

# GLOBAL MODELLING OF TRANSBOUNDARY AIR POLLUTION

DEFRA CONTRACT No. CPEA7

FINAL REPORT

NOVEMBER 2003 TO OCTOBER 2006

W.J. Collins<sup>1</sup>, M.G. Sanderson<sup>1</sup>, A.J. Manning<sup>1</sup>, A.L. Redington<sup>1</sup>,  
R.G. Derwent<sup>2</sup>

<sup>1</sup>Climate Research  
Met Office  
Exeter

<sup>2</sup>rdscientific  
Newbury  
Berkshire

## **Contents of this Report**

Introduction to the project

Executive Summary

### **I. Development of the Lagrangian models STOCHEM and NAME**

- (a) Introduction
- (b) STOCHEM
- (c) NAME

### **II. Scenario Assessment and Policy Support**

- (a) UNECE and CAFE - Role of long range transport and scenario assessment
  - 1. Background
  - 2. Ozone, methane and carbon monoxide under the IIASA scenarios
  - 3. Impacts of NO<sub>x</sub> emission changes
- (b) Additional Scenarios
  - 1. Impact of international shipping on sulphur deposition and surface ozone levels
  - 2. Eutrophication of Ecosystems: Changes in deposition to the EC15 countries
  - 3. Acidification of ecosystems: The role of climate change
- (c) Conclusions

### **III. Climate Change – Air Quality Interactions**

- (a) Exploring the Interactions
  - 1. Introduction and Policy relevance
  - 2. Effect of climate change on surface ozone levels
  - 3. Ozone levels in 2100: Further studies of climate change impacts
  - 4. Effect of changes in natural hydrocarbon emissions on surface ozone levels
  - 5. Effect of increasing levels of carbon dioxide on stomatal conductance and surface ozone concentrations
  - 6. Changes in emissions of nitrogen oxides (NO<sub>x</sub>)
- (b) Scenario Assessment and Interaction with IIASA
  - 1. Introduction
  - 2. Relationship between surface levels of O<sub>3</sub>, NO<sub>2</sub> and NO over Europe
  - 3. Effect of changes in European emissions on the rate of production of ozone
- (c) Contributions to Fourth Assessment Report of the IPCC
- (d) Conclusions

### **IV. Chairmanship of the UN ECE Task Force on Measurements and Modelling**

#### **V. Pollution Climate Modelling**

Introduction

- (a) NAME model analysis in response to ad hoc enquiries by Defra
- (b) UK and European contributions to secondary particulate levels
- (c) Estimation of contribution of natural sources to fine and coarse particles
- (d) Photochemical oxidant modelling within NAME
- (e) Conclusions

VI. Summary and Conclusions

VII. Recommendations for further work

Glossary

References

Annex A. Published papers and reports from this project

Annex B. Meetings attended.

## **Introduction to the Project**

Since 1979, the United Nations Economic Commission for Europe (UN ECE) Convention on Long-Range Transboundary Air Pollution (CLRTAP) has addressed some of the major international environmental problems of air pollution. It has since been extended by eight Protocols which identify specific transboundary issues. Since 1984, protocols for controlling sulphur, nitrogen oxides (NO<sub>x</sub>), volatile organic compounds VOCs, heavy metals, persistent organic pollutants and for the abatement of acidification, eutrophication and the formation of ground-level ozone O<sub>3</sub> have all been adopted under CLRTAP.

The objective of CLRTAP is to control air pollution and its effects and to develop an extensive programme for the monitoring and evaluation of the long-range transport of air pollutants. The object of the latest Protocol, signed in 1999 and named the Gothenburg Protocol, was to abate acidification, eutrophication and ground-level ozone. The goal of this Protocol, to be reached through a series of interim targets, is to achieve depositions not exceeding critical loads for acidification and eutrophication, and to achieve concentrations of ground-level ozone not exceeding critical levels for human health and damage to vegetation. The European Commission's Clean Air for Europe (CAFE) programme aims to provide a thematic strategy for air quality legislation in the European Union (EU).

Revisions of the Protocols and the building of new strategies have relied on sophisticated modelling of the emission, transport and deposition of air pollution to predict levels of pollutants under a range of scenarios. The models being used have become more sophisticated and better able to provide more accurate assessments of source-receptor relationships, and to describe the fate of air pollutants. The Task Force on Measurements and Modelling (TFMM) has been set up under the EMEP Protocol to the CLRTAP to provide qualified scientific information to support the development and further evaluation of the international protocols on emission reductions negotiated within CLRTAP.

Air pollution affects both the regional and global climate directly and indirectly, with the result that air pollution and climate change cannot be treated as distinct problems by policymakers. Many of the traditional air pollutants and greenhouse gases have common sources. Reducing these emissions offers the potential for simultaneous improvements for

both problems, resulting in short and medium term benefits for air pollution and long term benefits for climate change. There is a need to understand and quantify the links between regional air quality and climate change.

Methane ( $\text{CH}_4$ ) is both an ozone precursor and a greenhouse gas with both its sources and sinks likely to be affected by climate change. Some regional air pollutants, including tropospheric  $\text{O}_3$  and aerosols, are also important greenhouse forcing agents. Air pollutants such as  $\text{NO}_x$ , carbon monoxide (CO) and VOCs act as indirect greenhouse gases through their impact on the tropospheric distribution of hydroxyl radicals (OH) and hence the global-scale build-up of  $\text{O}_3$  and  $\text{CH}_4$ .

The Met Office has had a long involvement with the modelling of the long-range transport of acidic sulphur and nitrogen species and of ozone in Europe. It has also developed a sophisticated global Lagrangian chemistry model STOCHEM to study the build-up of greenhouse gases and aerosols.

In recent years, air pollution policies have been revised considerably to take into account the increased coverage of pollution networks and the publication of authoritative health-based air quality standards. Increasingly, air quality standards and the policy-based targets derived from them, are being set in terms of the number of occurrences allowed during each calendar year. This method of formulation implies that it is not simply the magnitude of the peak concentrations that are the most damaging, but also their recurrence.

In the past, it has been often the case that air quality standards have been expressed in terms of annual averaging time periods. Mean concentrations and air quality targets expressed in such terms are relatively robust and well defined quantities, statistically speaking. In urban areas, spatial variations in annual mean concentrations are strongly influenced by the distribution of emissions. Meteorological factors, in contrast, have relatively little influence on the overall spatial patterns of annual mean concentrations across particular urban areas. Emission inventories can then be useful policy tools in guiding air quality strategies and the achievement of air quality targets.

In contrast, the occurrence of pollution episodes and the magnitudes of the pollutant concentrations achieved within them are much more strongly influenced by meteorological

conditions than annual mean concentrations. Since they occur for relatively short periods, emissions during episodic conditions are often not well defined by annual inventories. The special features of each episode have to be resolved on a case by case basis. Furthermore, natural processes can lead to pollution episodes although such processes might make only negligible contribution to mean concentrations.

Some recent episodes that the Met Office has investigated, though not necessarily an exhaustive list, are given below to illustrate their range and diversity:

- Saharan dust episodes across England and Wales during March 2000.
- Sea salt aerosol across Wales during November and December 2000 and across Northern Ireland during March and May 1998.
- SO<sub>2</sub> pollution episode at Nottingham during 1998.
- Intercontinental transport of CO from forest fires in Alberta, Canada during August 1998 observed at the Mace Head monitoring site, Ireland.
- Long range transport of particles from forest fires near Moscow to PM<sub>10</sub> measured at monitoring sites from Scunthorpe to Edinburgh during September 2002.
- The movement and dispersion of the plume from the Buncefield depot fire, 2006.

The results from this project presented in this report are:

- I. To develop and validate state-of-the-art global chemistry-transport models for the air pollutants: NO<sub>x</sub>, SO<sub>2</sub>, NH<sub>3</sub>, CH<sub>4</sub>, VOCs, CO, O<sub>3</sub> and particulate matter PM. Developments are to focus on the links and feedbacks between climate change and air quality issues.
- II. To generate results with the global chemistry-transport model to guide the review and formulation of international policy agreements on emissions ceilings and air quality in the UN ECE and EU. An important consideration will be the extent to which improvements due to emission reductions within Europe may be offset by emission increases elsewhere, particularly for O<sub>3</sub> and PM.

- III. To evaluate the significance of international shipping and aviation on surface O<sub>3</sub> and the likely benefits arising from any reductions in emissions.
- IV. To begin the investigation and characterisation of the interactions between climate change and air quality, focusing on the benefits and disadvantages to Europe.
- V. To develop the NAME model further, as an aid to policy makers in their understanding of a range of specific issues relating to particulate matter both now and in the future.

The objectives of this work were to inform policy at DEFRA and the Devolved Administrations: the National Assembly for Wales (NAW), the Northern Ireland Executive, represented by the Department of the Environment in Northern Ireland (DoENI) and the Scottish Executive, represented by the Scottish Executive Environment and Rural Affairs Department (SEERAD).

## Executive Summary

1. In this report, two state-of-the-art models have been used to study current European air quality, and examine possible future changes under a variety of scenarios in the wider context of global atmospheric chemistry. Selected pollution episodes identified from surface measurements have also been studied, and the causes identified. The work described here has been orientated to illustrate to policy makers the fact that local, regional and global air quality problems are intrinsically linked.
2. The effect of different emission scenarios on surface ozone levels over Europe has been investigated, by examining the changes between the years 2000 and 2030. Three scenarios were chosen, IIASA CLE, (“likely”), IIASA MFR (“optimistic”) and SRES A2 (“pessimistic”). Under the SRES A2 scenario, ozone levels increase by 2 – 12 ppb. Under the CLE scenario, ozone levels have fallen by up to 6 ppb over much of Europe by 2030, and by up to 18 ppb under the MFR scenario. These results show that pollution levels can be controlled under current policies, and even greater reductions could potentially be achieved.
3. Ozone levels are predicted to rise over the Benelux countries and the southern half of the U.K. in the CLE and MFR scenarios. These results highlight the important non-linearity between the magnitude of emissions and ozone levels. Reductions in emissions of primary pollutants do not always lead to lower ozone levels.
4. The previous paragraphs summarised results from global emissions changes. Further studies on emissions changes showed that European air quality is improved even if just European emissions were reduced and the rest of the world did not reduce their emissions. Long-range transport of pollution still has a significant impact on European air quality. By 2030, emission reductions in Europe under the CLE scenario don’t give the full benefit as emissions from the rest of the world are still increasing. Under the MFR scenario, Europe benefits considerably by reducing its emissions, even if the rest of the world does not. The greatest ozone reductions over Europe are realised if all the world follows the MFR scenario

5. Emissions of primary pollutants from international shipping are predicted to rise in the future. These emissions are currently unregulated, and so they may have a greater impact on air quality over Europe as land-based emissions fall. Shipping-based emissions are responsible for between 4 and 16% of ozone levels over Europe, and approximately 10% of the total sulphur deposited over north-western Europe for the current time. Climate change has been shown to increase the deposition flux of acidifying compounds to land surfaces, owing to changes in the oxidation pathways of ammonia and sulphur dioxide.
6. Climate change has a large impact on modelled concentrations of ozone and other pollutants, even in the year 2030. Background ozone levels are smaller when climate change effects are included in simulations. Much of this reduction is due to increased levels of water vapour that in turn lead to greater destruction of ozone. However, the rate of exchange between the stratosphere and troposphere increases with climate change, and a greater proportion of surface ozone has a stratospheric origin. More work is needed to determine how the local production of ozone changes with climate change.
7. Source-receptor relationships have been widely used in policy discussions to quantify the relationships between emission sources and air concentrations or depositions at receptors. Here we begin the process of defining ozone source-receptor relationships where the precursor emissions sources,  $\text{NO}_x$  in particular, are located in North America and Asia and the receptors are located in Europe. A large set of STOCHEM model experiments have been carried out using month-long emission pulses of  $\text{NO}_x$ . Ozone responses have been followed at 21 EMEP monitoring site locations across Europe and the model calculations have been conducted for summer and winter. The ozone responses to the  $\text{NO}_x$  pulses contain a short-term (1 – 3 month) ozone increase above baseline followed by a long-term (10 – 15 year) decrease below baseline. The initial positive response is  $\text{NO}_x$ -driven and the long-term negative response is methane-driven. There appears to be significant gradients in these two responses and their extents of cancellation, depending where in each continent the  $\text{NO}_x$  pulse is emitted, and where in Europe the receptor is located
8. Increasing levels of carbon dioxide have an important indirect effect on surface ozone levels. When carbon dioxide levels rise, the plant stomata do not need to open as widely to allow sufficient carbon dioxide to enter, hence the rate of removal of ozone also

decreases. Simulations have shown that ozone levels may rise by about 10% owing to this effect under doubled carbon dioxide levels.

9. Results from many model simulations were submitted and included in the “Photocomp” experiment organised by ACCENT (A European network of excellence), which involved significant interaction with many other researchers across the globe. Six peer-reviewed publications were written by the organisers of the Photocomp experiment, and several were referred to in chapter 7 of the IPCC Fourth Assessment Report. Additionally, other publications from this contract and the previous one (EPG 1/3/164) were also referenced by the IPCC in chapter 7.
10. One consortium member has chaired the UN ECE Task Force on Measurements and Modelling. The EMEP model has been reviewed and found to be fit for purpose. The state of modelling of heavy metals and POPs was assessed, as well as air pollution monitoring strategies.
11. During the three year period of the contract the NAME dispersion model has been used to respond to several enquiries from Defra, most notably the dispersion of the smoke plume from the Buncefield depot fire which began on the 11<sup>th</sup> December 2005. Despite the number of unknown variables, NAME predicted the extent and movement of the smoke plume with a high degree of accuracy.
12. Unusually high levels of PM<sub>10</sub> were observed in the UK in May 2006. Dispersion modelling with NAME demonstrated that this episode was caused by long-range transport of smoke from agricultural burning and forest fires in western Russia. Russian fires have affected UK air quality at least twice since 2000 and such events are likely to occur in the future with implications for UK and European air quality.
13. The NAME model has been used to study the origin of secondary inorganic aerosols in the UK. The study covered 2002 and 2003 and found significant variation in the amount of imported aerosol from Europe with location in the UK. For example, France was the main contributor to UK sulphate aerosol levels, contributing over a third of the sulphate modelled at Barcombe Mills in 2003. Significant differences were also found between the results from the two years. These results reflect the importance of fully representing the

three dimensional transport of secondary aerosols over the European domain, and highlight the differences that can occur from year to year through meteorology alone. This work contributed to the Air Quality Expert Group Report on Particulate Matter in the United Kingdom.

14. The contribution of natural sources of aerosols to observed  $PM_{10}$  levels over the U.K. was examined using the NAME model. The focus was on sea salt aerosols and Saharan dust. The model was validated using measurement data from dust events in Spain. The model was subsequently used to examine the role of Saharan dust in an event in the U.K and the dust storm in Athens 2005. The NAME model was also used to forecast the passage of dust from the Sahara and direct the flights of aircraft used to make measurements.
15. The ability to model the advection of background pollutants (i.e., pollutants that exist throughout the atmosphere rather than being emitted from specific sources) has proved a difficult problem in the Lagrangian framework of the NAME model. A scheme has been devised which combines modelling ozone on both a three-dimensional grid and utilises existing model particles where available. This new scheme will be fed into the forthcoming Air Quality Forecasting System.

# Chapter I. Development of the STOCHEM chemistry-climate model and the NAME dispersion model.

## (a) Introduction

This chapter reports on the development of the STOCHEM model under Work Package I of the original contract. Additionally, a brief description of some developments made to the NAME model is also given. These improvements were necessary to meet objectives in other parts of the contract.

## (b) STOCHEM

### 1. General Description

STOCHEM is a three-dimensional Lagrangian chemistry-transport model. In this model, the atmosphere is divided into a number of air parcels with equal masses. STOCHEM is coupled directly to the Hadley Centre's climate models (HadCM3 and HadGEM1), from which many data such as winds, temperature and humidity are taken. Each air parcel holds the concentrations of over 70 chemical species, including nitrogen oxides (NO and NO<sub>2</sub>), ozone (O<sub>3</sub>), PAN, and the associated radicals such as the hydroxyl radical (OH) and perhydroxy radical (HO<sub>2</sub>). The chemical scheme includes the degradation mechanisms of many hydrocarbons, which are methane (CH<sub>4</sub>), ethane (C<sub>2</sub>H<sub>6</sub>), propane (C<sub>3</sub>H<sub>8</sub>), butane (C<sub>4</sub>H<sub>10</sub>), toluene (C<sub>6</sub>H<sub>5</sub>CH<sub>3</sub>), o-xylene (C<sub>6</sub>H<sub>4</sub>(CH<sub>3</sub>)<sub>2</sub>), ethene (C<sub>2</sub>H<sub>4</sub>) and propene (C<sub>3</sub>H<sub>6</sub>). An oxidation mechanism of the important naturally emitted hydrocarbon isoprene (C<sub>5</sub>H<sub>8</sub>) is also included. The full chemistry of the oxidation products of these hydrocarbons, such as peroxy radicals, acetone (CH<sub>3</sub>COCH<sub>3</sub>), methyl vinyl ketone (CH<sub>3</sub>COCH=CH<sub>2</sub>) and acetaldehyde (CH<sub>3</sub>CHO), is also included. In total, there are 176 chemical reactions and 18 photolysis reactions.

For some of the results presented in the following chapters, STOCHEM was coupled to the HadCM3 climate model. In this case, the atmosphere was divided into 50,000 air parcels, and the resulting concentrations of the chemical species were mapped onto a 5° × 5° horizontal grid, and 9 vertical levels, with an upper boundary of 100 hPa. When STOCHEM was coupled to the Hadley Centre's new climate model HadGEM1, the atmosphere was divided into 100,000 air parcels, and the concentrations were mapped onto a 3.75° × 2.5° horizontal grid, and 20 vertical levels, which extend to an upper boundary of 39 km.

## 2. Development of the STOCHEM model

### (i) Aerosols in STOCHEM-HadGEM1

Aerosols, or particulates, have a significant effect on air quality and human health. Small particles (PM<sub>10</sub>, i.e. those with a diameter less than 10 µm) are easily inhaled, where they cause inflammation in the lungs. Smaller particles, such as PM<sub>2.5</sub>, are more easily inhaled, and have a sufficiently long lifetime that they can be transported large distances from their source. Some types of aerosol, such as sulphate particles and mineral dust, can reflect incoming solar radiation and cool the atmosphere. Other types, such as black carbon and soot, produced from combustion of fossil fuels, can absorb incoming and reflected radiation, and warm the atmosphere. Aerosols have a wide range of sizes, and their lifetime is similar to that of ozone. Two types of aerosol have received comparatively less attention than others. First, secondary organic aerosols are produced from the oxidation of large hydrocarbons (terpenes) emitted by vegetation (and some anthropogenic emissions), and second, ammonium nitrate aerosols. The latter type is likely to increase in importance in the future, as emissions of sulphur dioxide fall, and ammonia emissions (one of the precursor gases) from agriculture increase.

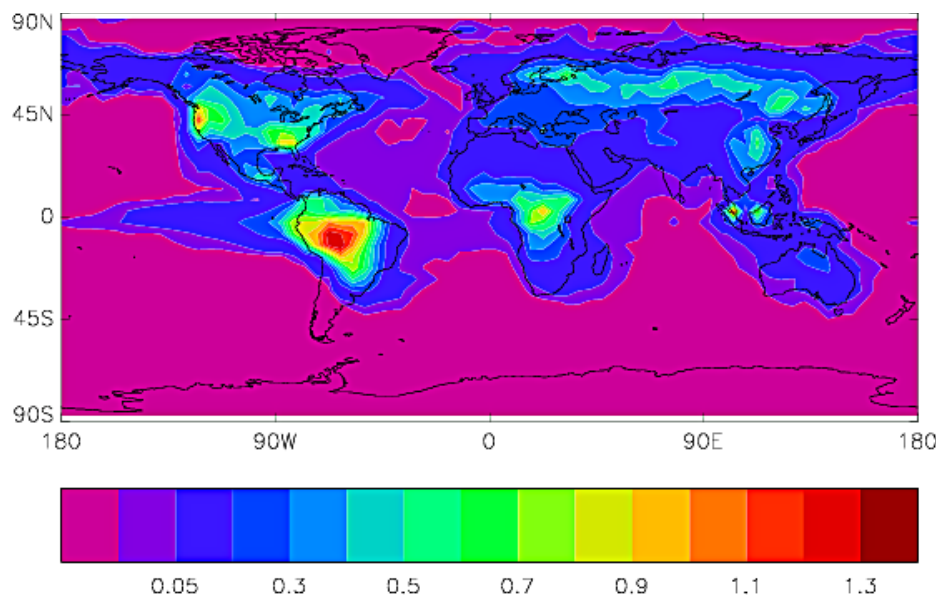


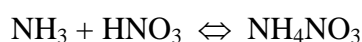
**Figure I-1.** Concentration of aerosols (ppb) produced from the oxidation of terpenes as predicted by STOCHEM.

### *Secondary organic aerosols*

A chemical scheme for generating secondary organic aerosols from terpenes has been developed and run in STOCHEM. Briefly, additional chemical reactions describing the oxidation of  $\alpha$ -pinene, a terpene emitted by many plants, were added to the STOCHEM mechanism. A full mechanism would require hundreds of reactions, so a simplified scheme was used instead (M.E. Jenkin, personal communication). A fixed percentage of the oxidation products were assumed to enter the aerosol phase. Initial results are shown in Figure I-1. Large concentrations of aerosols are found over the tropical forests, and over the boreal forests of the USA and Siberia.

### *Ammonium nitrate aerosols*

The largest anthropogenic contribution to global aerosol burdens is from sulphur emissions. However, ammonium nitrate is a significant fraction of anthropogenic aerosol over agricultural regions, such as Europe (principally the Netherlands), India, and China. Where there is an excess of ammonia over sulphate, ammonium nitrate aerosol may be formed,



It is likely that ammonium nitrate will increase in importance in the future, as sulphur dioxide emissions decrease, but ammonia emissions from intensive animal husbandry increase, and nitrogen oxide ( $\text{NO}_x$ ) emissions remain high. It is therefore important to include this species in studies of particulate matter levels, and hence air quality, of the future.

Ammonium nitrate is much more complex to model than ammonium sulphate. Ammonium sulphate is produced directly in the gas phase, and also in the aqueous phase, where it immediately precipitates as a solid. Once formed, it is no longer reactive. However, ammonium nitrate is volatile and can decompose back into its constituent parts ( $\text{NH}_3$  and  $\text{HNO}_3$ ), as shown in the above equation. A new scheme has been added to STOCHEM that takes into account the competition between sulphate and nitrate for the ammonia, and includes the effects of temperature and relative humidity on the volatility of the ammonium nitrate (Ackermann et al., 1995). An example of the predicted ammonium nitrate aerosol levels is shown in Figure I-2. The biggest concentration is over the Netherlands, but with substantial concentrations over the rest of Western Europe, South Asia and East Asia.

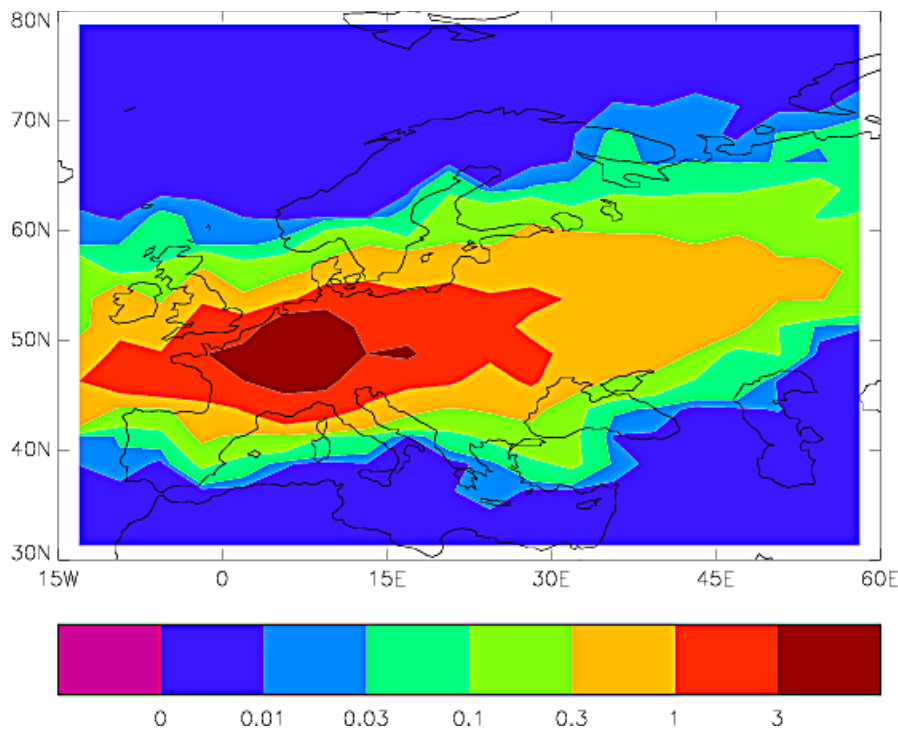


**Figure I-2.** Ammonium nitrate concentrations ( $\mu\text{g m}^{-3}$ ) at the surface.

(ii) Coupling of emissions schemes to model parameters

*Production of nitrogen oxides by lightning*

Lightning represents an important source of nitrogen oxides in the troposphere. Although the global production (which lies between 2 and 10 Tg N yr<sup>-1</sup>) is small compared to the total NO<sub>x</sub> emission (about 56 Tg N yr<sup>-1</sup>), a significant proportion is produced in the upper troposphere, where it may produce ozone and change the radiative balance of the atmosphere. In STOCHEM, the simple approach of Price and Rind (1992) has been implemented.

Convective cloud heights are used to calculate the number of lightning flashes, which are divided into cloud-to-ground and inter-cloud components. Cloud-to-ground flashes make up a smaller proportion of the total number of flashes, but are more energetic and produce more nitrogen oxides. The total NO<sub>x</sub> produced is then distributed vertically using the profiles derived by Pickering et al. (1998). Different profiles are used for tropical continental, mid-latitude continental, and maritime storms. An example of the lightning production of NO<sub>x</sub> is shown in Figure I-3. The majority of the production occurs in the tropics in the upper troposphere, but significant amounts are also produced at the surface.

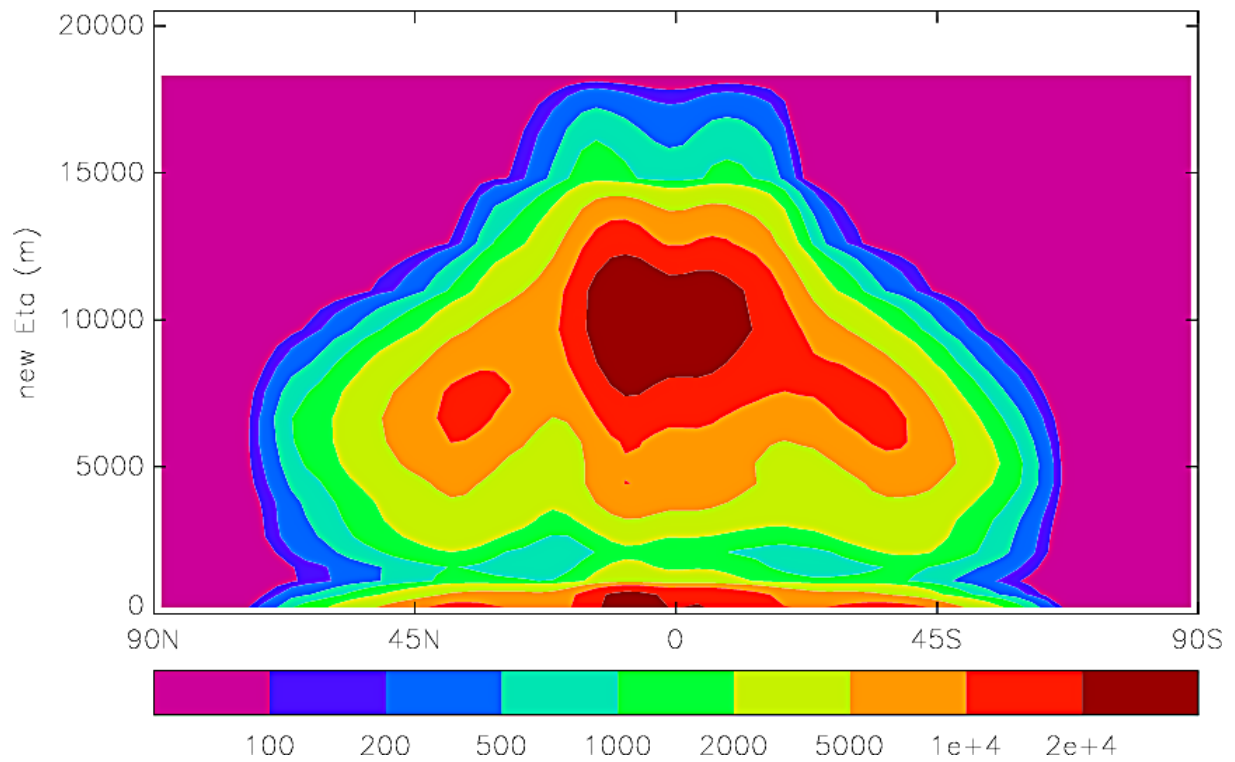


**Figure I-3.** Annual  $\text{NO}_x$  production rate by lightning. The units are  $\text{kg yr}^{-1}$ .

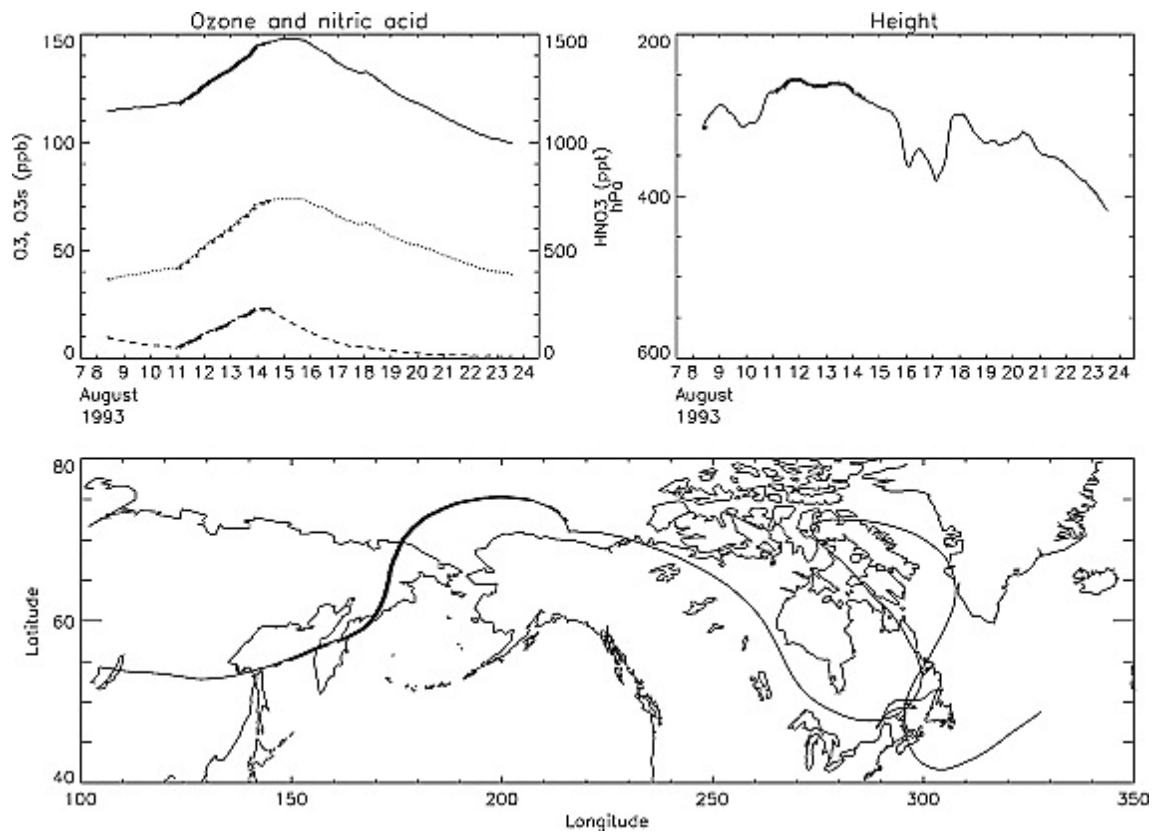


**Figure I-4.** An example of a parcel trajectory showing the levels of  $\text{O}_3$  (solid line), stratospheric ozone ( $\text{O}_3\text{s}$ , dotted line) and  $\text{HNO}_3$  (dashed line), and height. The thicker line segments indicate when the air parcel was above the tropopause.

### *Stratospheric Ozone*

Although stratospheric ozone is not an emitted species, stratosphere-troposphere exchange (STE) is an important process that influences both upper atmospheric and surface ozone levels. STOCHEM does not explicitly simulate chemical reactions in the stratosphere. All chemical and photolytic rates are set zero in this region. Ozone values within air parcels that enter the stratosphere are relaxed toward a climatology present within the climate model using a time constant of 20 days. As before, a source of oxidised nitrogen from the stratosphere is also included, having a value of one thousandth of the ozone flux. This oxidised nitrogen is assumed to be present as nitric acid, HNO<sub>3</sub>. Simulations using different time constants for the relaxation (e.g. 10 days) did not produce significantly different results.

### *Methane emission from wetlands*

Wetlands are a major source of the greenhouse gas methane, and currently account for about 20 % of the total methane source (IPCC, 2001). Most of the world's wetlands are found at high northern latitudes, in Canada and Siberia, but significant areas are also found in tropical regions. The exact emission of methane from wetlands in any year will be primarily controlled by the soil moisture and temperature, and is consequently highly variable. For example, in 1998 there was an anomalous increase in the methane growth rate, which in turn was due to an increase in emission from tropical wetlands, caused by warmer and wetter conditions in that year (Dlugokencky et al., 1998). In the future climate, if areas where wetlands are present become warmer and wetter, they could produce significantly more methane. Conversely, if the same areas become drier, then the methane emission may fall. It is clearly important to include such variability in long-term climate modelling studies. An interactive wetland methane emission scheme has been implemented into the Unified Model (Gedney and Cox, 2002), and the results are used in STOCHEM. Each model timestep, the soil moisture content and local topography are used to calculate the area of wetland in each model surface gridbox, and other data such as the organic carbon content are used to calculate the methane emission based on the formulae of Christensen and Cox (1995).

Modelled global wetland distributions are compared with the database of Aselmann and Crutzen (1989; with the updates for Alaska of Stillwell-Soller et al. (1995)) in Figure I-5. It should be noted that the modelled wetland distributions were generated entirely within the climate model – no actual measurements were used to construct them. The model predictions are in generally in good agreement with the observations, except over central Africa. In this

region, the precipitation amounts are too large in the climate model, and consequently the model predicts too much wetland area in this region.

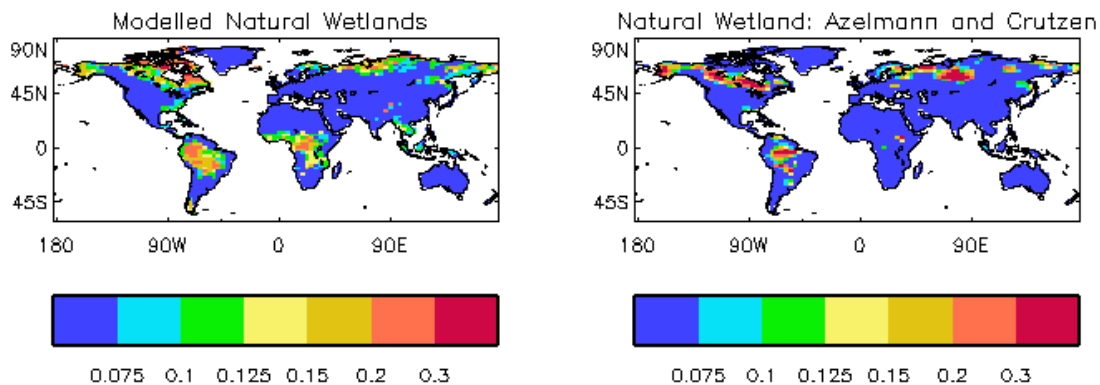


**Figure I-5.** Comparison of modelled wetland areas with the database of Aselmann and Crutzen (1989) as updated by Stillwell-Soller et al. (1995). The scale gives the fraction of each surface gridbox that is classed as wetland. The model reproduces the data very well except over Africa. See text for further information.

The zonal average wetland fractions, and annual methane emissions predicted by the wetland scheme are shown in Figure I-6. The average wetland fractions and emissions predicted by two other published wetland methane emission databases are also given for comparison. Again, the model is in good agreement with the other two databases, but overpredicts emissions in tropical regions. This overprediction is caused by the large wetland area modelled in central Africa as discussed above.

The effect of climate change and interannual variability in the model will now feed back onto the wetland emissions. Previously in STOCHEM, a simple wetland methane emission file was used which did not include any seasonal variation. Emission of methane from wetlands, particularly those at high northern latitudes, varies strongly with season. Little or no emission occurs during the winter months, whereas large emissions are produced in the summertime. We have now integrated STOCHEM using the interactive wetland methane emission scheme. The results are compared with a similar simulation which used the original fixed emission file and measurements from the NOAA/CMDL network in Figure I-7.

The methane levels at the sites chosen are strongly influenced by wetland emissions, and so will give a good indication of any improvement in the model simulation. Alert, Barrow and Cold Bay are situated close to wetland areas. Bermuda and Shemya are island locations

further from the source regions, and methane levels at the Seychelles are strongly influenced by emissions from India and areas containing rice paddies at certain times of the year. The STOCHEM data have been detrended to overlap with the observed data. The important features in this instance are the monthly and yearly variability in the methane levels, rather than their absolute values.

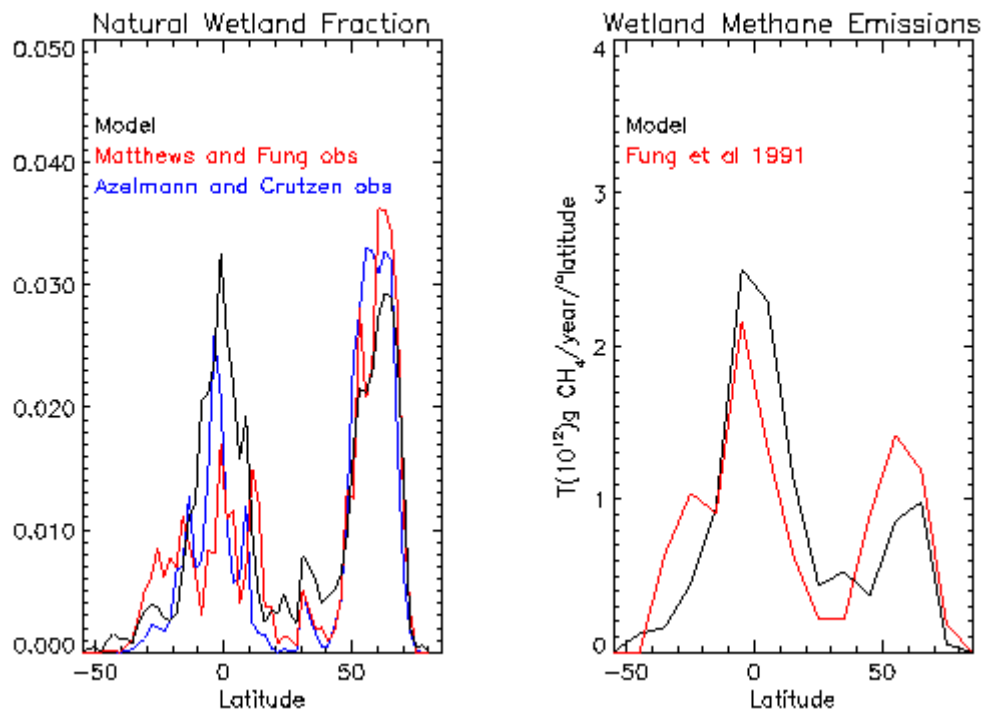


**Figure I-6.** Comparison of zonally averaged wetland fractions and methane emissions compared with two published databases. The left panel compares the wetland fraction in each 10° latitude band with the databases of Matthews and Fung (1987) and Aselmann and Crutzen (1989). The right panel compares the modelled annual methane emission from each 10° latitude band with the emissions calculated by Fung et al. (1991).

In Figure I-7, the methane levels from a STOCHEM integration using the original constant emission scheme are shown in blue, and the results using the interactive wetland scheme are shown in red. Monthly mean methane levels derived from surface measurements are represented by the triangles. At Alert, Barrow and Cold Bay, locations situated very close to wetlands, the simulation using the new scheme gives better results which contain less ‘noise’ than the results using the fixed wetland emissions. Although these locations are close to the wetland methane sources, transport still plays a role in determining the observed levels. The large peaks in the simulation using the fixed wetland emissions are likely to be caused by transport of air containing too much methane.

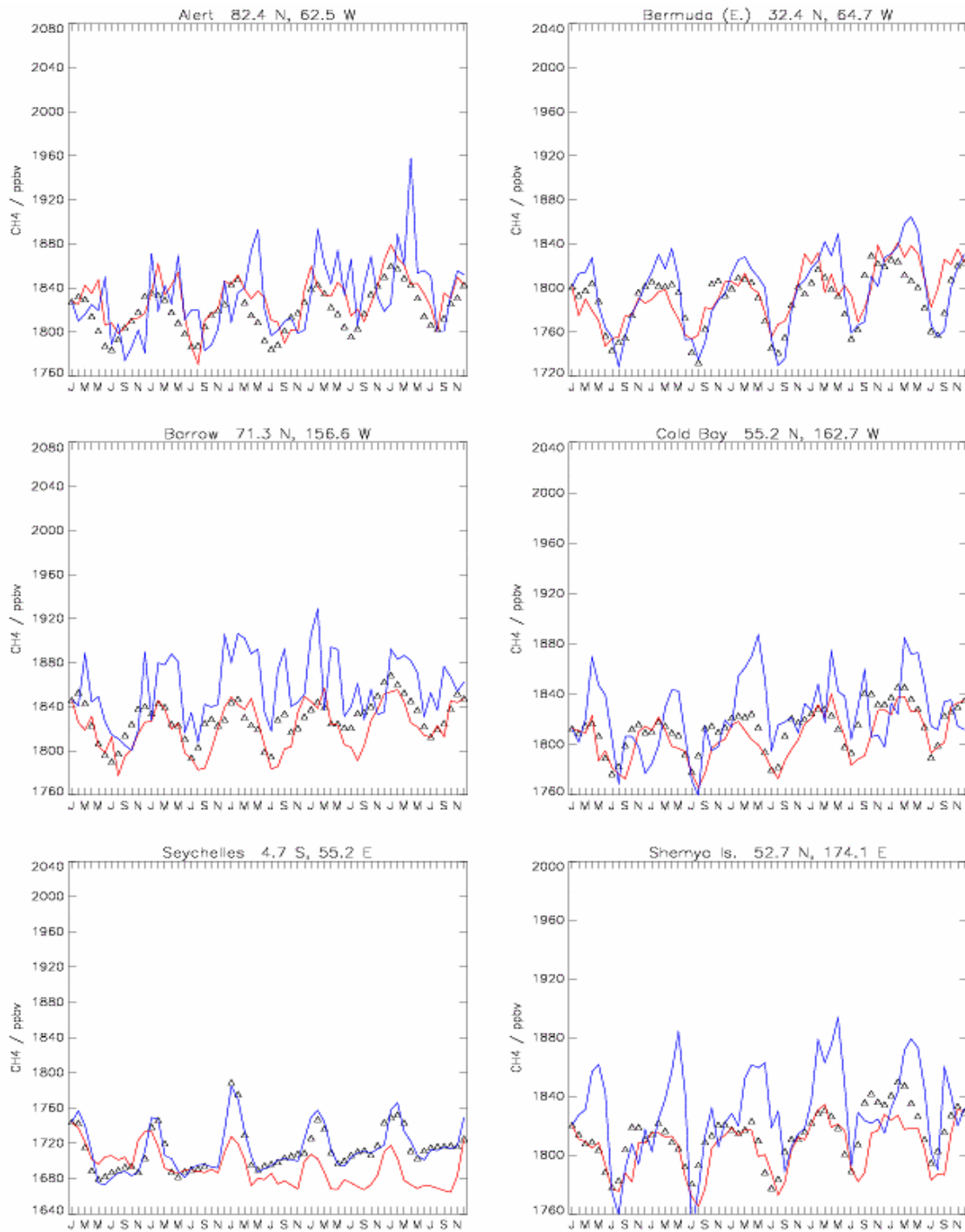


**Figure I-7.** Comparison of surface methane levels from two simulations using the STOCHEM model with measurements from the NOAA/CMDL network for the period 1991-1995. The red line is a simulation using the interactive wetland methane emissions scheme described in the text. The blue line is a simulation using a constant methane emissions source. The surface measurements are represented by triangles. In all cases, monthly mean concentrations are shown.

At Bermuda and Shemya, long-range transport of methane from wetlands is very important. The phase of the cycle in the methane levels in each simulation is similar, indicating that influence of the seasonality in the emission flux is less important here, and transport plays an important role in determining the methane levels at these locations. However, the amplitude is simulated more accurately when the new wetland scheme is used at Shemya, and the peaks in the springtime seen when the constant wetland emission is used are not present. At Bermuda, both simulations perform equally well.

During the period January to March, methane levels at the Seychelles are strongly influenced by emissions from India and the surrounding area. In this case, the simulation using the fixed wetland emissions is more accurate than when the interactive scheme is used. This result may be due to incorrect seasonal variation in the interactive scheme. In the present work, rice paddy emissions are modelled in the same way as natural wetlands. In reality, the seasonality will be determined by, for example, planting times and fertilizer use.

#### *Isoprene and terpene emissions from vegetation*

Vegetation emits a wide range of hydrocarbons and other compounds. One of the most important of these hydrocarbons is isoprene (2-methyl-1,3-butadiene). This species has an annual emission flux of about 570 Tg yr<sup>-1</sup> (Guenther et al., 1995), which is similar to that of methane. It is also very reactive, having a lifetime of just a few hours (Kesselmeier and Staudt, 1999), and so only affects surface chemistry (although some of the longer-lived products such as acetone and carbon monoxide can be transported to the free troposphere and other locations). If the surface levels of NO<sub>x</sub> are large enough, isoprene emissions will promote ozone formation. If they are low, isoprene can react directly with ozone and reduce its levels. The majority of isoprene is emitted in the tropics, which is where most of the methane is destroyed. The degradation of isoprene, like all hydrocarbons, begins by reaction with the hydroxyl (OH) radical. If isoprene emissions were to increase in a future climate, they could perturb the levels of the OH radical and change the lifetime of methane (Shallcross and Monks, 2000).

An extra module has been added to STOCHEM to calculate isoprene emissions, using the vegetation distribution from MOSES-II (Cox et al., 2001) and the well-established algorithms of Guenther et al. (1995). These algorithms were developed using field measurements of isoprene emissions, and use a standard emission for each vegetation category that is combined

with leaf-area indices (divided into sunlit and shaded fractions), temperature and surface radiation fluxes to calculate the actual isoprene emissions. The isoprene emissions are calculated every model time step (30 minutes).

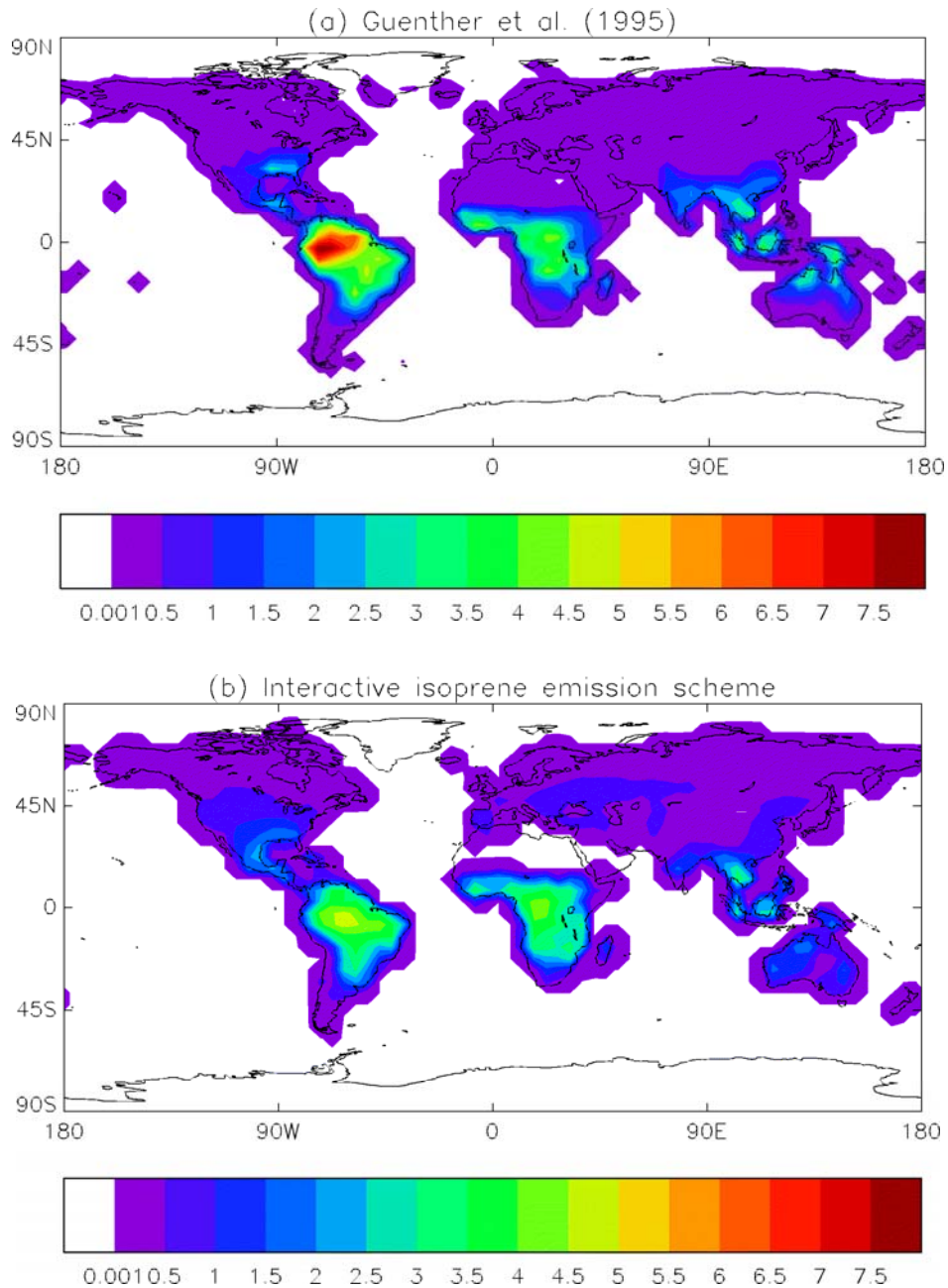


**Figure I-8.** Comparison of annual isoprene emissions from (a) Guenther et al. (1995), and (b) the interactive scheme in STOCHEM. The units are Tg isoprene per model gridbox per year. Both datasets have been scaled to a global total of 568 Tg yr<sup>-1</sup>.

The modelled isoprene emissions are compared with the emissions from Guenther et al. (1995) in Figure I-8. The latter authors used a global ecosystem database, satellite measurements of leaf area indices, and monthly mean temperature, precipitation and radiation

data to calculate an annual isoprene emission. Both datasets have maximum emissions from tropical forests in Amazonia, Africa and Indonesia, and much smaller emissions from other regions of the globe. The isoprene emissions calculated by Guenther et al. (1995) for Amazonia are larger than those from Africa and Indonesia. However, in STOCHEM the emissions from these three regions are almost the same. The surface scheme used by STOCHEM, MOSES-II, only has 5 vegetation types. However, Guenther et al. (1995) used the ecosystems database of Olson (1992), which has areas of 40 different vegetated types. The species of trees which emit isoprene in Amazonia are very different to those in Africa and Indonesia. It is not possible to represent this diversity in MOSES-II presently. Given the differences between these two studies, the isoprene emissions are in very good agreement.

### (iii) Dry deposition of ozone and other pollutants

Dry deposition may be defined as the irreversible uptake of a species at the surface in the absence of precipitation. In the previous version of STOCHEM, this quantity was calculated from an aerodynamic term, which was dependent on the stability of the boundary layer, and a surface term, whose value was fixed for each depositing species. In the current version of STOCHEM, the dry deposition velocity ( $v_d$ ) is calculated as the reciprocal of the sum of three resistance terms,  $v_d = 1 / (R_a + R_b + R_c)$ , where  $R_a$  is the aerodynamic resistance,  $R_b$  is the quasi-laminar resistance, and  $R_c$  is the surface resistance. All these resistance terms have units of reciprocal velocity ( $s\ m^{-1}$ ).

The aerodynamic term is calculated from the stability of the boundary layer. The quasi-laminar resistance,  $R_b$ , depends on the surface velocity and the depositing species, and represents diffusion across a narrow layer of air just above the surface. Finally, the surface resistance,  $R_c$ , is calculated from many individual resistance terms for the various surfaces, such as the surfaces of plant leaves, soils, water and ice. Many of these individual resistances depend on temperature or humidity. One important deposition route for many species, such as ozone and sulphur dioxide, is deposition via the stomata. Stomata are small pores on the surface of leaves that allow carbon dioxide to enter where it may be used for photosynthesis, and water to escape. The size of the stomata (and hence the resistance term) varies diurnally, and also with soil moisture. Other gases as well as carbon dioxide may enter the leaf via the stomata, and damage the plant. This new dry deposition scheme therefore may be used to calculate the fluxes of trace gases that deposit via the stomata only, as well as the total deposition.

The potential damage to plants from ozone is usually assessed using the AOT<sub>40</sub> scale. This quantity may be defined as the sum of the differences between hourly ozone concentrations and 40 ppb for each hour when the concentration exceeds 40 ppb during the growing season. However, this measure does not take into account any stresses the plant may be under. For example, if the soil is dry, the stomata will reduce in size to decrease water loss. Consequently, for a given ambient ozone concentration, less ozone will be absorbed by the plant. A more accurate way of assessing the effect of ozone on plants is to measure the total amount actually absorbed via the stomata. This second approach requires measurements of micrometeorological data such as temperature, surface wind profiles, humidity as well as the ozone concentrations. Damage to plants is closely related to stomatal uptake of ozone.

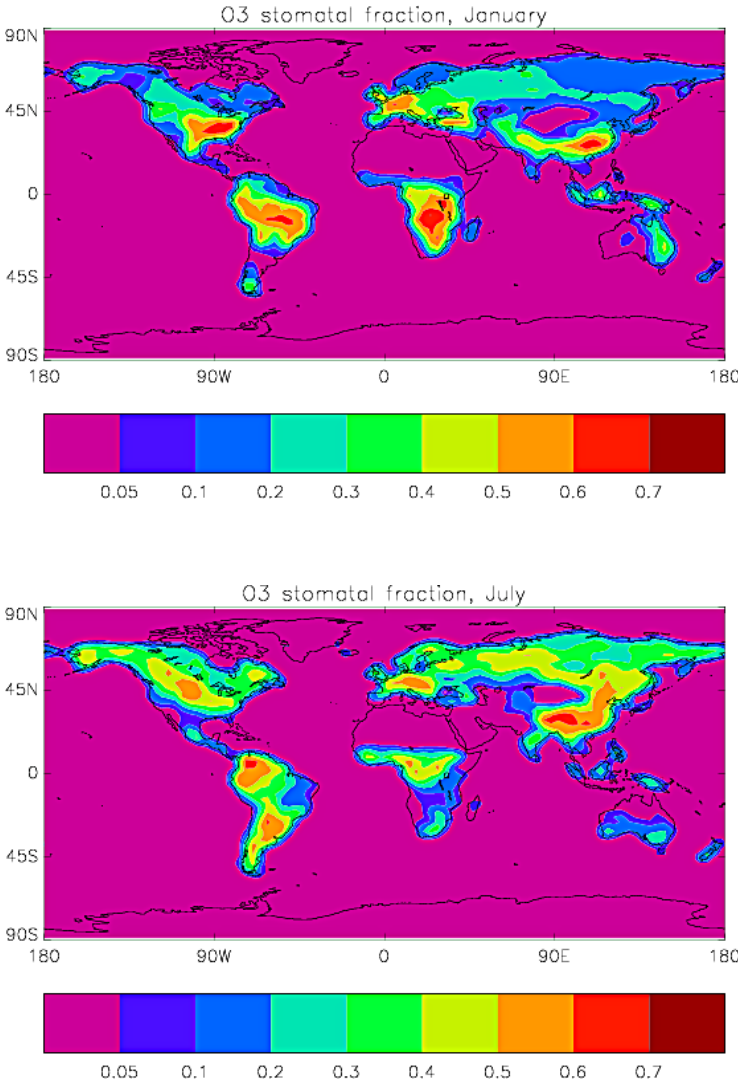


**Figure I-9.** Fraction of ozone deposited via the stomata of vegetation. Top panel – January. Bottom Panel – July.

The dry deposition module in STOCHEM has been used to calculate the fraction of ozone dry deposited via the stomata, and hence the flux of ozone taken up by the plant. An example of the modelled stomatal deposition fractions for January and July is shown in Figure I-9. In most vegetated locations, the percentage of ozone deposited via the stomata is at least 20 %, rising to 60 % or more in some locations. Any increase in surface ozone levels could therefore have a detrimental effect on the health of the vegetation. The locations with the highest uptake flux do not necessarily correspond to the areas where the stomatal contribution is largest. The surface ozone concentration is the main controlling factor.

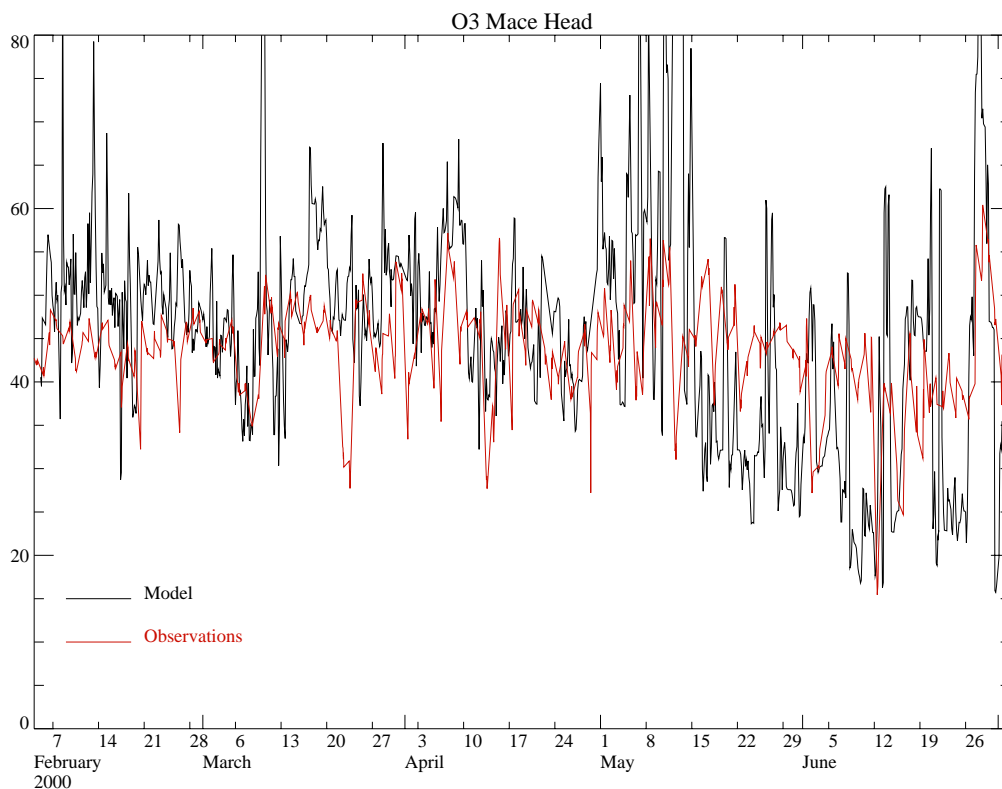


**Figure I-10.** Modelled and measured ozone levels at Mace Head for spring 2000. Units are ppb.

#### (iv) Evaluation of Long-Range Transport

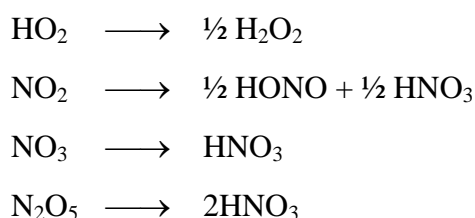
For detailed comparisons of model results with observations it is essential to drive the chemistry model with meteorological data appropriate for the period of the measurements. In particular, this approach reduces differences between modelled and measured trace gas concentrations due to interannual variability. STOCHEM is driven from the climate model, so to run specific periods, the meteorology has to be nudged towards observed data. Figure I-

10 shows 3-hourly modelled ozone concentrations for the grid square that includes Mace Head for the period February to June 2000. STOCHEM is driven by the climate model which in turn was nudged towards analyses for the year 2000 using ECMWF analyses. Measured hourly daytime ozone concentrations at Mace Head are shown for comparison. The comparison is very good, and although there are some modelled concentration peaks that are much larger than the measurements, there is a clear correspondence between the model results and the measurements.

(v) Heterogeneous reactions

Nitrogen oxides ( $\text{NO}_x$ ) play a very important role in the oxidation of hydrocarbons and the formation of ozone in the lower atmosphere. Correct representation of the reactions of nitrogen oxides in a model is therefore very important for simulating observed ozone levels, and predicting future levels and changes.

As well as the numerous gas-phase reactions, there are a number of important reactions involving nitrogen oxides that occur on the surfaces of aerosols, which are referred to as heterogeneous reactions. They are important because they convert reactive  $\text{NO}_x$  to less reactive forms of nitrogen oxides (referred to as  $\text{NO}_y$ ). Most of the reactions convert nitrogen oxides to nitric acid, which remains on the surface of the aerosol. However, one heterogeneous reaction produces nitrous acid (HONO), which is emitted back into the gas phase. HONO production will occur during the night time, allowing its concentrations to build up. It is readily photolysed, and so provides a large source of OH radicals and NO at sunrise. These reactions will have a strong influence on ozone levels, as the latter are strongly controlled by the levels of  $\text{NO}_x$ . The heterogeneous reactions considered in STOCHEM are shown below.



The rate constant for each heterogeneous reaction in STOCHEM is calculated from the total surface area of the aerosol, and a reaction probability. The sulphate aerosol surface area was estimated from the mass using the same size distribution as Dentener and Crutzen (1993), and

the reaction probabilities were taken from a review by Jacob (2000), as updated by Evans and Jacob (2005). Reactions on sea salt aerosols were also included by Dentener and Crutzen (1993), but were not considered in STOCHEM. The percentage changes in NO<sub>x</sub> and O<sub>3</sub> in STOCHEM have been arranged into the same regions and time periods used by Dentener and Crutzen (1993), and are compared with the latter's results in Table I-1. Although there are some differences between these two studies, a comparison of the results is still useful.

The results in Table I-1 show that both studies predict significant reductions in the levels of ozone and nitrogen oxides. The reductions in NO<sub>x</sub> levels in STOCHEM are generally (but not always) smaller than those of Dentener and Crutzen (1993), whereas there are larger differences in the ozone changes. Interestingly, the reduction in NO<sub>x</sub> and O<sub>3</sub> in the southern hemisphere (SH) in the period November to April in STOCHEM is greater than that modelled by Dentener and Crutzen (1993). The importance of sea salt aerosols should be greatest in this region. This unexpected result may also be due to differences in sulphate loadings between the two studies, and the greater number of reactions considered in STOCHEM. Generally, most of the changes in these two studies are within a factor of 2 of each other, which perhaps is reasonable, considering the differences.

**Table I-1.** Percentage changes in NO<sub>x</sub> and O<sub>3</sub> mixing ratios in the northern (NH) and southern hemispheres (SH), and the tropics, for the periods November to April (NA) and May to October (MO). The results from a similar study by Dentener and Crutzen [DC (1993)] are included for comparison.

	Species	NH		Tropics		SH		Global
		NA	MO	NA	MO	NA	MO	
STOCHEM	NO <sub>x</sub>	-54	-42	-22	-25	-23	-26	-33
DC (1993)		-75	-45	-22	-15	-13	-37	-49
STOCHEM	O <sub>3</sub>	-14	-1	-13	-14	-8	-8	-11
DC (1993)		-20	-13	-7	-6	-4	-10	-9

Global maps of the surface ozone changes show that, as indicated by the results in Table I-1, ozone levels are generally smaller when heterogeneous reactions are included. However, increases in ozone levels are observed in some regions. The seasonal mean changes in surface ozone levels over Europe, when heterogeneous reactions are included, are shown in Figure I-11. Positive values indicate that ozone values are larger when the heterogeneous reactions are included.

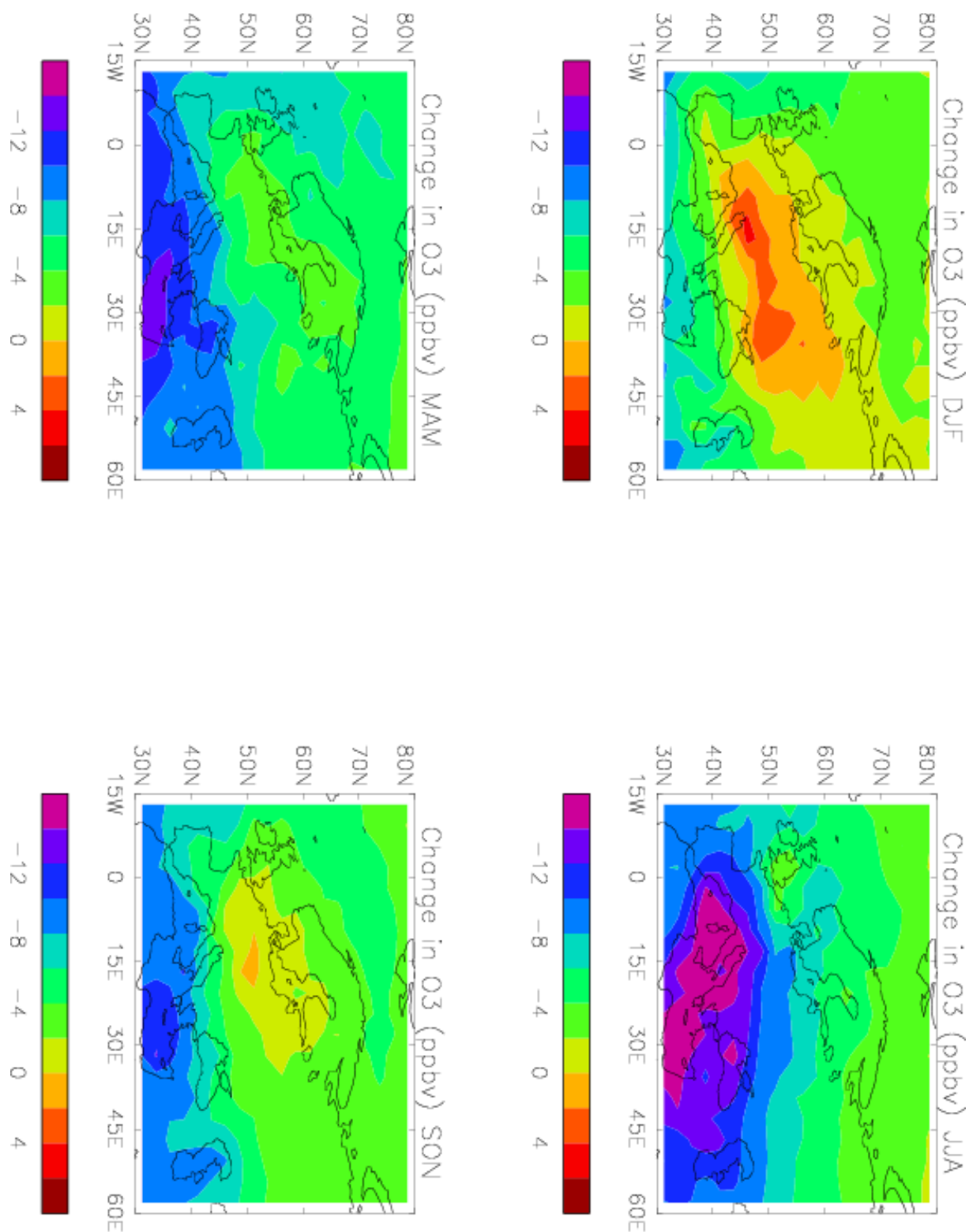


**Figure I-11.** Changes in seasonal mean surface ozone levels over Europe (ppb), from the addition of heterogeneous reactions. The seasons are winter (DJF), spring (MAM), summer (JJA) and autumn (SON). A positive value indicates that ozone levels are larger when the heterogeneous reactions are included.

It can be seen that, in the autumn and winter months, ozone levels over parts of central Europe are 2 – 4 ppb larger. In spring and summer, ozone values are always smaller when heterogeneous reactions are included, particularly over the Mediterranean area in summer, when substantial reductions are observed. These changes in ozone levels are likely to be due to changes in NO<sub>x</sub> levels. In summer, when insolation is at its greatest, photolysis of NO<sub>x</sub> leads to ozone production. Hence, reduction of NO<sub>x</sub> due to heterogeneous reactions leads to lower ozone levels.

In winter, when insolation is low, NO<sub>x</sub> is efficient at scavenging the oxidant radicals (OH and HO<sub>2</sub>), which are essential for catalysing ozone production. Hence heterogeneous NO<sub>x</sub> removal will increase ozone production. The heterogeneous HO<sub>2</sub> removal will always decrease ozone production rates, but will be more noticeable in winter. The regions of positive and negative change in winter (DJF) and summer (JJA) shown in Figure I-11 reflect the relative importance of the NO<sub>x</sub> and HO<sub>x</sub> removal.

### **(c) NAME**

#### **1) General description**

NAME is a Lagrangian dispersion model that simulates the movement of pollutants within the atmosphere in three dimensions and parameterises the key chemical and deposition processes occurring. Pollutant emissions are represented by releasing hundreds of thousands of air parcels, each able to represent the released mass of many different species. There are numerous applications of the NAME model including emergency response to, for example, nuclear incidents, volcanic eruptions and airborne spread of foot and mouth disease. The NAME model is also used routinely to provide air quality forecasts and to investigate pollution episodes.

The NAME air parcels are carried passively by the three dimensional wind field obtained from the Met Office's Numerical Weather Prediction (NWP) model (Cullen, 1993). Local turbulent motion is simulated using a random walk technique which requires a diffusion coefficient which is calculated from the local turbulent velocity variance and the Lagrangian timescale. Above the boundary layer these two quantities are fixed, but within the boundary layer they are defined in terms of the local atmospheric stability and local surface quantities. A detailed description can be found in Ryall and Maryon (1998). Wind and temperature data from the NWP model is also used to calculate boundary layer height in the model, using a

combination of Richardson number and parcel techniques (Ryall and Maryon, 1998). The model dry deposition scheme is based on a resistance analogy parameterisation to calculate a species dependent deposition velocity. It is applied to all air parcels within the boundary layer. The wet deposition method uses scavenging coefficients to model washout and rainout of pollutants.

In order to calculate loss terms for primary species and production terms for secondary species due to the chemical reactions occurring, it is necessary to calculate species concentrations from the masses carried by the air parcels. This is done by effectively constructing a three-dimensional grid over the model domain, and adding up the contributions to the mass of each species from the air parcels within that grid box, from which a concentration can then be calculated. Concentrations of background species, i.e. those species not directly released into the atmosphere, but that are globally present, are also held on this three-dimensional grid, and all the species concentrations are then passed to the chemistry module. After the chemistry has taken place, the new concentrations of the species and products carried on the air parcels must be converted back to masses and re-assigned back to the air parcels. By using the information about the plume of air parcels before the chemistry occurred, it is possible to allocate production and loss terms in proportion with the original amount of primary species carried in the parcel. This method reduces the artificial diffusion of a species within the chemistry grid box.

## 2) The Chemistry Scheme: Treatment of Radicals

The chemistry scheme was originally developed to model sulphate aerosol (Malcolm et al., 2000), releasing primary emissions of sulphur dioxide ( $\text{SO}_2$ ), nitric oxide (NO) and ammonia ( $\text{NH}_3$ ). The scheme was subsequently revised to improve the parameterisation of wintertime sulphate aerosol (Derwent and Malcolm, 2000) and to include nitrate aerosol chemistry (Redington and Derwent, 2002). The current chemistry scheme, used for this study, has undergone further development to include the release of primary emissions of carbon monoxide (CO), formaldehyde (HCHO), ethene ( $\text{C}_2\text{H}_4$ ), propene ( $\text{C}_3\text{H}_6$ ), isoprene ( $\text{C}_5\text{H}_8$ ), o-xylene ( $\text{C}_6\text{H}_4(\text{CH}_3)_2$ ), and toluene ( $\text{C}_6\text{H}_5\text{CH}_3$ ). The emissions from the volatile organic compounds (VOC's) are then scaled in the model in order to represent the released mass of the full VOC emission inventory.

The primary emissions are released on model particles. Secondary species produced in the chemistry scheme are also carried on the model particles. At the end of the chemistry timestep the mass of the secondary products are distributed amongst model particles carrying the appropriate primary species in proportion with the original amount of that primary species. The inclusion of these additional primary species and their associated chemistry has resulted in the addition of nearly a hundred extra chemical reactions. The gas and aqueous phase reactions are now the same as in STOCHEM (section I(a)).

As a result of these additional reactions, a key difference between the current chemistry scheme and that described in Redington and Derwent (2002) is that free radicals hydroxyl (OH) and hydroperoxy (HO<sub>2</sub>) are now modelled explicitly within NAME and are no longer read in from background fields. Ozone (O<sub>3</sub>) and hydrogen peroxide (H<sub>2</sub>O<sub>2</sub>) are also now calculated within the model, being initialised at the start of a model run using values taken from background fields provided by the STOCHEM model as previously described. It should be noted that ozone and hydrogen peroxide, along with other photo-oxidants, are still treated within the model as static three-dimensional fields in that they are not advected by the three-dimensional wind field as the species carried on model air parcels are. That is the concentrations vary with the local chemistry, but are not then spread downwind. This is a good approximation for short lived species such as OH and HO<sub>2</sub> but is less suitable for species with longer atmospheric lifetimes such as O<sub>3</sub> and H<sub>2</sub>O<sub>2</sub>. The ability to advect these background species was a key aim for the model development under this contract, and progress to this end is detailed in Chapter V section (d). The NAME modelling carried in under Chapter V section (b) was done using the model as described above.

The same ammonium nitrate aerosol formation scheme used in STOCHEM has been implemented in NAME. The formation of coarse mode aerosol nitrate is parameterised by the reaction of N<sub>2</sub>O<sub>5</sub> and nitric acid with natural dusts and sea salt and is described using a first order rate coefficient following the approach used in the European Monitoring and Evaluation Programme (EMEP) model (EMEP, 1998b).

The aqueous phase oxidation of sulphur dioxide by hydrogen peroxide and ozone makes an important contribution to the formation of sulphate aerosol. Aqueous phase chemistry is carried out if there is a non-zero cloud fraction and there is cloud water present. At the end of the time step it is assumed that the cloud has evaporated leaving particulate aerosol. This

would be automatically dissolved again at the start of the next chemistry time step if the cloud were still present. The mechanism used in the NAME model is based on that used in STOCHEM.

## **Chapter II. Scenario Assessment and Policy Support**

### **(a) UN ECE and CAFE – Role of Long Range Transport and Scenario Assessment**

#### 1. Background

##### (i) Policy Relevance

Air pollution has been a recognised problem since the 1970s, and various pieces of legislation have been implemented to improve air quality. In the last few years, Directive 2001/81/EC of the European Parliament and the Council on National Emission Ceilings (NECs) for certain pollutants has set upper limits on the emissions of the four pollutants responsible for acidification, eutrophication and ground-level ozone pollution (SO<sub>2</sub>, NO<sub>x</sub>, VOCs and ammonia) to be achieved by 2010. Each Member State has its own target, and the Directive leaves it largely to the Member States to decide which measures to take in order to comply. The pollutants concerned are transported in large quantities across national and international boundaries; consequently, it would be very difficult for individual Member States to meet the objectives within their territory by national action alone. Under the Clean Air for Europe (CAFE) programme, the NEC Directive will be revised to ensure that emissions of the four pollutants given above are consistent with interim objectives for 2020, which propose further reductions in emissions, particularly for NO<sub>x</sub> and VOCs.

Parallel to the development of the EU NEC Directive, the EU Member States together with Central and Eastern European countries, the United States and Canada have negotiated a multi-pollutant protocol under the Convention on Long-Range Transboundary Air Pollution. This piece of legislation is the Protocol to Abate Acidification, Eutrophication and Ground-level Ozone, and is also known as the Gothenburg Protocol, which was agreed in November 1999, and entered into force on the 17th May 2005. The Gothenburg Protocol sets emission ceilings for 2010 for the same four pollutants (SO<sub>2</sub>, NO<sub>x</sub>, VOCs and ammonia). Once the Protocol has been fully implemented, emissions from Europe should be significantly smaller. Specifically, emissions of sulphur should be cut by at least 63%, NO<sub>x</sub> emissions by 41%, VOC emissions by 40% and ammonia emissions by 17%, compared to 1990 values. The emission ceilings in the Gothenburg Protocol are equal to or less ambitious than those set out in the NEC Directive. An important element of the review of the Gothenburg protocol is the better understanding of the role of transport of air pollution on the hemispheric scale.

One role of the NEC Directive was to reduce the deposition of eutrophying compounds to soils, such that the area with a deposition of excess nitrogen will be 30% smaller in 2010 than in 1990. However, with these emissions reductions, the extent of any external influences on Europe's air quality becomes potentially a more important issue for policy-makers. By external influences, we mean any source of air pollution that either does not come under the policy control of the UN ECE or EU or emanates from a geographical region beyond the scope of the UN ECE and EU, but nevertheless contributes to the exceedance of critical loads for acidification and eutrophication, and of critical levels for ozone. The following sources potentially come into this category:

- sulphur and nitrogen deposition from shipping
- ozone from shipping
- global background ozone

The emission scenarios used are discussed further in section 1(iii) below. The potential changes in acidification and eutrophication of soils are described in part (b), which includes a comparison of the different emission scenarios with the emissions totals of the NEC Directive, and the changes in the deposition fluxes of nitrogen-containing compounds.

#### (ii) Role of Long Range Transport

The uniqueness of the STOCHEM Lagrangian transport scheme enables us to follow air parcels as they are advected around the globe. We have used this to identify the sources of ozone arriving at Mace Head, and to understand the rate of processing of the ozone as the air travels over the Atlantic. For this study, the fluxes for the various production and loss reactions contributing to the budget of ozone are recorded for all the air parcels passing over Mace Head. As an example, the data for one of these parcels is shown in Figure II-1. On the 24<sup>th</sup> February the parcel descends into the boundary layer over the US and picks up a pulse of NO<sub>x</sub> (~2 ppb), as well as dry depositing ozone to the surface. On this day there is large ozone production (mostly HO<sub>2</sub> + NO) but a larger destruction (mostly dry deposition). On the 25<sup>th</sup> the parcel leaves the boundary layer, so no longer dry deposits and the large production term gives a large increase in ozone. Over the next six days there is still sufficient NO<sub>x</sub> available that ozone production (HO<sub>2</sub> + NO<sub>2</sub>) and destruction (O(<sup>1</sup>D) + H<sub>2</sub>O and O<sub>3</sub> + HO<sub>x</sub>) are more or less in balance. The change in ozone due to mixing with other air parcels is shown in the

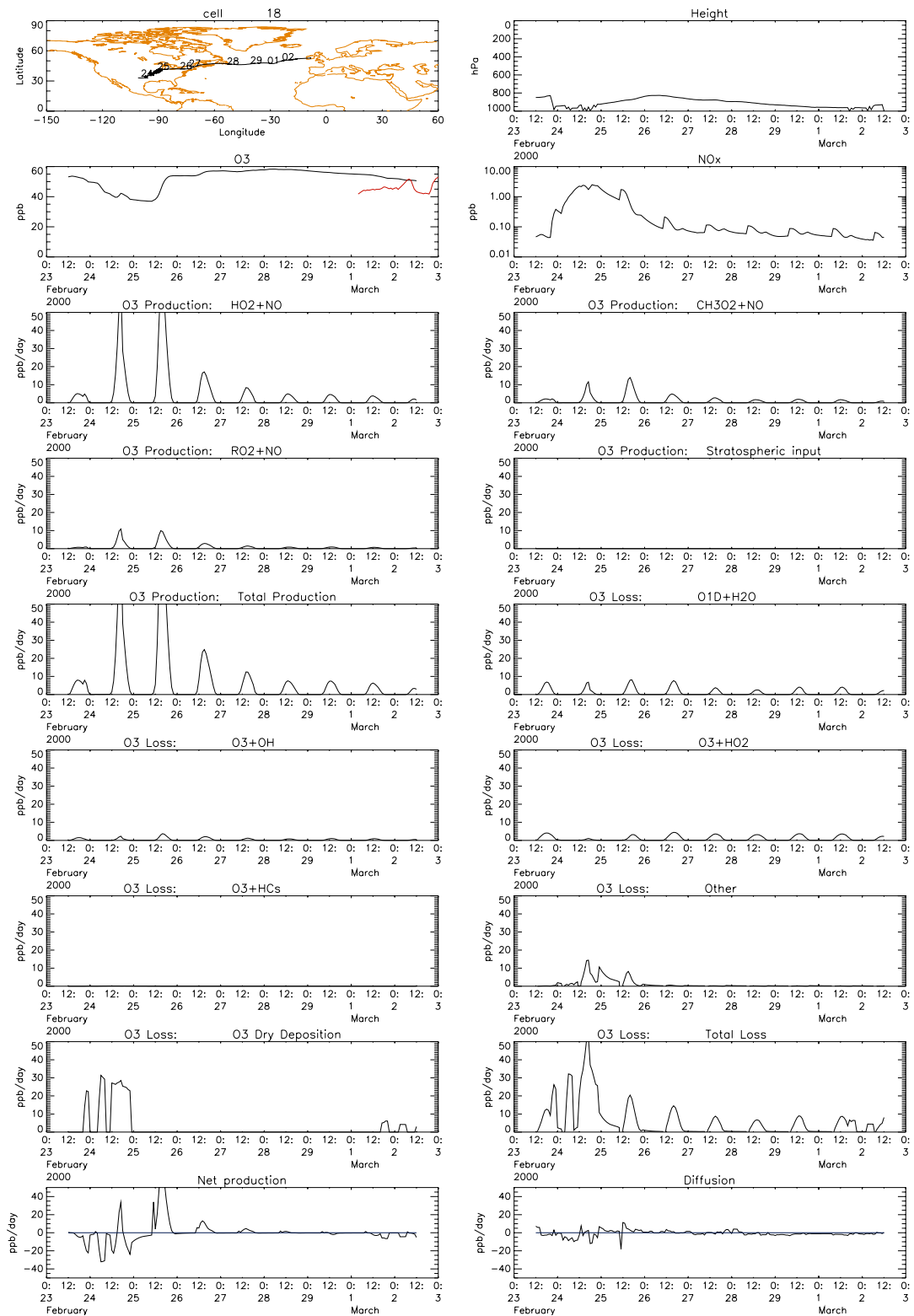


**Figure II-1.** Example of individual ozone budget terms for an air parcel as it travels from the USA and across the Atlantic Ocean to Mace Head, Ireland.

panel labeled “Diffusion” (bottom right of Figure II-1). This causes the ozone to decrease across the Atlantic. The parcel finally reaches the boundary layer over Mace Head on 2<sup>nd</sup>

March. The measured ozone for a day either side of the parcel arrival is shown in red in the plot labeled O<sub>3</sub>. This shows an ozone peak around the arrival time.

The trans-Atlantic parcel following experiments outlined above have been further developed. The model was run for one year using 100,000 air parcels, and the climate model's winds are continually nudged towards ECMWF analyses for the year 2000. 1202 air parcels passed within 1° solid angle of Mace Head in the boundary layer. Of those 81 had come from the North American boundary layer in the previous 20 days. These represent direct pollution from North America. All the 81 parcels crossed the Atlantic in the lower troposphere below 600 hPa. An example of a trajectory is shown in Figure II-2.

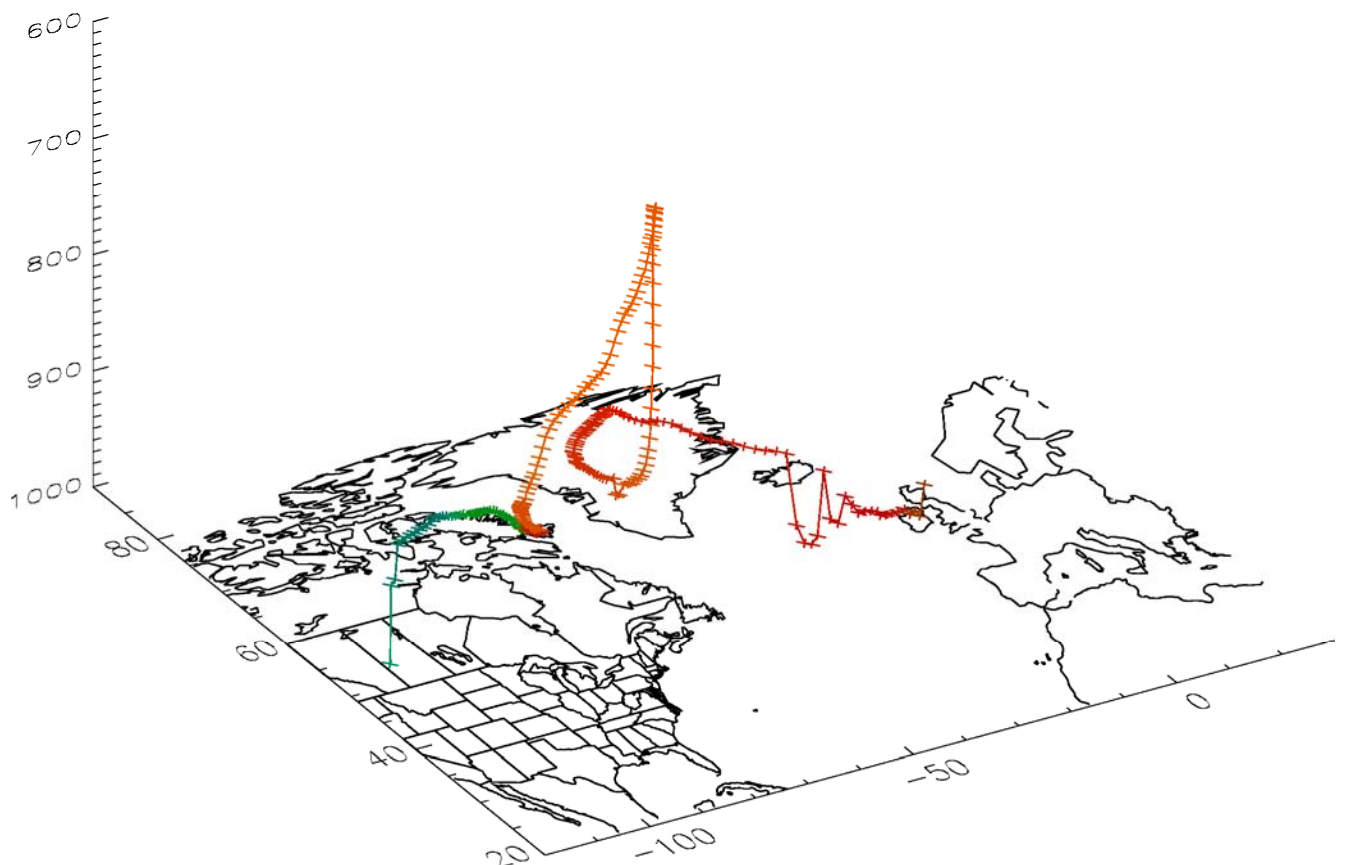


**Figure II-2.** Parcel trajectory coloured by ozone level. Blue: 25 ppb, Green 30 ppb, Red 35 ppb, and Orange 40 ppb.

The fact that the air parcels remained in the lower troposphere might seem to contradict studies such as Stohl and Trickl (1999), which have shown there is significant transport to Europe in the upper troposphere. This happens when polluted boundary layer air in the western Atlantic is lifted up over a frontal system in a warm conveyor belt and transported rapidly at high altitudes to Europe. However, the polluted air has generally been observed in the free troposphere using lidar measurements, not at the surface. The warm conveyor belt does eventually bring this pollution down to the surface, but this process tends to happen over central and Eastern Europe, not over the British Isles. This has a significant impact on the amount of ozone reaching the British Isles from America.

### (iii) Emission Scenarios

In previous studies with STOCHEM, we have pointed out the importance of the coupling between the regional and global scale distributions of tropospheric ozone. The rising global or hemispheric baseline concentrations of ozone will act to offset some of the ozone air quality improvements brought about by regional scale pollution control measures. We have shown how the hemispheric ozone baseline concentrations in Europe arise from intercontinental contributions from North America and Asia. All of these conclusions depend on the adequacy and completeness of the emission inventories employed. Furthermore, where the conclusions address the future situation, additional uncertainties come into play from the choice of the underlying emission scenario. Much of this earlier work has been based on the IPCC SRES emission scenarios (Nakićenović et al., 2000).

IIASA has developed an entirely new set of global emission inventories for the man-made sources of SO<sub>2</sub>, NO<sub>x</sub>, CO, CH<sub>4</sub> and VOCs for each year from 1990 through to 2030. The global inventories are spatially disaggregated at 1° x 1° resolution and have been constructed from separate spatially-gridded inventories for up to 12 different emission source categories, including road transport, power stations and so on. Two distinct scenarios have been developed and are termed CLE and MFR. The former (Current LEGislation) assumes current legislative plans are implemented fully, and the latter (Maximum Feasible Reductions) assumes that the maximum feasible emission reductions are applied. The CLE and MFR scenarios may be thought of as “likely” and “optimistic”, respectively. The IPCC SRES A2 scenario has also been used, and may be thought of as a “pessimistic” view of the future. As an example, the time development of global anthropogenic NO<sub>x</sub> emissions in the CLE and MFR scenarios in the major northern hemisphere continents are illustrated in Figure II-3.

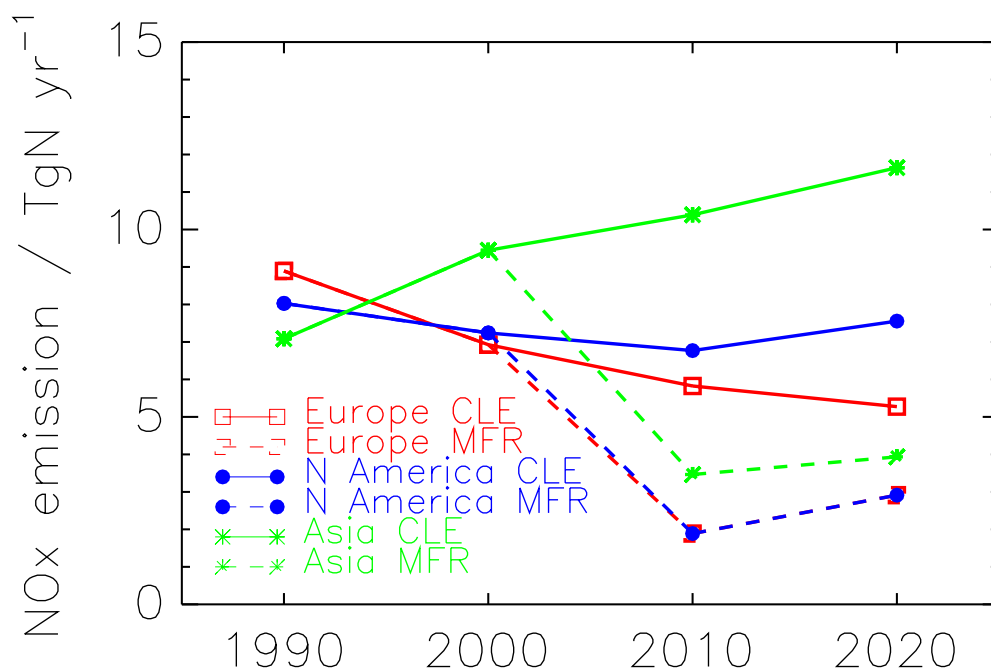


**Figure II-3.** Anthropogenic NO<sub>x</sub> emissions from three different continents in the two IIASA scenarios CLE and MFR, over the period 1990 through to 2020.

## 2. Ozone, Methane and Carbon Monoxide under the IIASA scenarios

### (i) Introduction

In this section, modelled levels of ozone, methane and carbon monoxide over Europe using the IIASA scenarios for the period 1990 – 2030 will be presented and discussed, although the bulk of the work focuses on ozone levels. Ozone measurements at Mace Head, Ireland, began during 1987 and have continued through to the present day. The hourly ozone observations have been sorted by air mass origins to derive a set of monthly mean ozone concentrations for air masses arriving at Mace Head that have passed over the North Atlantic Ocean only. By definition, these air masses represent an external influence on Europe’s air quality. The mean ozone concentrations in these air masses characterise the ozone background for the British Isles and for much of North West Europe. A trend analysis of these mean ozone concentrations in background air masses has revealed a statistically significant upwards trend of +0.47 ppb yr<sup>-1</sup> over the period from 1987 through to 2002.

## (ii) Present and Future Ozone Levels over Europe

Since a rising ozone background can ultimately work against the reduction in peak ozone levels due to European regional pollution controls, it is an important issue to understand the extent to which these background ozone trends may continue in the future. Future ozone levels over Europe over the period from 1990 to 2030 have been investigated with the global Lagrangian model STOCHEM using the three scenarios described earlier,

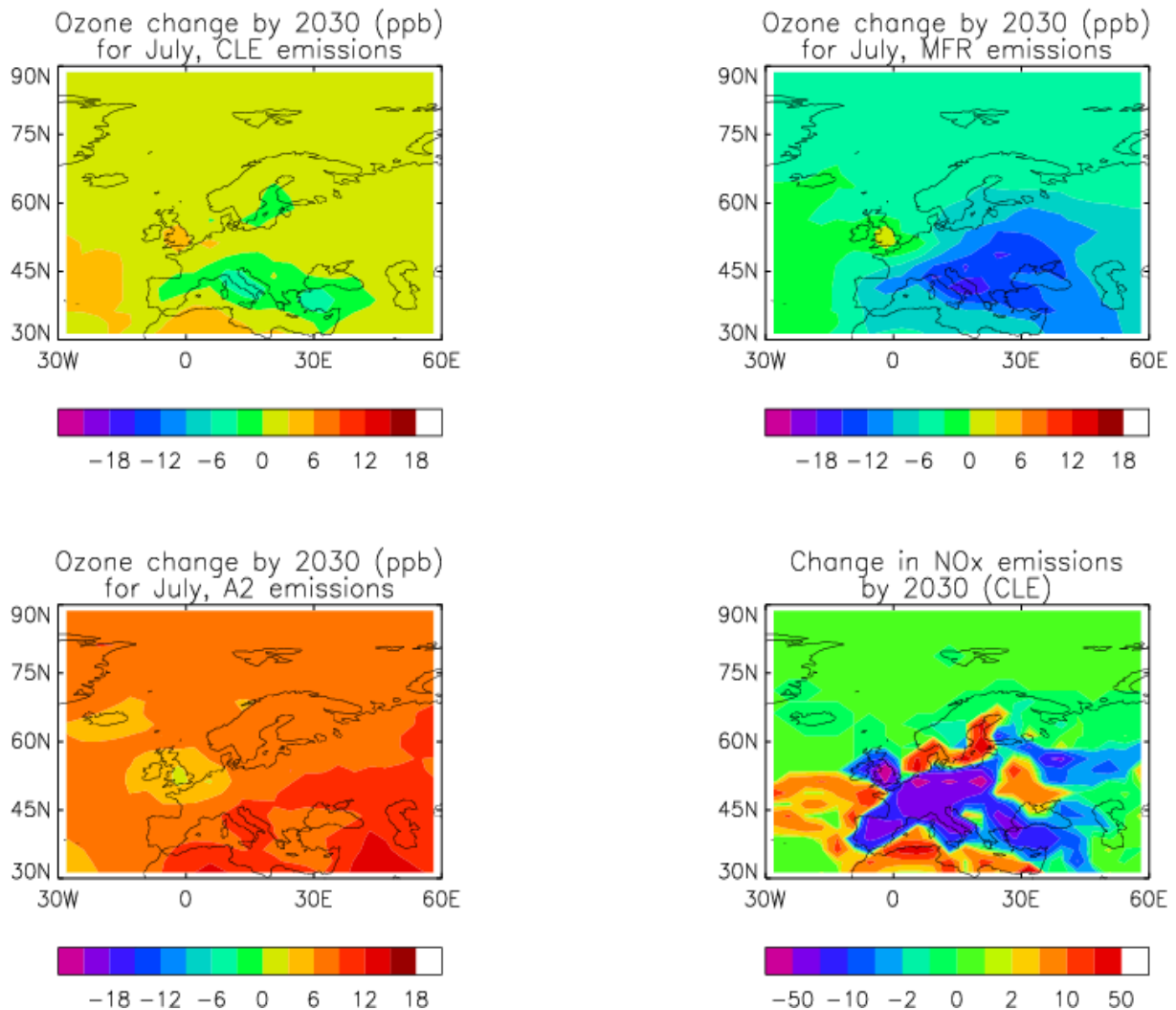
- IPCC SRES scenario A2
- IIASA CLE
- IIASA MFR

Figure II-4 shows the impact on European surface ozone concentrations of predicted changes in emissions between 2000 and 2030 according to the scenarios CLE and MFR from IIASA, and the SRES A2 scenario. In this case, STOCHEM was integrated for six years with the same emissions, and the results shown in Figure II-4 are the differences between the five year mean surface ozone values predicted for 2030 and 2000.

European ozone precursor emissions such as  $\text{NO}_x$  are predicted to fall in both IIASA scenarios (lower right picture in Figure II-4). Larger decreases are predicted in the MFR scenario than in the CLE scenario. Across the rest of the world, American sources decrease in CLE whereas Asian sources increase. In the MFR scenario all sources decrease (see Figure II-3 for a summary). The predicted ozone levels follow the emissions with decreases of up to 4 ppb in the CLE scenario, and up to 14 ppb in MFR. This dramatic decrease in MFR is due not only to the local emission cuts over Europe, but also to the influence of Asian sources which increase in CLE but decrease in MFR. The SRES A2 scenario is much more pessimistic. It assumes that emissions will continue to rise in all regions, ignoring any legislative changes. Hence the European ozone concentrations increase by up to 8 ppb in this scenario. The A2 scenario was developed based on figures for 1990. Its predictions for 2000 European emissions have already been shown to be too large.

Clearly, future ozone levels in Europe are highly scenario dependent, and increase in the IPCC SRES A2 and IIASA CLE scenarios, but decrease in the IIASA MRF scenario. These

changes in sign and magnitude of the ozone trend reflect the different relative trends in precursor emissions in the major continents of North America, Europe and Asia.



**Figure II-4.** The predicted change in ozone from 2000 to 2030 due to emissions changes according to three scenarios. Also shown is the change in NO<sub>x</sub> emissions from 2000 to 2030 in the CLE scenario.

(iii) Methane, carbon monoxide and ozone at Mace Head for the period 1990-2030

The time development of the baseline concentrations of methane, carbon monoxide and ozone at Mace Head, Ireland over the period from 1990 through to 2030 have been studied using a combination of observations from the University of Bristol, and STOCHEM model calculations using the emission scenarios from the IPCC and IIASA described earlier. With the range of emission scenarios for man-made ozone precursor emission sources available, a wide range of model trends were predicted for the period up to 2030. The time development of methane, carbon monoxide and ozone in the various model experiments, and the

observations for the period 1990-2003, are illustrated in Figure II-5. Two model runs were performed using each of the CLE and A2 scenarios to investigate the effect of climate change. One of these runs used meteorology generated using fixed levels of carbon dioxide (marked “CLE” and “A2”), and the second used meteorology generated with increasing levels of carbon dioxide (marked “CLE-cc” and “A2-CLE”). A comparison of the two runs for each scenario will illustrate the effect of climate change on the model results. A third run using the CLE scenario and observed sea-surface temperatures (SSTs), marked as “CLE-sst”, was also performed.

The observed growth in methane levels is predicted well by the model when the CLE-cc scenario is used. Methane levels tend to be overpredicted when the other scenarios are used, particularly for the CLE scenario. Interestingly, the effect of climate change is negligible before the year 2020 when the A2 scenario is used. The use of real SSTs has not changed the predicted methane levels under the CLE scenario; the methane levels predicted by the two runs “CLE” and “CLE-sst” are essentially identical.

The model does not reproduce the observed levels or interannual variability in the carbon monoxide levels. This result suggests that emissions of carbon monoxide, or precursor gases, are too small, or the oxidation of the precursor gases does not produce sufficient carbon monoxide. In the IIASA scenarios, the model results show little interannual variability, and falling levels of carbon monoxide with time. In the A2 scenarios, the carbon monoxide levels rise over the modelled time period. Climate change has little effect in both cases.

The modelled ozone levels generally surround the observations, although no one scenario reproduces the observations exactly. Results using the IIASA scenarios show a weak upward trend (except the CLE-sst scenario which has almost no trend), whereas the SRES scenarios have produced a stronger upward trend. Once again, the effect of climate change is more marked when the CLE scenario is used than when the A2 scenario is used. In the former case, ozone levels are 1 – 2 ppb smaller when climate change effects are included, but there is no real change in the latter case.

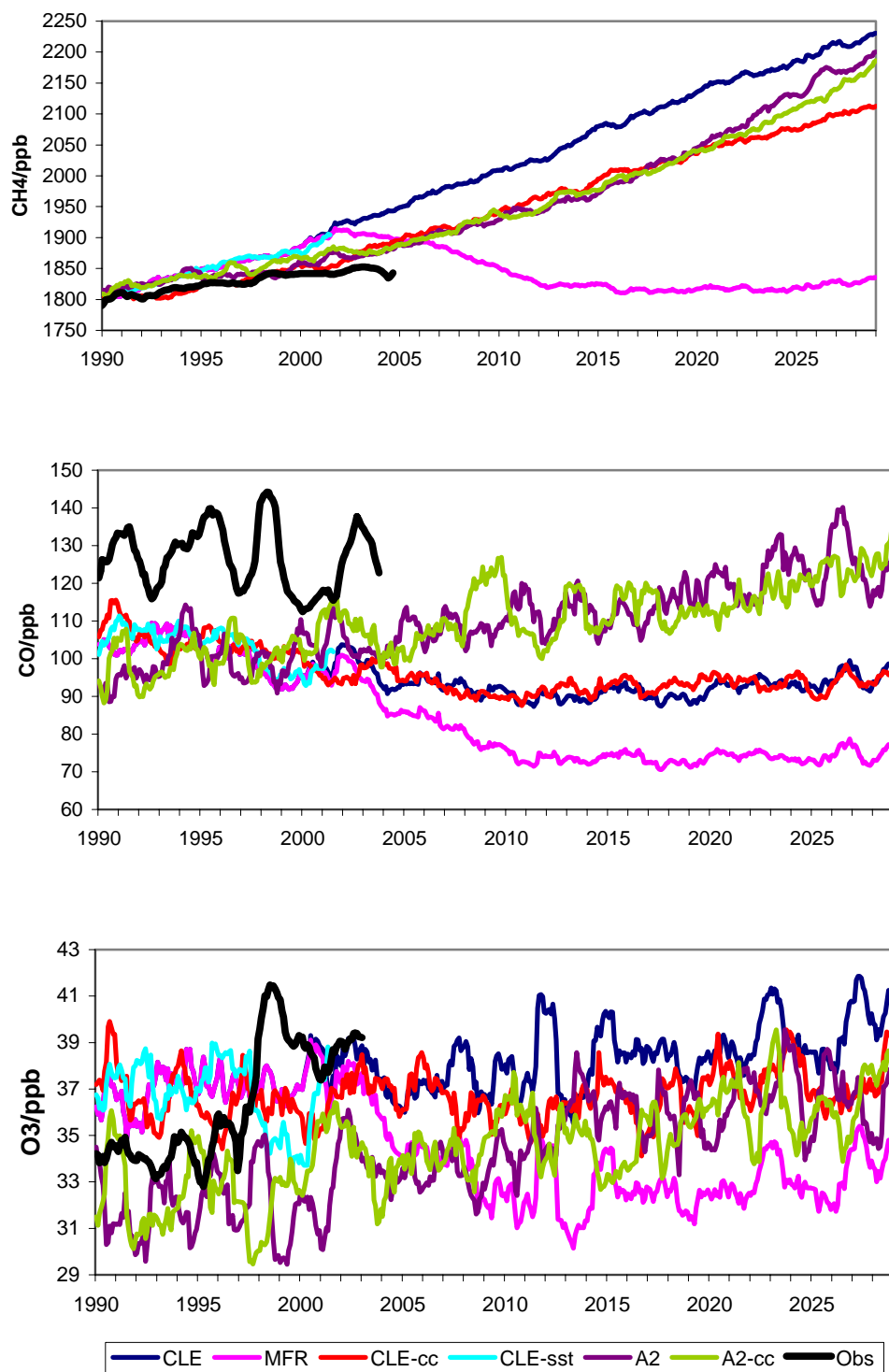


**Figure II-5.** 12-month running mean of observed (1990-2003) and modelled (1990-2030) mixing ratios for CH<sub>4</sub> (upper panel), CO (middle panel), and O<sub>3</sub> (lower panel) at Mace Head. In all cases, the observations are shown by the thick black line.

To summarise, in the scenario based on current planned air pollution controls (IIASA CLE), methane shows a strong upward trend, ozone shows a weaker upward trend, and carbon

monoxide is approximately flat in baseline air masses. In one of the more pessimistic IPCC SRES scenarios, A2, all three gases show future increases. However, in the scenario based on maximum feasible emission reductions, (MFR), all three trace gases decline. By 2030, projected climate change reduces the growth in CH<sub>4</sub>, but has insignificant effects on baseline CO and O<sub>3</sub> in these simulations. Global or hemispheric ozone precursor emissions and their controls exert a potentially large external influence on Europe's air quality. This influence is currently not taken into account in future European air quality policy formulation. This study of the trends in baseline methane, CO and ozone at Mace Head is designed to be used in the Unified EMEP modelling studies by assisting with the development of future ozone scenarios over Europe up to the year 2030.

### 3. Impacts of NO<sub>x</sub> emission changes

#### (i) Introduction

Emissions of nitrogen oxides (NO<sub>x</sub>) from human activities, together with those of methane (CH<sub>4</sub>), carbon monoxide (CO) and volatile organic compounds (VOCs), take part in controlling the oxidizing capacity of the troposphere and hence the atmospheric lifetime of methane and its global-scale build-up. The growth in NO<sub>x</sub> emissions from human activities since pre-industrial times has also brought about a global-scale increase in the tropospheric ozone burden. Because tropospheric ozone is a radiatively-active trace gas, this increase since pre-industrial times is associated with a positive radiative forcing of climate which is separate from that due to methane. The Intergovernmental Panel on Climate Change (IPCC) report that, considering only trace gases, the radiative forcings due to methane and tropospheric ozone are the second and third most important after carbon dioxide. Despite the magnitude of these radiative forcings, NO<sub>x</sub> emissions and tropospheric ozone precursor gases have, in general, not been included in the basket of trace gases within the Kyoto Protocol to the United Nations Framework Convention on Climate Change.

Policy actions on climate change need to take into account the relative magnitudes and timescales of the many radiative forcing agents, such as CO<sub>2</sub>, CH<sub>4</sub> and O<sub>3</sub>, and processes, such as land-use change and global aviation. A range of different climate change metrics have been proposed but here, attention will be given to two metrics in particular: radiative forcing (RF) and global warming potential (GWP). RF is an instantaneous property of the atmosphere and has been extensively defined, reviewed and utilised by the IPCC (IPCC, 1990). It quantifies the impact on the transmission of radiation through the atmosphere due to

changes in the trace gas distributions since pre-industrial times, but takes no account of how long such changes will persist in the absence of the human activities that are driving them. The GWP concept has also been reviewed and promulgated by the IPCC. This concept is built around the time-weighted radiative forcing of a trace gas, following the emission of a pulse of that trace gas, expressed relative to the behaviour of a corresponding pulse of CO<sub>2</sub>. Both radiative forcing and atmospheric persistence are therefore merged into a single index.

There are many questions concerning the wisdom of combining all the biogeochemical properties of the trace gases into a single climate change metric (Fuglestedt et al., 2003, and references therein). There are questions concerning the relationship between radiative forcing and climate response and whether the same climate sensitivity parameter is appropriate for all trace gases and radiative forcing agents (Hansen et al., 1997; Joshi et al., 2003). There are also proposals for different indices based on climate responses such as global temperature (Shine et al. 2003). Here, the concern is that there is no simple robust relationship between trace gas emission and radiative forcing for some radiative forcing agents, particularly tropospheric ozone precursors, and this contributes further to uncertainty and hesitancy on the part of policymakers.

The emission of an instantaneous pulse of a short-lived trace gas, such as NO<sub>x</sub>, causes an immediate and localized change in the oxidizing capacity of the troposphere and induces perturbations in the distributions of CH<sub>4</sub> and O<sub>3</sub>. These perturbations persist long after the pulse of NO<sub>x</sub> has decayed away. The perturbations are dispersed and advected and may become well-mixed on the hemispheric and global scales, at least for CH<sub>4</sub>. The CH<sub>4</sub> perturbation decays away with an adjustment time constant, which lies within the range 10 – 15 years (IPCC, 2001), and hence is significantly longer than the atmospheric lifetime. Short-lived trace gases indirectly cause radiative forcing responses that are global in character and persist over decadal time-scales. The difficulty is that the magnitudes of the CH<sub>4</sub> and O<sub>3</sub> responses appear to depend on where and when the pulse of the short-lived trace gas was emitted (Berntsen et al., 2005). Emissions of NO<sub>x</sub> from aircraft in the upper troposphere and lower stratosphere have a much stronger effect on ozone than if the same amounts of NO<sub>x</sub> were emitted at the surface (Fuglestedt et al. 1996; IPCC, 1999). Fuglestedt et al. (1999) found a much higher sensitivity for upper tropospheric O<sub>3</sub> to reductions in NO<sub>x</sub> emissions from surface sources in Asia and Australia compared with North America and Europe.

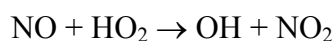
In previous studies, we have employed a chemistry-climate model to study the radiative forcings generated by aircraft NO<sub>x</sub> emissions (Stevenson et al., 2004) and surface sources of CO, NO<sub>x</sub> and CH<sub>4</sub> (Derwent et al., 2001) and VOCs (Collins et al., 2002). Here, a similar approach has been adopted to study the radiative forcings due to CH<sub>4</sub> and O<sub>3</sub> perturbations generated by surface NO<sub>x</sub> emissions. Attention has been given to the spatial variations in the emission and forcing relationships, and the mechanisms that drive them.

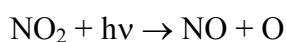
#### (ii) Radiative Forcing from Surface NO<sub>x</sub> Emissions

The transient behaviour of CH<sub>4</sub> and O<sub>3</sub> in response to emission pulses of NO<sub>x</sub> were investigated using the Lagrangian CTM model STOCHEM. Each model run was initialised using the same set of trace gas mixing ratios on 1<sup>st</sup> October 1997 and integrated using analysed wind fields to run through to 1<sup>st</sup> January 1998. At that point, two model experiments were initiated. The first model experiment, the base case, continued on from the previous run without change until 31<sup>st</sup> December 1998. In the second model experiment, the transient case, the NO<sub>x</sub> emission source was increased so that a pulse containing an additional 2 Tg NO<sub>x</sub> as N was emitted at a constant rate up to the 31<sup>st</sup> January 1998. At this point, the NO<sub>x</sub> emissions were reset to the base case value and the model experiment was continued until 31<sup>st</sup> December 1998. The impacts of the pulse of NO<sub>x</sub> on the composition of the model troposphere were followed by taking differences between the base and transient cases. Increases in mixing ratio between the two model experiments were termed ‘excess’ mixing ratios and decreases, ‘deficits’.

In the first set of transient experiments, the emission pulses were applied during January 1998 using a constant emission flux over an area of 80° longitude by 40° latitude centred on each of North America, Europe and Asia. The size of the emission pulse was completely arbitrary and was chosen to be small enough so that the model responses were in their linear range, yet large enough to bring about discernible changes in mixing ratios.

In response to the NO<sub>x</sub> emission pulses, systematic differences were found in trace gas mixing ratios between the two model experiments. An immediate increase was observed in the OH and O<sub>3</sub> mixing ratios through the following reactions (hν denotes photolysis):





These excess OH and O<sub>3</sub> mixing ratios built up in the regions where the NO<sub>x</sub> emission densities had been perturbed and the areas immediately downwind of them. The increased OH mixing ratios in the transient case led to increased OH + CH<sub>4</sub> reaction fluxes and ultimately to decreased CH<sub>4</sub> mixing ratios. The deficit in the CH<sub>4</sub> mixing ratios steadily built up and stabilized both in magnitude and spatial distribution during the first 4-6 months and then began to decay away steadily during the rest of the year. In previous studies (Derwent et al., 2004), we have shown that CH<sub>4</sub> excesses and deficits decay away with a time constant of between 10 and 15 years, the CH<sub>4</sub> perturbation time constant. Excess O<sub>3</sub> mixing ratios reached a peak during January and February, then decayed away rapidly during March and April. This peak is the short-term positive ozone perturbation. The decay in ozone mixing ratios continued during May and June, taking the excess ozone below zero, producing an ozone deficit in the transient case. This deficit stabilized during the remainder of the first year and began decaying away slowly. It was associated strongly with the CH<sub>4</sub> deficit. It was found that this CH<sub>4</sub>-driven O<sub>3</sub> deficit decayed away with the same 10 – 15 year time constant as the CH<sub>4</sub> deficit. This deficit is the long-term negative ozone perturbation.

Time-integrated perturbations to the global burdens of CH<sub>4</sub> and O<sub>3</sub>, both short-term positive and long-term negative, were calculated from the differences in the respective burdens between the transient and base case model experiments. Two contributions were required for this: the first was estimated from the model results in the first year; the second was obtained by extrapolating the model results from the end of December 1998 onwards using the methane adjustment time. In all cases, a CH<sub>4</sub> adjustment time constant of 11.5 years from previous studies (Stevenson et al., 2004) was used. It should be noted that this adjustment time is longer than the methane lifetime. For the time-integrated perturbations to the CH<sub>4</sub> burdens, both contributions were negative and the second term dominated over the first by at least an order of magnitude. For the time-integrated perturbations to the O<sub>3</sub> burdens, the contributions were of opposite sign. The first term was positive, being dominated by the initial NO<sub>x</sub>-driven perturbation, and the second term was negative, being dominated by the CH<sub>4</sub>-driven O<sub>3</sub> perturbation. Although the magnitude of the CH<sub>4</sub>-driven perturbation was tiny compared with the initial NO<sub>x</sub>-driven, its persistence meant that it dominated on a time-

integrated basis. The methane perturbation changed the overall impact of NO<sub>x</sub> from an ozone source to an ozone sink over the long term.

The time-integrated perturbations in the global burdens of CH<sub>4</sub> and O<sub>3</sub> were then converted into time-integrated radiative forcings using the methodologies detailed in our previous work on aircraft NO<sub>x</sub> perturbations (Stevenson et al., 2004). Table II-1 presents the time-integrated radiative forcings due to the perturbations in the global burdens of CH<sub>4</sub> and O<sub>3</sub> following the emission of a NO<sub>x</sub> pulse in each of North America, Europe and Asia during January, normalized to a pulse of 1 Tg NO<sub>2</sub>. The radiative forcing perturbations spanned a factor about five for methane, with European NO<sub>x</sub> emissions showing the least response and Asian emissions, the greatest response. The short-lived positive ozone forcings spanned about a factor of two but the long-lived negative forcings covered a factor of close to 20. Taking the sum of all the three terms, the net radiative forcings from Asia, North American and European NO<sub>x</sub> emission pulses were -0.94, -0.46 and -0.06 mW m<sup>-2</sup> yr<sup>-1</sup>, respectively.

**Table II-1.** Time-integrated radiative forcings due to changes in the global burdens of methane and ozone in response to NO<sub>x</sub> emission pulses applied to different regions during January, normalized to 1 Tg NO<sub>2</sub>.

Geographical Region	Latitude range	Longitude range	Radiative forcing from CH <sub>4</sub> mW m <sup>-2</sup> yr <sup>-1</sup>	Radiative forcing from O <sub>3</sub> (short) mW m <sup>-2</sup> yr <sup>-1</sup>	Radiative forcing from O <sub>3</sub> (long) mW m <sup>-2</sup> yr <sup>-1</sup>
				Initial +ve	Long-lived -ve
Asia	0° - 40°N	60° - 140°E	-1.30	0.56	-0.21
N America	10° - 50°N	130° - 50°W	-0.83	0.49	-0.12
Europe	30° - 70°N	10°W - 70°E	-0.25	0.2	-0.01

### (iii) Radiative Forcing from Asian Surface NO<sub>x</sub> Emissions

In a second set of transient experiments, NO<sub>x</sub> emission pulses of 0.2 Tg NO<sub>x</sub> as N were applied during January 1998 as constant emission fluxes over areas of 10° longitude x 10° latitude centred on the main regions of Asia. Table II-2 shows the time-integrated perturbations in the global burdens of CH<sub>4</sub> and O<sub>3</sub> that resulted from the NO<sub>x</sub> emission pulses applied to the different Asian regions. CH<sub>4</sub> responses varied by a factor of about 7 across the

regions whereas O<sub>3</sub> responses varied by a factor of about 6 in the initial short-term positive and by a factor of 16 in the long-term negative phases. The net radiative forcing from all terms varied from -0.13 mW m<sup>-2</sup> yr<sup>-1</sup> for the NO<sub>x</sub> emission pulse emitted in Afghanistan to -2.01 mW m<sup>-2</sup> yr for that in Java and hence covered a factor 15 in range.

**Table II-2.** Time-integrated radiative forcings due to changes in the global burdens of methane and ozone in response to NO<sub>x</sub> emission pulses from different regions of Asia during January, normalized to 1 Tg NO<sub>2</sub>.

Geographical Region	Latitude range	Longitude range	Radiative forcing from CH <sub>4</sub> mW m <sup>-2</sup> yr <sup>-1</sup>	Radiative forcing from O <sub>3</sub> (short) mW m <sup>-2</sup> yr <sup>-1</sup> Initial +ve	Radiative forcing from O <sub>3</sub> (long) mW m <sup>-2</sup> yr <sup>-1</sup> Long-lived -ve
Afghanistan	30°-40°	60°-70°	-0.53	0.47	-0.08
Kashmir		70°-80°	-0.54	0.45	-0.07
China 1		80°-90°	-0.81	0.53	-0.13
China 2		90°-100°	-0.74	0.49	-0.11
China 3		100°-110°	-0.51	0.37	-0.06
China 4		110°-120°	-0.44	0.31	-0.04
Korea		120°-130°	-0.59	0.36	-0.07
Japan		130°-140°	-0.81	0.50	-0.12
Pakistan	20°-30°	60°-70°	-0.61	0.37	-0.07
India 2		70°-80°	-0.38	0.18	-0.03
India 1		80°-90°	-0.38	0.25	-0.03
Burma		90°-100°	-0.44	0.28	-0.04
China 5		100°-110°	-0.39	0.28	-0.03
China 6		110°-120°	-0.42	0.28	-0.04
India 3	10°-20°	70°-80°	-0.69	0.22	-0.09
Thailand 2		90°-100°	-0.72	0.21	-0.10
Thailand 1		100°-110°	-0.81	0.25	-0.14
Philippines		130°-140°	-1.1	0.40	-0.16
Malaysia	0°-10°	100°-110°	-1.81	0.89	-0.31
Borneo		110°-120°	-1.60	0.69	-0.26
Java	-10°-0°	100°-110°	-2.59	1.04	-0.47



the end of the experiment. As with the radiative forcing, the ozone response at Mace Head to the NO<sub>x</sub> emission pulse in Asia thus had two phases: an initial short-term positive phase representing increased ozone production from the additional NO<sub>x</sub>, followed by a long-term negative phase representing decreased ozone production driven by the decreased methane concentrations due to depletion by the NO<sub>x</sub> pulse.

Table II-3 presents the time-integrated initial short-term positive and the long-term negative ozone responses at Mace Head in ppb-months driven by 0.2 Tg NO<sub>x</sub> pulse emitted in January in the different regions of Asia. The time-integrated short-term ozone responses at Mace Head decrease markedly with latitude, from +0.6 ppb-months for pulses emitted in China to close to zero for those emitted in Java and Borneo. In contrast, the time-integrated long-term ozone responses are negative and somewhat smaller in absolute magnitude, but show a much reduced latitudinal variation. The result is that the total time-integrated ozone responses vary from about +0.5 to -0.2 ppb months across Asia, for 0.2 Tg NO<sub>x</sub> pulses emitted during January.

**Table II-3.** The time-integrated initial short-term positive and the long-term negative ozone responses at Mace Head in ppb-months driven by 0.2 Tg NO<sub>x</sub> pulse emitted in January in the different regions of Asia.

	Positive phase	Negative phase	Net		Positive phase	Negative phase	Net
Afghanistan	0.53	-0.11	0.42	India 3	0.03	-0.06	-0.03
Borneo	0.04	-0.14	-0.10	Japan	0.57	-0.13	0.44
Burma	0.24	-0.06	0.18	Java	0.01	-0.21	-0.20
China 1	0.61	-0.14	0.47	Kashmir	0.52	-0.10	0.42
China 2	0.59	-0.12	0.47	Korea	0.37	-0.08	0.29
China 3	0.45	-0.08	0.37	Malayasia	0.04	-0.16	-0.12
China 4	0.31	-0.05	0.26	Pakistan	0.24	-0.08	0.16
China 5	0.24	-0.05	0.19	Philippines	0.11	-0.11	0.00
China 6	0.20	-0.04	0.15	Thailand 1	0.10	-0.10	-0.00
India 1	0.19	-0.05	0.14	Thailand 2	0.03	-0.06	-0.03
India 2	0.10	-0.04	0.06				

This work has been extended to an analysis of 0.1 Tg NO<sub>x</sub> pulses emitted in 10° latitude × 10° longitude regions of North America during July, see Table II-4. The time-integrated ozone responses at Harwell, Oxfordshire, are presented on this occasion. Despite the smaller pulse sizes, the time-integrated initial short-term ozone responses are somewhat larger in the North American cases compared with the Asian cases. The long-term ozone responses are negative in sign and are comparable in absolute magnitude to those Asian cases. Hence, the same cancellation effects are seen in the total ozone responses at low latitudes.

**Table II-4.** The time-integrated initial short-term positive and the long-term negative ozone responses at Harwell, Oxfordshire, in ppb-months driven by 0.1 Tg NO<sub>x</sub> pulse emitted in July in the different regions of North America.

	Positive phase	Negative phase	Net		Positive Phase	Negative Phase	Net
Washington	0.18	-0.08	0.09	Colorado	0.15	-0.12	0.03
Idaho	0.32	-0.1	0.22	Kansas	0.13	-0.07	0.06
Montana	0.50	-0.10	0.39	Kentucky	0.23	-0.09	0.14
Minnesota	0.40	-0.10	0.31	Washington DC	0.34	-0.11	0.23
Ontario	0.74	-0.11	0.62	Mexico	0.03	-0.14	-0.11
Quebec	0.99	-0.12	0.87	Mexico	0.07	-0.21	-0.14
New Brunswick	1.23	-0.14	1.09	Texas	0.05	-0.14	-0.09
Newfoundland	1.25	-0.13	1.11	Mexico	0.05	-0.13	-0.08
California	0.06	-0.13	-0.07	Honduras	0.03	-0.36	-0.33
Nevada	0.16	-0.09	0.06				

Table II-5 shows how the initial short-term and long-term ozone responses to the 0.1 Tg NO<sub>x</sub> pulse emitted in the Quebec – New York square during July vary with location across Europe. It is clear that the initial short-term responses decrease markedly as the receptor location moves both northwards into Scandinavia and eastwards in central Europe. Since the variations across Europe in the long-term responses are less important, then the net responses also decrease both northwards and eastwards across Europe.

**Table II-5.** The time-integrated initial short-term positive and the long-term negative ozone responses at various locations across Europe in ppb-months driven by 0.1 Tg NO<sub>x</sub> pulse emitted in July in the Quebec-New York region.

	Positive phase	Negative phase	Net		Positive phase	Negative phase	Net
Mace Head	0.88	-0.13	0.75	K-Pusztta	0.36	-0.12	0.23
Illmitz	0.41	-0.13	0.28	Montelibretti	0.28	-0.15	0.13
Taenikon	0.53	-0.12	0.41	Preila	0.69	-0.09	0.60
Kosetice	0.56	-0.12	0.44	Kollumerwaard	0.74	-0.11	0.63
Waldhof	0.70	-0.11	0.59	Birkenes	0.76	-0.10	0.66
Frederiksborg	0.62	-0.09	0.53	Jarczew	0.65	-0.10	0.54
Lahemaa	0.78	-0.07	0.71	Monte Vehlo	0.71	-0.15	0.56
Tortosa	0.58	-0.14	0.44	Aspreveten	0.68	-0.09	0.59
Virolahti	0.62	-0.07	0.56	Iskrba	0.36	-0.13	0.23
Revin	0.76	-0.12	0.64	Starina	0.37	-0.12	0.26
Harwell	0.99	-0.12	0.88				

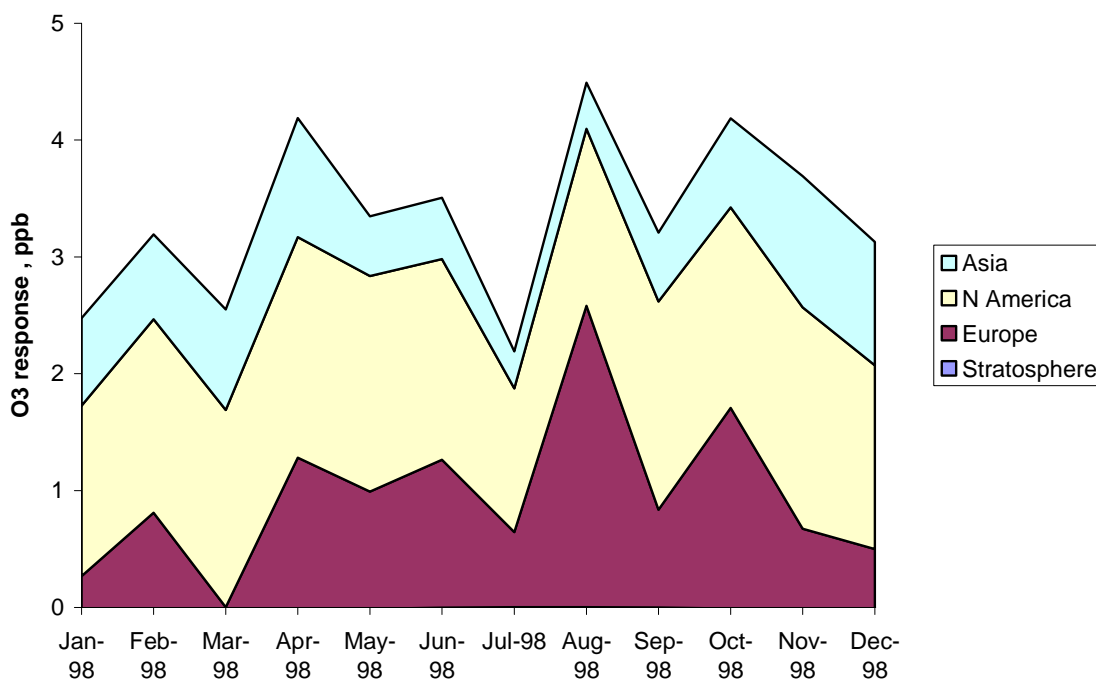


**Figure II-7.** The impact of a 50% reduction in global man-made NO<sub>x</sub> emissions from the different continents on the mean surface ozone level over Europe. The ozone response is the reduction in modelled ozone levels when the NO<sub>x</sub> emissions are reduced. The stratospheric contribution is negligible in all cases.

Additional model experiments have been performed with STOCHEM to study the intercontinental attribution of the surface ozone levels observed across Europe. Experiments have been performed to investigate the influence of a 50% reduction in man-made emissions of carbon monoxide, NO<sub>x</sub> and VOCs on the intercontinental contributions from North America and Asia, and local European emissions. As an example, Figure II-7 shows the influence of a 50% reduction in global anthropogenic NO<sub>x</sub> emissions on the different continental ozone contributions. A 50% reduction in global man-made emissions of NO<sub>x</sub> would lead to a decrease in the intercontinental contribution from North America to ozone in Europe of about 0.8 – 1.9 ppb and 0.5 – 0.7 ppb from Asia. The corresponding decreases for a 50% reduction in man-made CO emissions were 0.1 – 0.3 ppb from North America and 0.1 – 0.2 ppb from Asia. The corresponding reductions in AOT<sub>40</sub> exposure levels were significantly larger in percentage terms. On this basis, it was concluded that reductions in tropospheric ozone precursor emissions from the other major northern hemisphere continents could produce appreciable reductions in ozone exposure levels within Europe. European air quality policy development could benefit appreciably from global or hemispheric scale policy actions to reduce tropospheric ozone precursor emissions.

## **(b) Additional Scenarios**

### 1. Impact of international shipping on sulphur deposition and surface ozone levels

#### (i) Introduction

Observations have shown that there were marked differences in the apparent trends in sulphur deposition across the different regions of the British Isles over the period from 1986-1997. Although trends in sulphur deposition were clearly downwards in Eastern England, no obvious trends were apparent along the Atlantic Ocean and Irish Sea fringes of the UK. The suggestion was made that this might reflect a dominating contribution from sources of sulphur arriving in westerly air masses with different apparent trends in the sulphur contents of the associated precipitation. A number of potential sources of sulphur deposition in westerly air masses could be considered as reasonable possibilities, including recirculation of European air masses, North American SO<sub>2</sub> sources, and emissions from international shipping crossing the North Atlantic Ocean. Levels of NO<sub>x</sub> are generally very low over the oceans, and so emission of NO<sub>x</sub> by shipping could influence ozone levels in these regions, and hence the background levels over the UK.

Global emission fields of SO<sub>2</sub>, NO<sub>x</sub>, CO, CH<sub>4</sub> and NMVOCs from anthropogenic sources were taken from the IIASA CLE scenario for the years 1990 and 2000. Emissions of NO<sub>x</sub> and SO<sub>2</sub> from international shipping are not included in the IIASA scenarios; instead, they were based on the EDGAR 3.2 shipping inventories for 1995 (Olivier et al., 1999). The emissions from international shipping were assumed to have an annual growth rate of +1.5% per year (Dentener et al., 2004). STOCHEM simulations were performed with and without the inclusion of the shipping emissions of SO<sub>2</sub> and NO<sub>x</sub>, so that the contribution of shipping to sulphur deposition and surface ozone levels over Europe may be assessed.

(ii) Sulphur deposition over Europe

The annual mean deposition flux of sulphur to Europe for the year 2000 is shown in Figure II-8. Additionally, the flux value is written on the 16 model grid squares that cover the UK. Modelled total sulphur deposition from all sources peaks in central Europe with a maximum deposition of over 2000 mg S m<sup>-2</sup> yr<sup>-1</sup>, see Figure II-8. A ridge of high deposition above 1000 mg S m<sup>-2</sup> yr<sup>-1</sup> extends towards the UK, leading to peak deposition over the UK in excess of 1600 mg S m<sup>-2</sup> yr<sup>-1</sup>. The total sulphur deposition field shows the presence of a finger of increased deposition passing across the Atlantic Ocean corresponding to the deposition contour of 200 – 500 mg S m<sup>-2</sup> yr<sup>-1</sup>. In the western fringes of the British Isles, total sulphur deposition lies within the range 150 – 250 mg S m<sup>-2</sup> yr<sup>-1</sup>. All these features appear to correspond closely with observations of sulphur deposition.

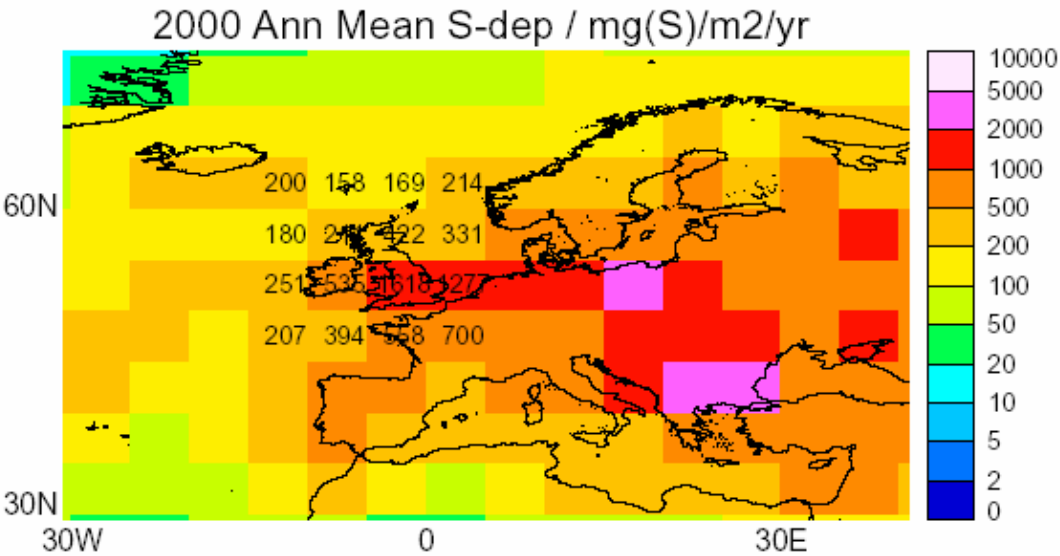


**Figure II-8.** Annual sulphur deposition field in mg S m<sup>-2</sup> yr<sup>-1</sup> for 2000 from all sources. The flux value is written on the 16 model grid squares that cover the UK.

The modelled sulphur deposition fluxes from international shipping alone are shown in Figure II-9. They peak at just over 400  $\text{mg S m}^{-2} \text{ yr}^{-1}$  over the North Sea and Baltic Sea, and are above 200  $\text{mg S m}^{-2} \text{ yr}^{-1}$  over the south west approaches and Brittany. As a percentage, shipping contributes about 30% of the total deposition flux to the south-west approaches, and nearly 60% over East Anglia and the near continent. Over the British Isles, shipping contributes between 10% and 27% of the total sulphur deposition. These results were derived from a short simulation however, and some variability between years is expected. The assumed rate of growth of shipping may also be too large or too small. Despite these uncertainties, it is concluded that international shipping makes a significant contribution to total sulphur deposition along the Atlantic Ocean seaboard of Europe, over the North Sea and over the Baltic Sea.

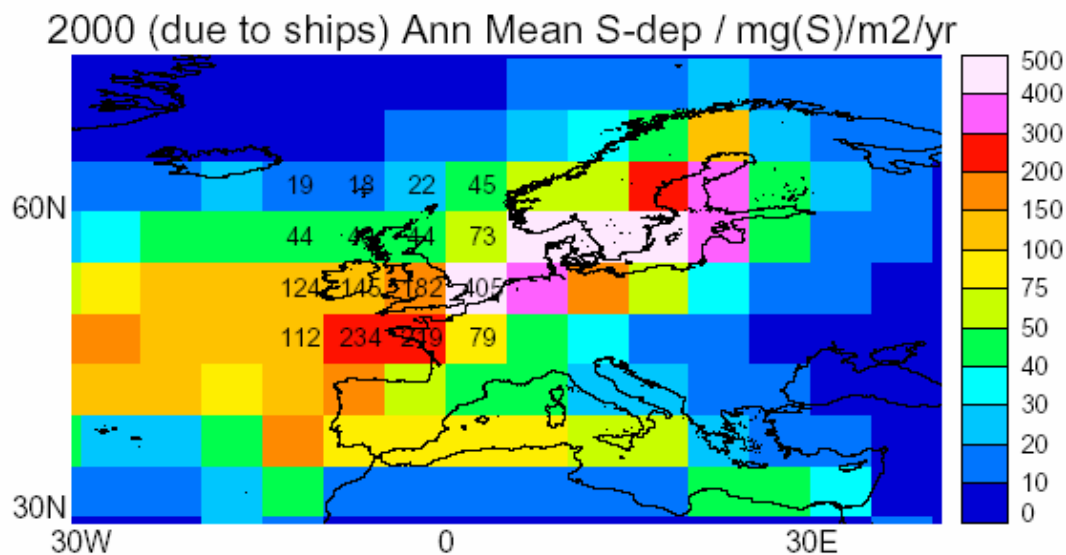


**Figure II-9.** The annual sulphur deposition field in  $\text{mg S m}^{-2} \text{ yr}^{-1}$  for 2000 from international shipping alone. The flux value is written on the 16 model grid squares that cover the UK

### (iii) Ozone levels over Europe

$\text{NO}_x$  levels are observed to be extremely low over oceans and so it is not surprising therefore that  $\text{NO}_x$  emissions from international shipping have been postulated to have some significance for the chemistry of the marine boundary layer. The STOCHEM simulations described above have also been used to identify the role played by  $\text{NO}_x$  emissions from international shipping in influencing the global surface ozone distribution over Europe during the summertime.

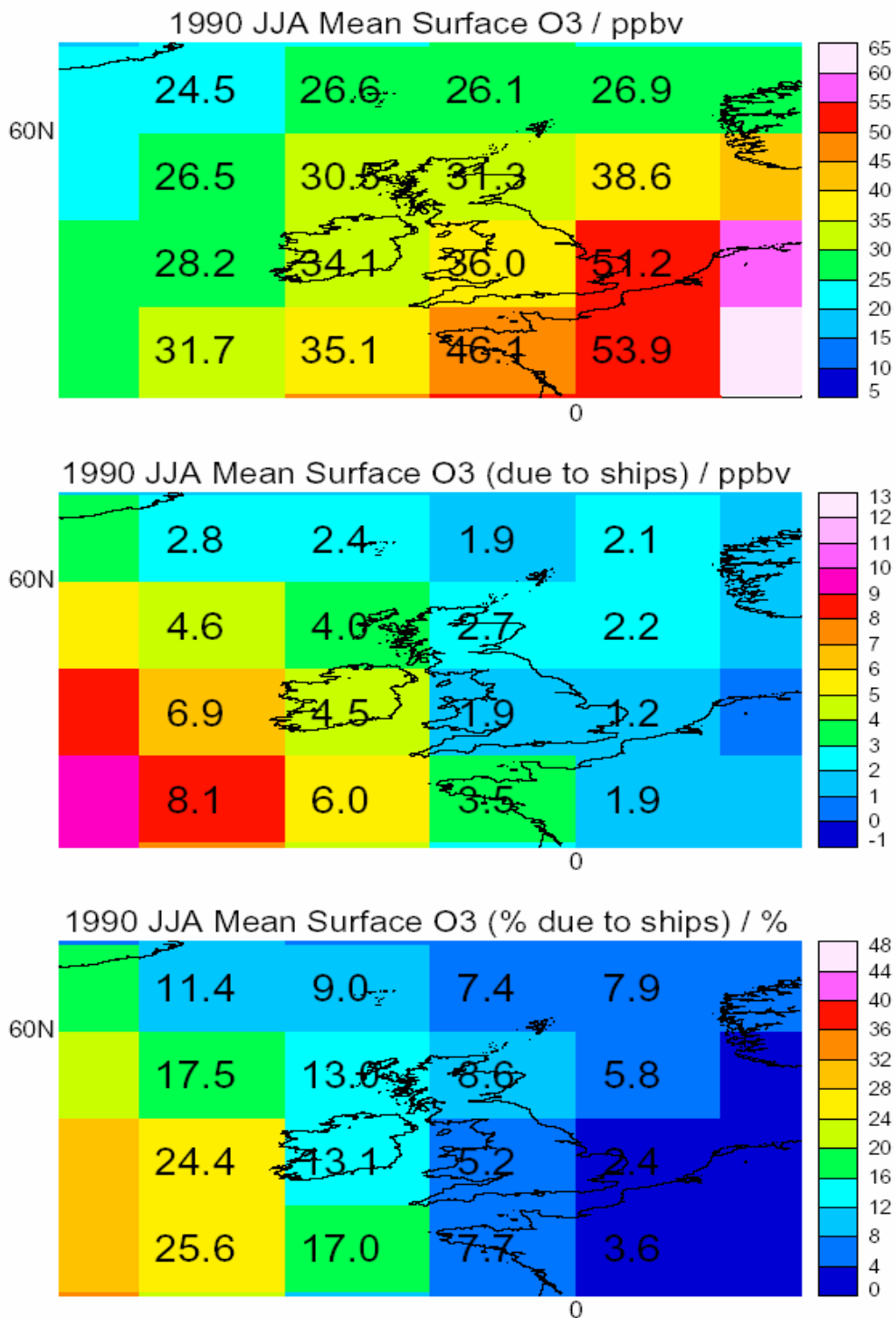


**Figure II-10.** Mean ozone concentrations calculated for June through to August 1990 (JJA) from all sources (upper panel), and from international shipping alone (middle panel). The lower panel shows the percentage of the mean ozone that has resulted from international shipping NO<sub>x</sub> emissions.

The mean surface ozone distribution over the British Isles in 1990 during June-August is shown in Figure II-10. The upper panel presents the mean ozone distribution resulting from all sources and shows values ranging from 30 to 51 ppb over the British Isles. The middle

panel gives the contribution due to international shipping emissions alone, revealing values in the range from 1.2 to 4.5 ppbv.

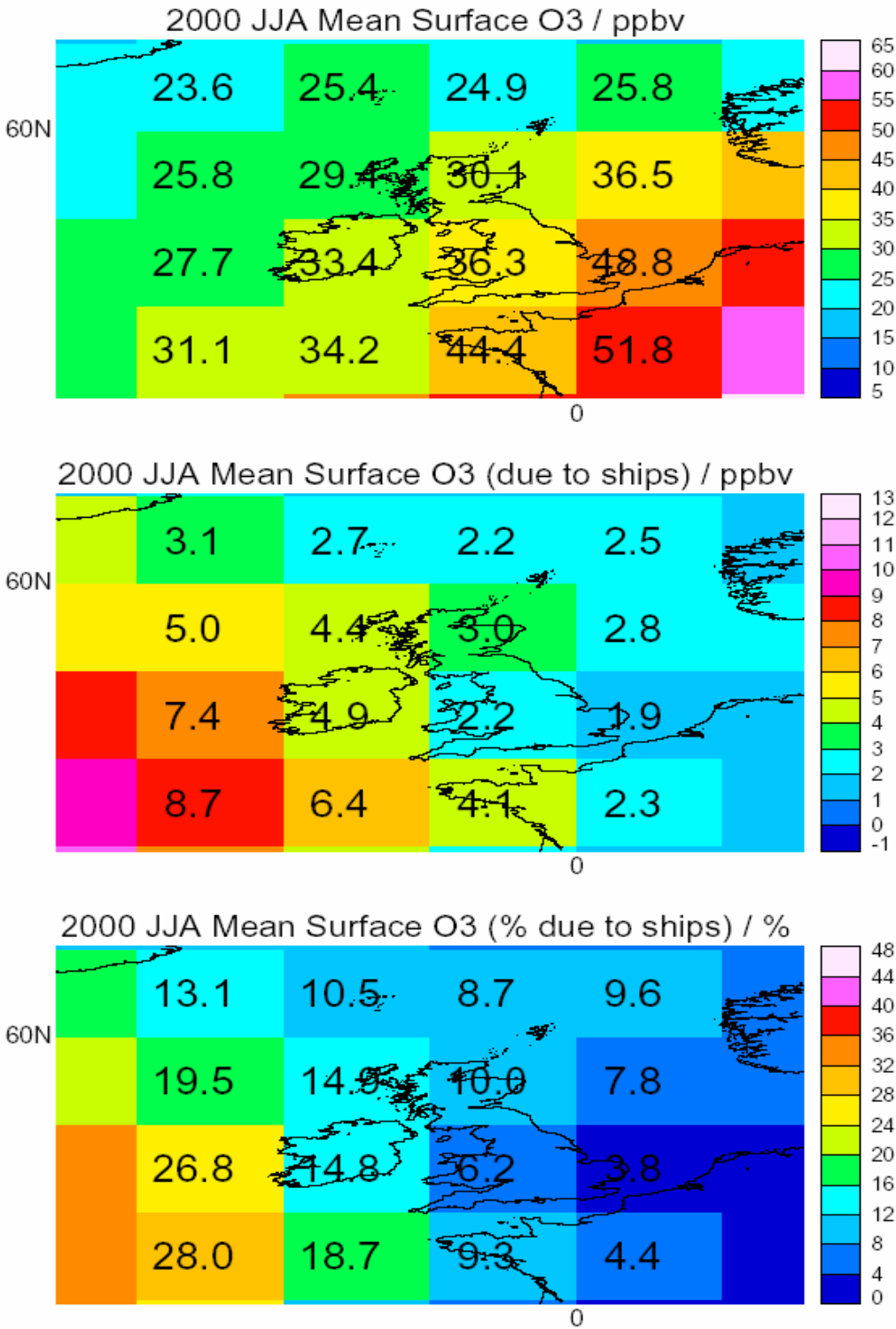


**Figure II-11.** Mean ozone concentrations calculated for June through to August 2000 (JJA) from all sources (upper panel), and from international shipping alone (middle panel). The lower panel shows the percentage of the mean ozone that has resulted from international shipping.

By the year 2000, European legislation limiting emissions has begun to reduce the mean ozone concentrations by up to 3 ppb. In contrast, the contribution from international shipping had increased slightly (compare the middle panels of Figure II-10 and Figure II-11). In both 1990 and 2000, substantial ozone concentrations were predicted to occur during the summertime in the south west approaches to the British Isles from international shipping, reaching between 8 and 9 ppb. During the rest of the year, ozone production from international shipping emissions was substantially reduced compared with the summertime. Uncertainty in these results comes from assumptions about the changing NO<sub>x</sub> emissions from shipping. Nevertheless, shipping emissions do contribute significantly to surface ozone levels over parts of Europe.

## 2. Eutrophication of Ecosystems: Changes in deposition to the EC15 countries

Eutrophication of ecosystems is an acknowledged problem in parts of Europe. Deposition of excess nitrogen, originating from agriculture and other anthropogenic activities, results in stimulated growth of plants, changes in species distribution, and loss of biodiversity. The NEC Directive has set down reductions in emissions of SO<sub>2</sub>, NO<sub>x</sub>, VOCs and NH<sub>3</sub>, aimed at reducing the deposition fluxes of eutrophying species by 30% by 2010, relative to 1990. Each country in the EC15 has an emission ceiling, which must be reached by 2010. These emissions reductions will also impact on air quality, because the NO<sub>x</sub> and VOCs are key primary species whose reactions produce ozone, PAN, and other air pollutants. The total emissions target for the EC15 countries are shown in Table II-6. The emissions from these countries under the IIASA scenarios CLE 2000, CLE 2030, and MFR 2030 (see section II(a).1(iii)) are also given in Table II-6. The emissions of NO<sub>x</sub> and SO<sub>2</sub> under both the CLE 2030 and MFR 2030 are smaller than the NECD target for 2010, but the VOC and NH<sub>3</sub> emissions are larger. Emissions of ammonia were not specified by IIASA. Instead, the ammonia emissions specified under the ACCENT Photocomp experiment were used (Dentener et al., 2006), and are given in the last column of Table II-6. Global ammonia emissions are assumed to have increased by 2030, although emissions from Europe have fallen, and exceed the EC15 total. The majority of the increased ammonia emissions originate from agricultural activities.

The STOCHEM model was integrated for 5 years using each of the scenarios in Table II-6. The climate data used were for the year 2000 in all cases. Although the CLE 2030 scenario is a projection for the year 2030, it is used here as a proxy for 2010. The annual deposition

fluxes of oxidised and reduced nitrogen compounds to the EC15 countries averaged over these 5 years are given in Table II-7. The deposition fluxes of oxidised nitrogen are significantly reduced in all of the 2030 scenarios compared with the present-day (CLE 2000) simulation. The oxidised nitrogen fluxes are 19% and 43% smaller in the CLE 2030 and MFR 2030 scenarios respectively. A comparison of the CLE 2030 and MFR 2030 fluxes shows that the deposition of oxidised nitrogen compounds could be reduced even further if extra legislation to reduce emissions even further was introduced.

**Table II-6.** Sum of emissions targets for EC15 countries under the NEC Directive, and corresponding land-based emissions under IIASA scenarios. Units are kilotonnes yr<sup>-1</sup>.

EC15 Emissions	SO <sub>2</sub>	NO <sub>x</sub>	VOC	NH <sub>3</sub>
Target for 2010	3850	6519	6510	3110
CLE 2000	7645	11442	9922	5144
CLE 2030	2710	5518	10385	4022
MFR 2030	1021	2902	8762	4022

Deposition fluxes of reduced nitrogen compounds are smaller in the 2030 scenarios, by 11%. However, the emissions have been reduced by 22%. A significant shift in the proportions of ammonia and ammonium sulphate could explain the results, because ammonia has a much shorter lifetime (0.9 days) than ammonium sulphate (about 5 days). However, the proportion of the reduced nitrogen deposition fluxes that is ammonia has changed by only 3%. It is likely that deposition of reduced nitrogen compounds from locations outside of the EC15 countries is offsetting the benefit of the emissions reductions.

**Table II-7.** Annual deposition fluxes of oxidised and reduced nitrogen compounds to the EC15 countries. Units are ktonnes (N) yr<sup>-1</sup>.

Scenario	Oxidised N / ktonnes yr <sup>-1</sup>	Reduced N / ktonnes yr <sup>-1</sup>
CLE 2000	1993	2870
CLE 2030	1615	2557
MFR 2030	1139	2567
CLE 2030 + cc	1640	2613

The effect of climate change on the deposition fluxes can be seen by comparing the CLE 2030 and CLE 2030 + cc rows. The extra simulation CLE 2030 + cc used a projected climate for 2030 from previous integrations of the climate model. The deposition fluxes are only 1.5 – 2% larger when the 2030 climate was used. For 2010, the impact of climate change on nitrogen deposition is likely to be smaller, and essentially negligible.

Critical loads for nitrogen deposition to Europe are listed by Bobbink and Roelofs (1995) for a variety of vegetation types, and are uncertain by as much as a factor of 2. It is not straightforward to map the vegetation types listed by these authors to those used in the model simulations. The critical loads generally range between 5 and 20 kg N ha<sup>-1</sup> yr<sup>-1</sup>. The modelled nitrogen deposition fluxes under both the present-day (CLE 2000) and future (CLE 2030) simulations are greater than 5 kg N ha<sup>-1</sup> yr<sup>-1</sup> over most of Europe, except for parts of Sweden, Norway and Finland. The areas of Europe where the modelled nitrogen deposition fluxes exceed 10, 15 and 20 kg N ha<sup>-1</sup> yr<sup>-1</sup> under each of these two scenarios are shown in Table II-8. The emissions in the CLE 2030 scenario from the EC15 countries are closest to the limits of the NEC Directive.

**Table II-8.** Areas where nitrogen deposition flux exceeds critical loads.

Critical load / kg N ha <sup>-1</sup> yr <sup>-1</sup>	Area where critical load exceeded / 10 <sup>6</sup> ha		
	10	15	20
CLE 2000	452	159	22
CLE 2030	260	51	7

The areas where a given critical load are exceeded are substantially reduced in the CLE 2030 scenario, by 43, 67 and 67% for the limits of 10, 15 and 20 kg N ha<sup>-1</sup> yr<sup>-1</sup> respectively. These results suggest that the emissions reductions under the NEC Directive will reduce the areas of Europe having excess nitrogen deposition by more than 30%, which is the target value under the Directive. These results are, however, subject to large uncertainties. The emissions of the CLE 2030 scenario do not match the targets under the NEC Directive exactly. The emissions of NO<sub>x</sub> are smaller, but the ammonia emissions used are larger. The Directive also aims to reduce areas having excess nitrogen deposition by 30% by 2010 relative to 1990, whereas deposition fluxes for the years 2030 and 2000 have been used here. The formation and deposition of ammonium nitrate was not included in these particular simulations, although it

is not clear what the effect on the modelled deposition fluxes of nitrogen would be. Further uncertainties originate from the low resolution of the model, the treatment of the oxidation of sulphur and nitrogen compounds in cloud water, and the representation of the deposition processes.

### 3. Acidification of Ecosystems: The role of climate change

We have further investigated the potential acidification of global ecosystems in the present day and the 2090s, as a continuation of the work described in part (3) above. The deposition of nitrogen and oxidised sulphur compounds to ecosystems can lead to an effect known as acidification. Acid deposition is a recognised problem in Europe and North America, but there is potential for considerable damage to ecosystems in developing countries (Kuylenstierna et al., 2001). The most sensitive regions are old acidic tropical areas with high rainfall such as the Amazon basin, central Africa and south-east Asia. Some of the ecosystems in these areas have the potential to partly mitigate the effects of acid deposition. The adsorption of sulphate ions releases hydroxide ions which will neutralise acidity (Kuylenstierna et al., 1995). It is also likely that tropical soils and ecosystems will respond differently to increased nitrogen input than temperate soils. Productivity is unlikely to increase, and the excess nitrogen will result in increased fluxes from the soil to the air and water with little time lag (Matson et al., 1999).

Reactive nitrogen is emitted as nitric oxide, NO (oxidised form) and ammonia, NH<sub>3</sub> (reduced form). NO is produced from combustion processes (fossil fuel and biomass burning), and is rapidly transformed into other species such as nitric acid (HNO<sub>3</sub>) which deposits readily to most surfaces. Significant amounts of NO are also produced by lightning and soils (IPCC, 2001). Ammonia is emitted mainly from intensive livestock agriculture. Emissions from soils and vegetation are possible, depending on environmental conditions. A small amount of ammonia emitted into the troposphere is oxidised via reaction with the hydroxyl radical, and some is deposited back to the surface (Adams et al., 1999). Ammonia readily dry deposits to most surfaces; measured surface resistances to ammonia deposition are small (Erisman et al., 1994, and references therein). Consequently, the lifetime of ammonia is quite short (0.9 days (Adams et al., 1999)), and so this species will be deposited close to its source regions. A significant amount dissolves into cloud water to form the ammonium ion which in turn combines with sulphate ions to form ammonium sulphate aerosols which will also be deposited to the surface. Ammonium sulphate has a longer lifetime than ammonia

(approximately 5 days (IPCC, 2001)), and can be transported larger distances from its source regions and impact a greater area.

Simulations using STOCHEM were run to examine the magnitude and changes in the deposition fluxes of acidifying compounds (nitric acid, sulphuric acid aerosols, and ammonium sulphate) between the present day and the 2090s. The effects of climate and increases in emissions on the deposition fluxes were investigated separately. The possible exceedance of critical loads for acidification for the 1990s and 2090s has been assessed. Four simulations were used, and are summarised in Table II-9. All emissions were taken from the IS92a scenario. Each chemistry-climate coupled model simulation lasted for 6 years, and results from the first year were excluded from the analysis. The climate data used to drive these simulations, including the vegetation changes, were generated in a previous integration of the Hadley Centre model, similar to that of Cox et al. (2000). This integration used carbon dioxide emissions specified by the IS92a scenario (IPCC, 1994).

**Table II-9.** Summary of scenarios used for acid deposition studies.

Simulation	Climate	Vegetation	Emissions
A	1990s	1990s	1990s
B	1990s	1990s	2090s
C	2090s	2090s	1990s
D	2090s	2090s	2090s

The emission and deposition fluxes of nitrogen and sulphur species are summarised in Table II-10. The deposition of oxidised nitrogen species is greater in the 2090s owing to increased emissions. There has been a shift in the deposition of the reduced nitrogen species, ammonia and ammonium sulphate. In the future simulation (D), more of the ammonia has been converted to ammonium sulphate than in the present day (A), and less ammonia is deposited back to the surface. In all simulations, the reaction of ammonia with the hydroxyl radical (OH) is a minor sink and will not be considered further. The total deposition flux of ammonia, and the aqueous phase reactions which form ammonium sulphate, have similar

magnitudes. In simulation A, for the 1990s, dry and wet depositions are the largest sinks for ammonia. However, in the future simulation (D), the formation of ammonium sulphate is the most important sink.

Two sensitivity integrations were performed to test the effect of emission increases (simulation B) and climate (simulation C) at 2100 levels on the nitric acid and ammonia sinks. Not surprisingly, larger emissions of nitric oxide result in increased deposition fluxes of nitric acid. The effect of climate change on the deposition fluxes can be seen by comparing column A with C, and B with D, in Table II-10. For the oxidised nitrogen species, climate change acts to increase the deposition flux of nitric acid at the expense of other nitrogen compounds. More ammonia is converted to ammonium sulphate as well. From the data in columns A and B of Table II-10, it can be seen that increasing the emissions (simulation B) has the largest effect on the ammonia – ammonium conversion, and increases the production of ammonium sulphate. Increasing the emissions of precursor gases has a larger impact on the ammonia – ammonium conversion than climate change.

**Table II-10.** Summary of 5 year mean nitrogen and sulphur deposition fluxes, and total acid deposition flux to land surfaces only for each simulation (see Table II-9).

Flux (Tg S or N yr <sup>-1</sup> )	A	B	C	D
NO emission	58.1	105.3	58.1	105.3
NO <sub>2</sub> deposition	5.2	11.1	4.8	10.0
HNO <sub>3</sub> deposition	51.1	90.8	52.7	93.5
Ammonia emission	53.7	53.7	53.7	53.7
Ammonia deposition	29.0	26.4	27.8	24.9
Ammonium deposition	23.4	26.1	24.3	27.5
SO <sub>2</sub> emission	85.2	156.2	85.2	156.2
Sulphate deposition	34.5	45.4	36.6	49.7

Increased emissions of pollutants such as nitrogen oxides and hydrocarbons, and climate change, therefore encourage production of nitric acid from nitric oxide, and ammonium sulphate from ammonia. Part of the latter change is due to more aqueous phase oxidation of sulphur dioxide by hydrogen peroxide, which in turn produces more ammonium sulphate. Climate change also affects the relative importance of each of the ammonia and sulphur sinks. In these simulations, the cloudiness (and hence amount of liquid water in clouds) has also

increased in the future climate, further encouraging the dissolution and ionisation of ammonia and sulphur dioxide. These results demonstrate that the sulphur and reduced nitrogen cycles are closely connected.

A map of the sensitivity of ecosystems to acidic deposition has been presented by Kuylenstierna et al. (2001), which divides the ecosystems into 5 sensitivity classes. The critical loads corresponding to each sensitivity class are given in Table II-11. Following the method of Kuylenstierna et al. (2001), the deposition flux of base cations was subtracted from the total acid deposition flux to give the net acid deposition flux, using the equation: Net acid equivalent =  $f[\text{NH}_4^+] + f[\text{HNO}_3] + 2 \times f[\text{SO}_4^{2-}] - 2 \times f[\text{Ca}^{2+}]$ . The notation  $f[\text{X}]$  means the total (wet + dry) deposition flux of species X (with units in moles  $\text{m}^{-2} \text{yr}^{-1}$ ). The base cation deposition fluxes were derived from dust deposition fields calculated by Woodward et al. (2005) for the 1990s and 2090s, assuming in each case that 10 % of the dust was calcium which is used as a proxy for the carbonate content and hence the buffering ability of the dust (Kuylenstierna et al., 2001). The future dust loading and deposition flux is predicted to be significantly greater in the future owing to climate change induced desertification in Amazonia (Cox et al., 2000; Woodward et al., 2005).

From the map of critical loads for acidification presented by Kuylenstierna et al. (2001), the most sensitive areas to acid deposition (class 1 in Table II-11) extend from the southernmost part of China to Malaysia and Indonesia. Significant parts of Amazonia, parts of the south-eastern U.S.A., and a smaller area of central Africa are also assigned to this class. The rest of the southern half of China, central Africa and Amazonia are assigned to class 2. These sensitive areas are interspersed, particularly in Amazonia. Most of the remaining areas are assigned to classes 4 and 5. The upper value from the low range of the critical loads for each sensitivity class in Table II-11 will be used in the first instance.

The net acid deposition fluxes in the tropical and subtropical regions for the 1990s and 2090s are shown in Figures II-16(a) and II-16(b) respectively. Areas where the critical loads are exceeded are ringed. For the present day (Figure II-12(a)), the areas where the critical loads are exceeded are confined to the eastern U.S.A. and southern China, and a small part of southern Amazonia. A very few areas in central Africa are close to exceeding the critical loads. By the 2090s (Figure II-12(b)), areas of exceedance in south-east Asia are

considerably larger, extending from all of southern China to Indonesia. Critical loads for a small part of central India may also be exceeded. Critical loads for Amazonia are not exceeded, owing to the increased base cation deposition flux in turn caused by desertification in this region. Acid deposition fluxes over the eastern U.S.A. still exceed the critical loads.

**Table II-11.** Critical loads for acidic deposition (from Kuylenstierna et al., 2001). The low range for classes 2 – 4 increase in line with critical load ranges used in Europe. For the most highly buffered soils (class 5), there is essentially no critical load. The high range of critical loads is simply double the low range, and accounts for the uncertainty in these estimates.

Sensitivity Class	Range of critical loads (meq m <sup>-2</sup> yr <sup>-1</sup> )	
	Low Range	High Range
1	0 – 25	25 – 50
2	25 – 50	50 – 100
3	50 – 100	100 – 200
4	100 – 200	200 – 400
5	> 200	> 400

The base cation deposition flux and critical load used will clearly influence which areas are exceeded. To test the sensitivity to these two quantities, the same test used by Kuylenstierna et al. (2001) was used, where the base cation flux was increased by a factor of 4, and the highest critical load for each sensitivity class was used (Table II-11). Figure II-12(c) shows the acid deposition flux (total acid flux minus the base cation flux) when the larger base cation flux is used. The areas experiencing acid deposition fluxes above the corresponding critical loads over south-east Asia are smaller, but significant areas are still exceeded. As in the other future scenario (Figure II-12 (b)), no critical loads over Amazonia are exceeded. The overall acid deposition fluxes over the U.S.A. are reduced, but despite this reduction, the critical loads for the eastern part are still exceeded. These results suggest that acid deposition over south-east Asia and the eastern U.S.A. will be a problem in the future if preventative measures are not taken to reduce emissions of nitrogen and sulphur compounds. Technology to reduce emissions of sulphur and oxidised nitrogen already exists, and it is likely that these technologies will be employed to reduce acid deposition fluxes in Asia (Pham et al., 2005). It is likely that ammonia emissions will increase in importance in the future as emissions of sulphur and oxidised nitrogen species are reduced.

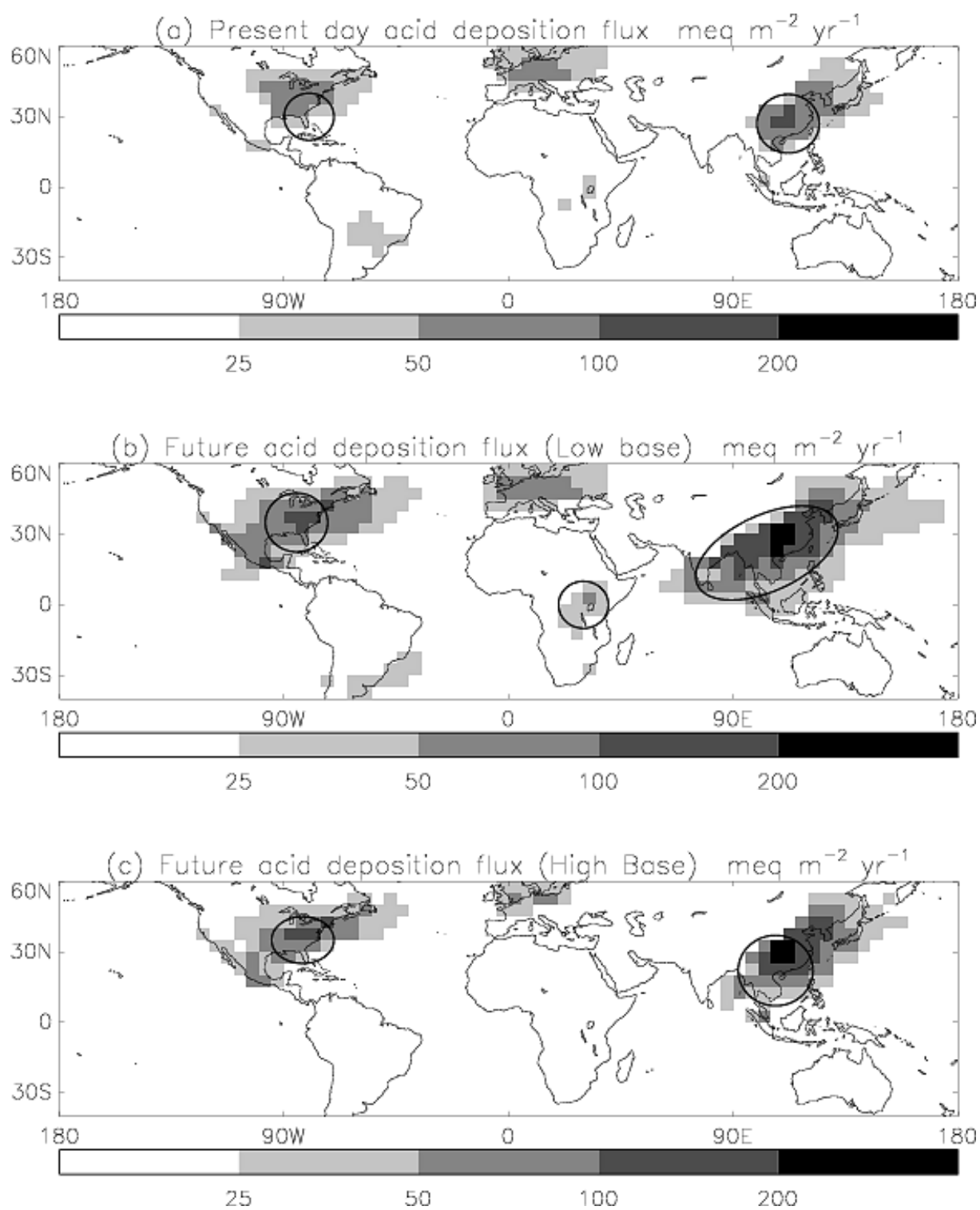


**Figure II-12.** Net acid deposition fluxes to land surface. (a) Present day flux (1990s). (b) Future deposition flux (2090s) from simulation D. (c) Future deposition flux but using a base cation flux 4 times larger. The units are milliequivalents ( $\text{meq m}^{-2} \text{yr}^{-1}$ ) in all cases. The ringed portions of each map indicate areas where the critical loads are exceeded. See text for further details.

The critical loads for Europe were not exceeded in any of the scenarios, although the net acid deposition flux is larger in the future than the present. Emissions of SO<sub>2</sub> from Europe have been substantially reduced over the last 30 years, and are assumed to fall further in the IS92a scenario. Emissions of ammonia, and deposition of ammonium compounds, may therefore become more important in the future.

### **(c) Conclusions**

In this chapter, surface ozone levels over Europe for 2030 have been projected using several scenarios developed by IIASA. Ozone levels remain fairly constant under current legislation (CLE), but much greater reductions are realised under the maximum feasible reductions (MFR) scenario. However, in both of these projections, ozone levels rise over the southern half of the UK, and the Benelux countries. The levels of nitrogen oxides in these regions are very large, and act to remove hydroxyl radicals (OH) by forming nitric acid vapour, which is readily removed from the atmosphere. When the emissions of nitrogen oxides are reduced, this removal of hydroxyl radicals becomes less important, meaning there are larger levels of hydroxyl radicals and hence greater ozone production.

Further assessment of the IIASA scenarios was achieved with 40 year simulations from 1990 to 2030, and examining the projected levels of ozone, methane and carbon monoxide at Mace Head. In the CLE scenario, methane levels exhibited a strong upward trend, ozone levels a weaker upward trend, and carbon monoxide levels remained approximately constant in baseline air masses. In one of the more pessimistic IPCC SRES scenarios (A2), marked increases in all three gases are projected. However, in the scenario based on maximum feasible emission reductions, (MFR), the levels of all three trace gases decline. By 2030, projected climate change reduces the growth in CH<sub>4</sub>, but has an insignificant effect on baseline CO and O<sub>3</sub> levels. Global or hemispheric ozone precursor emissions and their controls potentially exert a strong influence on European air quality. This influence is currently not taken into account in future European air quality policy formulation. Other work has shown that control of methane levels will also reduce ozone levels.

The radiative forcing due to changes in ozone and methane levels driven by pulses of NO<sub>x</sub> emitted from various locations have been investigated. The response of modelled ozone levels at Mace Head to these pulses has also been examined. A “baseline” simulation with no pulses was used as a reference. Initially, an increase in ozone levels is simulated, followed by

a much longer lived decrease, when compared with the baseline simulations. The long-term decrease is caused by reduced methane levels.

NO<sub>x</sub> pulses emitted from Asia had the largest overall radiative forcing, followed by pulses from North America and finally Europe. Using NO<sub>x</sub> emission pulse from various locations in Asia, the time-integrated short-term ozone responses at Mace Head increased markedly with latitude, from approximately zero for those pulses emitted in Java and Borneo to +0.6 ppb-months for pulses emitted in China. In contrast, the time-integrated long-term ozone responses are negative and somewhat smaller in absolute magnitude, but show a much reduced latitudinal variation. Overall, the total time-integrated ozone responses vary from about -0.2 to +0.5 ppb-months across Asia

Further experiments were run, using pulses of NO<sub>x</sub> from the USA, and examining the ozone response at many locations within Europe. The net responses decrease both northwards and eastwards across Europe, driven by the initial short-term response. The variations across Europe in the long-term responses are less important.

The impact of emissions of NO<sub>x</sub> and SO<sub>2</sub> from shipping on European ozone levels and sulphur deposition fluxes were assessed. For the year 2000, shipping emissions contributed between 4 and 15% of modelled surface ozone levels. As legislation such as the NEC Directive and Gothenburg Protocol come into force, land-based emissions will fall and the importance of emissions from international shipping will increase. Legislation to control emissions from shipping, as well as land-based sources, will be needed to control future ozone levels. Deposition of sulphur from shipping was also significant, particularly in coastal regions.

One aim of the NEC Directive is a reduction of 30% of land area having excess nitrogen deposition, in order to combat eutrophication. STOCHEM was integrated using two IIASA emissions scenarios, CLE 2000 as a control, and CLE 2030 as a proxy for the emission limits agreed under the NEC Directive for 2010. Using the modelled deposition fluxes, the changes in the areas having excess nitrogen deposition were calculated using several different critical loads. Significant reductions in areas having excess nitrogen deposition were modelled. Although the critical loads and modelled deposition fluxes are subject to large uncertainties,

the results suggest that the 30% reduction in areas having excess nitrogen deposition will be achievable.

Changes in the deposition fluxes of nitrogen and sulphur compounds, and the impact of climate change on the deposition fluxes, was further assessed for the years 2000 and 2100. Climate change was found to increase acid deposition globally, owing the increased production of ammonium sulphate which in turn is caused by a larger proportion of the oxidation of SO<sub>2</sub> occurring in cloud liquid water, as opposed to the gas-phase. The critical loads for acid deposition are highly uncertain. However, the results indicate that large parts of south-east Asia could be at risk. There was little impact over Europe, owing to the smaller emissions and hence deposition fluxes in this region.

It is important to note that the low resolution of the global model used means that small areas in Europe or elsewhere experiencing high deposition fluxes of eutrophying and/or acidifying compounds will not be identified. Models with higher spatial resolutions that can include local topography and more accurate emissions are needed. The transport of relevant compounds from outside the domain of interest could be provided by the global model.

## Chapter III. Climate Change – Air Quality Interactions

### (a) Exploring the interactions

#### 1. Introduction and Policy Relevance

In the United Kingdom, air quality targets for 2005 (DETR, 2000) have been set for a variety of pollutants, such as benzene, nitrogen dioxide, particulates and ozone. These compounds have an impact on human health. They are all primary pollutants except ozone, as they are emitted directly from sources such as vehicle exhausts. Ozone, however, is a secondary pollutant, because it is made from photochemical reactions in the atmosphere involving the primary pollutants. Control of ozone levels is more difficult owing to the complex and variable reactions involved in its production and destruction. The same levels of primary pollutants may produce quite different levels of ozone depending on the meteorological conditions. On top of this, climate change is another process which has to be considered when making decisions on pollutant reduction policies. The chemical reactions involved in the formation and destruction of ozone are temperature dependent, and if the future climate is warmer, these reactions will proceed more quickly and produce more ozone. However, the water vapour in the air will increase, resulting in increased destruction of ozone. The target set for U.K. ozone levels, to be achieved by the end of 2005, is a daily maximum of 50 ppb, which must not be exceeded more than 10 times per year (DETR, 2000). Results from several different scenarios to assess the effect of climate change and other influences on surface ozone levels over Europe are presented below. They concentrate on summer values, as this is the time of year when the highest surface ozone values are observed. Finally, the likelihood of meeting the air quality target for ozone now and in the future is discussed.

A series of experiments have been described in Chapter II to look at the effect of different emissions scenarios on European ozone levels. An extension to these experiments was to look at the effect of climate change on emissions of methane and isoprene, and surface ozone levels in the year 2030. It is often assumed that climate change is negligible at 2030, but this assumption is not necessarily true. As an example, Figure III-1 (reproduced from Stott et al., 2004) shows significant increases in European summer temperatures, between approximately 0.5 and 2.0 °C by 2030.

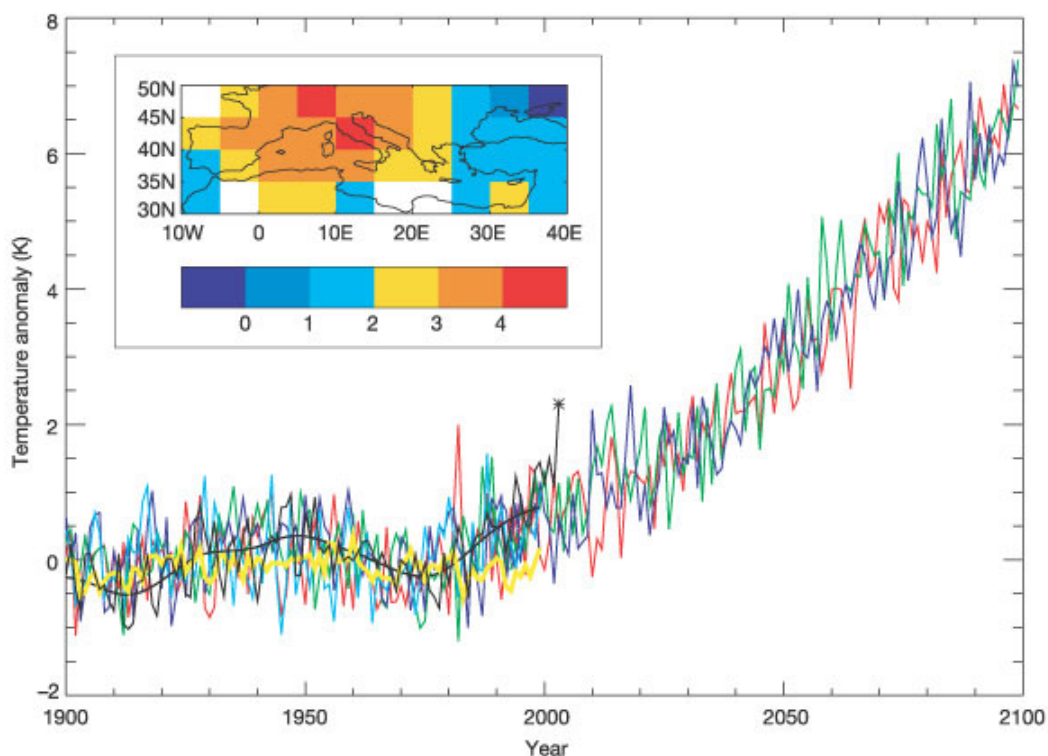


**Figure III-1.** Changes in European surface summer temperature compared to the 1960-1990 mean (from Stott et al., 2004). Observed temperatures are shown by the black line, and a smoothed version by the heavy black line. Modelled temperatures from four simulations including both anthropogenic and natural forcings to 2100, including changes in greenhouse gas and sulphur emissions according to the SRES A2 scenario for the future, are indicated by the red, green, blue and turquoise lines. The model response to purely natural forcings is shown by the yellow line. The observed 2003 summer temperature is shown by an asterisk. The inset shows observed summer 2003 temperature anomalies in °C.

## 2. Effect of climate change on surface ozone levels

### (i) Introduction

It is expected that the future climate will be warmer than the present one. The rates of the chemical reactions that form ozone are temperature dependent, and will proceed more rapidly in a warmer environment. However, there will also be more water vapour in a warmer atmosphere, which will result in greater destruction of ozone. Photolysis of ozone produces an oxygen atom, which can either reform ozone via reaction with oxygen molecules, or produce the OH radical via reaction with water vapour:  $O(^1D) + H_2O \rightarrow 2 OH$ . The latter reaction therefore represents a sink for ozone (Johnson et al. 2001). In this section, the effect of climate change alone on projected ozone levels is investigated. Further impacts of climate change are investigated in sections 3, 4 and 5.

(ii) Surface ozone levels in 2030

Figure III-3 shows the impact climate change has on the projected surface ozone levels in 2030. In the simulations used here, natural emissions were fixed at 1990 levels, so the effect of climate change alone could be assessed. The top left panel is the same as in Figure II-11, showing the projected change in ozone due solely to emissions changes under the CLE scenario. The top right panel shows the effect of the same emissions change, but now the climate used is appropriate for 2030. The projected ozone levels are significantly smaller, by approximately 3 ppb over Europe. The difference between these two simulations, illustrating the effect of climate change alone, is shown in the lower picture. Over much of Europe the change in ozone levels as a consequence of climate change by 2030 is larger than that due to emissions changes under the CLE scenario. The effects of climate change therefore make the projected ozone levels more uncertain.

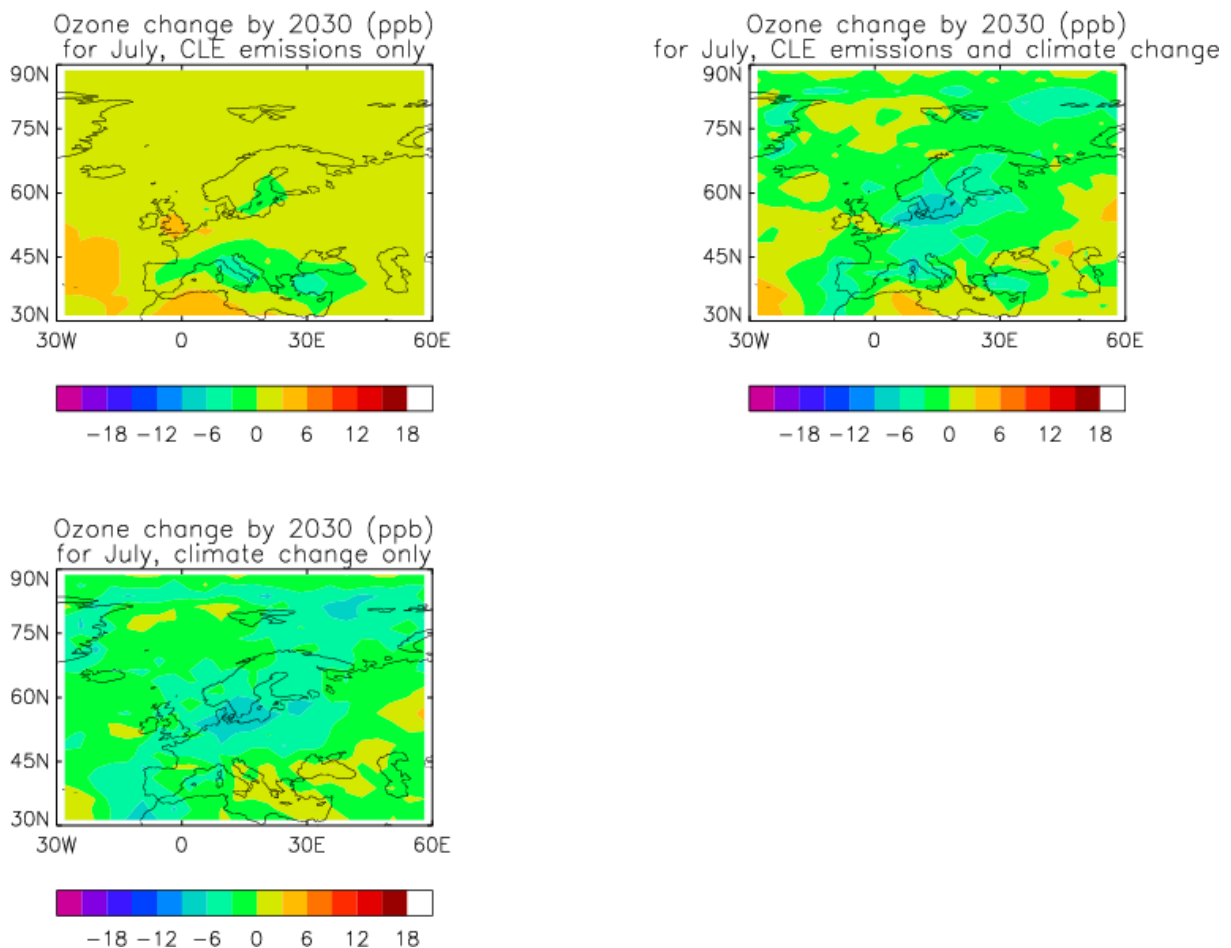


**Figure III-2.** Changes in surface ozone between 2000 and 2030. The top left panel shows the ozone differences due to changing emissions according to the IIASA CLE scenario. The top right panel shows the ozone differences using the same emissions changes, and using the appropriate climate for 2030. The lower plot is the difference between the top two.

(iii) Surface ozone levels in 2090s

Two further simulations have been performed with the STOCHEM model to assess the effect of climate change on surface ozone levels over Europe for the present day and the 2090s (Johnson et al., 2001). In each case the model was run for 110 years continuously for the period 1990 to 2100. The control run had constant greenhouse gas concentrations and hence a fixed climate. In the climate change run greenhouse gas concentrations were allowed to increase according to the SRES A2 scenario, which results in the climate slowly warming over the course of the simulation. In both simulations, the anthropogenic emissions of reactive gases such as nitrogen oxides, carbon monoxide and hydrocarbons increased according to the SRES A2 scenario, but the vegetation distribution and natural hydrocarbon emissions were fixed and did not vary between each year of the simulation.

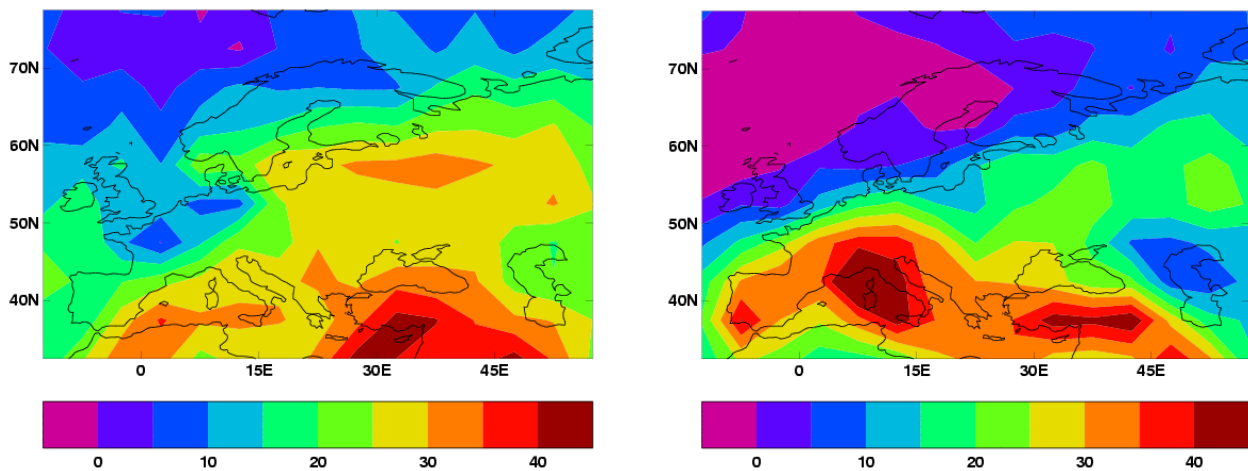


**Figure III-3.** Change in summertime surface ozone levels in ppb over Europe: (a) Left panel - between the 2090s and the 1990s with a fixed 1990s climate (control run); (b) Right panel - as the control run but uses a changed climate.

Figure III-3(a) shows the change in summer mean surface ozone levels over Europe owing to increased emissions of pollutants only (control run). The ozone levels over northern Europe have increased by 5 – 20 ppb, and are 25 – 40 ppb higher over eastern and southern Europe. Figure III-3(b) shows the same difference but includes the effects of climate to change as well. It can be seen that pattern of ozone increases in this run are quite different. Over northern Europe, the ozone levels have increased by a smaller amount, 5 – 15 ppb, whereas over all of southern Europe the ozone changes are 30 – 40 ppb, slightly higher than in the control run. The effect of climate change in these simulations is complex. The reduction in ozone values over northern Europe is caused by an increase in the ozone destruction rate via

the reaction of oxygen atoms with water vapour, as described above. However, southern Europe has become warmer and drier, and so the ozone destruction rate is correspondingly smaller. Production of ozone is expected to increase in a warmer climate and this may exceed the increase in the destruction rate.

### 3. Ozone levels in 2100: Further studies of climate change impacts

#### (i) Introduction

In section 2, it has been shown that climate change, through changes in temperature and humidity, is generally expected to decrease tropospheric ozone by increasing the ozone destruction rate. However, climate change can increase the direct input of ozone into the troposphere by enhancing the rate of exchange of air between the stratosphere and the troposphere. This enhanced exchange is driven by increases in the Brewer-Dobson circulation, which in turn are caused by increased propagation of planetary waves into the stratosphere (Butchart and Scaife, 2001). In the next section, the impact of increased stratosphere-troposphere exchange (STE) on modelled surface ozone values is shown. Afterwards, the impacts of combinations of climate change, STE, and also stratospheric ozone levels on surface ozone is explored.

#### (ii) Changes in stratosphere-troposphere exchange (STE)

We have carried out two simulations with STOCHEM using trace gas emissions for the 1990s in both cases, but climatologies for the 1990s and 2090s respectively (Collins et al., 2003). A stratospheric ozone climatology for the 1990s was used for both runs, allowing the effect of enhanced STE alone on tropospheric ozone levels to be elucidated. Chemical reactions were switched off in the stratosphere, although ozone levels in air parcels in the stratosphere were relaxed toward those of the climatology. When the 2090s climate was used, the stratospheric input of ozone increased by 37% compared with the 1990s. Although the overall tropospheric burden of ozone decreased due to the increased destruction rate, there were local ozone increases. These increases were most evident in the upper troposphere, but could sometimes be observed at the surface. The modelled concentrations of ozone and the stratospheric ozone component (marked as O3\_strat) at Mace Head are shown in Figure III-4 for each of the simulations. The present day ozone is simulated well at Mace Head, with a peak in April. The future simulation projects that this ozone peak may occur earlier in the spring, in March. The proportion of stratospheric ozone at the surface is higher in the 2090s compared to the 1990s due to the increased rate of exchange between the troposphere and the stratosphere. In

the 2090s, the total ozone mixing ratio is lower in the summer, due to the larger destruction rate caused by increased humidity, but higher in February and March due to the increased rate of stratosphere-troposphere exchange. Other studies (Zeng and Pyle, 2003; Sudo et al. 2003; Shindell, 2004 – personal communication) have found that allowing the stratospheric ozone chemistry to respond to climate change results in a doubling of the rate of stratosphere-troposphere exchange of ozone.

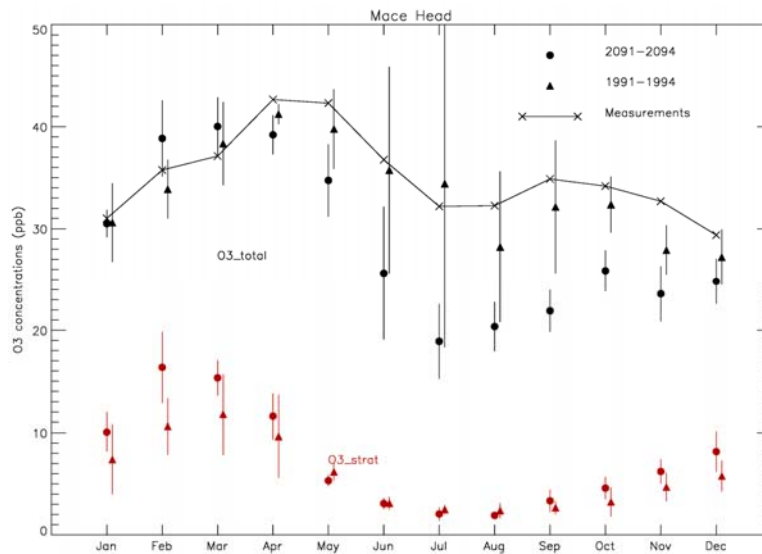


**Figure III-4.** Ozone levels at Mace Head using climatologies for the 1990s and 2090s. The data in red marked “O3\_strat” are the levels of ozone transported from the stratosphere into the troposphere. Monthly mean measurements of ozone for the 1990s are also shown.

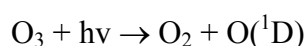
(iii) Impacts of climate, emissions and stratospheric exchange on ozone levels

Several further simulations were performed to further assess the combined effects of climate change, changes in emissions, and stratosphere-troposphere exchange on tropospheric ozone levels between the present day (2000) and the year 2100. The simulations are summarised in Table III-1. In each case, the model was “spun-up” for 4 months, and then run for a further 5 years. The results shown in Figure III-5 and Figure III-6 are monthly mean differences in the surface ozone levels between simulations 2, 3 and, 4 and simulation 1, averaged over the 5 years for January and July respectively. The absolute ozone levels from simulation 1 are also shown for each month.

**Table III-1.** Summary of simulations to assess future ozone changes.

Simulation	Climate	Stratospheric Ozone	Surface Emissions
1	2000	2000	2000
2	2100	2100	2100
3	2000	2100	2100
4	2100	2000	2100

The predicted increases in surface ozone levels for 2100 are shown in Figures III-7(b) and III-8(b). The largest changes in ozone are in the tropical regions, particularly over parts of Africa, South America and south-east Asia. Interestingly, a small decrease is predicted over China and the tropical Pacific Ocean. The ozone changes between simulations 1 and 3 are shown in Figures III-7(c) and III-8(c). Simulation 3 has future stratospheric ozone levels and precursor emissions, but a present day climate. The peak ozone increases over land are similar to those in simulation 2 (see Figures III-7(b) and III-8(b)), but the ozone levels over the oceans are 10 – 15 ppb greater. This change is due to the water vapour feedback on ozone levels. The increased temperatures in the future climate used in simulation 2 means that the atmosphere will hold more water vapour, resulting in increased ozone destruction via the reactions



Countering this effect, the flux of ozone from the stratosphere into the troposphere in simulation 2 will be greater than in simulation 3, owing to the increased rate of stratosphere-troposphere exchange in the warmer climate (Collins et al., 2003). The rate of destruction of ozone via the water vapour feedback dominates, so that the surface ozone levels are lower in simulation 2 than simulation 3. However, the proportion of the surface ozone that is stratospheric in origin is larger, as was discussed in section 3(ii).

In simulation 4, the effect of just the stratospheric ozone changes can be seen by comparing panels (b) and (d) for each of Figures III-7 and III-8. The peak ozone levels over land are essentially unchanged, but the ozone values in the tropical Pacific Ocean are 5 ppb lower in simulation 4 than simulation 2. Similar changes can also be seen in the Atlantic Ocean at

mid-latitudes. The effect of stratospheric ozone changes is smaller than climate and emission changes, but should not be ignored.

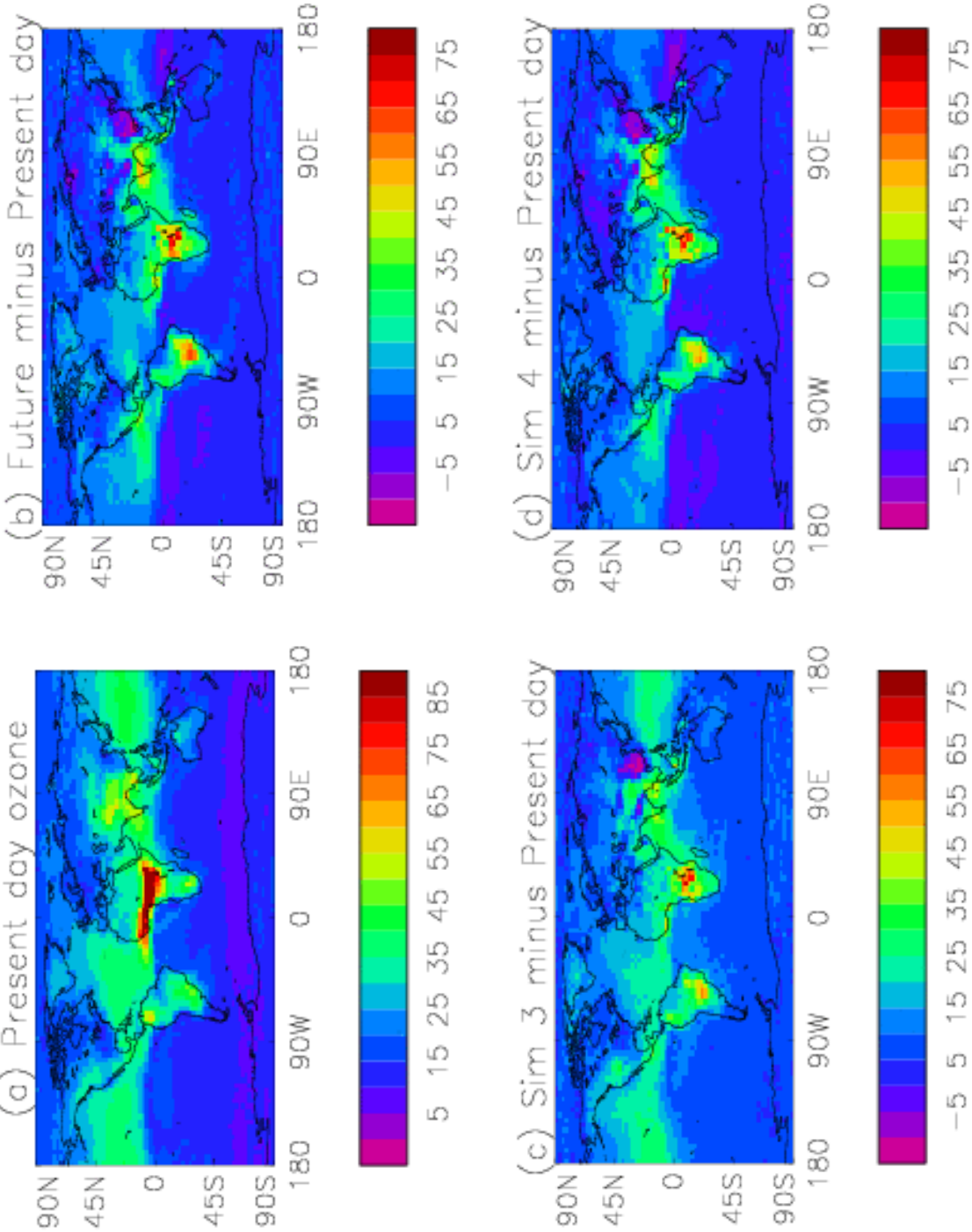


**Figure III-5.** Present day and changes in surface ozone levels for January (ppb).

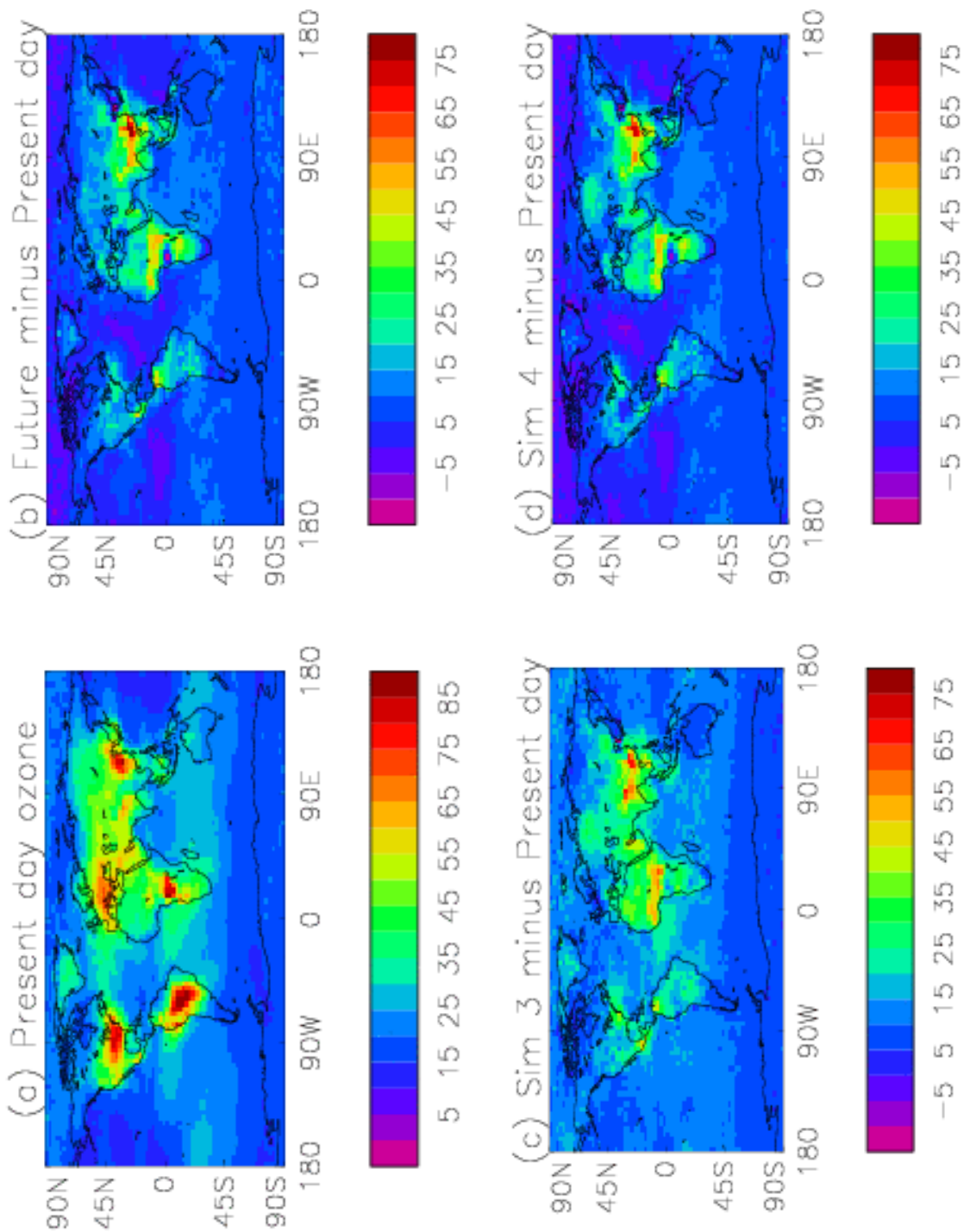


**Figure III-6.** Present day and changes in surface ozone levels for July (ppb).

#### 4. Effect of changes in natural hydrocarbon emissions on surface ozone levels

##### (i) Introduction

Vegetation emits a wide range of hydrocarbons and other VOCs, of which the most important (from a chemistry viewpoint) is isoprene. Isoprene is highly reactive, and has a lifetime of

just a few hours or less in the atmosphere. Isoprene emissions exert a strong control on surface ozone levels, and generally act to increase ozone levels (Wang and Shallcross, 2001; Lee et al., 2006). The emissions of isoprene depend on temperature and light intensity, and are expected to increase in the future as the climate warms.

Methane is produced in significant quantities by wetlands. The production of methane depends on the temperature and moisture content of the wetland, and the type of vegetation, as the depth of the roots affects how much methane is drawn up through the plant and released from the stomata (Gedney et al., 2004). Globally, methane levels control ozone levels (Wild and Prather, 2000), so enhanced methane emissions from wetlands could increase surface ozone levels.

In the following sections, the emissions of isoprene and methane in the future are estimated. Climate change can also cause a shift in the pattern of vegetation (Cox et al., 2000), and the impact of a changed vegetation distribution on modelled surface ozone levels, and the dry deposition of ozone, which is an important removal mechanism, is explored. Finally, the impact of increased isoprene emissions and vegetation pattern changes on modelled future surface ozone levels are investigated.

#### (ii) Emission of isoprene and methane in 2025

The STOCHEM chemistry model was run for 35 years, from 1990 to 2025 continuously, using the interactive methane and isoprene emission schemes described in Chapter I. Over that time the isoprene and wetland methane emissions increased (relative to the emissions predicted for the 1990s) owing to the increased temperatures. The vegetation map used was also regularly updated, using the predictions described by Sanderson et al. (2003). The emission increases are illustrated in Figure III-7. The top panel shows the changes in isoprene emissions. Both positive and negative changes are visible. Although isoprene emissions have declined over much of North America, Europe and Asia, mostly due to vegetation changes, a large increase is predicted from tropical forests. Globally, isoprene emissions are greater in 2025 than 1990.

The biggest changes in methane emissions have occurred in tropical regions (lower panel of Figure III-7), and are all positive, owing to the increased temperatures. By 2025, the impact

of a warmer climate on the higher latitudes doesn't seem to be as large. The change in the zonal mean methane concentrations is shown in Figure III-8. Again, the largest changes are seen in the tropics, where the largest increases in methane emissions are predicted.

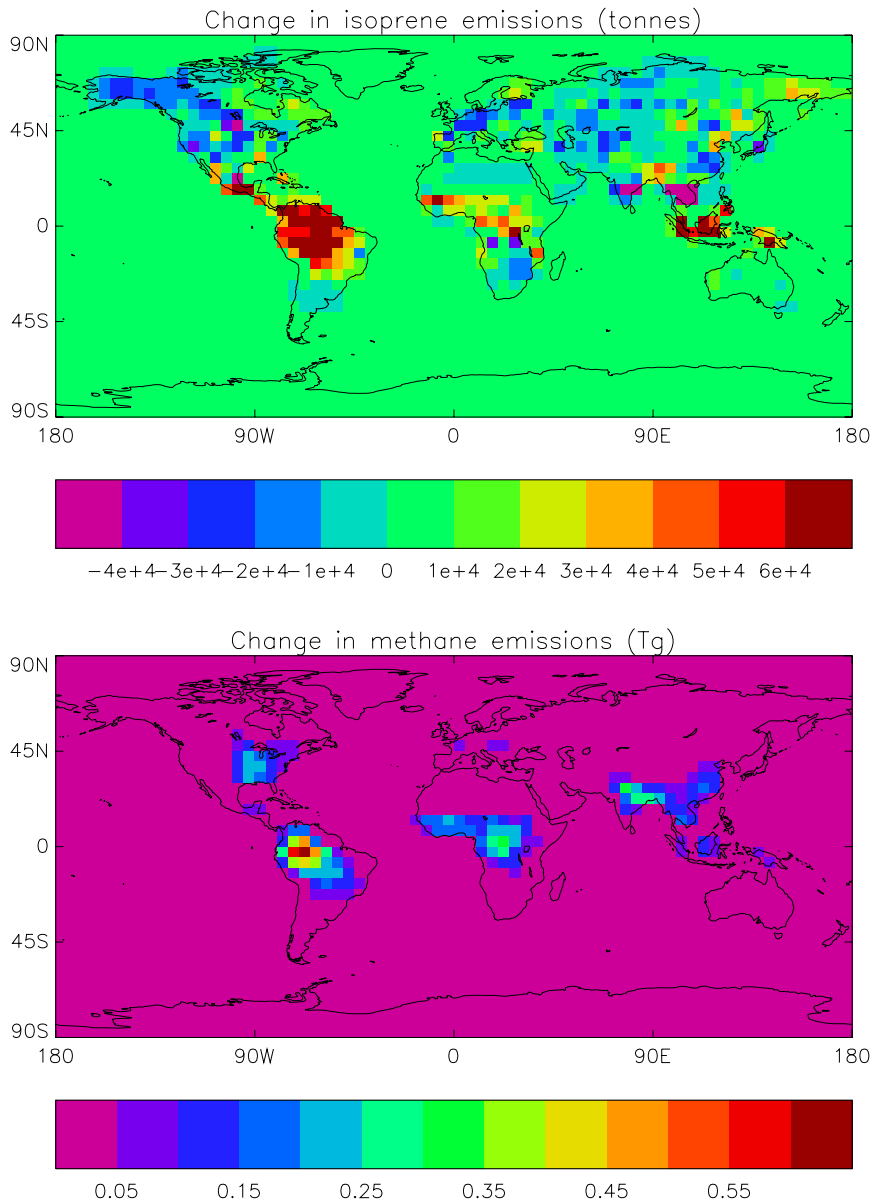


**Figure III-7.** Changes in isoprene emissions (upper panel) and methane emissions from wetlands (lower panel) between 1990 and 2025 due to climate change. A positive value indicates that emissions in 2025 are larger than those in 1990. The differences are annual means in both cases.

The increased isoprene emissions may be expected to impact on the methane levels. Isoprene reacts rapidly with the hydroxyl radical (OH), and reaction with OH is the major sink for methane. The isoprene emissions have increased in the tropics, which is where the majority

of the methane destruction also occurs. OH radical concentrations are largest in the tropics because levels of water vapour and radiation are the largest. Hence the extra isoprene emitted may deplete the OH levels and extend the methane lifetime. However, a comparison of the methane lifetime from this simulation with that from a similar run with no changes in isoprene emissions showed that the lifetime was just 0.1 years longer with the increased isoprene emissions. It is concluded that, by 2025, changes in isoprene emissions have little impact on the methane lifetime.

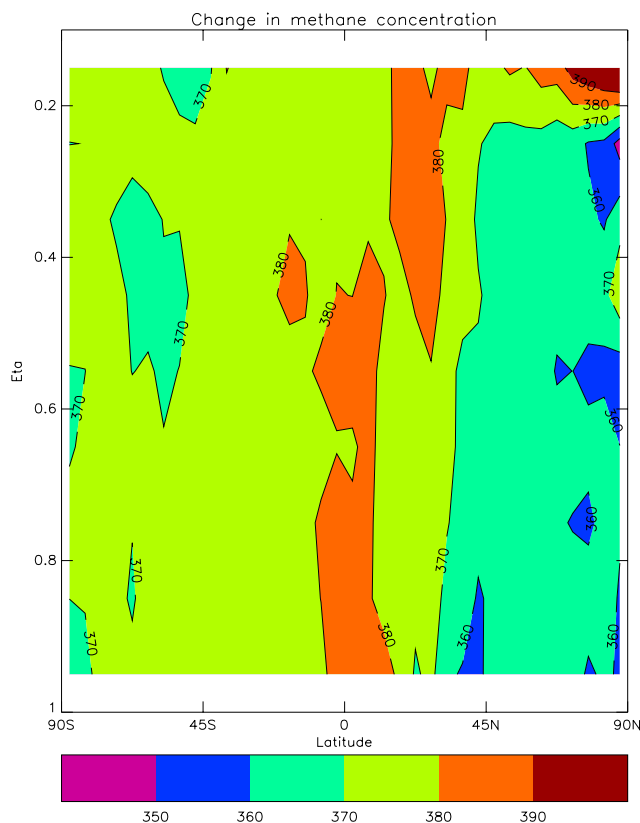


**Figure III-8.** Changes in zonal mean methane concentration between 1990 and 2025 (ppb) owing to increased emissions from wetlands and isoprene emissions. The vertical coordinate decreases from 1.0 at the surface to 0.2 at 200 hPa.

(ii) Effect of vegetation changes on surface ozone levels

In a future climate, with higher temperatures and increased levels of carbon dioxide, a shift in vegetation patterns is likely (for example, Cox et al., 2000). Emissions of reactive gases from vegetation such as isoprene will also respond to climate. In this set of simulations, isoprene emissions were modelled using the well-established algorithms developed by Guenther et al. (1995). To examine the effect of changed vegetation and hence natural hydrocarbon

emissions on surface ozone levels, we have run two experiments using emissions and a climatology for the 2090s, which were identical except for the vegetation maps used. In the first experiment, the vegetation map used was for the 1990s, and in the second the changed vegetation map from Cox et al. (2000) for the 2090s was used. Over Europe, the density of vegetation has increased in the future climate, owing to larger carbon dioxide concentrations and the higher temperatures.

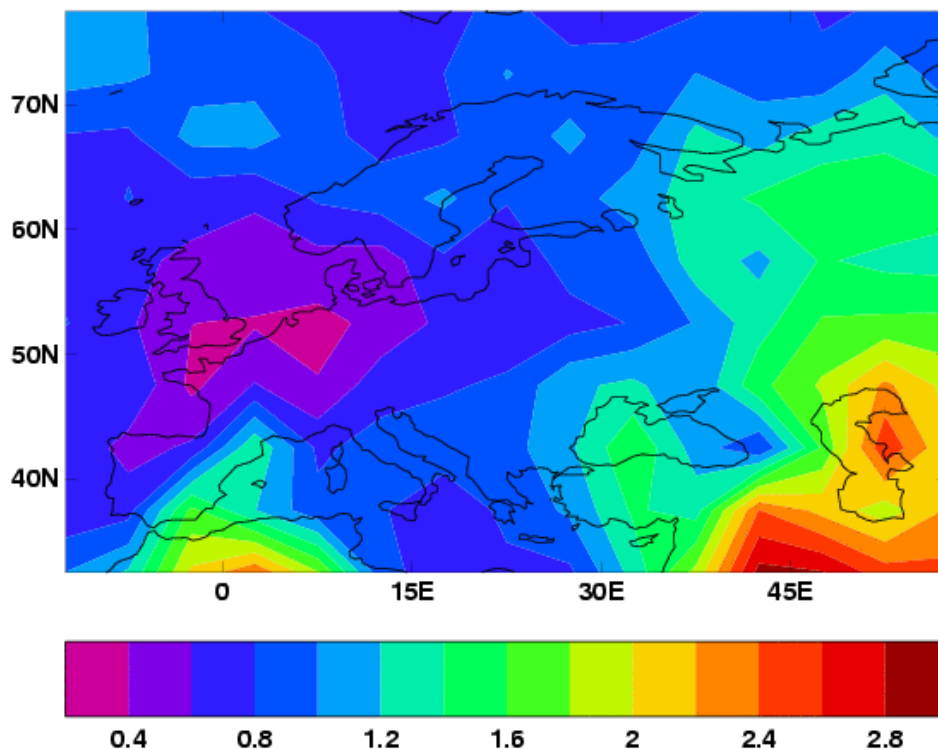


**Figure III-9.** Difference in summertime surface ozone values in ppb between 1990 and 2095.

Figure III-9 shows the difference in the summer surface ozone concentrations between the two simulations. The ozone changes are all positive, indicating that the predicted surface ozone values are greater when the vegetation distribution for the 1990s was used. This result indicates that the larger isoprene emissions from the 2090s vegetation distribution have resulted in a slightly greater rate of ozone destruction. The largest changes are seen over south-east Europe, but are only about 2.6 ppb. Over the majority of Europe, the change in surface ozone levels is 1.6 ppb or less. Hence changes in natural hydrocarbon emissions only have a small impact on predicted future surface ozone levels over Europe.

(iii) Effect of vegetation changes and isoprene emissions on the dry deposition of ozone

In section 4, the effect of changing isoprene emissions alone on future surface ozone levels was examined. Ozone is also dry deposited to the surface. Dry deposition is an important loss mechanism for many trace gases and aerosols. It may be defined as the irreversible uptake of a species at the surface in the absence of precipitation. Further details have been given in Chapter I. Climate change may affect dry deposition via a number of pathways. If a surface becomes wetter or drier, the surface resistance will change, depending on the solubility of the depositing trace gas. Another indirect effect of climate change likely to effect ozone dry deposition is changes in the distribution of vegetation. Any such change will also alter the isoprene emissions from vegetation, which have a significant effect on the chemical production and loss of ozone. Changes in the dry deposition flux of ozone will also affect the surface concentrations.

**Table III-2.** Model runs to assess the effect of climate change on surface ozone levels

Run Number	Climatology	Vegetation	Natural Emissions
1	2090s	2090s	Fixed
2	2090s	1990s	Fixed
3	2090s	2090s	Varying
4	2090s	1990s	Varying
5	1990s	1990s	Varying

To investigate the effect of changing vegetation distribution and isoprene emissions on ozone deposition, five runs with STOCHEM were integrated for 2 years. In all cases, the first year was treated as model spin-up, and results from the second year only were analysed. The first run used a climatology and emissions for the 2090s, and the vegetation map from Cox et al. (2001), where the levels of carbon dioxide had been increased according to the IS92a scenario. One of the main effects predicted by the Hadley Centre model is a drying out of the Amazon region followed by significant dieback of the vegetation (Cox et al., 2001). The second run was identical except that a vegetation map for the 1990s was imposed. The natural isoprene emissions were kept the same (at 2090 levels) in both runs, and were changed on a monthly timescale. The third and fourth runs were identical to the first and second, except that isoprene emissions were calculated interactively every model time step (1 hour in this case), but scaled so that the annual emission was the same in both cases. Finally, the fifth

run was a control, and used a vegetation map and climatology for the 1990s. These runs are summarised in Table III-2. In all cases, methane emissions from wetlands were calculated using the interactive scheme described in Chapter I.

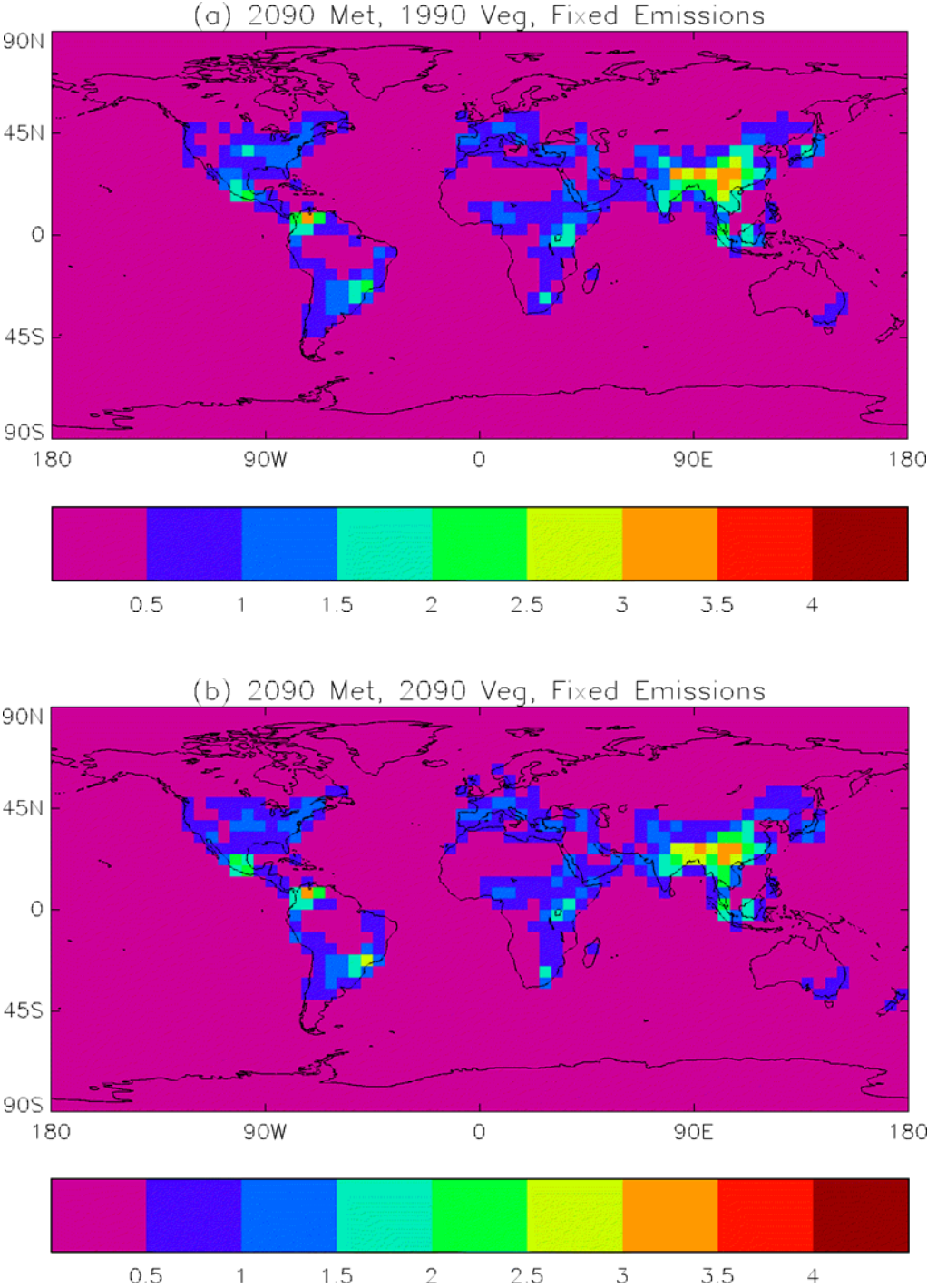


**Figure III-10.** Change in annual ozone dry deposition flux, compared to the 1990s control run, when the isoprene emissions are held at 1990 levels. The scale gives the change in deposition flux in  $\text{Tg O}_3 \text{ yr}^{-1}$ . Top panel, run 2 – run 5. Bottom Panel, run 1 – run 5.

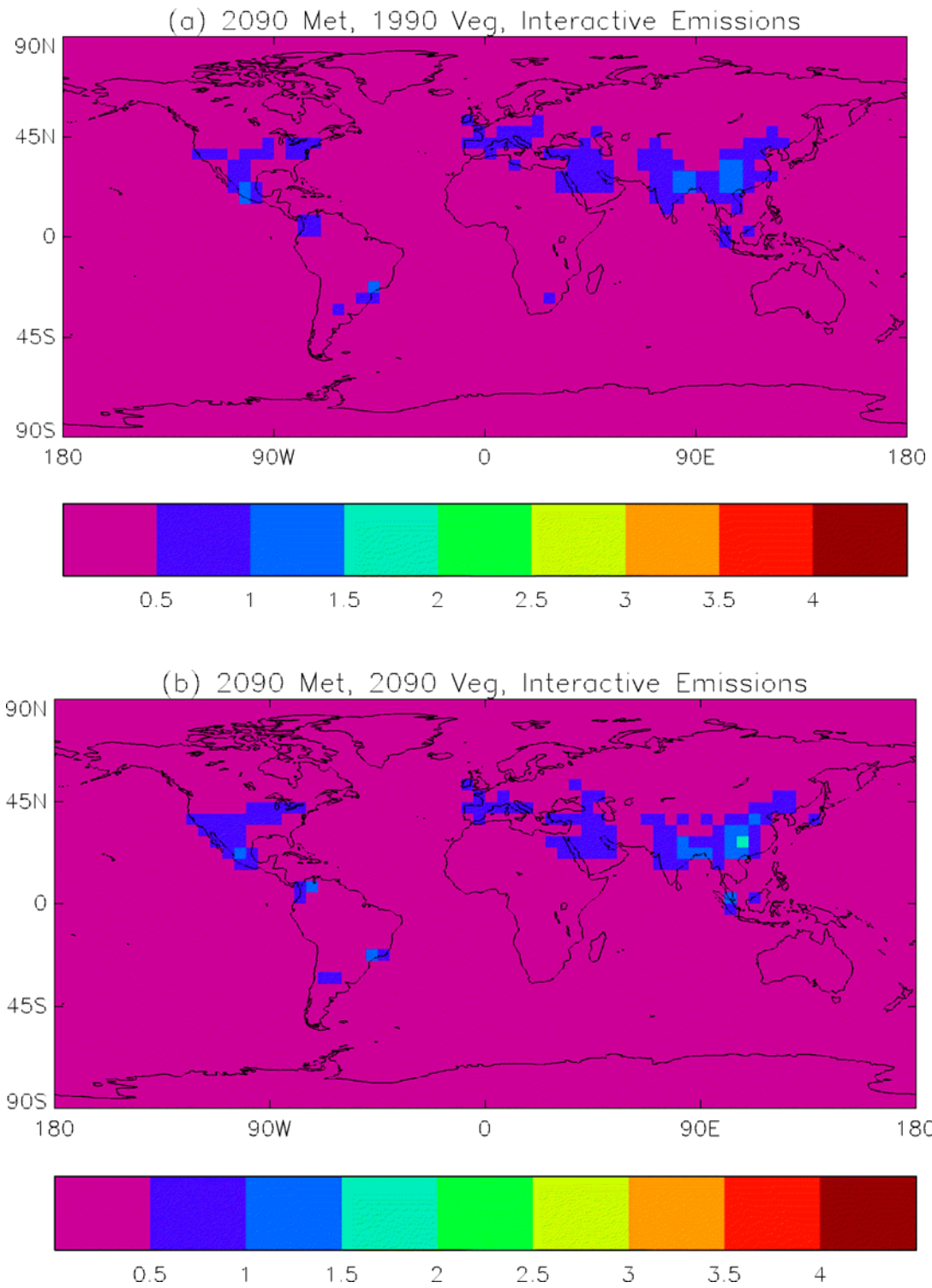


**Figure III-11.** Change in annual ozone dry deposition flux, compared to the 1990s control run, when the isoprene emissions are calculated interactively. The scale gives the change in deposition flux in Tg O<sub>3</sub> yr<sup>-1</sup>. Top panel, run 4 – run 5. Bottom Panel, run 3 – run 5.

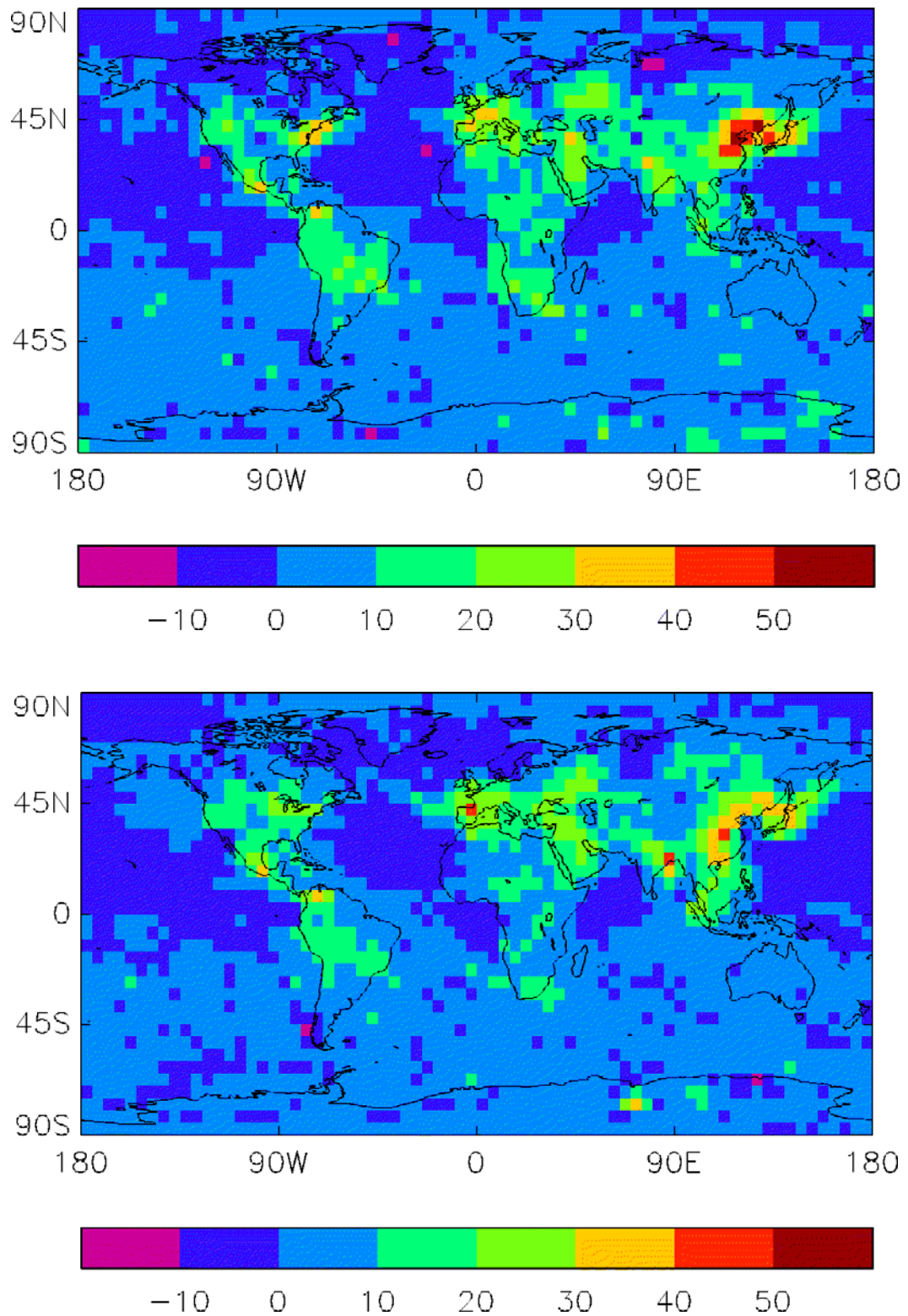


**Figure III-12.** Change in monthly mean surface ozone levels (in ppb) for July between the 2090s and 1990s (a) with fixed vegetation (Top panel, run 4 minus run 5) and (b) with changing vegetation (Bottom panel, run 3 minus run 5).

The changes in annual ozone dry deposition fluxes are shown in Figure III-10 and Figure III-11. There is little difference between each pair of runs with the same natural emissions (varying or fixed) but different vegetation maps (i.e. runs 1 and 2, and runs 3 and 4). Over Europe, 66.4 Tg O<sub>3</sub> yr<sup>-1</sup> are deposited to the surface in the 1990s control run (run 5). First, the two future runs with fixed natural emissions of isoprene (runs 1 and 2) are considered. In run 1, when 2090s (i.e. changed) vegetation is specified, 106.3 Tg O<sub>3</sub> yr<sup>-1</sup> are deposited at the surface over Europe, and 103.7 Tg O<sub>3</sub> yr<sup>-1</sup> when the 1990s vegetation distribution is used (run 2). Slightly more ozone is deposited in the changed vegetation scenario than with fixed vegetation, even though the ozone levels in the climate change scenario are slightly lower. However, the vegetation distribution and ozone levels over Europe are very similar in both runs. Most of the changes in ozone levels have occurred elsewhere. This result indicates that changes in vegetation alone as a result of climate change do not have a large effect on the amount of ozone deposited over Europe.

In the next two experiments (runs 3 and 4), the emissions of isoprene were calculated interactively using the scheme described in Chapter I, and will therefore respond to changes in vegetation cover. Larger differences in surface ozone levels between these two runs were observed at some locations, particularly in the summer months. The changes in surface ozone levels for July in each run are shown in Figure III-12.

When the vegetation distribution for the 1990s was used (i.e. fixed vegetation, run 4), very large summer ozone levels over northern China and Japan, central Europe, and the Eastern USA were predicted, and these levels exceed the WHO health limit of 60 ppb. However, when the changed (i.e. 2090s) vegetation distribution was used (run 3), the summer ozone levels were up to 30 ppb lower in these locations, and a much smaller area exceeded the WHO limit. Despite these changes in surface ozone levels, the amount of ozone deposited globally only decreased by 6.5 Tg yr<sup>-1</sup> when the changed vegetation map was used. The amount of ozone dry deposited over Europe did not change significantly between these two runs, 92.3 Tg yr<sup>-1</sup> in run 3 and 92.7 Tg yr<sup>-1</sup> in run 4.

To summarise, the amount of ozone deposited to the surface of Europe changes significantly between the 1990s and 2090s. The annual flux changes from 66.4 Tg yr<sup>-1</sup> in the 1990s (run 5) to 92.3 Tg yr<sup>-1</sup> (run 3) or 106.3 Tg yr<sup>-1</sup> (run 1). The effect of fixing the isoprene emissions is to increase the ozone deposition flux by 14 Tg yr<sup>-1</sup>, or 15 %. Experiments where the isoprene

emission flux was kept the same, but the vegetation map was changed to that for the 1990s only caused the ozone deposition flux to change slightly. These results show that vegetation changes alone, as a result of climate change, have little effect on the amount of ozone dry deposited over Europe. Changes in emissions of precursor gases have the largest effect on ozone levels and deposition fluxes.

## 5. Effect of increasing levels of carbon dioxide on stomatal conductance and surface ozone concentrations

### (i) Introduction

The levels of carbon dioxide (CO<sub>2</sub>) in the atmosphere have increased over the last 200 years, from about 280 ppm in the pre-industrial era (before 1750) to 375 ppm in the year 2000. This increase in carbon dioxide levels is caused mostly by the burning of fossil fuels, with a smaller contribution from land-use changes (IPCC, 2001). Levels of CO<sub>2</sub> are predicted to rise further unless emissions are reduced substantially. The global mean surface temperature is predicted to rise between 1.2 and 5.8 °C by 2100.

As well as the effect of warmer climate on reaction rates and humidity, as discussed in the previous sections, there is an additional indirect impact of carbon dioxide on ozone levels and ozone deposition fluxes, namely on the stomatal conductance. Stomata are small pores on the surface of leaves, which allow carbon dioxide for photosynthesis to enter the plant, and water to escape. Plant growth generally increases with larger levels of CO<sub>2</sub>, as most are limited by the availability of CO<sub>2</sub> (Taiz and Zeiger, 1991). However, the stomatal conductance falls, as the pores do not need to open as widely to allow sufficient CO<sub>2</sub> to enter the leaf. The water efficiency of the plant will also be increased. Using data published in Taiz and Zeiger (1991) the stomatal conductance was found to fall to 62% of its original value if the current level of CO<sub>2</sub> in the atmosphere was doubled.

Many trace gases are dry deposited to vegetation, where they are taken up by the leaf surface (cuticles), the stems and branches, and also via the stomata. Consequently, as CO<sub>2</sub> levels rise, the dry deposition fluxes of trace gases such as ozone, NO<sub>2</sub> and SO<sub>2</sub> will fall, as the stomatal conductance will also decrease. The surface concentrations of depositing trace gases may therefore rise. This effect of CO<sub>2</sub> on dry deposition may also be important for assessing damage to plants by ozone deposition in the future.

(ii) Model simulations

An atmosphere-only version (HadGAM1) of the Hadley Centre’s climate model HadGEM1 (Johns et al., 2004) was coupled to the STOCHEM chemistry model. The version of STOCHEM used for this work has the same model of natural hydrocarbons as described above. Dry deposition fluxes of trace gases are calculated using a “big leaf” multiple resistance model (Smith et al., 2000).

Three model simulations were used to assess the effect of increasing CO<sub>2</sub> levels on stomatal conductance, surface trace gas concentrations, and two air pollution metrics. They are summarised in Table III-3. First, a control simulation (number 1) was run, which used a climatology and CO<sub>2</sub> levels for the year 2000. The second simulation involved the calculation of two stomatal conductances, using current and doubled levels of CO<sub>2</sub>. The stomatal conductances calculated using doubled CO<sub>2</sub> levels were only passed to STOCHEM for use in the dry deposition module. In the third simulation, the stomatal conductance was calculated using doubled CO<sub>2</sub> levels only, and was used in both the climate model and STOCHEM. In this third case, the water vapour concentration at the surface may change, owing to reduced transpiration, and hence changes in cloud amount, precipitation, and meteorology are likely. In all the simulations, anthropogenic emissions of primary pollutants were taken from the IIASA CLE scenario for the year 2000 (Dentener et al., 2005). This scenario reflects the current perspectives of individual countries on future economic development and takes into account the anticipated effects of presently decided emission control legislation in individual countries.

**Table III-3.** Summary of model simulations

Simulation	Stomatal conductance used:	
	STOCHEM	GCM
1	1xCO <sub>2</sub>	1xCO <sub>2</sub>
2	2xCO <sub>2</sub>	1xCO <sub>2</sub>
3	2xCO <sub>2</sub>	2xCO <sub>2</sub>

In all simulations, to save time spinning up the model, and to help constrain the results, global methane mixing ratios were specified across the model domain, using results from a previous model integration using the same emission scenario (Dentener et al., 2005; Stevenson et al.,

2005a). This approach has been used recently for a multi-model ensemble prediction of current and future tropospheric ozone changes (Stevenson et al., 2006). Each model simulation lasted for 16 months.

(iii) Changes in stomatal conductance

The changes in stomatal conductance between simulations 1 and 2, averaged over all vegetation types, are shown in Figure III-13. A negative value indicates that the stomatal conductance is smaller in simulation 2 (which has doubled CO<sub>2</sub> levels) than simulation 1. In all areas of the globe, the changes are negative, indicating that the stomatal conductance is smaller when doubled CO<sub>2</sub> levels are used. The conductance is generally 0.5 – 1.5 mm s<sup>-1</sup> smaller over large parts of the land masses in all four seasons.

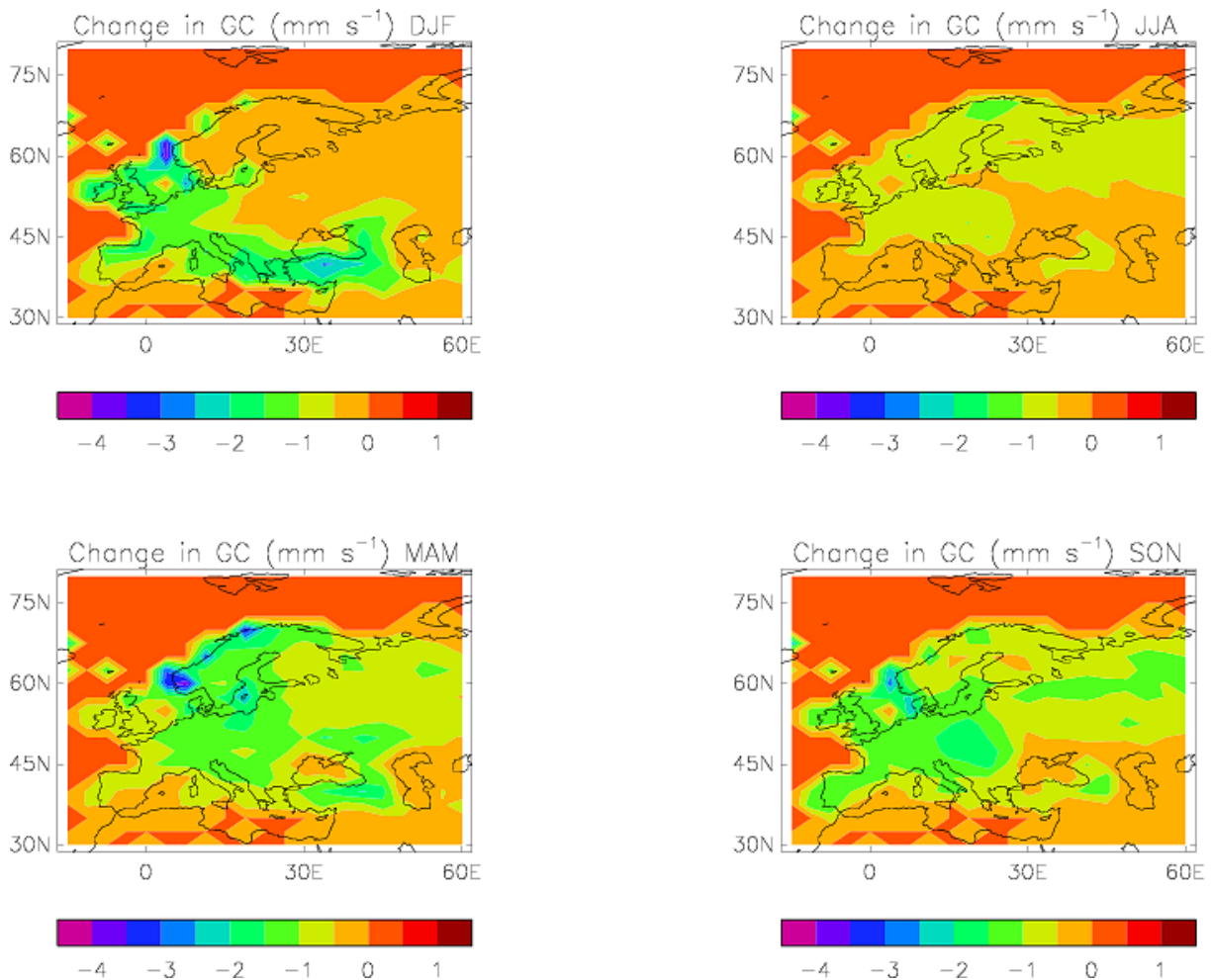


**Figure III-13.** Changes in seasonal mean stomatal conductance GC (mm s<sup>-1</sup>) for winter (DJF), spring (MAM), summer (JJA) and autumn (SON) when the CO<sub>2</sub> level is doubled. A negative value indicates that the stomatal conductance is smaller in simulation 2 than simulation 1. See Table III-3 and text for more details.

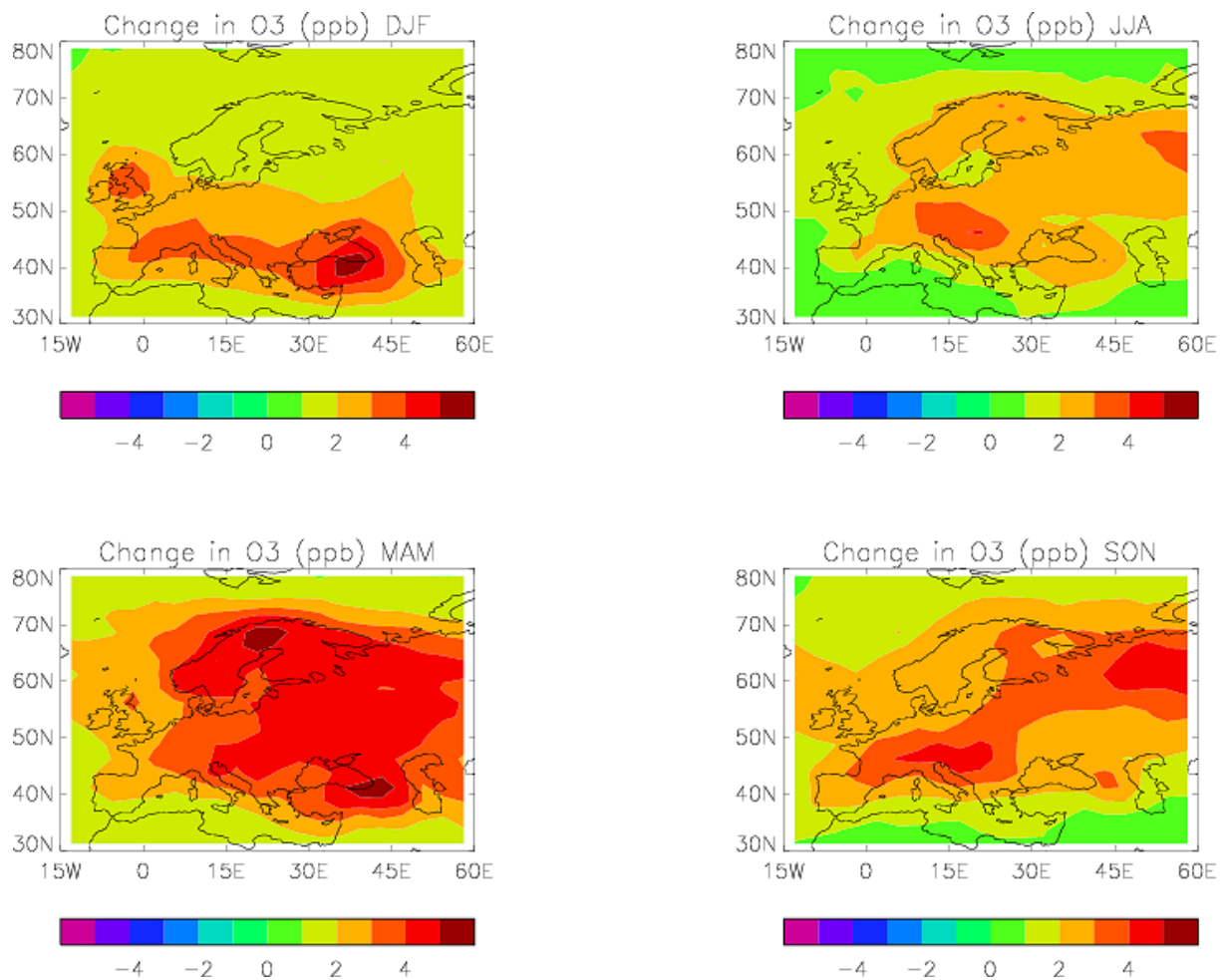


**Figure III-14.** Changes in seasonal mean surface ozone concentrations (ppb) for winter (DJF), spring (MAM), summer (JJA) and autumn (SON) when the stomatal conductance calculated using a doubled  $\text{CO}_2$  value is passed to the chemistry model. A positive value indicates that the ozone levels are larger in simulation 2 than simulation 1. See Table III-3 and text for more details.

The changes in surface ozone levels between simulations 1 and 2 in the four seasons are shown in Figure III-14. These changes demonstrate the effect of reduced stomatal conductances (and hence smaller dry deposition fluxes) on surface ozone levels caused by doubled  $\text{CO}_2$  concentrations, but with no change in meteorology. In all four seasons, the ozone levels are larger, by up to 8 ppb, although a change of 3 – 4 ppb is seen over the majority of the northern hemisphere land masses. A comparison of Figures III-13 and III-14 shows that areas with increased surface ozone levels are approximately correlated with areas that have reduced stomatal conductance. This result demonstrates that deposition to plants via the stomata is an important loss mechanism for ozone.

The distributions of the changes in surface ozone levels are very different in each season. The largest changes are seen in the spring (MAM), when most of the vegetation and crops are growing, and the stomata will be fully open. In this case, the surface ozone levels are 3 – 5 ppb larger over most of Europe. Changes of similar magnitude are also seen in the autumn (SON). The smallest impact of the doubled CO<sub>2</sub> levels on stomatal conductance is seen in the summer (JJA). The deposition flux of ozone via the stomata is smallest during this period, reflecting the drier soils.

Changes in the surface levels of other important pollutants, such as nitrogen oxides (NO<sub>x</sub>, NO + NO<sub>2</sub>) and peroxyacetyl nitrate (PAN) were also examined. Both of these species play an important role in ozone formation, and are also dry deposited. However, there was essentially no change in the surface levels of NO<sub>x</sub> and PAN. In the present work, the change in the dry deposition fluxes of NO<sub>x</sub> and PAN is clearly too small to impact on their modelled concentrations. The reduced stomatal conductance therefore appears to have little effect on the concentrations of NO<sub>x</sub> and other species containing oxidised nitrogen.

In simulation 3, doubled CO<sub>2</sub> levels were used to calculate stomatal conductances for the land surface exchange of water vapour as well as ozone. The rate of transpiration of water from plants, and hence surface water vapour concentrations, will be reduced, with consequent changes in cloud cover, surface temperature, and meteorology. A comparison of results from simulations 1 and 3 will show the difference in surface concentrations of trace gases caused by both meteorology and dry deposition changes. The changes in stomatal conductance between simulations 1 and 3 are different to those modelled in simulations 1 and 2, owing to increased levels of soil moisture. The patterns of the changes are broadly similar to those shown in Figure III-13, but the differences are smaller. As an example of the changes in the state of the modelled atmosphere, the differences in seasonal mean specific humidity in the lowest model layer are shown in Figure III-15. A negative value indicates that the humidity in simulation 3 is smaller than in simulation 1. These four plots are “noisy”; to fully assess the impact of changed stomatal conductance on the meteorology, longer simulations (e.g. 10 years) would be needed. Both positive and negative changes are simulated. Overall, the specific humidity at the surface in simulation 3 is smaller than in simulation 1, as expected, owing to reduced transpiration by vegetation caused by smaller stomatal conductances. There is some similarity in the patterns of changes in the stomatal conductances and specific

humidity, which can be seen by comparing Figure III-13 and Figure III-15. Generally, where the conductance is reduced, the humidity has fallen.

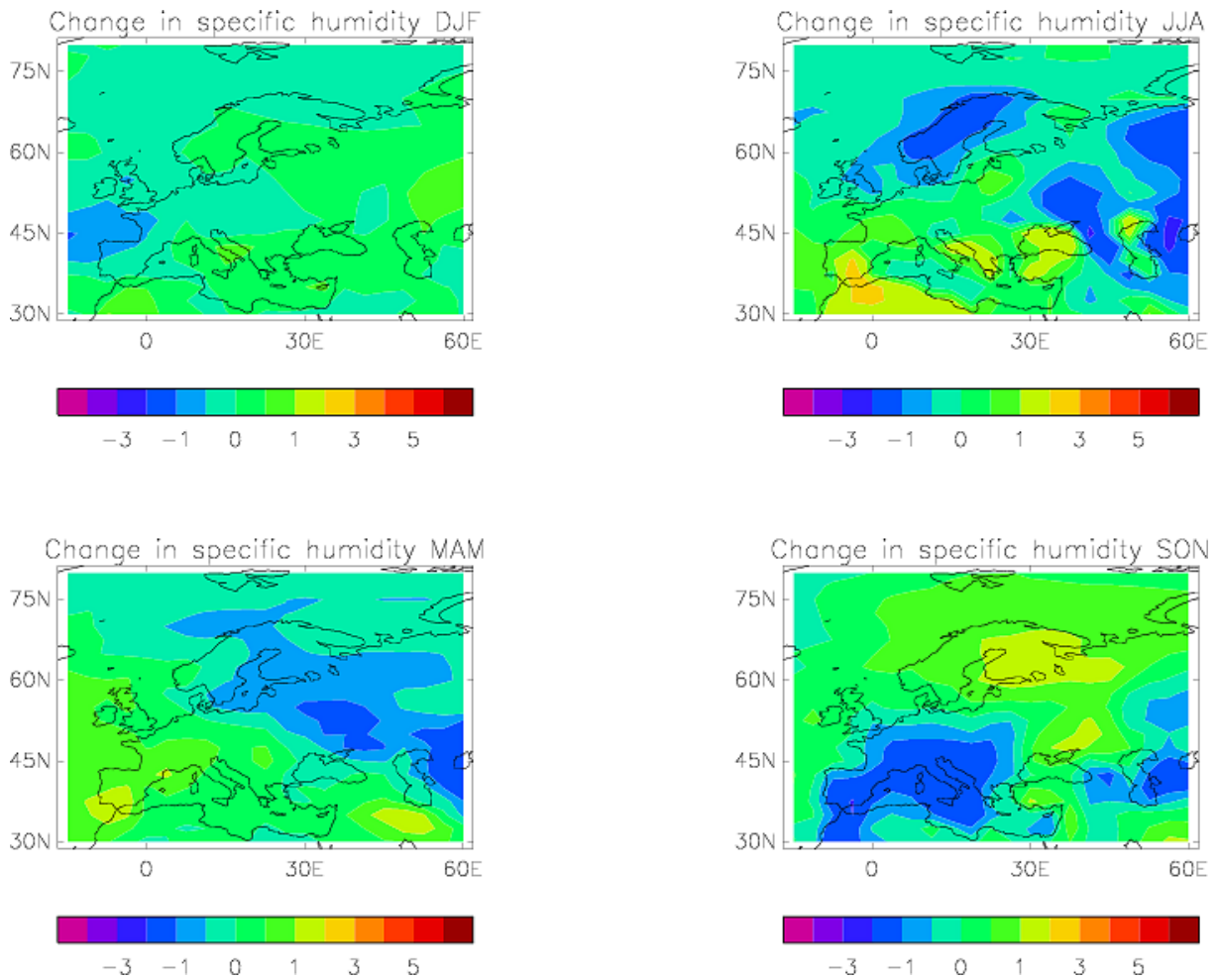


**Figure III-15.** Changes in specific humidity ( $\text{g}(\text{H}_2\text{O}) / \text{kg air}$ ) in the lowest model layer between simulations 3 and 1 for winter (DJF), spring (MAM), summer (JJA) and autumn (SON). A negative value indicates that the humidity in simulation 3 is smaller than that in simulation 1. See Table III-3 and text for more details.

The changes in surface ozone values between simulations 1 and 3 are shown in Figure III-16, and are very different to those in Figure III-14. There are many areas with reduced ozone levels, as well as areas with larger ozone levels. Again, much longer simulations would be needed to fully assess the impact of changed meteorology on the ozone levels. These changes will be caused by differences in humidity and meteorology as discussed previously, as well as a reduced dry deposition flux. The greatest ozone increases are now seen in the summer (JJA) over much of Europe, and are as large as 16 ppb. Smaller increases in ozone levels between 8 and 10 ppb are also seen in spring and autumn. However, there are areas

experiencing a reduction in surface ozone levels in the same time period, most notably over Western Europe in winter, and the North Sea and Scandinavia in summer. Part of the reason for the increased ozone levels is the reduced water vapour concentrations (caused by reduced transpiration from plants) which in turn result in less ozone removal via the reaction of  $O(^1D)$  with water vapour. There is no real correlation between the changes in humidity shown in Figure III-15, and the ozone levels in Figure III-16, suggesting that differences in meteorology and hence transport of pollutants are responsible for the majority of the ozone changes.

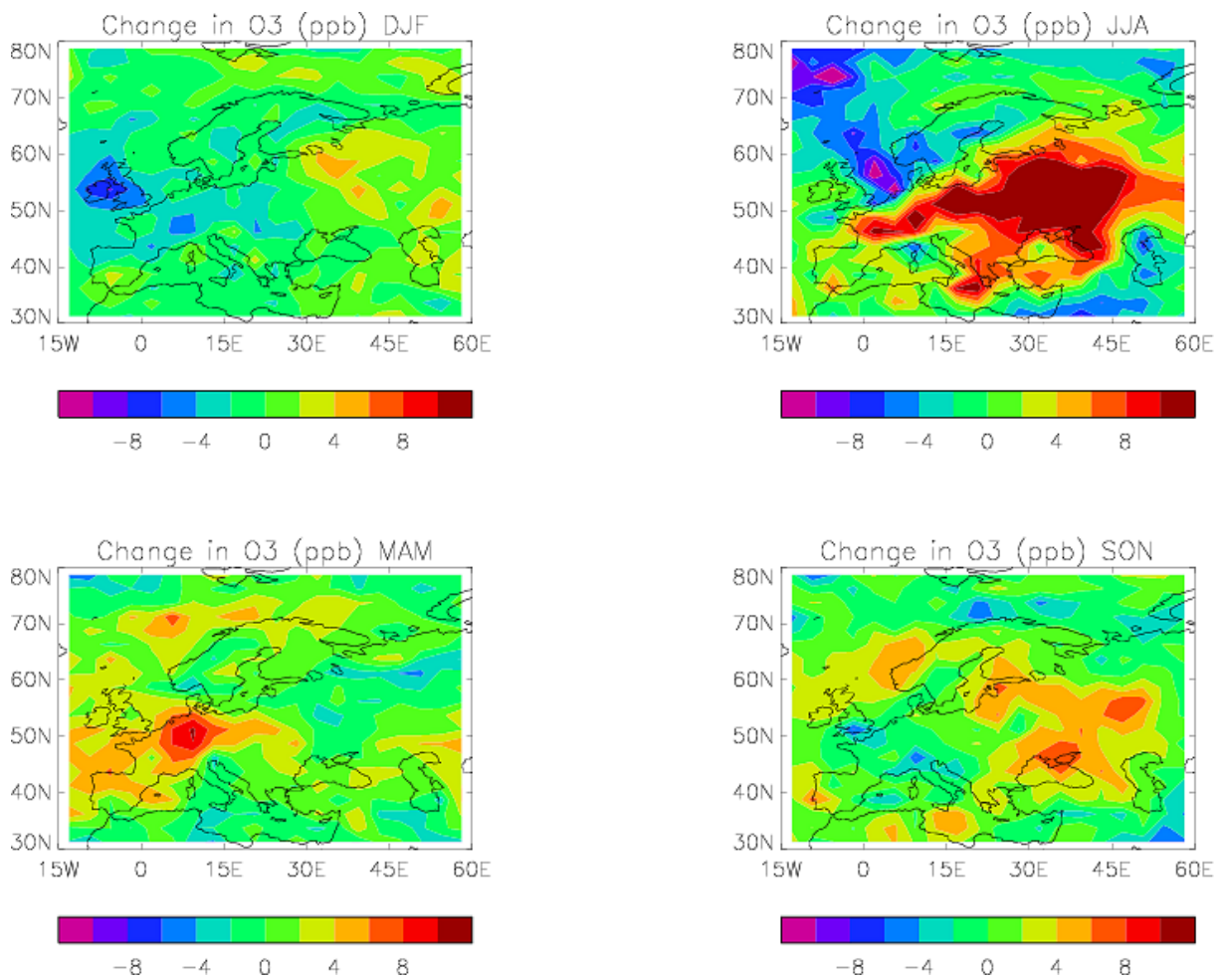


**Figure III-16.** Changes in seasonal mean surface ozone concentrations (ppb) for winter (DJF), spring (MAM), summer (JJA) and autumn (SON) when the stomatal conductance calculated using a doubled  $CO_2$  value is passed to the entire model. A positive value indicates that the ozone levels are larger in simulation 3 than simulation 1.

The changes in the surface concentrations of other trace gases were also investigated (data not shown).  $NO_x$  levels did not change significantly between simulations 3 and 1, except over

parts of northern Europe, where they were 2 – 4 ppb larger; these areas correspond to areas with reduced ozone levels in Figure III-14. PAN levels were nearly the same in each simulation, and the magnitude of the largest changes in each season was less than 1 ppb. As was discussed briefly above, ozone deposited via the stomata causes damage to the interior of the plant, reducing photosynthesis and growth, and, in the case of crops, significant reductions in yield will occur. For example, it has been estimated that reductions in NPP (net primary productivity) between 2.6 and 6.8 % have occurred in the U.S.A. during the period 1988-2000 owing to ozone damage (Felzer et al., 2004). Wang and Mauzerall (2004) estimated that in east Asia, ozone damage was responsible for reductions in wheat yields of 1 – 9 %, with an associated value of 3.5 billion US\$ for 1990. Greater reductions in crop yields, particularly in Europe, China and the U.S.A., are likely in the future if ozone levels are not controlled (Felzer et al., 2003; Wang and Mauzerall, 2004).

#### (iv) Changes in ozone damage metrics

Until recently, the metric AOT<sub>40</sub> has been used to assess possible damage to vegetation by ozone. The AOT<sub>40</sub> metric may be defined as the sum of the differences between hourly ozone concentrations and 40 ppb for each hour when the concentration exceeds 40 ppb during the relevant growing season (Ashmore et al., 2004). However, this metric is based purely on observed ozone concentrations. It cannot take into account the actual flux of ozone entering the plant via the stomata. If the plant is experiencing drought conditions, the stomatal openings will be small or even closed completely. Hence, for a given set of ozone concentrations, the AOT<sub>40</sub> metric will be the same, but the actual amount of ozone taken up by the plant will be very different, depending on the soil moisture. A new air pollution metric, referred to as CUO (cumulative stomatal uptake of ozone) has recently been derived (Pleijel et al., 2004). This scale uses the cumulative uptake of ozone over a given period of time, and therefore will be controlled by both the ozone concentration and the stomatal conductance. The CUO metric has been shown to give a better correlation with crop yield than the AOT<sub>40</sub> scale (Pleijel et al., 2004). A comparison between the AOT<sub>40</sub> and CUO scales for predicting damage to trees by ozone was made by Matyssek et al. (2004). Although the two scales did correlate well, there was considerably more scatter in the comparison of the observed yields with the AOT<sub>40</sub> values than the CUO figures.

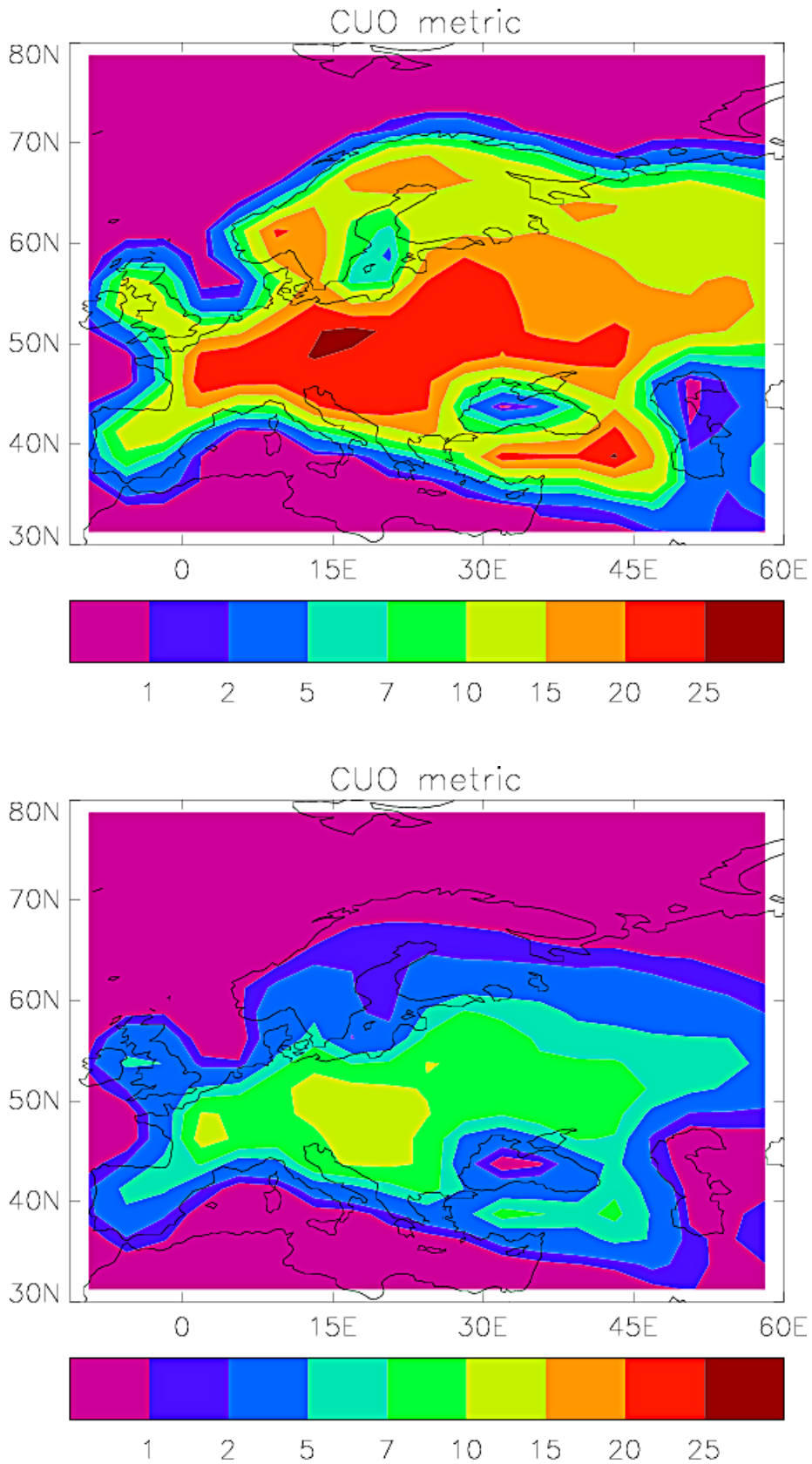


**Figure III-17.** CUO metric calculated from simulation 1, control run (top panel), and simulation 2 (lower panel). See Table V and text for more details.

The CUO values calculated over Europe from simulations 1 (control) and 2 are shown in Figure III-17 (see also Table III-3). In this instance, it has been assumed that the growing season in Europe lasts from March to May. For the control simulation, the CUO values range from 5 to 25 (Figure III-17, top panel). Pleijel et al. (2004) calculated values between 2 and 10 for various sites in Europe using the EMEP model for the 1990s.

The CUO values for simulation 2 are shown in the lower panel of Figure III-17. It is clear that they are much smaller than those from the control simulation, owing to the reduced ozone deposition fluxes resulting from smaller stomatal conductances in response to the increased CO<sub>2</sub> levels. In this instance, AOT<sub>40</sub> values would be larger than the control simulation, owing to the increased surface ozone concentrations. The CUO and AOT<sub>40</sub> metrics will therefore give different indications about the damage to vegetation. The AOT<sub>40</sub> values, as they have risen, imply that more damage is being done to the plants, whereas the CUO values, based on the actual stomatal uptake of ozone, indicate that less damage is being done.

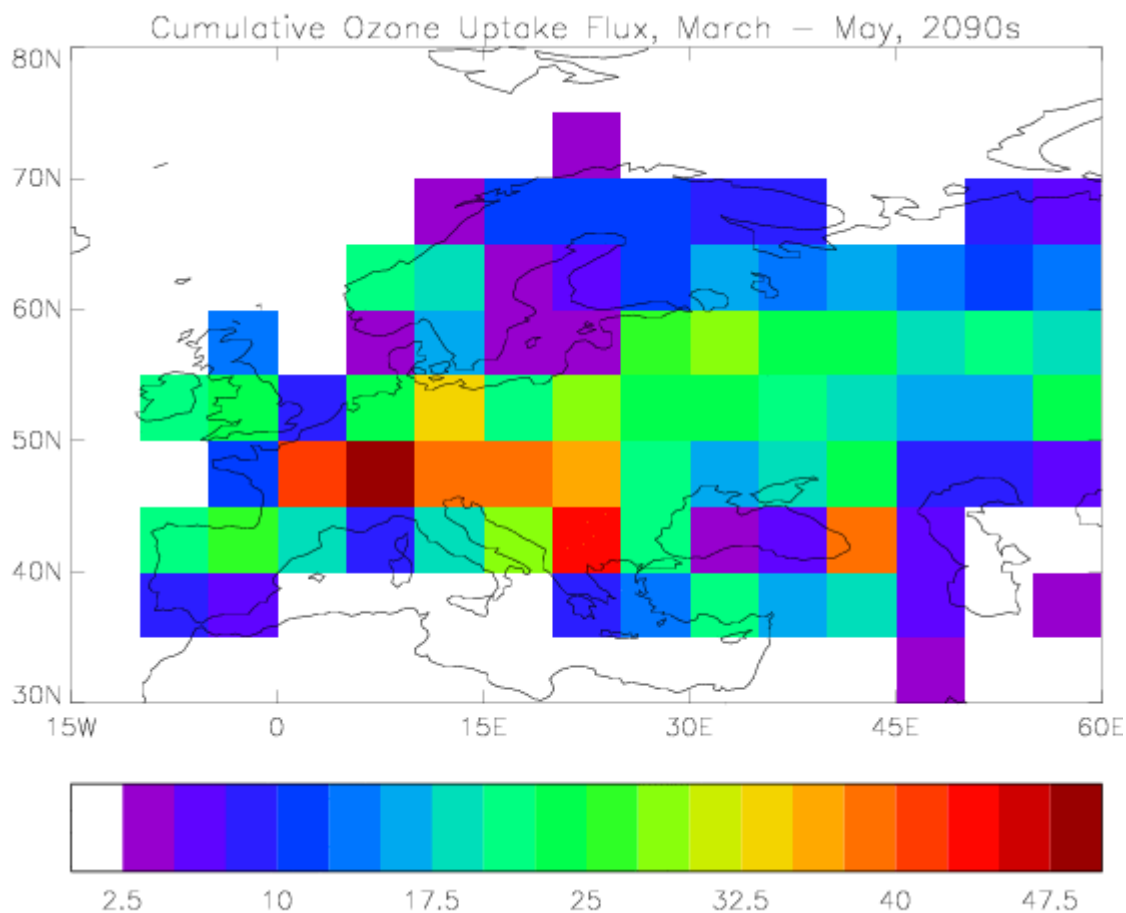


**Figure III-18.** Cumulative ozone uptake flux over Europe for the period March to May, 2090s. The CUO flux is expressed in units of  $\text{mmol m}^{-2}$ .

CUO values have also been calculated for the 2090s, and are shown in Figure III-18. The magnitudes are larger than those for the present day in Figure III-17, owing to the greater surface ozone levels modelled in the 2090s. The largest values are over central Europe, with smaller values found in coastal regions.

In the above calculation, no account of plant damage was included. There are two complex interactions which could occur if plant damage is considered. First, the rate of growth of plants, and hence CO<sub>2</sub> uptake and moisture input into the boundary layer via transpiration will be reduced, which could impact on the climate and surface chemistry. Secondly, damaged plants will take up less ozone owing to reduced transpiration, and so surface ozone levels could increase further as the overall surface sink for ozone will be reduced in magnitude. These interactions will be the subject of future studies.

## 6. Changes in emissions of nitrogen oxides (NO<sub>x</sub>)

### (i) NO<sub>x</sub> production by lightning

Lightning is generated in large convective clouds, and produces significant amounts of nitrogen oxides in the atmosphere, which contribute between 8 and 16 % of the global total NO<sub>x</sub> production (IPCC, 2001). Significant amounts are produced near the tropopause and the surface, which can have an important effect on ozone levels. In STOCHEM a parameterization whereby NO<sub>x</sub> emissions over land are proportional to the 5<sup>th</sup> power of the convective cloud height (Price and Rind, 1992) has been implemented.

STOCHEM was integrated using anthropogenic emissions suitable for the 1990s, but climatologies for the 1990s and 2090s. Biomass burning emissions were also kept constant in both runs. The effect of any changes in lightning emissions may be found by comparing results from these two runs. The production of NO<sub>x</sub> by lightning is expected to increase in the future, since a warmer land surface should induce more vigorous convection. However, it was found that the production decreased slightly, from 9.3 Tg(N) yr<sup>-1</sup> in the 1990s to 9.1 Tg(N) yr<sup>-1</sup> in the 2090s. The pattern of this change can be seen in the top left plot of Figure III-19. While emissions have increased over much of the land area as expected, lightning NO<sub>x</sub> has decreased over the Amazon region. The reason for this is a positive feedback in the climate model of declining precipitation and decreasing vegetation cover in the Amazon (Cox et al., 2000). In this climate model prediction, the Amazon dries out, resulting in less vigorous convection and hence less lightning. The climate change impact on lightning is the

dominant factor in the changes in  $\text{NO}_y$  deposition, tropospheric ozone column and the surface deposition of ozone (see Figure III-19). Biogenic emissions and deposition also respond to the changing climate. Changes in the  $\text{NO}_y$  deposition over the ocean are due to changes in the precipitation patterns. Ozone dry deposition is also affected by changing vegetation amounts and surface characteristics, as has been described in detail in section 4.

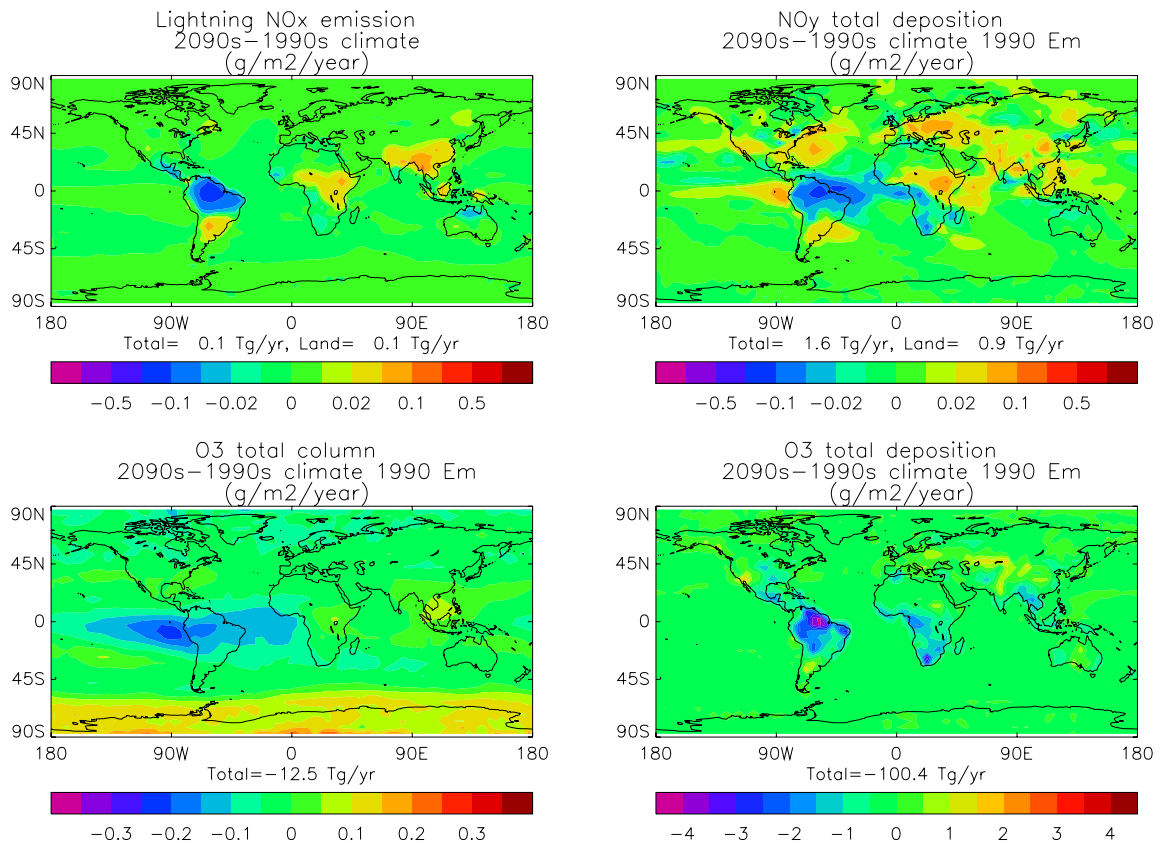


**Figure III-19.** Effect of climate change on production of  $\text{NO}_x$  by lightning,  $\text{NO}_y$  deposition flux, total ozone column and the ozone dry deposition flux. The data shown above have been averaged over 5 years.

The STOCHEM model was integrated again using the climate and emissions for the 2090s, but without production of  $\text{NO}_x$  by lightning. The changes in summer surface ozone levels are shown in Figure III-20. Negative values indicate that the ozone levels have fallen when the lightning  $\text{NO}_x$  emissions are neglected. Ozone levels have fallen over all of Europe, but the largest changes are only 2.0 – 2.5 ppb over eastern and parts of southern Europe. Over northern and western Europe, the changes are only 1 ppb or less. This result suggests that production of  $\text{NO}_x$  by lightning does not have a significant impact on summer surface ozone levels over Europe.

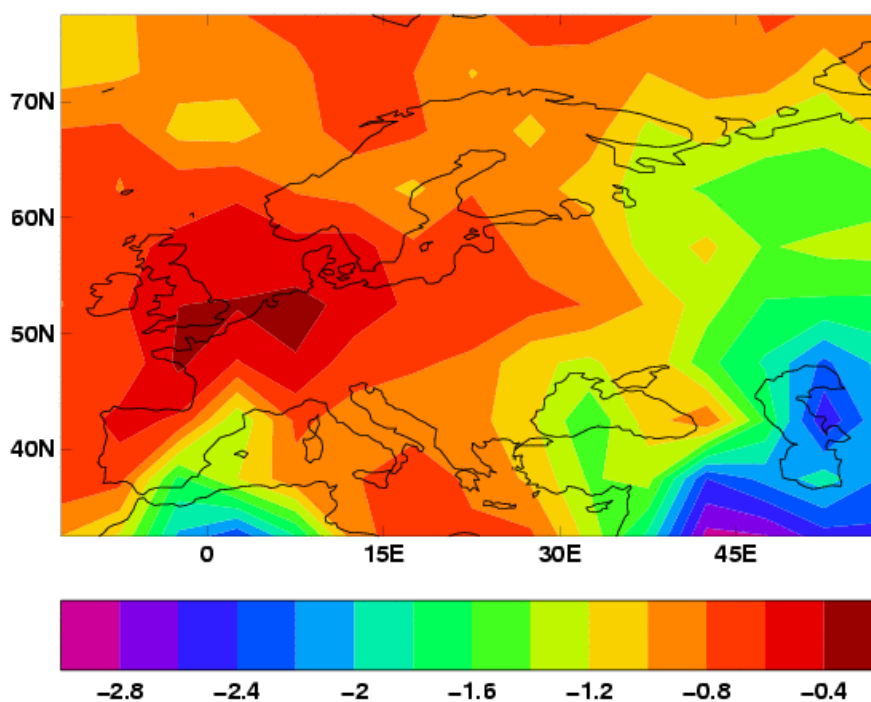


**Figure III-20.** Change in 2090s summertime ozone levels when production of  $\text{NO}_x$  by lightning is neglected. Units are ppb.

(ii) Effect of anthropogenic  $\text{NO}_x$  emission changes on surface ozone levels

Nitrogen oxides are major primary pollutants. At their source, they exist as  $\text{NO}$  only, but once emitted, part conversion to  $\text{NO}_2$  occurs rapidly. Substantial reductions in emission of this pollutant are required in the DEFRA air quality strategy. We have used the STOCHEM model to assess the effect of a 50 % reduction in global anthropogenic  $\text{NO}_x$  emissions on current summer ozone levels. The change in ozone values over Europe resulting from such a reduction are shown in Figure III-21. A negative value indicates that the ozone levels have fallen as a result of reducing the  $\text{NO}_x$  emissions. The biggest changes are seen over Spain and the eastern Mediterranean and beyond, where the ozone levels have fallen by 6 – 10 ppb. Interestingly, the ozone values over the North Sea and Scandinavia have risen by 4 – 6 ppb. This increase seems to be due to reduced titration of  $\text{OH}$  by  $\text{NO}_2$ , resulting in higher  $\text{OH}$  levels, and consequently more oxidation of primary VOCs to produce peroxy radicals that oxidise  $\text{NO}$  to  $\text{NO}_2$ , which in turn readily photolyses to produce ozone. Reductions in emissions of hydrocarbons and carbon monoxide as well as  $\text{NO}_x$  may be needed to achieve the required reductions in surface ozone levels over the U.K.

It has been shown that climate change, emissions and other atmospheric processes exert an important influence on the summertime surface levels of ozone over Europe. Climate change, resulting in higher temperatures and higher amounts of water vapour, acts to reduce the modelled levels of ozone by 8 – 14 ppb. Reducing the anthropogenic emissions of  $\text{NO}_x$  by 50 % reduced ozone levels over most of Europe by 4 – 10 ppb, but the ozone levels increased slightly in a few locations. Vegetation changes and in turn isoprene emissions as a response to climate change had a small effect on ozone levels over Europe, where the ozone levels only changed by 4 ppb or less. The interaction between climate, emissions and chemistry is highly complex. Significant reductions in emissions of ozone precursors do not necessarily yield large decreases in surface ozone levels.

The current predictions of present day surface summertime ozone levels using STOCHEM lie within the range 40 – 50 ppb. Most of the predictions of 2090s surface levels are well above this range, up to 90 ppb in a few locations. Although climate change and possibly vegetation changes act to reduce the ozone levels to some extent, considerable effort will be needed if the air quality targets are to be met.

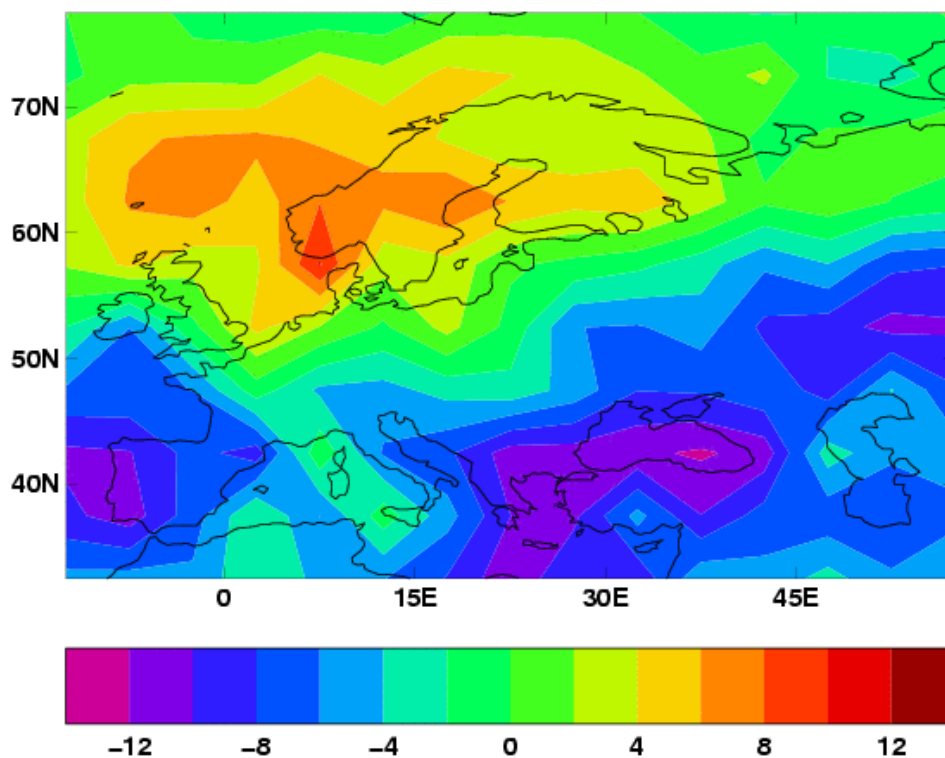


**Figure III-21.** Change in present day summertime ozone levels when anthropogenic emissions of  $\text{NO}_x$  are reduced by 50 %. Units are ppb.

## **(b) Scenario Assessment and Interaction with IIASA**

### 1. Introduction

The effect of climate change in its various forms on surface ozone levels has been investigated in part (a) above. In this part, further experiments exploring the effects of emissions changes on surface ozone levels over Europe are presented and discussed. The IIASA scenarios CLE and MFR, described in more detail in Chapter I, are used throughout.

### 2. Relationship between surface levels of O<sub>3</sub>, NO<sub>2</sub> and NO over Europe

Ozone changes over Europe between the years 2000 and 2030 have already been reported. Here, we show further analysis of these results, focusing on levels of NO<sub>x</sub> (the sum of the concentrations of NO and NO<sub>2</sub>), O<sub>3</sub> and total oxidant, OX (the sum of the concentrations of O<sub>3</sub> and NO<sub>2</sub>) over Europe. By using measurements of NO, NO<sub>2</sub> and O<sub>3</sub> in urban environments, and plotting observed OX levels as a function of NO<sub>x</sub> for daylight hours only, Clapp and Jenkin (2001) and Mazzeo et al. (2005) obtained a linear relationship between these two quantities. The data at the lowest levels of NO<sub>x</sub> were not used in their analyses, as the linear relationship does not hold there. The positive intercept on the ordinate axis gives the regional contribution to oxidant levels, and the difference between the intercept and the OX level is the local contribution to total oxidant. The more important quantity is the regional contribution to OX levels, which can therefore be found by extrapolating the linear relationship from higher NO<sub>x</sub> values to zero NO<sub>x</sub>. At this level, all the oxidant will be O<sub>3</sub>. This relationship is illustrated in an idealised form in Figure III-22.

The same analysis is applied to monthly mean levels of OX and NO<sub>x</sub> generated from STOCHEM over Europe, to see if a similar relationship is present on a regional scale. If so, it would be a useful tool for policy makers. Only results from a present-day integration, which used emissions from the IIASA CLE scenario for the year 2000, are considered.

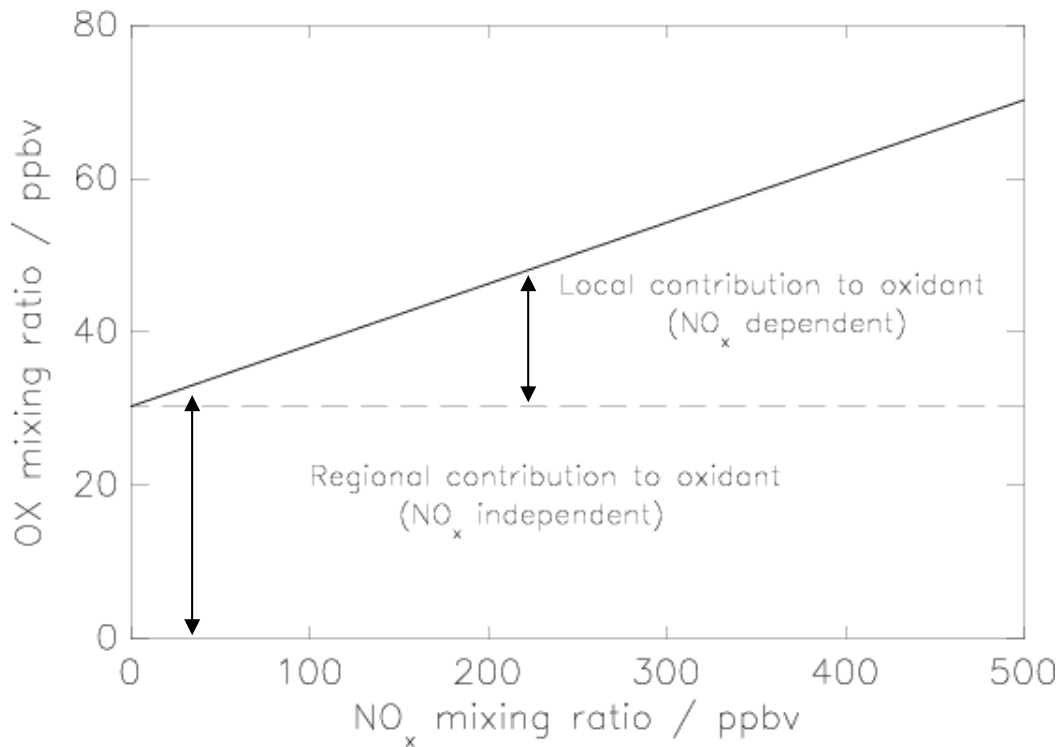


**Figure III-22.** Illustration of the idealised relationship between total oxidant (OX) and  $\text{NO}_x$  levels, allowing local and regional contributions to total oxidant to be calculated.

The total oxidant metric (OX) calculated from the model results as a function of  $\text{NO}_x$  levels is shown in Figure III-23 for winter and summer respectively. It is clear that the relationship between OX and  $\text{NO}_x$  in the modelled data is very different to that illustrated in Figure III-22. The modelled  $\text{NO}_x$  levels are representative of large areas, and are much smaller than those measured in urban environments (compare the x-axes of Figure III-22 and Figure III-23). However, the important regional contribution to total oxidant can be calculated, which in these two cases is 22 ppb and 45 ppb for winter and summer respectively. The regional contribution to oxidant levels can therefore be found directly from modelled data from STOCHEM without the need to extrapolate from higher  $\text{NO}_x$  values. As already indicated, when the  $\text{NO}_x$  level is zero, all the oxidant present must be ozone. The regional contribution to oxidant is therefore a measure of the regional contribution to surface ozone levels, which is an important quantity for formulating policy decisions on the control of ozone levels. If, for example, the regional contribution of oxidant (i.e. ozone) is 30 ppb, and the observed levels are 35 ppb, then local reductions in emissions will have little effect on the total ozone levels. However, if the observed values were much larger than the regional contribution, local emissions changes may have a large impact on the observed ozone levels.

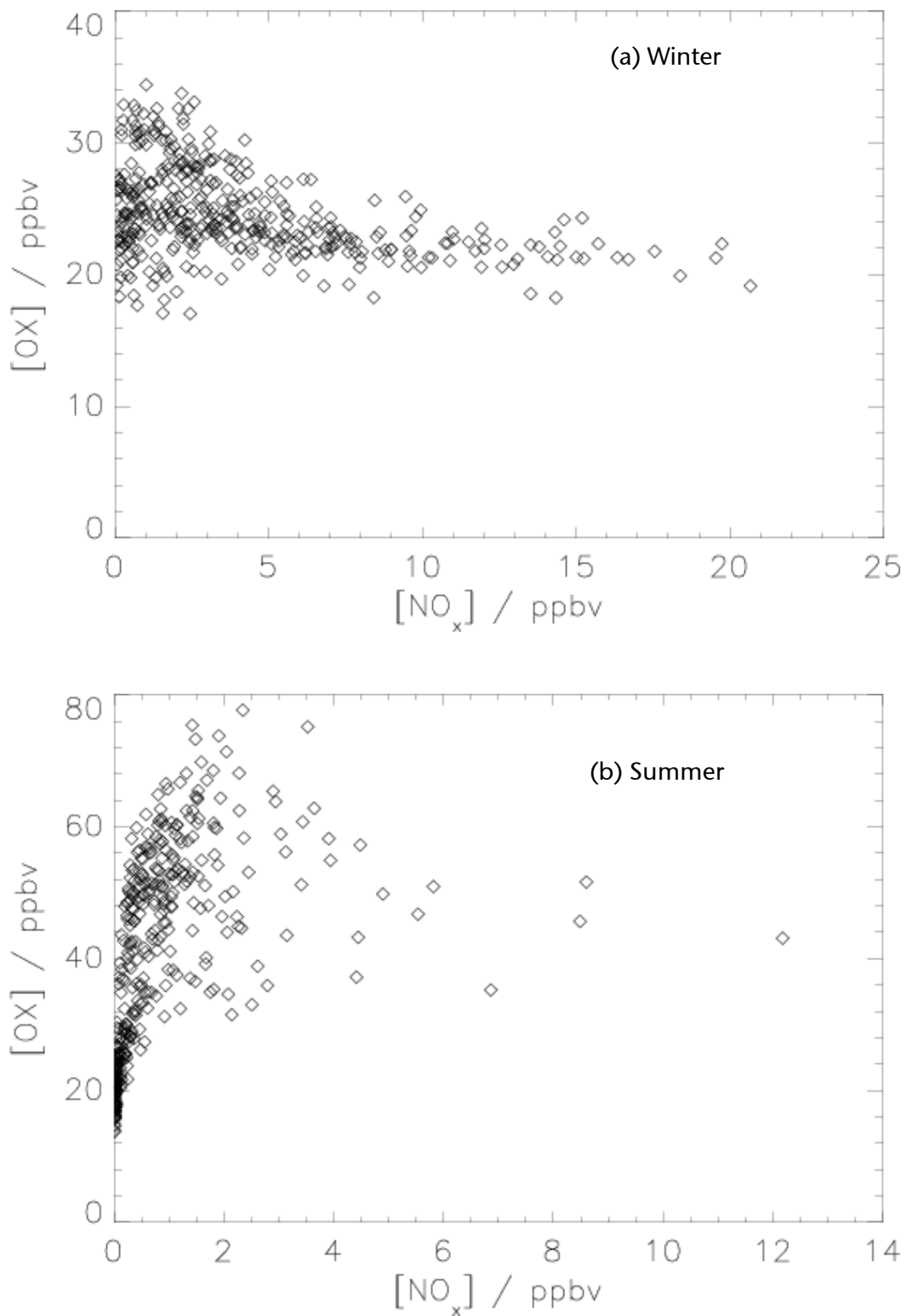


**Figure III-23.** Scatterplots of total oxidant (OX) as a function of NO<sub>x</sub> for (a) winter and (b) summer.

### 3. Effect of changes in European emissions on the rate of production of ozone

Previously we have investigated the effect of the IIASA scenarios on European surface ozone by 2030. These IIASA scenarios predict emission changes throughout the world. The UK is likely to have the most influence on pollution control policy within Europe. Therefore, we have repeated the scenarios by only changing the emissions within Europe (defined for this experiment as a box from 35 °N to 70 °S and 30 °W to 30 °E). For the European emissions, we have excluded changes in shipping by 2030. The effects of these emission changes on July surface ozone are shown in Figure III-24, along with the results obtained by changing the global emissions for comparison. For the three simulations with the MFR scenario, the results are nearly identical when the MFR emissions are used globally or just over Europe. This result demonstrates that nearly all the European surface ozone reduction comes from the changes in European emissions, i.e. Europe receives all the benefit of its emission controls. The contribution of the rest of the world (including shipping) is less than 1 ppb in the MFR scenario (lower right panel), and this small increase is likely to be due to shipping emissions still rising. However, in the CLE scenario the European-only case predicts a larger ozone reduction than when the CLE changes are imposed globally (top and middle left panels). The benefit to European ozone is offset by a contribution of around 2 ppb from the rest of the world (lower left panel). This reflects the fact that in the CLE scenario the global ozone background is predicted to increase by 2030 owing to continuing emissions increases, particularly in Asia.

To explore the implications for the UK further, these experiments were extended to determine whether controls on European NO<sub>x</sub>, hydrocarbon or carbon monoxide would be more effective in reducing ozone levels. These simulations are summarised in Table III.4. A control simulation was included, which used emissions from the CLE scenario for the year 2000 for both Europe and the rest of the world. Simulation 1 used the same emissions, except that all the European emissions were replaced with those from the MFR scenario for the year 2030. Three more scenarios were run (numbers 2 – 4), where the 2000 emissions were used, but just the NO<sub>x</sub>, VOC or CO emissions in turn were replaced by those from the 2030 MFR scenario over Europe. It should be noted that emissions of primary pollutants from shipping (NO<sub>x</sub> and SO<sub>2</sub>) were the same (at 2000 levels) in all simulations. In this way, the class of primary pollutants that exert the strongest control over the production rate and surface concentrations of ozone over Europe can be identified.

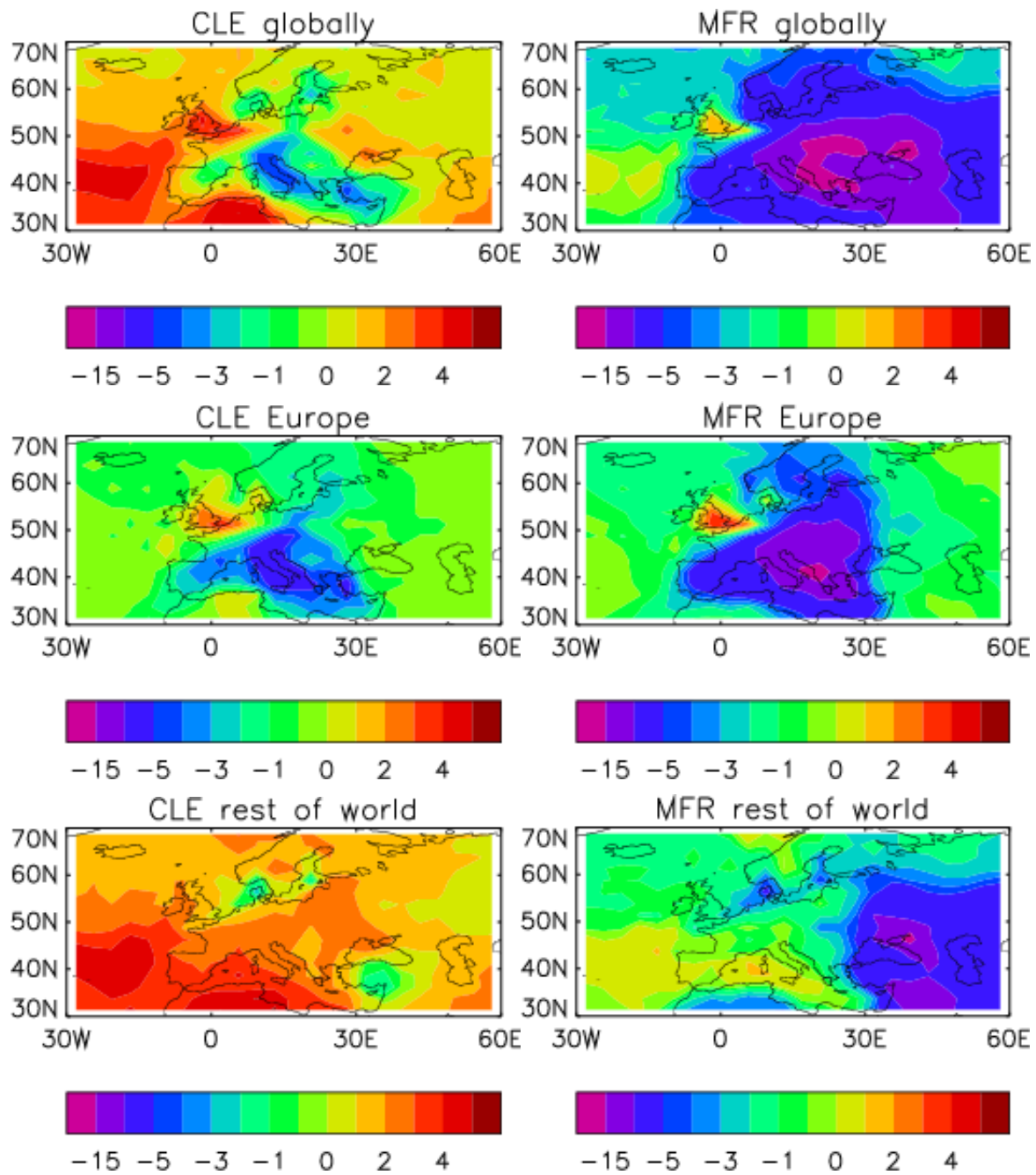


**Figure III-24.** The change in July surface ozone (in ppb) by 2030. Top row: effect of IIASA global emissions changes. Middle row effect of implementing IIASA emissions changes over Europe only. Bottom row: effect of implementing IIASA emissions changes over the rest of the world but excluding Europe.

The production rate of ozone as a function of the  $\text{NO}_x$  concentration for each European surface grid square for simulations 1 and 2 are shown in Figure III-26. The exact units of the ozone production rates are not important; rather, the focus should be on the changes from the control to each of the simulations. The cross (×) symbols are the results from the standard

scenario (control run), using emissions for the year 2000. The squares represent the results from the scenarios where the European emissions have been replaced by those from the MFR scenario. In each panel of Figure III-26, the eight locations that cover the U.K. are highlighted in red (see also Figure III-25).

**Table III-4** .Effect of changing European land-based emissions on the production rate of ozone. Emissions from shipping were the same in all five simulations.

Simulation	NO <sub>x</sub>	VOC	CO
Control	2000	2000	2000
1	2030 MFR	2030 MFR	2030 MFR
2	2030 MFR	2000	2000
3	2000	2030 MFR	2000
4	2000	2000	2030 MFR

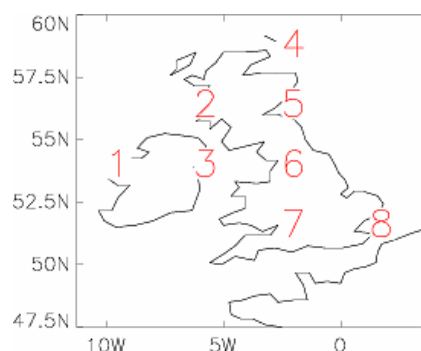


**Figure III-25.** Map showing the locations of the 8 locations in the STOCHEM model that cover the U.K.

Figure III-26(a) shows the change in the production rate of ozone when all European land-based emissions are changed to those from the 2030 MFR scenario (simulation 1; see Table III-4). Positive slopes indicate ozone production decreasing with decreasing NO<sub>x</sub>, negative slopes indicate ozone production increasing with decreasing NO<sub>x</sub>. Under the MFR scenario NO<sub>x</sub> emissions are predicted to decrease over all European points. Over most of Europe, including Scotland and Northern Ireland, the production rate of ozone falls when the emissions are reduced. Figure III-26(b) shows almost the same changes in the ozone production rates when just the European NO<sub>x</sub> emissions are changed to those from the MFR scenario. This result indicates that European ozone levels are strongly controlled by local

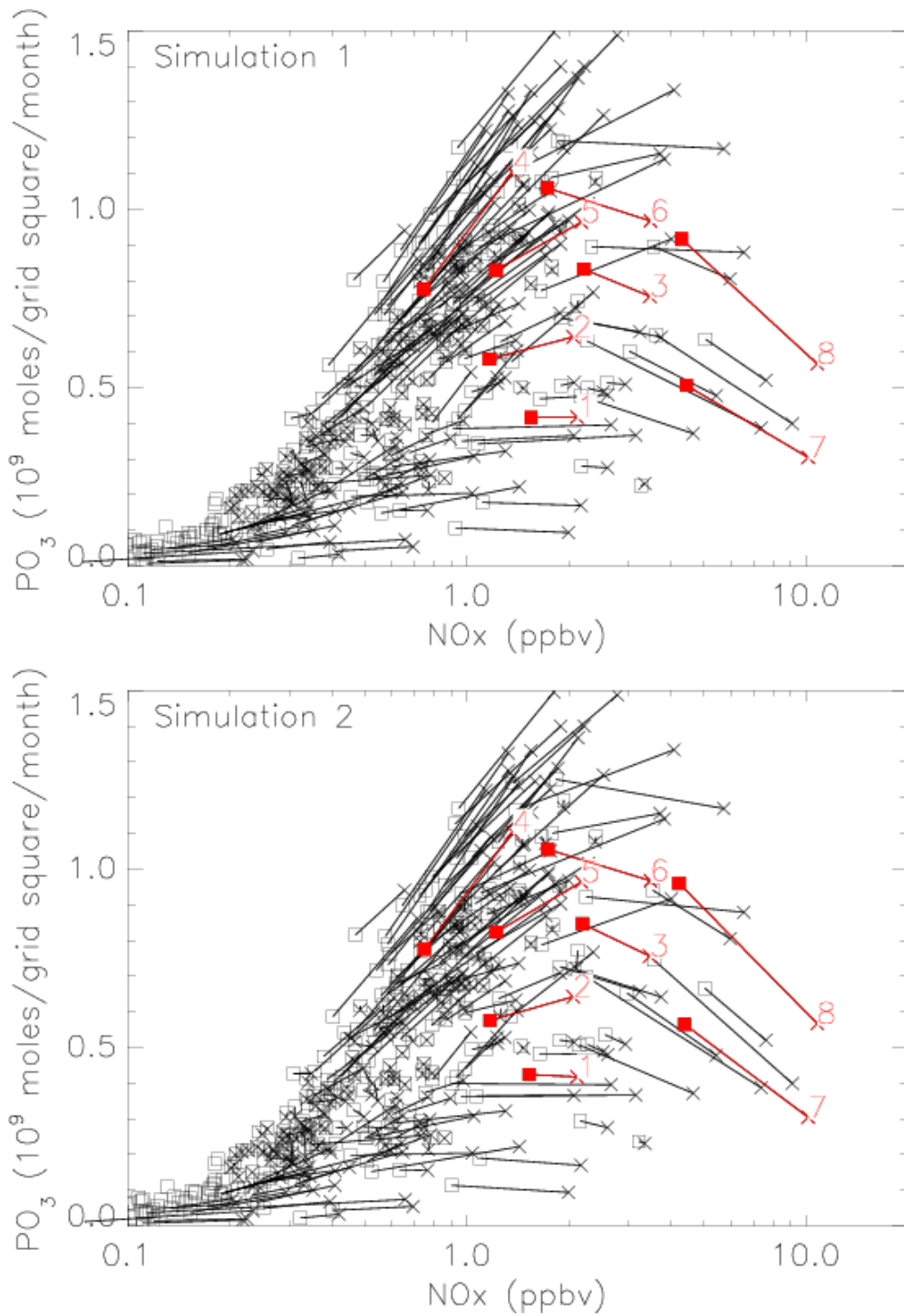


**Figure III-26.** Change in the ozone production rate ( $PO_3$ ) as a function of  $NO_x$  concentration. The cross ( $\times$ ) symbol represents results from the control simulation, and the squares results from (a) simulation 1 and (b) simulation 2. The eight points covering the UK are numbered and highlighted in red (see Figure III-25).

$NO_x$  emissions. However, over the southern half of the U.K. (and Benelux), a sharp increase in the ozone production rate occurs. These particular locations are numbered 3, 6, 7 and 8 on Figure III-26. The ozone production rate has only risen in areas which have the largest  $NO_x$

concentrations in the control simulation. In these cases, the levels of  $\text{NO}_x$  are sufficiently large that reactions removing ozone and  $\text{HO}_x$  dominate over the production terms.

Changes in the ozone production rates for simulations 3 (reduced VOC emissions) and 4 (reduced CO emissions) were also examined. However, in these two cases, the changes were very small. For simulation 3, the ozone production rate fell slightly at locations with the largest  $\text{NO}_x$  concentrations, but was almost unchanged elsewhere. For simulation 4, there was essentially no change in the ozone production rate at all locations.

The changes in monthly mean surface ozone concentrations for July between the control run and each of simulations 1 – 4 are shown in Figure III-25. The top 2 panels show the results from simulations 1 and 2. A large decrease in ozone in each of these two simulations of up to 15 ppb is evident over most of Europe, except for the southern half of the U.K., Belgium and the Netherlands. In these latter areas, the ozone levels have risen by 2 – 4 ppb.  $\text{NO}_x$  levels are highest in this region, and when the  $\text{NO}_x$  emissions are reduced, the sinks for ozone and  $\text{HO}_x$  are also reduced and ozone levels rise.

A very different change in surface ozone levels is apparent in Figure III-27 when the European emissions of VOCs (simulation 3) and CO (simulation 4) are reduced. A reduction in surface ozone levels over parts of Europe is found, but the magnitude is much smaller than in simulations 1 and 2. In simulation 3, ozone levels fall by up to 2 ppb, whereas in simulation 4 they have fallen by only 0.5 ppb or less. Interestingly, in simulation 3, a small increase in surface ozone (less than 2 ppb) is seen over most of France, and a small decrease in ozone (0 – 0.5 ppb) occurs over the U.K.

The results presented in Figure III-25 and Figure III-26 indicate that reducing emissions of  $\text{NO}_x$  on a European scale will reduce the ozone production rate and surface ozone levels over most of continental Europe. However, owing to the high levels of  $\text{NO}_x$  over the southern half of the U.K., Belgium, and Holland, the ozone levels will rise when the  $\text{NO}_x$  emissions are reduced, owing to reduced oxidant removal. Over the next 20 years, a policy of reducing European  $\text{NO}_x$  emissions will increase ozone values over the southern half of the U.K. However, European VOC controls are shown to benefit the UK ozone.

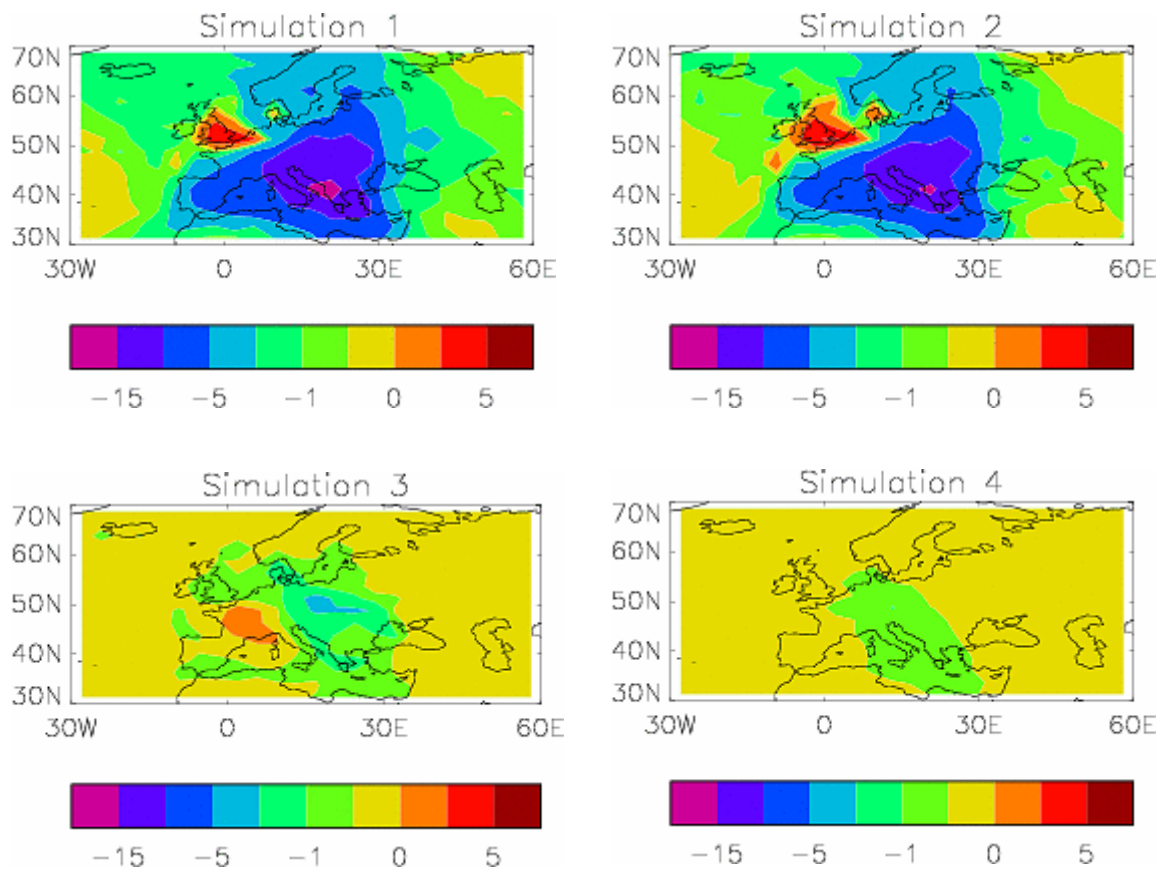


**Figure III-27.** Changes in monthly mean surface ozone concentrations for July for each of the four simulations described in Table III-4. A positive value indicates that the ozone level is greater in the given simulation than the control scenario.

### (c) Contributions to Fourth Assessment Report of the IPCC

A large number of model simulations using the IIASA and SRES A2 scenarios have been used to perform many experiments for the IPCC Fourth Assessment report. These results have been used in multi-model ensemble studies of various chemical and climate change topics. The papers published from this work are given in Annex A. This work also involved considerable interaction with other researchers through the ACCENT Photocomp experiment.

First, several simulations were performed using combinations of climate, stratospheric ozone levels and emissions for the pre-industrial, present day and future (2100). The results were used to assess the impact of radiative forcing due to ozone increases since pre-industrial times, and the sensitivity of the forcing to different parts of the climate system (Gauss et al., 2006). A further paper examining possible changes in tropospheric ozone levels and an examination of the ozone budget has also been published (Stevenson et al., 2006).

Second, numerous simulations were run using the IIASA emission scenarios for the years 2000 and 2030, and the SRES A2 scenario for the year 2030 as well. Results from these simulations were used to assess future changes in surface ozone levels, including the effects of climate change as well as emission changes, and air pollution metrics (Dentener et al., 2006a), the same changes in carbon monoxide levels (Shindell et al., 2006), and the deposition of acidifying and eutrophying substances (Dentener et al., 2006b).

Finally, additional simulations were used with and without emissions from shipping to assess the contribution of ship exhaust on modelled ozone and NO<sub>x</sub> levels in the present day and future (Eyring et al., 2006).

#### **(d) Conclusions**

The impact of climate change and stratosphere-troposphere exchange on projected future ozone levels was assessed. Climate change was found to have the largest effect, owing to the water vapour feedback, resulting in increased ozone destruction. Stratosphere-troposphere exchange is expected to be greater in the future, because the rate of exchange is predicted to be larger, and hence more ozone can be transferred to the troposphere, and also because by 2100 stratospheric ozone levels are predicted to be larger than the present day. Although climate change acts to reduce ozone levels, the proportion of surface ozone that has a stratospheric origin is projected to be larger in the future.

Natural hydrocarbons emitted by vegetation play an important role in controlling surface ozone levels. For example, high isoprene emissions caused by the exceptional temperatures during the 2003 heat wave were partly responsible for the elevated (> 100 ppb) ozone levels measured over the south-eastern half of the UK (Lee et al., 2006). Most isoprene emissions occur in the tropics, which is where most of the methane destruction occurs. However, elevated isoprene emissions had a negligible impact on the modelled methane lifetime (< 0.1 years). The vegetation distribution may also change with climate (Cox et al., 2000). An experiment using the changed vegetation from the simulations of Cox et al. (2000), but climate and anthropogenic emissions for the 1990s, showed there to be very little change in the modelled surface ozone levels over Europe. The deposition fluxes of ozone were also fairly similar. Vegetation changes alone have little effect on modelled surface ozone levels.

Changes in the emissions of precursor gases, both anthropogenic and natural, have a much greater impact.

A major sink for ozone is dry deposition, which occurs partly via the stomata on the leaves of plants. Increasing carbon dioxide levels mean that the stomata do not need to open as widely to allow sufficient CO<sub>2</sub> for photosynthesis to enter the plant. Consequently, the dry deposition flux of ozone may be reduced. The seasonal mean change in surface ozone levels under doubled CO<sub>2</sub> conditions were in the range 1-6 ppb over Europe (up to 15% larger), although the pattern was very different between each season. The largest overall increase occurred in spring. This indirect impact of CO<sub>2</sub> on surface ozone levels is smaller than other effects, such as climate change itself and changes in emissions, but is not negligible.

The change in the ozone damage metrics AOT<sub>40</sub> and CUO between the present day and the 2090s was investigated. Although ozone levels rise, less ozone is taken up by plants, owing the reduced stomatal conductances and higher levels of CO<sub>2</sub>. Consequently, projected values of AOT<sub>40</sub>, which are based purely on surface ozone concentrations, are larger, but CUO values are smaller, as they are the sum of ozone absorbed via the stomata. The AOT<sub>40</sub> metric therefore gives a misleading result, and may not be suitable for assessing future damage to vegetation by ozone.

The impact of NO<sub>x</sub> produced by lightning on surface ozone levels over Europe was investigated. Changes in climate, and shifts in vegetation, both affect global lightning intensities and the NO<sub>x</sub> production. However, no significant impact on modelled surface ozone levels was found, at least for the 2090s.

The impact of global and Europe-only emissions changes on monthly mean surface ozone levels over Europe for July was investigated. Under the MFR scenario, the ozone changes over Europe were similar when the whole world was assumed to follow this scenario, and when just Europe dies so. Hence, Europe would receive most of the benefits from introducing strict emissions controls on European emissions. However, transport of ozone and precursors from other locations partly offsets these benefits, so it is in European interests to encourage other countries to implement tighter emissions controls. The high NO<sub>x</sub> levels over southern parts of the UK and the Benelux countries mean that reducing the emissions results in greater ozone production, owing to non-linearities in the ozone-NO<sub>x</sub> chemistry. An

extra simulation for the present day where global NO<sub>x</sub> emissions were reduced by 50% projected that ozone levels over the UK remained approximately the same. Current policies to control air pollution over Europe are projected to maintain ozone levels at current levels. However, significantly greater reductions in ozone are achievable if emissions are cut further. Ozone levels over Europe are primarily controlled by the emissions of nitrogen oxides, and substantial reductions (of the order of 50%) are needed to control ozone levels over the southern half of the UK and Benelux countries.

Many model experiments were submitted under the ACCENT Photocomp model intercomparison experiment, which projected surface ozone levels for 2030, and examined the radiative forcing since preindustrial times due to tropospheric ozone increases. Several of the papers resulting from this experiment have been cited in Chapter 7 of the IPCC Fourth Assessment Report.

## **Chapter IV: Chairmanship of the UN ECE EMEP Task Force on Measurements and Modelling (TFMM)**

The EMEP Task Force on Measurement and Modelling organized a review of the EMEP Unified Model as part of the review process for the UN ECE Gothenburg Protocol and for the Preparation of the EU CAFÉ strategy. The format of the review was discussed at the 4<sup>th</sup> meeting of the TFMM in Valencia, Spain during 2003 and it was agreed that it would contain three elements: (i) an examination of the parameterisations employed in the model; (ii) an evaluation of the model performance against observations; and (iii) a consideration of the source-receptor relationships provided by the model. A workshop was convened in Oslo (Norway) in November 2003 to complete the review. The workshop concluded that the EMEP Unified Model represented a substantial development and enhancement compared to the previous EMEP models. Nevertheless, the workshop recommended that consideration should be given to a number of issues in both the short term and long term within the future development programme for the modelling. It was important to discuss these issues in order to give some guidance for the future activities of MSC-W.

The EMEP Unified Model review showed that the model was fit for policy purposes with regard to some compounds, but for others, such as particulate matter, further work was needed. Work on secondary organic aerosols in PM was continuing. The identification of the contribution of primary organic aerosols, however, required a large improvement in the emission inventories. Concerns were expressed about the delay in having a policy tool available to describe the whole of the particulate mass. The review had also shown that the EMEP model underestimated peak ozone concentrations, in common with other state-of-the-art ozone models. The model was however, suitable for the assessment of vegetation exposures and for the assessment of human health effects on the regional scale.

Resources under this work programme have been used to organize and manage the 5<sup>th</sup> meeting of the UN ECE EMEP Task Force on Measurements and Modelling in Prague from 29<sup>th</sup> March to 1<sup>st</sup> April 2004. The meeting has been organised as a joint meeting of the TFMM and the WMO GAW programme. The main agenda items were:

- The EMEP Monitoring Strategy
- The Review of the EMEP Eulerian model

- The EMEP Assessment Report
- The Review of the EMEP MSC-E modelling activities.

With the agreement of DEFRA, additional resources under this item were used to draft a chapter on ozone for Part I of the EMEP Assessment Report. Attendance was also supported at the meeting of the Task Force on Health at Bonn, Germany to discuss the long-range transboundary transport of ozone and particles within Europe. A chapter has been prepared on transboundary ozone for the Task Force on Health report. In this chapter, the annual mean daily maximum 8-hour mean ozone concentrations at sites over the UK were examined. Locations with the lowest values of this metric had increasing trends since 1990. Locations with the largest values had decreasing trends. Attendance was also supported at the EMEP Particulate Matter Workshop organised by the US EPA on particulate matter monitoring and modelling.

The TFMM organised and managed a Workshop in Oslo, Norway on the implementation of the EMEP monitoring strategy. This workshop was held during the 22<sup>nd</sup> to 24<sup>th</sup> November 2004 and helped the EMEP-CCC to understand the different priorities and choices within the monitoring strategy. The objective of the workshop was to discuss methodologies and technical requirements needed to implement the level 2 and level 3 activities defined by the EMEP monitoring strategy. Emphasis was given to: size resolved aerosol chemistry, gas/particle distribution of semi-volatile nitrogen species, elemental carbon (EC) and organic carbon (OC) determination, and methodologies for VOC determination. The workshop addressed the needs in relation to supersite activities that are being initiated nationally.

The 6<sup>th</sup> meeting of the Task Force on Measurement and Modelling was held in Zagreb, Croatia during April 2005. The main agenda items covered the topics:

- EMEP monitoring strategy:
- Source-receptor relationships
- Technical Reports by MSC-W
- Technical Reports by MSC-E
- Preparation of the review of the MSC-E models on heavy metals and POPs - status

- GAW and EMEP interaction
- EURODELTA intercomparison results
- CITY-DELTA and downscaling
- EMEP and ACCENT programme cooperation

A workshop was organized at the Meteorological Synthesising Centre-East in Moscow to review and evaluate the performance of the EMEP models for heavy metals (HMs), mercury, and persistent organic pollutants (POPs). The main aim of the workshop was to establish whether the EMEP MSC-E models on HMs and POPs are state-of-the-art and fit for the purpose of evaluating the contribution of long-range transport to the environmental impacts caused by heavy metals and persistent organic pollutants.

Based on an evaluation of the model formulations, an examination of inter-comparisons between monitored data as well as with other models, the workshop drew the following conclusions regarding the performance of the MSC-E models with respect to policy applications. Concerning the MSC-E HM models, it was concluded that the HM air concentrations and deposition levels estimated with the MSC-E HM model were found to be in good agreement with those estimated with other transport models in the various intercomparison exercises. The transboundary fluxes of HMs calculated with the MSC-E HM model corresponded well with and were within the range of those obtained with other transport models. The MSC-E HM model is suitable for the evaluation of the long range transboundary transport and deposition of HMs in Europe. However, significant difficulties still remain with official emissions data for lead and cadmium. Furthermore, significant uncertainties are associated with the chemistry of elemental mercury in all models, and with the representation of HM dry deposition.

It was concluded that the MSC-E POP models were based on up-to-date information and conformed to those employed in most of the other models used to simulate the behaviour of POPs in the environment. Remaining differences in process descriptions are caused by several specific assumptions underlying the set-up of each particular model. A main goal of the POP model intercomparison exercise is to make these assumptions transparent. The general level of agreement found between the different POP models in the model

intercomparison exercise was encouraging given the wide range of model approaches and structures employed. Nevertheless, a number of significant discrepancies were identified that will require further investigation. Within the limitations of current understanding of the sources and emissions of POPs, and of their fate and behaviour in the environment, the MSC-E POP model represents the state-of-the-science. It is also considered fit for the purpose of evaluating the contribution of long range transport to the environmental impacts caused by POPs.

The 7<sup>th</sup> meeting of the Task Force on Measurement and Modelling was organized at the Finnish Meteorological Institute at Helsinki, Finland during May 10th-12th 2006. The meeting was well-attended and covered the following topics:

- Implementation of the EMEP monitoring strategy:
- Review of the MSC-E models on heavy metals, mercury and POPs
- EURODELTA model intercomparison results
- Fine-scale urban modelling and downscaling regional models
- Particulate Matter assessment report
- Technical Reports by MSC-W
- Technical Reports by MSC-E
- GAW and EMEP programme cooperation
- EMEP and ACCENT programme cooperation
- Remote sensing datasets.

Preparations are under way for a Workshop to discuss the preparation of the EMEP PM Assessment Report in Paris during November 2006.

## Chapter V: Pollution Climate Modelling

### Introduction

So far, the work presented in this report has described results obtained using the STOCHEM global model. In this chapter, results obtained with the NAME dispersion model under Work Package VI regarding a range of issues concerned with regional scale pollution are presented, focusing on particulate matter. Descriptions of analysis of specific events in response to ad hoc enquiries by Defra are presented in part (a). Work to support the AQEG committee is described in parts (b) and (c), and work to enable a more complete picture of aerosol formation and composition is given in part (d).

### **(a) NAME model analysis in response to ad hoc enquiries by Defra**

#### 1. The Buncefield Oil Depot Fire

An explosion occurred at the Buncefield oil depot in Hemel Hempstead, Hertfordshire, (51.76° N, 0.429° W) at approximately 06:00 GMT on Sunday 11th December 2005. The explosion was heard over a wide area and is thought to have been caused by a leak from a petrol storage tank. The blaze is the largest industrial fire to date and at the height of the blaze, 20 tanks, each reported to hold up to three million gallons of refined fuel, were on fire.

Throughout the incident, the Met Office provided advice on the predicted spread and transport of the plume. Extensive modelling of the plume was undertaken using the NAME model. In modelling the plume from the Buncefield oil depot fire, three dimensional meteorological data from the mesoscale version of the Met Office's numerical weather prediction model was used with a horizontal resolution of approximately 12 km. There was a large degree of uncertainty in the source release details and consequently a number of assumptions, or estimates based on the available observations, were adopted. Due to the intense heat of the fire, the plume was highly buoyant and rose vertically within the atmosphere. The large amount of vertical wind shear present on 11th December enabled the height attained by the plume to be estimated by comparing NAME output with satellite imagery (see Figure V-1). This suggested that the plume reached a height of 3000 m above ground level on 11th December which was supported by a single pilot report from a commercial airline. On 12th December, winds were from a north-easterly direction at all levels and therefore, this method could not be repeated (satellite imagery

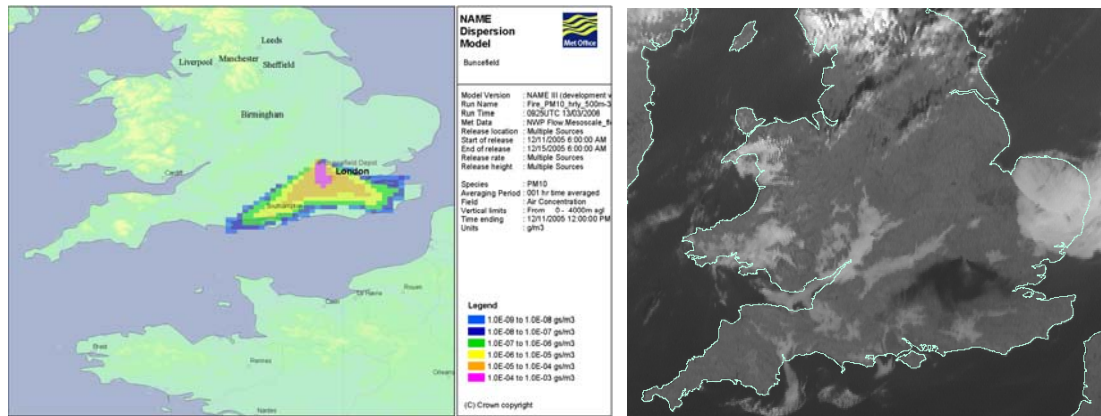
did not show the plume on subsequent days due to the presence of cloud). It was assumed that the plume reached a lower height of 2000 m on 12th December taking into account the effects of fire fighting activities. In addition, there was also a large degree of uncertainty in the quantity and content of material being released. Initial modelling exercises therefore assumed a unit release rate of a tracer. These were useful in predicting the transport and geographical spread of the plume but were not expected to give accurate estimates of concentrations within the plume.

Following the event, estimates of emission rates for various species were obtained from estimates of total emissions from the fire together with the following suggested release rate scaling factors; 1.0 for the period 06:00 GMT on 11/12/05 to 06:00 GMT on 12/12/05, 0.9 for 06:00 GMT on 12/12/05 to 06:00 GMT on 13/12/05, 0.4 for 06:00 GMT on 13/12/05 to 06:00 GMT on 14/12/05 and 0.2 for 06:00 GMT on 14/12/05 to 06:00 GMT on 15/12/05 (Noel Nelson, DEFRA, private communication). A 96 hour release, scaled to the above values, and a worst case scenario assuming 100% of 105 million litres burnt, were modelled.

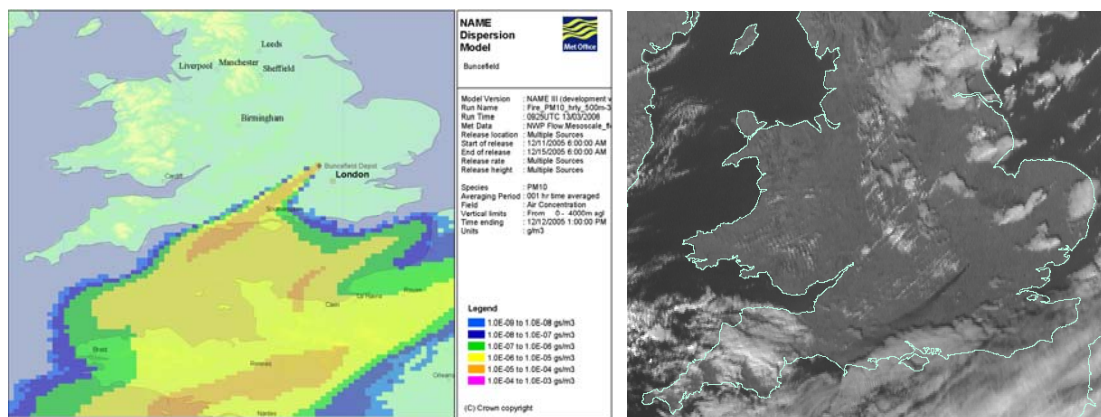
The rise of the plume due to buoyancy was taken into account in the release height. A release between 500 m and 3000 m was modelled during the period 06:00 GMT on 11th December and 06:00 GMT on 12 December. The release was then reduced to a height between 500 m and 2000 m from 06:00 GMT on 12 December onwards. The choice of 500 m as the lower height limit is somewhat arbitrary but is based on observations that the plume remained elevated (suggesting that it was above the boundary layer) together with information from the Facilities for Airborne Atmospheric Measurements BAe 146-301 aircraft, operated jointly by the Met Office and NERC, which made extensive measurements from within the plume during 13 December and reported that it flew through the plume at a height of 500 m above the ground on 13 December at a distance of approximately 78 km from the oil depot.

Figure V-1 and V-2 show the comparison between satellite imagery and NAME predicted hourly averaged fields of  $PM_{10}$  concentrations over a height range between 0 and 4000 m above ground, at 12:00 GMT on 11 December and at 13:00 GMT on 12 December. There is good agreement between the geographical spread of the NAME predicted plume and satellite observations. Modelled hourly averaged boundary layer concentrations of  $PM_{10}$  from NAME (see Figure V-3) suggest that, during Sunday 11 December, the plume was present mainly above the boundary layer. Some material from the plume could, however, be present at lower levels over the south-east of the UK although boundary layer concentrations were predicted to

be low. On Monday 12 December, NAME predicted potential grounding of the plume both in the UK to the south-west of the oil depot, over the Channel, and into northern France. Maximum hourly averaged boundary layer concentrations of PM<sub>10</sub> were predicted to reach values of approximately 150 µg m<sup>-3</sup> near to the source.



**Figure V-1.** Comparison between NAME predicted plume and satellite imagery at 12:00 GMT on 11/12/05. The plume is the black area over and around London on the satellite image.



**Figure V-2.** Comparison between NAME predicted plume and satellite imagery at 13:00 GMT on 13/12/05. The plume is the diagonal black line on the satellite image.

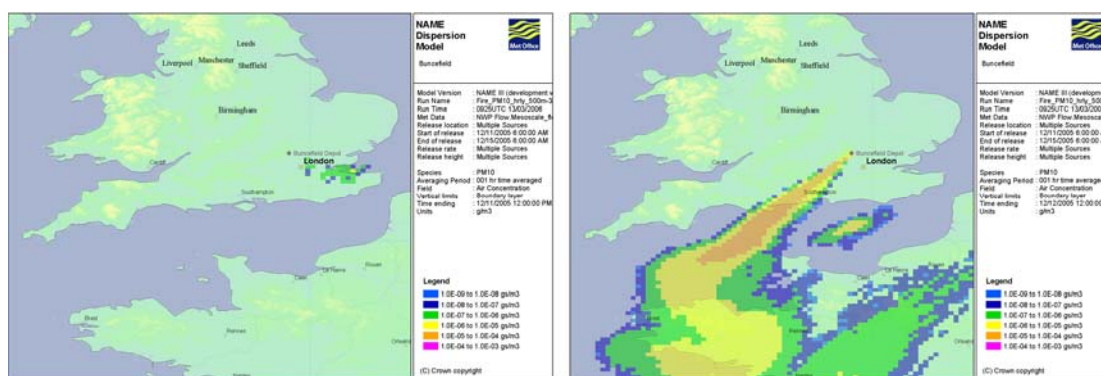


**Figure V-3.** NAME predicted hourly averaged boundary layer concentrations of PM<sub>10</sub> at 12:00 GMT on 11/12/05 and 12:00 GMT on 12/12/05.

The predicted boundary layer concentrations from NAME are clearly highly sensitive to the lower boundary of the plume (taken here to be at a height of 500 m). Work is continuing to improve our understanding of the plume's behaviour and incorporate this into the modelling of the plume. In addition, further work is planned to enable the initial rise of the buoyant plume to be modelled provided that appropriate estimates of the plume's properties (e.g. temperature) can be obtained. Further details of the modelling work undertaken are described in appendix E of the report on the Buncefield explosion (Targa et al., 2006).

## 2. UK PM<sub>10</sub> episode linked to Russian forest fires

Unusually high levels of PM<sub>10</sub> were observed by UK automatic urban and rural air quality monitoring network (AURN) sites in Scotland and north-east England between 8th and 10th May 2006. During this time, the Met Office also received a number of calls reporting the appearance of "yellow dust" on vehicles near the east coast. This dust was attributed to pollen that had been transported from Denmark following a sudden onset of the pollen season there and a press-release was issued to this effect on 9 May. On 10 May, the Met Office received an ad-hoc request from Defra to provide more information on the particulate pollution incident to enable them to brief the minister.

The synoptic pattern from 7-10 May 2006 was controlled by a high pressure system over northern Scandinavia, which slowly moved west during this time (Figure V-4) and created a strong easterly flow over northern Europe. UK weather was dominated by a frontal system that split the country north-west to south-east; areas to the east of the fronts received air from Europe and the east, whilst areas to the west of the fronts received "clean" air from the Atlantic. This frontal system moved slowly westwards during the period considered, gradually exposing more of the UK to the easterly air mass.

Satellite images from early May show a plume of material spreading over northern Europe, the North Sea and the UK in the easterly air mass (Figure V-5). The coincident timing of the movement of this plume over the UK and the raised UK PM<sub>10</sub> levels suggested a link between the two. At the time (and still), the origin and content of the plume were uncertain and it was not clear whether the plume contained PM<sub>10</sub>. The Met Office considered three hypotheses for the cause of the increased PM<sub>10</sub>: (i) smoke from Russian fires, (ii) pollen from Northern Europe and (iii) European pollution.

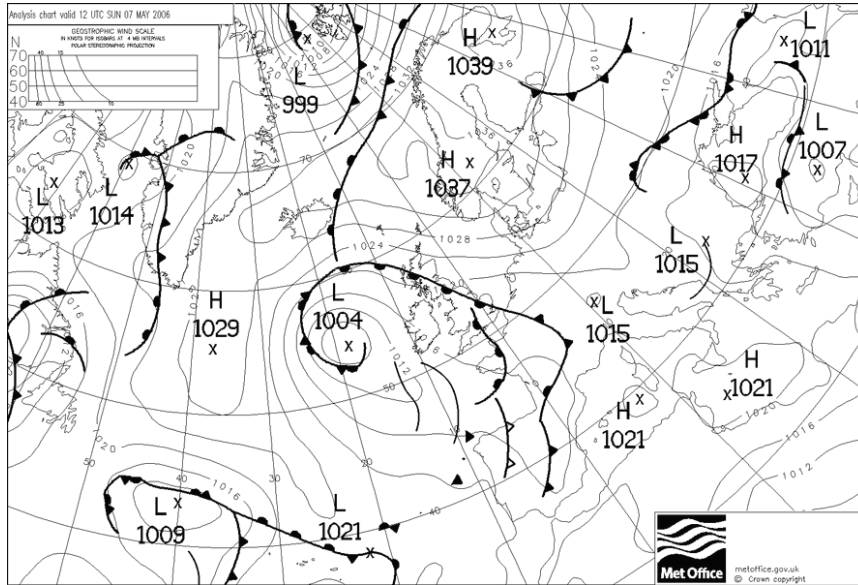


**Figure V-4.** Synoptic situation at 12:00 UTC on 7 May 2006 showing the frontal system over the UK that dominated the weather at this time.

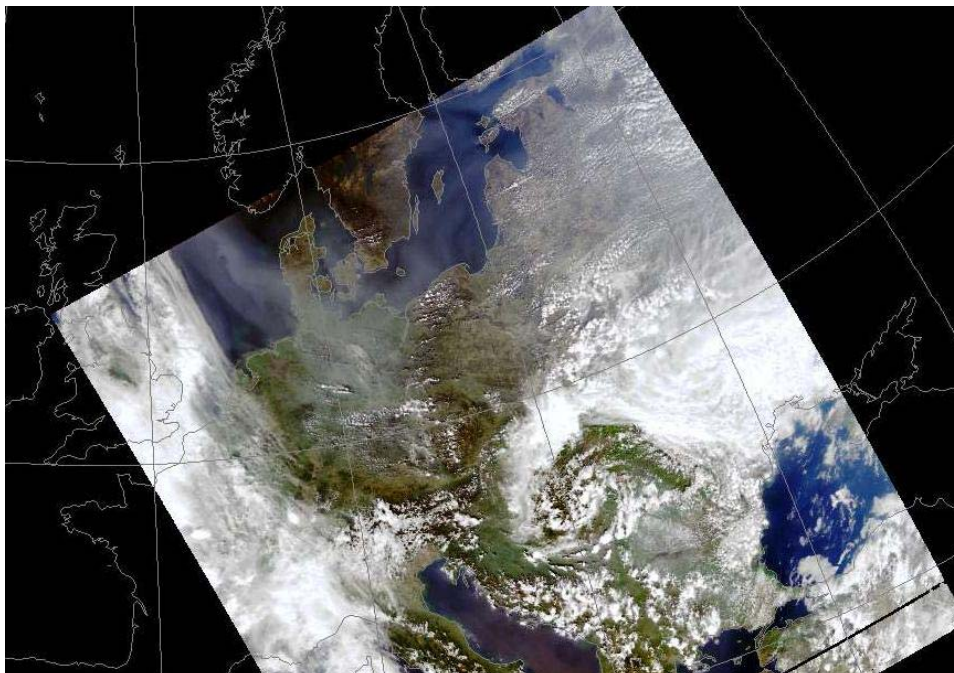


**Figure V-5.** Cropped MODIS image of central Europe on 6 May 2006 showing an apparent haze or smoke cloud over northern Europe and the North Sea (image credit NASA).

In early May, many areas of western Russia were experiencing forest fires started by incineration of dry grass and rubbish. Satellite data from the Moderate Resolution Imaging Spectroradiometer (MODIS) on 1 May showed that a large number of fires were burning in Russia and that smoke from the fires was travelling west, passing over several countries in

Eastern Europe. The apparent haze over the Baltic Sea, Germany and the North Sea in Figure V-5 could well be smoke from these fires. Alternatively, the haze seen in this and other satellite images of the UK and northern Europe during 6-10 May could have been due to large releases of pollen from Denmark, Germany and Eastern Europe that occurred at this time. This latter explanation agrees with the reports of pollen from the east coast of the UK, but without detailed analysis of the plume or the filters from the PM<sub>10</sub> stations is impossible to prove. Finally, although high particulate pollution in the northern UK is not common during the spring, long-range transport of pollutants from Europe is possible under the right meteorological conditions and could not be ruled out.

The Met Office's standard meteorology products and satellite data were available during the episode, as were near real-time observational data from AURN sites across the UK. In addition, NAME was run in both forwards and backwards modes to reveal more about the source and transport of the air masses present over the UK at the time. In backwards mode, thousands of neutrally buoyant inert particles are released from the receptor over a given period and followed backward in time. The particles are moved using negated 3-D winds and a random walk turbulence scheme. The grid box location of each particle at each time step is recorded over the duration of the model run and collated together into an air origin map. The result is a map of all of the possible sources of air over the duration of the model run, reaching the receptor within a given time window. This approach is a substantial improvement over the simple back-trajectories used in previous air pollution studies, as it incorporates the effects of detailed 3-D wind structure and atmospheric turbulence and amalgamates the routes of many thousands of single trajectories.

During the period of interest, air source maps were produced for a selection of sites in the UK. For each site, the model was run backwards for four days for two arrival periods on each day: 00:00 to 03:00 and 12:00 to 15:00. Each run used global meteorology, which has a horizontal resolution of 40 km by 40 km and 40 vertical levels. Particle position information was collected on a 40 km horizontal by 200 m vertical grid extending from 20° W to 50 °E and 30° N to 70° N.

The air source maps demonstrated that on 8 May – the day with the highest PM<sub>10</sub> concentrations – the air mass reaching Scotland and north England had travelled over the Russian fire region and northern Europe (Figure V-6(a)). On the following day, when

measured PM<sub>10</sub> concentrations were somewhat lower, the source of the air was more widespread. This result suggests that the fires were a likely source of the increased PM<sub>10</sub>.

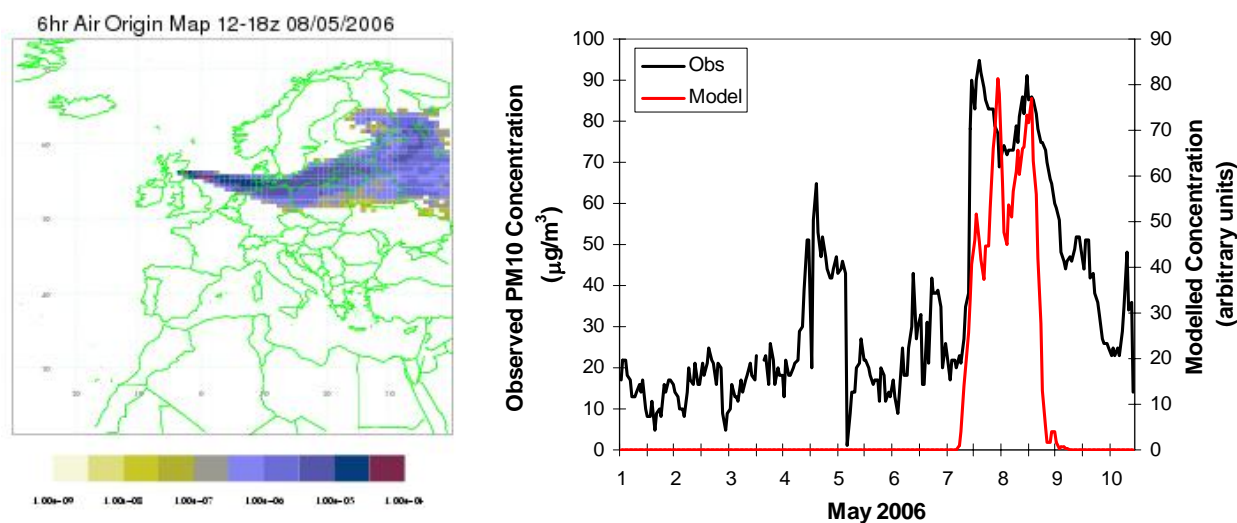


**Figure V-6** (a) Air source map for Edinburgh for the afternoon of 8 May. The colour scale indicates the relative amount of air originating from that grid square and the box indicates the approximate fire area. (b) PM<sub>10</sub> concentrations observed at Edinburgh compared to modelled levels scaled to fit on the same axis.

Forward NAME runs from the fire area were carried out starting on 1 May using the same meteorology and horizontal output grid as the backwards runs. As no site-specific data were available for the fire burn area, a burn region of 38 °E – 50 °E, 53.5 °N – 57.5 °N was estimated from MODIS images. Time series output of modelled concentrations were produced for observing sites in the UK and locations in Europe for comparison to the observed levels. Model results showed good agreement with the timings and relative magnitudes of the observed PM<sub>10</sub> peaks at most sites (see Figure V-6(b)). Only emissions from the burnt region were included in the simulation, hence the modelled PM<sub>10</sub> levels are zero except when the plume from the fires passes over Edinburgh.

The transport of air over Denmark, Germany and northern Europe prior to its arrival in Scotland means that the presence of pollen or anthropogenic pollution cannot be ruled out. The size of birch pollen grains (the major species released at this time), however, suggests that pollen may not have been a major contributor, as at 20 µm they are larger than the PM<sub>10</sub> cut-off size.

Air mass climatologies for London were produced using NAME back runs for each day in April and May from 1995-2004 inclusive. They demonstrated that it is not unusual for air to pass over Denmark and northern Europe before reaching the UK during this time of year (Figure V-7). This result suggested that long-range transport of pollution from Europe was unlikely to be the main cause of such exceptional PM<sub>10</sub> levels. Comparison of the trends of PM<sub>10</sub> levels to those of other typical anthropogenic pollutant species (NO<sub>x</sub>, CO, SO<sub>2</sub>, O<sub>3</sub> etc) also demonstrated that levels of other species generally remained low during the incident.

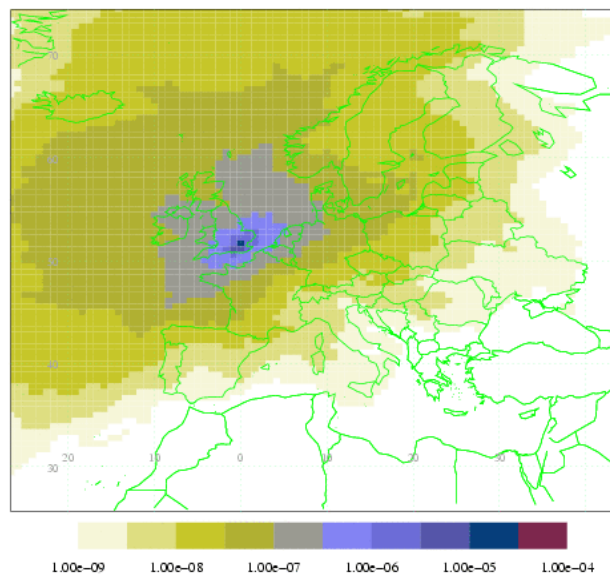


**Figure V-7.** Air mass origins for London for May (1995-2004 inclusive). Colours indicate the relative contribution to the air at 0-200 m over London from each grid square.

To summarise, forwards and backwards NAME modelling of the PM<sub>10</sub> incident in May 2006 demonstrated that the high PM<sub>10</sub> observed in Scotland and Northern England was most probably due to agricultural fires in Russia. Model results for a fire source in western Russia agreed well with the timings and relative magnitudes of observations at sites in Scotland, England and Northern Ireland. Although some transport of pollen to the UK occurred during this time, it was unlikely to be the major contributor to the PM<sub>10</sub> levels owing to its large size.

The locations of the high PM<sub>10</sub> concentrations in May were controlled by the synoptic meteorological situation, with the frontal system initially limiting the extent of the plume to Scotland and northern England. Under different meteorological conditions more of the UK could have been exposed to high PM<sub>10</sub>. Long-range transport of fire emissions from Russia to Europe has occurred also in 2002 and 2003. This frequency of pollution suggests that

future transport of fire emissions to Europe from Russia should be expected if the meteorological conditions are suitable and the practice of agricultural burning continues. Increases to UK and European air pollution levels are likely in such instances, which may have serious implications for the ability of countries to conform to national and EU air quality legislation targets.

### 3. Dust storm over Athens

An unusual dust event was observed over Greece on Sunday 17 April 2005. The city of Athens, as well as other parts of Greece, was enveloped in a thick yellow dust cloud that was part of a large-scale transport of a dust cloud from Africa. The event received wide coverage on television and the daily press, with scientists talking about ‘the highest dust concentrations in the last 15 years’. A picture of this event from the MODIS instrument is shown in Figure V-8. A number of observations were made at the time of the event, including concentrations of PM<sub>10</sub>. These data enabled a comparison of predicted concentrations from the NAME atmospheric dispersion model with these observations to investigate the event, and evaluate the dust scheme in NAME.

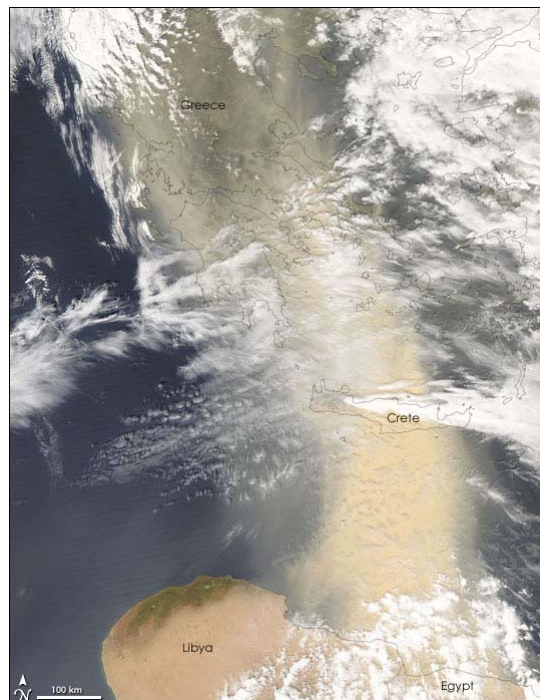


**Figure V-8.** Picture from the MODIS sensor on the AQUA satellite. The dust plume can be seen clearly, extending from Africa, over the Mediterranean Sea, Crete, and mainland Greece. The picture was taken at 11:45 UTC, at about the time of the onset of maximum dust concentrations in Athens.

Values of the maximum and 24 hour average concentrations of dust in three size distributions, and the total, are listed in Table V-1, as well as a summary of observations made at Athens International Airport. The maximum value of PM<sub>10</sub> from NAME (highlighted in red) and the 24 hour mean PM<sub>10</sub> level (highlighted in green) in Table V-1 agree remarkably well with the observations.

**Table V-1.** Dust concentrations from NAME and some observations at Athens International Airport (AIA) in  $\mu\text{g m}^{-3}$ .

NAME Results:	Total	PM <sub>10</sub>	PM <sub>2.5</sub>	PM <sub>1</sub>
Maximum values				
BL	6939	<b>2437</b>	584	230
0-100 m	11408	2855	1142	400
100-500 m	7200	2449	673	367
500 – 1000 m	15200	6645	1204	271
1000 – 2000 m	39015	21391	2838	585
24 h average				
BL	1483	<b>483</b>	114	37
0-100 m	1548	440	133	54
100-500 m	1419	530	122	45
500 – 1000 m	2675	1250	241	53
1000 – 2000 m	4368	2423	424	105

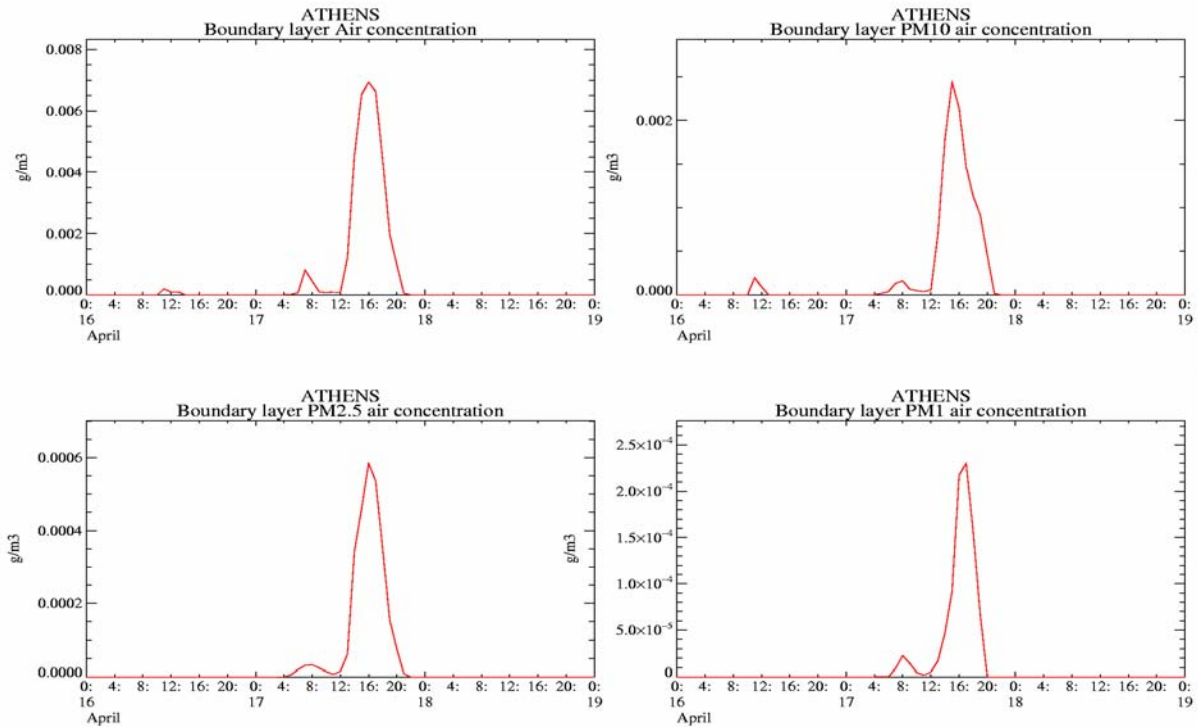
Observed values:

24 h average value of PM<sub>10</sub> at AIA = **502**  $\mu\text{g m}^{-3}$

Max value of PM<sub>10</sub> at AIA = **2384**  $\mu\text{g m}^{-3}$  at 1500 UTC – 1600 UTC.

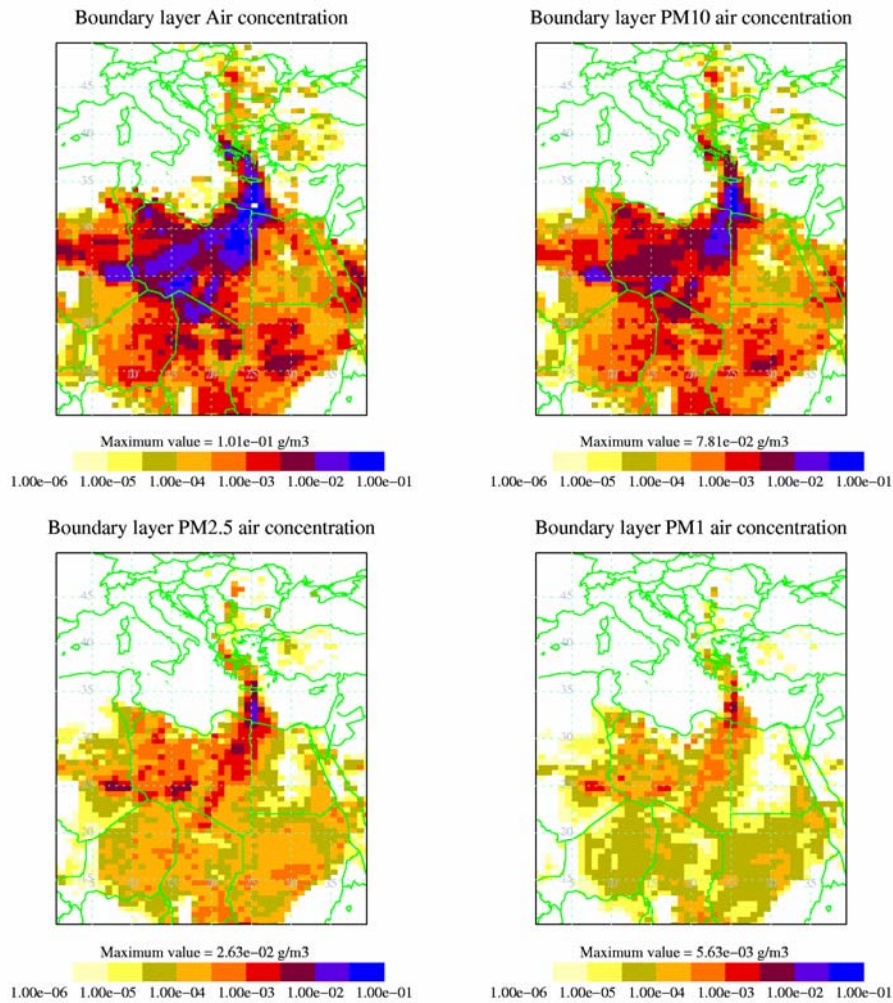
Figure V-9 shows time series of boundary layer concentrations over Athens from 0000 UTC on 16 April 2005, to 0000 UTC on 19 April 2005 predicted by NAME. The dust storm lasted for approximately 8 hours. The peak in the PM<sub>1</sub> concentrations is narrower than the three larger dust sizes.

Figure V-10 shows the spatial distribution of boundary layer concentrations at 1500 UTC, from the NAME dust forecast. The maximum concentrations, shown in blue/dark colours, correspond rather well with the dust cloud observed on the satellite picture in Figure V-8.



**Figure V-9.** Time series of boundary layer air concentrations of various dust particle size ranges over Athens, from NAME model run. The units are  $\text{g m}^{-3}$  in all cases. The dust event was severe and lasted for approximately 8 hours.

To summarise, dust transport is frequently observed in spring over Greece, but is usually manifested as “coloured” rain. The absence of precipitation in the event studied here made it rather unusual and allowed the dust concentrations to reach high levels near the surface. The Met Office atmospheric dispersion model NAME, running using meteorological data from the Met Office Unified Model at global N216 resolution, seems to capture the dust event of 17 April 2005 over Athens Greece remarkably well. Sensitivity tests (such as starting the model from different days, and either using different parameterisations or removing some entirely) produced virtually identical results to the ones shown here. Furthermore, trajectory runs (not shown) proved very useful in helping to identify and track different air masses significant for the event.



**Figure V-10.** Boundary Layer concentrations from NAME model run. Valid at 1500 UTC on 17 April 2005. (a) All size particles, (b) PM<sub>10</sub>, (c) PM<sub>2.5</sub>, (d) PM<sub>1</sub>.

## (b) UK and European contributions to secondary particulate levels

### 1. Introduction

The Met Office's Lagrangian dispersion model NAME has been used to model sulphate and nitrate aerosol formation over a European wide area for the years 2002 and 2003. This work was carried out in support of AQEG and contributed to the Air Quality Expert Group Report on Particulate matter in the United Kingdom, published in 2005.

## 2. Modelling the contribution of sulphate and nitrate aerosols to observed particulate levels

In order to calculate the species concentrations required for the chemistry scheme, a three-dimensional grid is constructed over the model domain. The model was driven using EMEP<sup>1</sup> 2001 emissions data on a 50 km grid, and so this resolution was also used for the chemistry calculations. Five vertical layers were used (0-100 m, 100-300 m, 300-800 m, 800-5000 m, 5000-20000 m) and the extent of the model domain was 10° W to 16° E and 44° N to 60° N. Emissions of 13 primary species are used, including seven VOC's (formaldehyde, ethene, propene, isoprene, o-xylene, toluene and 1,3-butadiene) which are then scaled to represent the full VOC emission inventory. Details of the chemistry scheme can be found in Redington et al (2001).

Thirty locations in the UK and Ireland were studied. The NAME results were processed to obtain the percentage contribution from each country (or group of countries) within the model domain to that location during 2002 and 2003.

In order to assess the ability of NAME to simulate sulphate aerosol on a daily basis, measurement data have been obtained for sulphate aerosol at five rural sites in the UK from the Air Quality Archive<sup>2</sup>. The five rural locations are Yarner Wood in the south west of England, Barcombe Mills in the south east of England, High Muffles in the north east of England, Eskdalemuir in Scotland and Lough Navar in Northern Ireland. NAME results have also been compared with nitrate aerosol data from Harwell for 2002<sup>3</sup>. Table V-2 presents a set of four standard statistics, correlation, bias, normalised mean square error (nmse) and percentage within a factor of two (Hanna and Chang, 1995), for NAME predictions versus observations in the years 2002 and 2003. A negative bias indicates under-prediction. Overall, the statistics show a general improvement in the year 2003 compared with 2002. The correlations are higher, the biases are closer to zero, the nmse's are closer to zero, and the percentages within a factor of two are larger. The model setup was exactly the same for the two years; thus, it seems that either the meteorology used for 2003 was better than that used for 2002, or that it was easier to predict pollution episodes with the type of meteorological events seen in 2003. There was a version change of the unified model in August 2002, so it is possible that this is responsible for the improvement seen.

---

<sup>1</sup> <http://www.emep.int/>

<sup>2</sup> <http://www.airquality.co.uk/archive/index.php>

<sup>3</sup> Data courtesy of Prof. Roy Harrison at Birmingham University

**Table V-2.** Correlation, bias, normalised mean square error (nmse) and percentage within a factor of two calculated for daily average model data versus observed data from five rural measurement sites for 2002 and 2003.

	correlation		bias ( $\mu\text{g}/\text{m}^3$ )		nmse		% within a factor of 2	
	2002	2003	2002	2003	2002	2003	2002	2003
Barcombe Mills	0.28	0.50	0.29	-0.15	2.23	1.31	41.7	41.4
Yarner Wood	0.40	0.62	0.14	-0.15	1.86	1.71	32.7	38.4
High Muffles	0.35	0.58	0.30	0.05	2.95	2.29	33.0	40.1
Eskdalemuir	0.39	0.47	0.14	0.08	2.35	2.27	28.6	33.4
Lough Navar	0.57	0.56	0.07	-0.06	2.87	1.96	24.1	26.0

The correlations achieved over the two years range from 0.28 to 0.62, which is a reasonable achievement given the coarse spatial resolution and the lack of any temporal variation in the emissions data emissions. Use of detailed UK National Atmospheric Emissions Inventory (NAEI) data would provide better spatial resolution over the UK; however, it was not used in this study due to the computational cost of running with high resolution source data. The UK sulphur dioxide emissions are dominated by a relatively few very large emitters, and another potential area for improvement would be to know exactly when these sources were active, i.e. have hour by hour variation of emissions rather than an annual average for each source.

The model production of sulphate aerosol is also limited by the spatial and temporal resolution of the moisture variables from the driving meteorological data. Large amounts of sulphate can be produced in the aqueous phase via oxidation by hydrogen peroxide and ozone, which requires accurate knowledge of cloud amount and cloud liquid water content in three dimensions.

Comparison of daily average modelled and observed sulphate aerosol levels at Yarner Wood are shown in Figure V-11 and Figure V-12 for 2002 and 2003 respectively. These results are typical of those seen at the other sites and some general comments can be made which allow a better understanding of the statistics presented in Table V-2. As demonstrated by the correlations it is clear that the model is capturing the large scale variation of the sulphate aerosol very well (see, for example, January, February and March 2003 in Figure V-12). What the model is not able to do so well is represent the shorter timescale variations with the same level of accuracy.

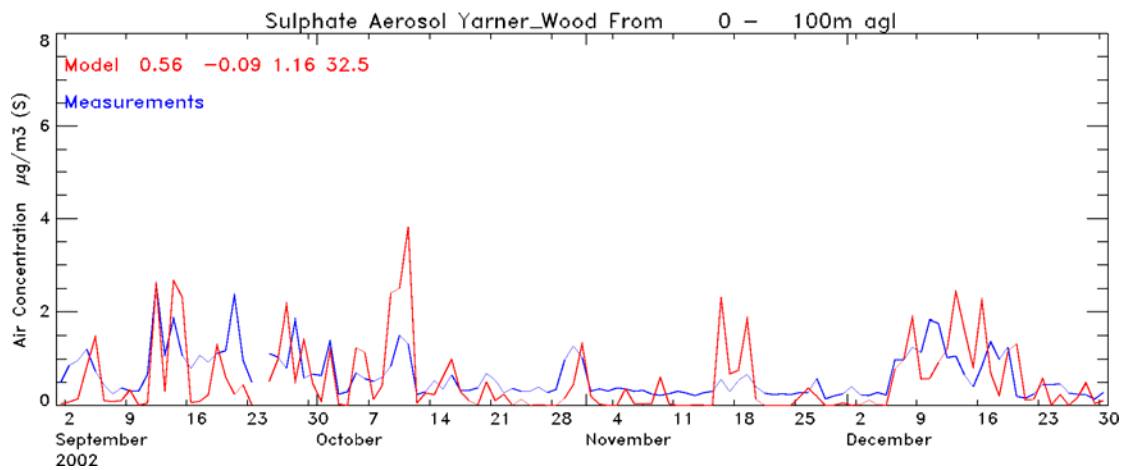
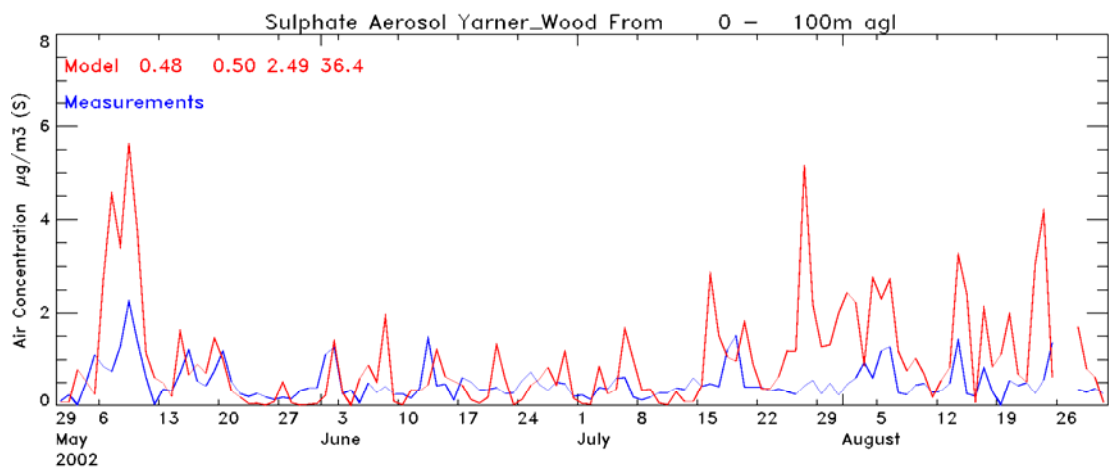
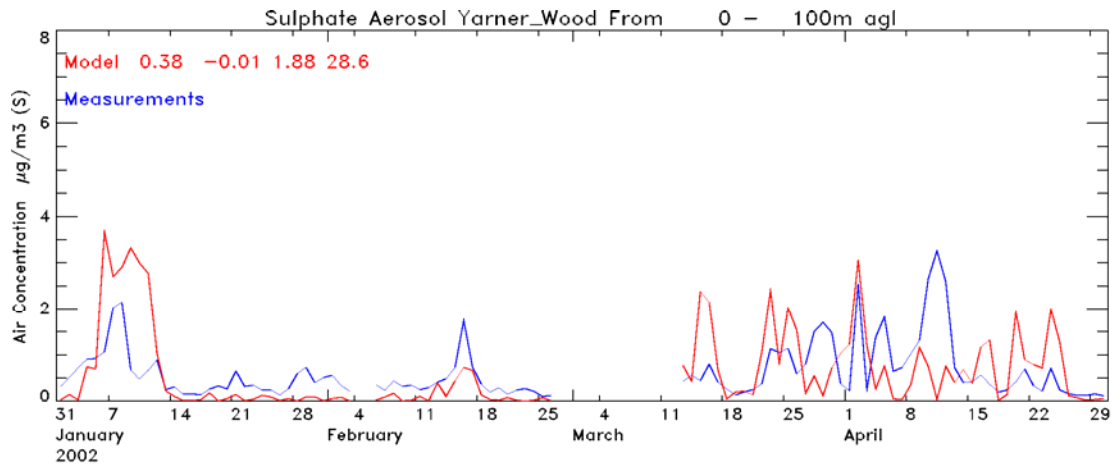


**Figure V-11.** Modelled and observed daily average sulphate aerosol loadings (in  $\mu\text{g m}^{-3}$ ) at Yarner Wood for 2002.

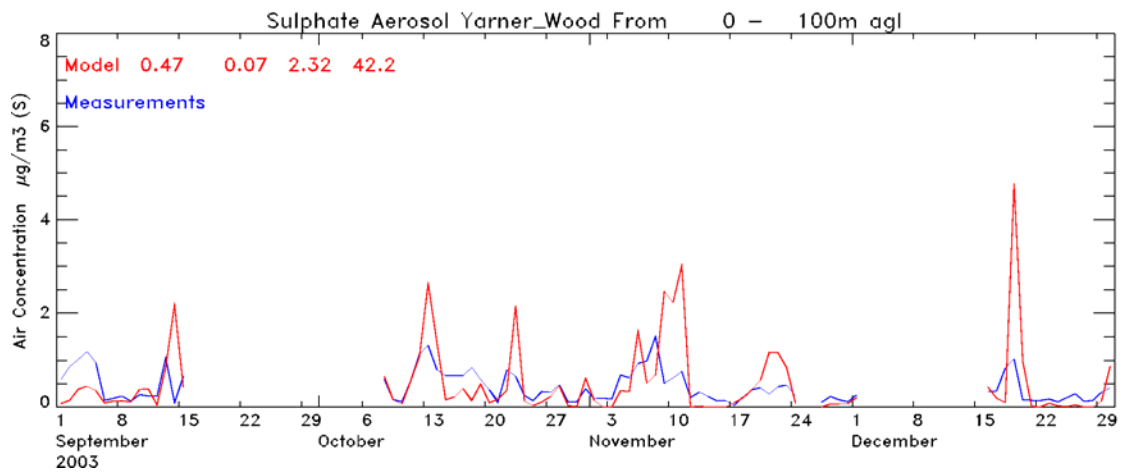
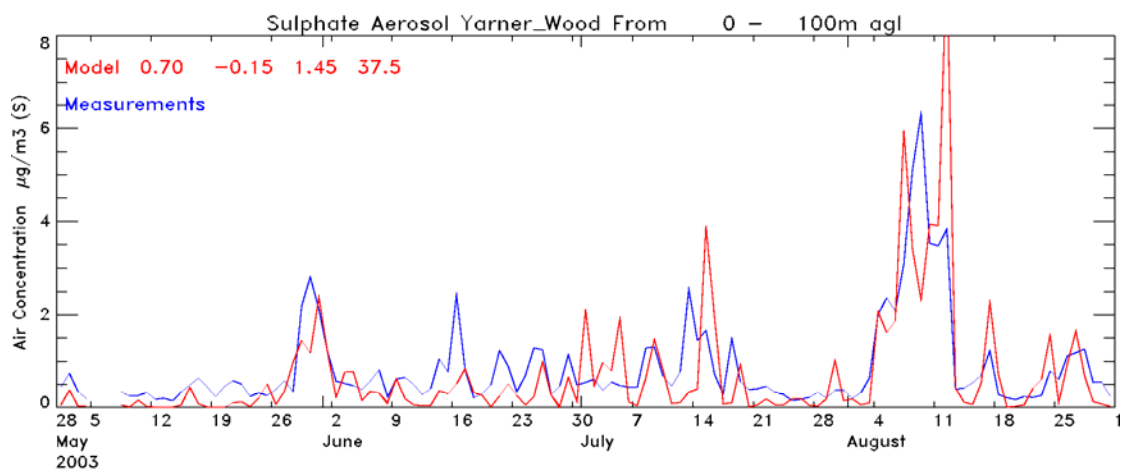
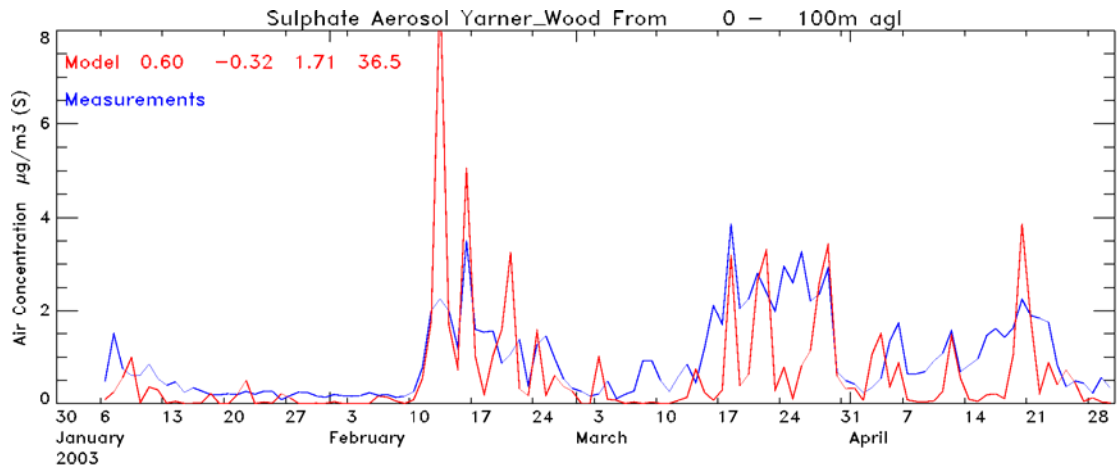


**Figure V-12.** Modelled and observed daily average sulphate aerosol loadings (in  $\mu\text{g m}^{-3}$ ) at Yarner Wood for 2003.

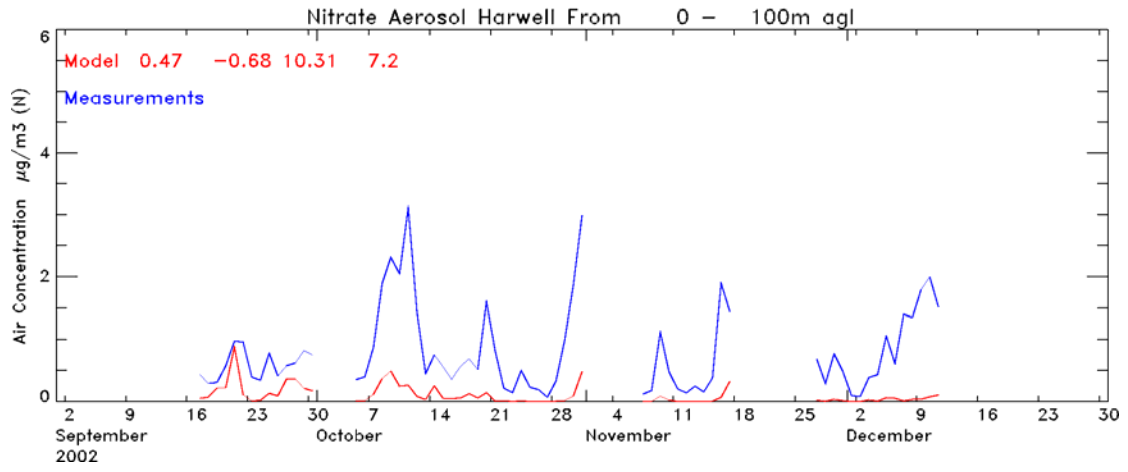
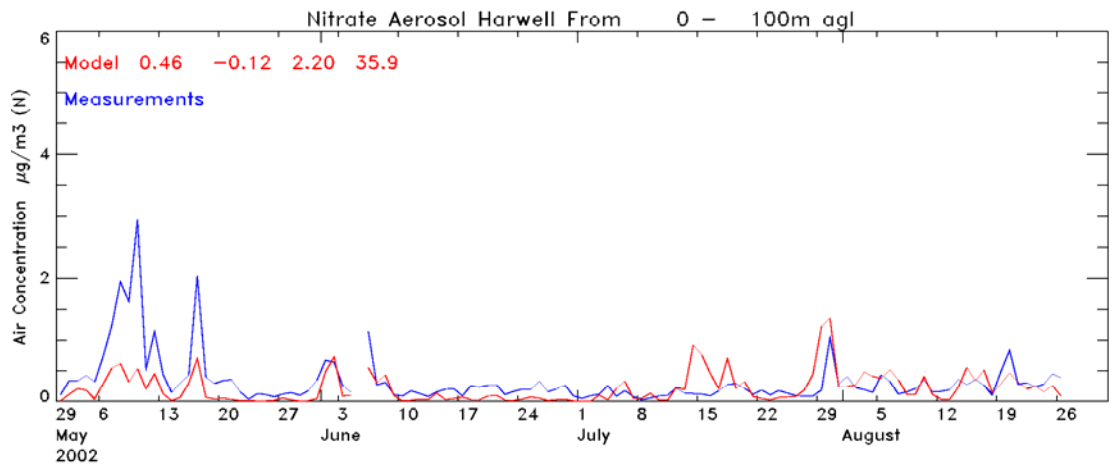
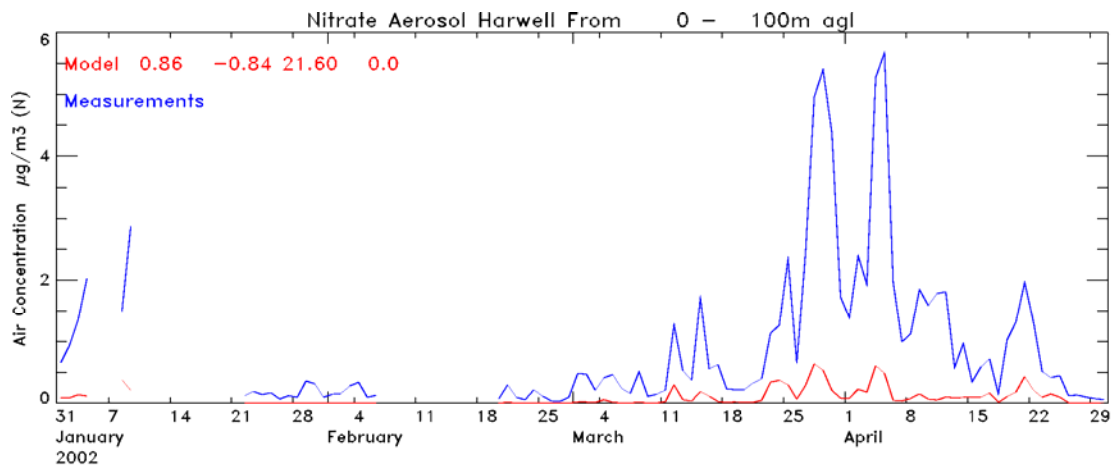


**Figure V-13.** Modelled and observed daily average nitrate aerosol loadings (in  $\mu\text{g m}^{-3}$  of N) at Harwell for 2002.

The relatively low bias values seen in Table V-2 are deceptive. The data shown in Figure V-11 and Figure V-12 reveal that the NAME model is often over-predicting the observed peaks in aerosol (for example, 6<sup>th</sup>-14<sup>th</sup> January 2002), but under-predicting the low background levels (for example, from January 2002 to mid February 2002). The result is a cancelling effect in the bias calculation and thus a relatively low overall bias. On average, sulphate aerosol levels in 2002 are over-predicted but in 2003 are under-predicted. The normalised mean square error gives a better indication of the difference between the modelled and the observed values and highlights the problems in predicting the correct magnitudes. Looking at Figure V-11 and V-12, it appears that the percentage of modelled aerosol levels within a factor of two is more likely to be dominated by the under-prediction of the low aerosol values. Generally speaking, more of the over-predicted peaks are still within a factor of 2 of the observations, compared with the low background levels, which are outside of this range.

Figure V-13 shows daily averaged model nitrate aerosol levels plotted against measurement data from Harwell for 2002. The statistics for each four month period are shown on the plot in red in the following order: correlation, bias, normalised mean square error and percentage within a factor of two. During the period from June to October both the measured and modelled nitrate aerosol concentrations are low and the model performs reasonably well. During the periods January to May and October to December, however, measured values are at times much higher, most notably during April, and the model fails to capture the increased magnitudes. Nitrate aerosol modelling is the subject of ongoing research.

### 3. Assessing the origin of sulphate and nitrate aerosol in the UK for 2002

The next stage of this work was to calculate the attribution of sulphate and nitrate aerosol, so that the proportion of aerosol arriving at each site from individual countries could be found. Table V-3, Table V-4 and Table V-5 show the percentage contribution to modelled sulphate aerosol, nitrate aerosol and sulphur dioxide respectively at thirty locations by the given countries during 2002. Some countries have been grouped and it should be noted that the model domain does not cover the full extent of some countries (for example, Norway, Sweden and Italy).

Looking at Table V-3, Table V-4 and Table V-5, the model predicts that (as a percentage of the total for that species) sulphate aerosol from external sources makes the greatest contribution to observed levels within the UK. Sites to the south and east of the UK receive

the greatest import from other countries, of which the larger part originates from France. Lough Navar and Belfast, (Northern Ireland) and Mace Head, (Ireland) have large contributions from Ireland as would be expected. Substantial Irish contributions are also seen at northern and western UK sites e.g. Eskdalemuir, Narberth and Edinburgh. The contribution from other European countries can be seen to fall off markedly with distance from the UK as would be expected.

In contrast to Table V-3, the percentage contributions shown in Table V-5 for sulphur dioxide show that UK emissions are dominant. Emissions from France have a large effect on the London sites and in the south and east generally, reaching a maximum of 19.4% of sulphur dioxide at Barcombe Mills. The percentage of sulphate aerosol arriving at Barcombe Mills from France is 38.1 %, demonstrating clearly how the generation and transport of the secondary species can have a more dominant effect than the primary species. It should be noted that the attribution for the secondary species includes aerosol formed during the travel time of the primary species from the country of origin (i.e. sulphur dioxide in this case).

A comparison of the percentage contributions for sulphate and nitrate aerosols in Table V-3 and Table V-4 show that sites are generally less influenced by European nitrate aerosol than they are by European sulphate aerosol. For example, 63 % of nitrate aerosol at Barcombe Mills is of UK origin compared with 38 % of sulphate aerosol. Given the relatively poor results for modelled nitrate aerosol when compared with Harwell measurement data, it is not appropriate to draw too many conclusions from the nitrate attribution data.

Figure V-14 shows how the modelled concentration of sulphate aerosol at Yarner Wood can be attributed to the country of origin on a daily basis, and Figure V-15 and Figure V-16 show the corresponding plots for sulphur dioxide and nitrate aerosol. It is interesting to note the differences between Figure V-14 and Figure V-15. For example, looking at the first two weeks of January, the sulphur dioxide concentration level is around 2 ppb with a reasonable contribution from France. This European import is much more evident in the corresponding relatively high level of model sulphate seen. The larger peak in sulphur dioxide on 12<sup>th</sup> - 19<sup>th</sup> February, however, produced very little sulphate aerosol, presumably due to the shorter travel time of the air mass as it consists of sulphur dioxide of UK and Irish origin.

**Table V-3.** Percentage contributions to sulphate aerosol in 2002 at the listed sites.

Site	UK	Atlantic	Ireland	France	Benelux	Germany	Denmark	North Sea	Norway	Sweden	Poland/ Baltic	Czech/ Austria	Italy/Med/ Switz/Yugo
<b>Barcombe_Mills</b>	38.2	7.6	3.5	38.1	5.1	4.8	0.7	1.0	0.0	0.1	0.1	0.3	0.5
<b>Belfast</b>	37.7	5.8	40.9	6.7	2.4	4.2	0.8	0.8	0.0	0.2	0.2	0.3	0.1
<b>Bexley</b>	44.1	6.3	3.4	31.0	6.8	5.4	0.8	1.1	0.0	0.1	0.2	0.4	0.4
<b>Birmingham</b>	60.3	6.1	6.8	15.3	4.7	4.2	0.9	0.8	0.0	0.1	0.2	0.3	0.2
<b>Birmingham East</b>	60.3	6.0	6.7	15.4	4.7	4.3	0.9	0.9	0.0	0.1	0.2	0.3	0.2
<b>Blaise_Castle</b>	53.6	9.0	6.3	21.0	4.1	3.6	0.6	0.7	0.0	0.1	0.1	0.4	0.4
<b>Bloomsbury</b>	46.7	6.4	3.6	28.8	6.5	5.1	0.9	1.1	0.0	0.1	0.2	0.4	0.4
<b>Bristol</b>	52.9	9.2	6.1	21.7	4.1	3.7	0.6	0.7	0.0	0.1	0.1	0.4	0.4
<b>Cardiff</b>	52.9	9.9	8.0	19.5	4.0	3.6	0.5	0.7	0.0	0.1	0.1	0.4	0.4
<b>Edinburgh</b>	65.8	3.5	14.0	7.3	2.5	3.7	1.2	1.2	0.0	0.2	0.3	0.2	0.1
<b>Eskdalemuir</b>	60.0	4.0	18.1	7.7	2.6	4.3	1.2	1.2	0.0	0.2	0.3	0.3	0.1
<b>Haringey1</b>	47.1	6.2	3.5	28.2	6.7	5.2	0.9	1.1	0.0	0.1	0.2	0.4	0.4
<b>Harwell</b>	53.6	7.0	4.3	23.7	4.9	3.8	0.9	0.8	0.0	0.1	0.1	0.4	0.4
<b>High_Muffles</b>	60.9	3.4	8.7	11.4	5.6	6.1	1.3	1.7	0.0	0.2	0.2	0.3	0.2
<b>Hull</b>	59.7	3.5	7.2	13.4	6.5	6.3	1.1	1.5	0.0	0.1	0.2	0.3	0.2
<b>Leeds</b>	64.5	3.5	9.2	10.4	4.3	5.0	1.1	1.2	0.0	0.1	0.2	0.3	0.1
<b>Leicester</b>	60.2	5.2	5.8	15.9	5.4	4.9	0.9	1.0	0.0	0.1	0.2	0.3	0.2
<b>Lough_Navar</b>	24.1	7.3	51.3	7.4	2.7	4.7	0.8	0.7	0.0	0.1	0.2	0.4	0.1
<b>Mace_Head</b>	23.4	9.3	43.9	10.1	3.8	6.4	1.0	0.9	0.1	0.2	0.2	0.4	0.2
<b>Middlesbrough</b>	61.0	3.6	10.0	10.7	4.9	5.8	1.4	1.6	0.0	0.2	0.2	0.4	0.2
<b>Narberth</b>	39.9	15.1	19.8	13.9	4.2	4.9	0.6	0.8	0.0	0.1	0.1	0.4	0.3
<b>Newcastle</b>	61.5	3.8	11.3	10.1	3.9	5.0	1.7	1.6	0.1	0.3	0.3	0.4	0.1
<b>Rochester</b>	40.7	6.0	3.1	33.8	7.4	6.0	0.8	1.2	0.0	0.1	0.2	0.4	0.4
<b>Southampton</b>	44.8	9.4	4.3	31.4	3.8	3.7	0.8	0.8	0.0	0.1	0.1	0.3	0.5
<b>Stoke_Ferry</b>	51.4	4.7	4.3	20.8	8.1	7.0	1.2	1.6	0.0	0.1	0.2	0.4	0.2
<b>Strathvaich</b>	54.7	5.6	17.9	8.6	3.2	4.4	2.5	2.0	0.1	0.3	0.5	0.2	0.1
<b>Sutton</b>	45.4	6.8	3.6	30.6	5.9	4.8	0.8	1.0	0.0	0.1	0.1	0.4	0.4
<b>Swansea</b>	48.2	11.3	13.1	16.8	4.1	4.2	0.7	0.7	0.0	0.1	0.1	0.4	0.4
<b>Thurrock</b>	43.3	6.1	3.3	31.5	7.1	5.7	0.8	1.2	0.0	0.1	0.2	0.4	0.4
<b>Yarner_Wood</b>	36.0	17.7	12.4	23.3	4.2	4.3	0.5	0.7	0.0	0.1	0.1	0.2	0.5

**Table V-4.** Percentage contributions to nitrate aerosol in 2002 at the listed sites.

Site	UK	Atlantic	Ireland	France	Benelux	Germany	Denmark	North Sea	Norway	Sweden	Poland/ Baltic	Czech/ Austria	Italy/Med/ Switz/Yugo
Barcombe_Mills	63.1	1.1	0.4	22.7	8.2	2.6	0.3	1.2	0.0	0.0	0.0	0.2	0.2
Belfast	66.6	3.5	12.8	6.8	4.4	2.8	0.5	2.1	0.1	0.1	0.0	0.2	0.1
Bexley	67.1	0.8	0.3	16.9	9.8	3.1	0.3	1.4	0.0	0.0	0.0	0.2	0.1
Birmingham	80.2	1.3	0.7	7.5	5.5	2.5	0.6	1.4	0.0	0.0	0.0	0.2	0.2
Birmingham_East	80.2	1.2	0.7	7.5	5.6	2.5	0.6	1.4	0.0	0.0	0.0	0.2	0.2
Blaise_Castle	75.1	2.2	1.0	11.7	5.6	2.4	0.4	1.0	0.0	0.0	0.0	0.2	0.3
Bloomsbury	70.3	0.9	0.4	15.1	8.6	2.8	0.3	1.3	0.0	0.0	0.0	0.2	0.2
Bristol	74.7	2.2	1.0	12.1	5.7	2.4	0.4	1.0	0.0	0.0	0.0	0.2	0.3
Cardiff	75.6	2.7	1.5	10.9	4.9	2.3	0.4	0.9	0.0	0.1	0.0	0.2	0.4
Edinburgh	81.7	1.1	2.0	4.3	4.1	2.4	0.7	3.2	0.0	0.1	0.0	0.1	0.1
Eskdalemuir	78.9	1.3	2.7	4.8	4.9	2.7	0.8	3.4	0.0	0.1	0.1	0.2	0.1
Haringey1	70.8	0.8	0.4	14.5	8.6	2.8	0.3	1.3	0.0	0.0	0.0	0.2	0.2
Harwell	74.9	1.3	0.5	12.7	6.4	2.2	0.4	1.0	0.0	0.0	0.0	0.2	0.2
High_Muffles	77.6	0.7	0.7	5.2	6.7	3.9	0.8	4.0	0.0	0.1	0.0	0.2	0.1
Hull	77.5	0.6	0.5	6.5	7.1	3.6	0.6	3.4	0.0	0.0	0.0	0.2	0.1
Leeds	79.7	0.9	0.9	5.6	5.5	3.3	0.9	2.7	0.0	0.0	0.0	0.2	0.2
Leicester	78.8	0.9	0.6	8.0	6.3	2.8	0.5	1.7	0.0	0.0	0.0	0.2	0.2
Lough_Navar	47.2	5.6	27.8	7.6	4.4	3.9	0.6	1.8	0.1	0.2	0.1	0.4	0.3
Mace_Head	43.3	7.3	31.4	6.6	5.2	4.0	0.3	1.0	0.1	0.2	0.0	0.3	0.3
Middlesbrough	77.9	0.9	0.9	5.3	6.4	3.5	0.8	3.8	0.0	0.1	0.0	0.2	0.1
Narberth	71.5	6.9	5.0	8.0	4.1	2.6	0.5	0.8	0.0	0.0	0.0	0.2	0.3
Newcastle	79.6	0.9	1.2	4.8	5.5	2.9	0.8	3.9	0.0	0.1	0.0	0.3	0.1
Rochester	61.5	0.7	0.3	19.9	11.8	3.5	0.3	1.6	0.0	0.0	0.0	0.2	0.1
Southampton	70.4	1.8	0.7	17.1	6.0	2.2	0.3	1.0	0.0	0.0	0.0	0.2	0.3
Stoke_Ferry	70.4	0.6	0.4	10.6	10.7	4.0	0.4	2.7	0.0	0.0	0.0	0.2	0.1
Strathvaich	76.3	2.8	3.4	5.1	3.9	2.8	1.0	4.3	0.1	0.2	0.0	0.1	0.1
Sutton	68.9	1.0	0.4	16.7	8.4	2.7	0.3	1.2	0.0	0.0	0.0	0.2	0.2
Swansea	75.2	4.0	2.7	9.2	4.4	2.5	0.7	0.8	0.0	0.0	0.0	0.1	0.4
Thurrock	65.6	0.8	0.3	17.5	10.4	3.2	0.3	1.4	0.0	0.0	0.0	0.2	0.1
Yarner_Wood	66.4	6.0	3.0	15.5	5.1	2.5	0.3	0.7	0.0	0.0	0.0	0.1	0.4

**Table V-5.** Percentage contributions to sulphur dioxide in 2002 at the listed sites.

Site	UK	Atlantic	Ireland	France	Benelux	Germany	Denmark	North Sea	Norway	Sweden	Poland/ Baltic	Czech/ Austria	Italy/Med/ Switz/Yugo
Barcombe_Mills	72.8	2.0	0.5	19.4	3.4	1.2	0.1	0.4	0.0	0.0	0.0	0.2	0.0
Belfast	64.3	1.9	30.9	1.3	0.4	0.6	0.1	0.3	0.0	0.0	0.1	0.1	0.0
Bexley	83.2	1.2	0.4	10.5	3.0	1.0	0.1	0.3	0.0	0.0	0.0	0.2	0.0
Birmingham	95.6	0.9	0.6	1.5	0.7	0.5	0.0	0.2	0.0	0.0	0.0	0.1	0.0
Birmingham_East	95.7	0.8	0.6	1.4	0.6	0.4	0.0	0.2	0.0	0.0	0.0	0.1	0.0
Blaise_Castle	89.8	2.8	1.0	4.1	1.3	0.7	0.1	0.2	0.0	0.0	0.0	0.1	0.0
Bloomsbury	84.2	1.4	0.5	9.3	2.9	1.1	0.1	0.4	0.0	0.0	0.0	0.2	0.0
Bristol	89.2	2.9	0.9	4.5	1.3	0.7	0.1	0.2	0.0	0.0	0.0	0.1	0.0
Cardiff	90.8	3.0	1.0	3.3	1.0	0.6	0.0	0.2	0.0	0.0	0.0	0.1	0.0
Edinburgh	98.1	0.2	0.8	0.3	0.2	0.2	0.0	0.2	0.0	0.0	0.0	0.0	0.0
Eskdalemuir	95.4	0.5	2.1	0.7	0.4	0.4	0.1	0.3	0.0	0.0	0.1	0.1	0.0
Haringey1	84.9	1.3	0.5	8.8	2.8	1.1	0.1	0.4	0.0	0.0	0.0	0.2	0.0
Harwell	90.9	1.5	0.6	4.5	1.5	0.7	0.0	0.2	0.0	0.0	0.0	0.1	0.0
High_Muffles	97.0	0.3	0.6	0.7	0.6	0.4	0.1	0.3	0.0	0.0	0.0	0.1	0.0
Hull	97.7	0.2	0.3	0.6	0.5	0.3	0.0	0.2	0.0	0.0	0.0	0.1	0.0
Leeds	97.6	0.3	0.6	0.5	0.4	0.3	0.0	0.2	0.0	0.0	0.0	0.1	0.0
Leicester	95.9	0.6	0.5	1.4	0.7	0.5	0.0	0.2	0.0	0.0	0.0	0.1	0.0
Lough_Navar	38.3	3.2	52.6	2.4	1.0	1.4	0.2	0.6	0.0	0.0	0.1	0.2	0.0
Mace_Head	15.5	1.7	79.8	0.9	0.8	0.8	0.1	0.2	0.0	0.0	0.0	0.1	0.0
Middlesbrough	95.8	0.4	1.0	0.8	0.7	0.6	0.1	0.4	0.0	0.0	0.0	0.1	0.0
Narberth	66.5	20.8	5.2	4.5	1.4	1.0	0.1	0.3	0.0	0.0	0.0	0.2	0.0
Newcastle	95.0	0.5	1.5	0.9	0.8	0.7	0.1	0.5	0.0	0.0	0.1	0.1	0.0
Rochester	81.5	0.8	0.3	12.8	3.1	0.9	0.1	0.3	0.0	0.0	0.0	0.1	0.0
Southampton	79.1	3.4	0.8	12.8	2.3	1.0	0.1	0.3	0.0	0.0	0.0	0.2	0.0
Stoke_Ferry	86.4	1.0	0.7	5.8	3.5	1.5	0.1	0.8	0.0	0.0	0.1	0.2	0.0
Strathvaich	84.1	2.8	5.2	2.4	1.2	1.6	0.6	1.6	0.1	0.1	0.3	0.1	0.0
Sutton	82.2	1.6	0.5	10.9	3.0	1.1	0.1	0.3	0.0	0.0	0.0	0.2	0.0
Swansea	84.8	6.7	2.2	3.9	1.1	0.8	0.1	0.2	0.0	0.0	0.0	0.1	0.0
Thurrock	83.5	1.0	0.4	10.5	3.0	1.0	0.1	0.3	0.0	0.0	0.0	0.2	0.0
Yarner_Wood	67.5	15.0	2.2	11.7	2.0	1.0	0.1	0.3	0.0	0.0	0.0	0.1	0.0

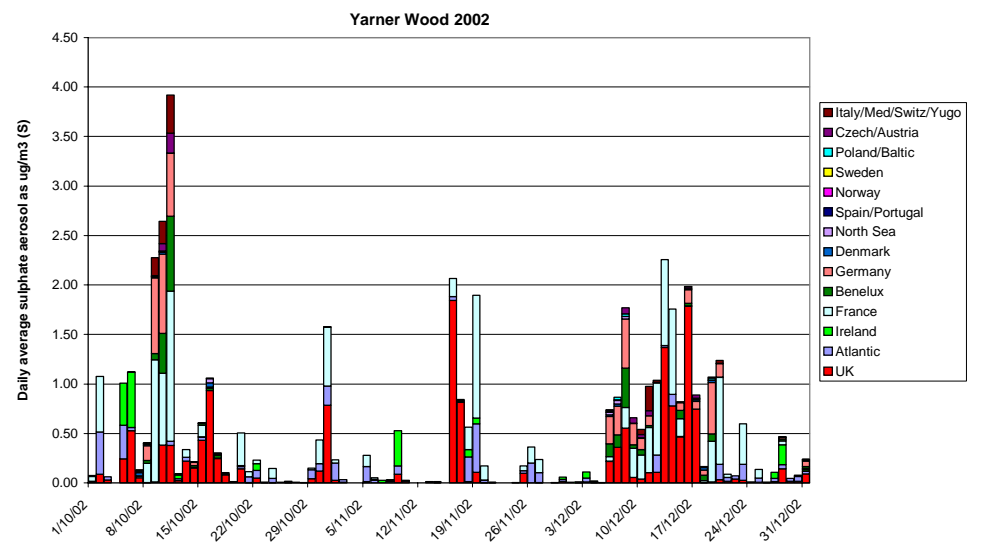
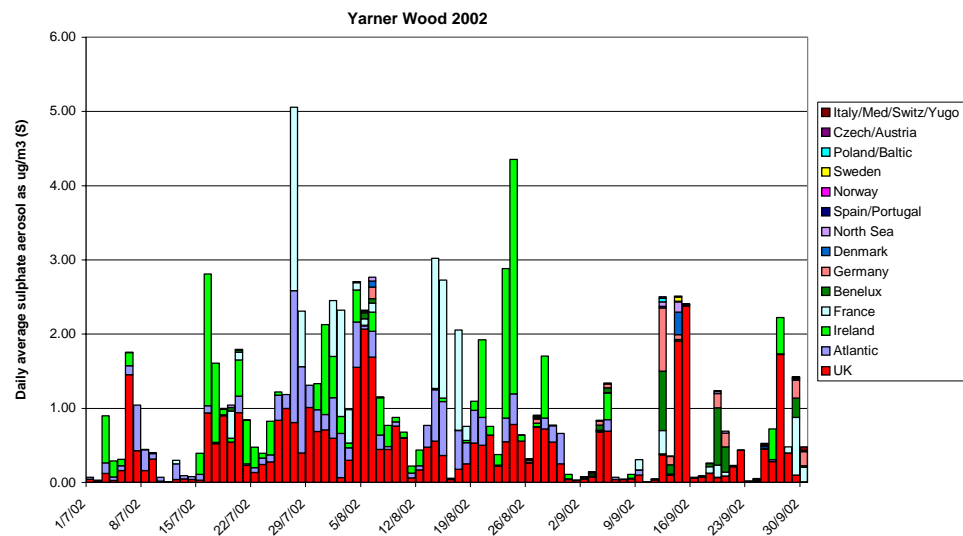
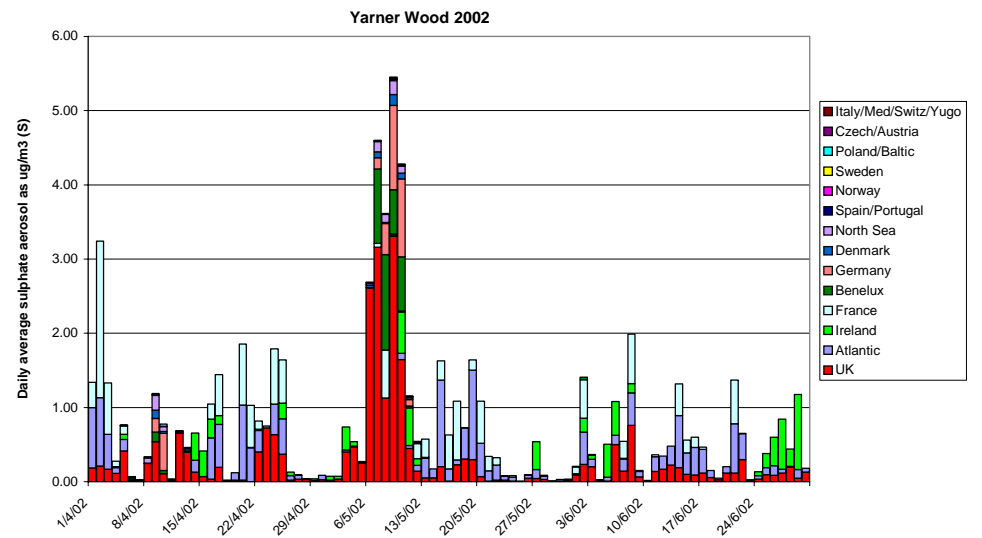
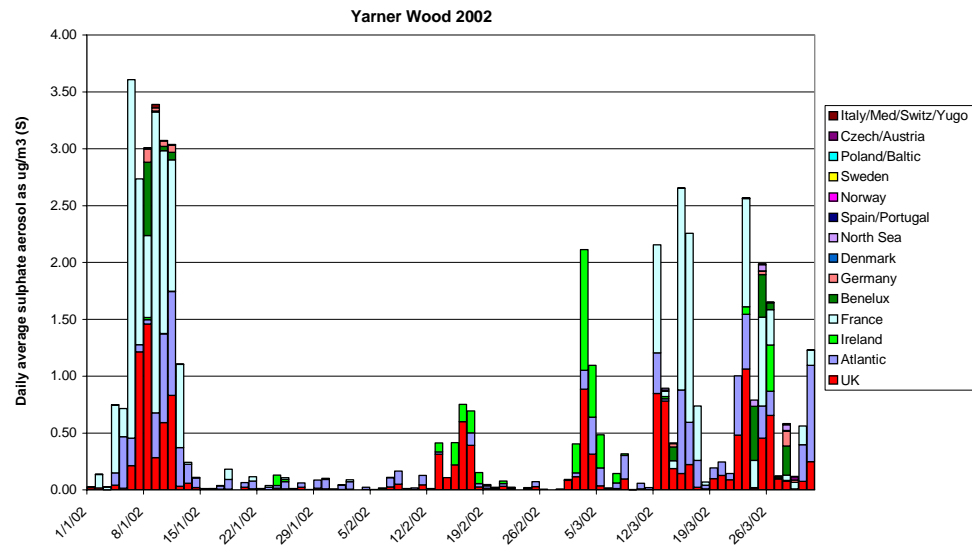


**Figure V-14.** Daily attribution of sulphate aerosol at Yarner Wood for 2002.

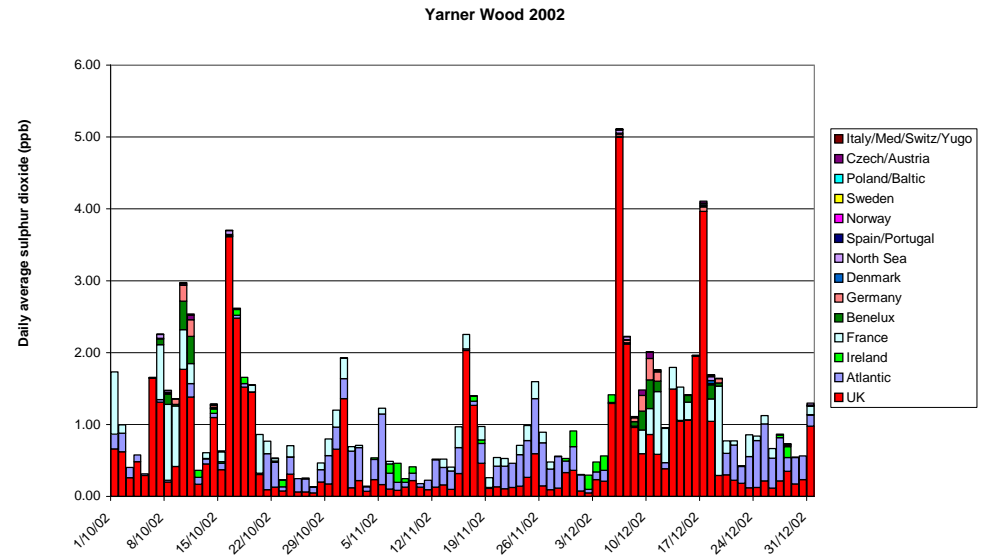
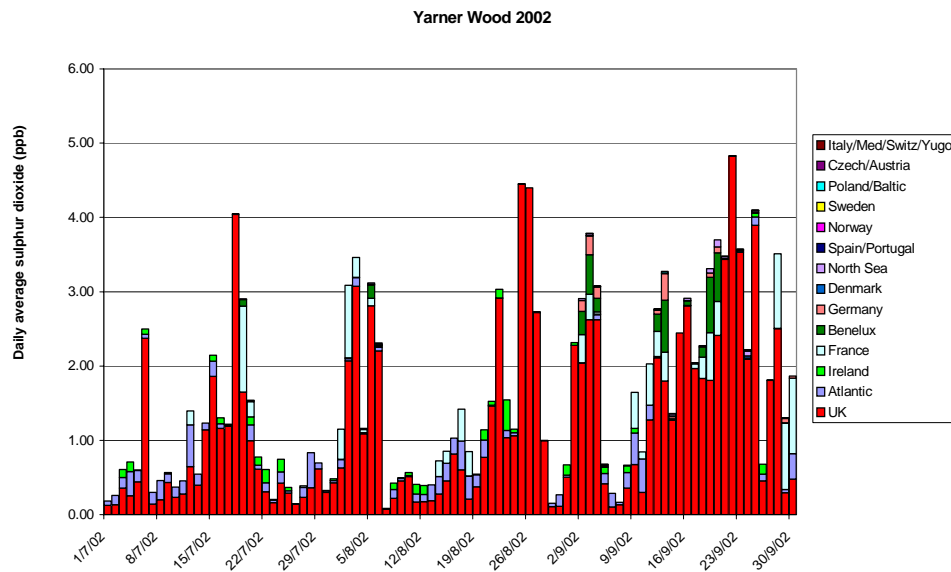
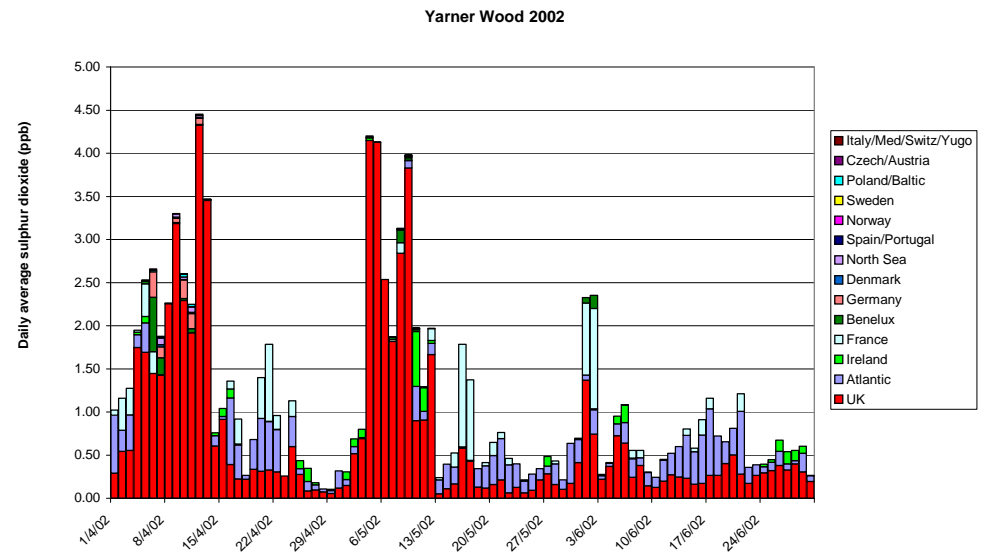
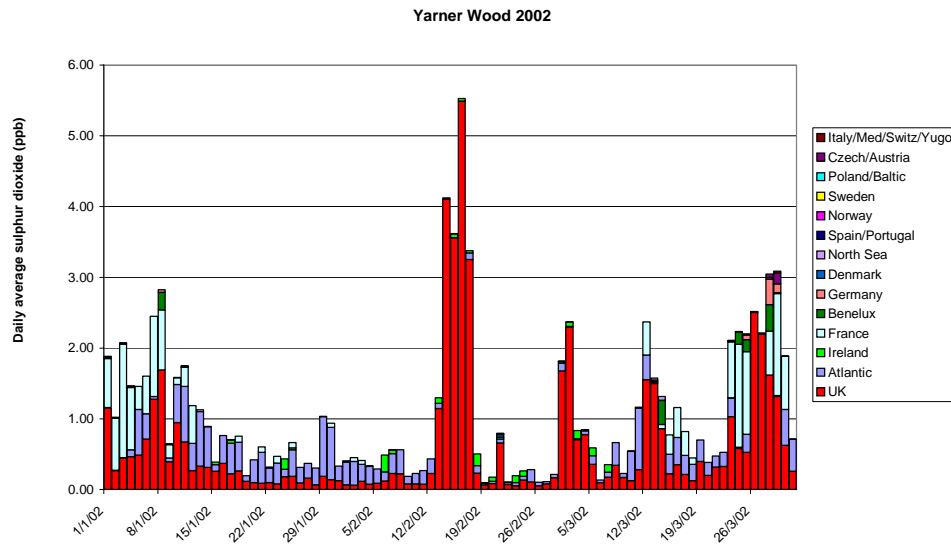


Figure V-15. Daily attribution of sulphur dioxide at Yarner Wood for 2002.

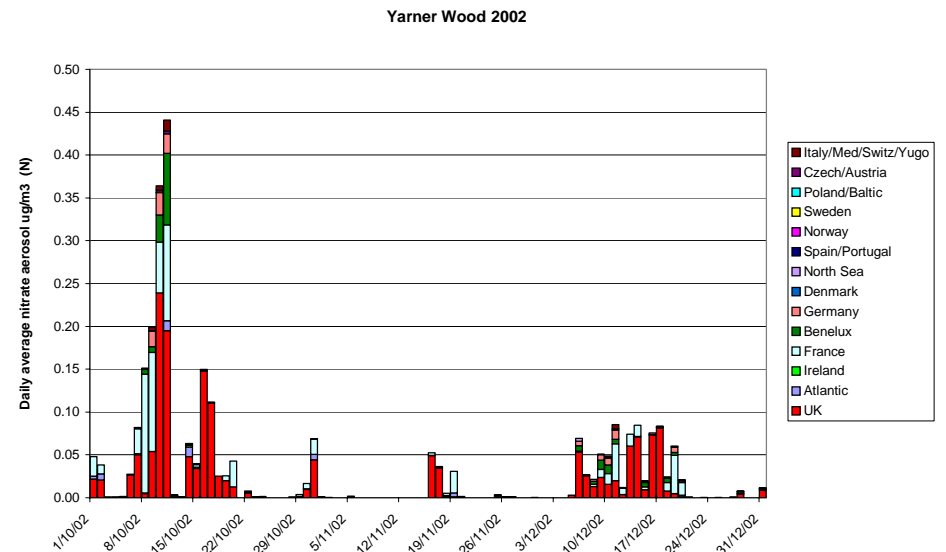
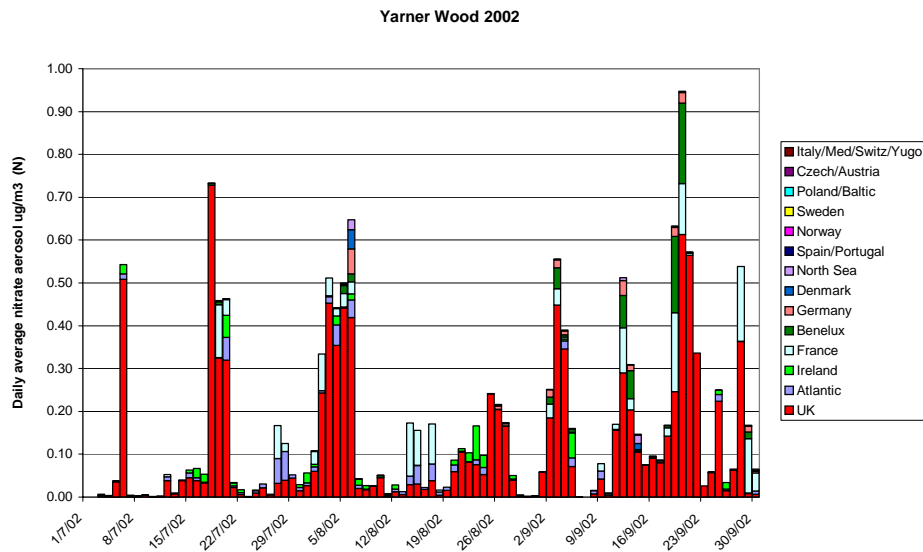
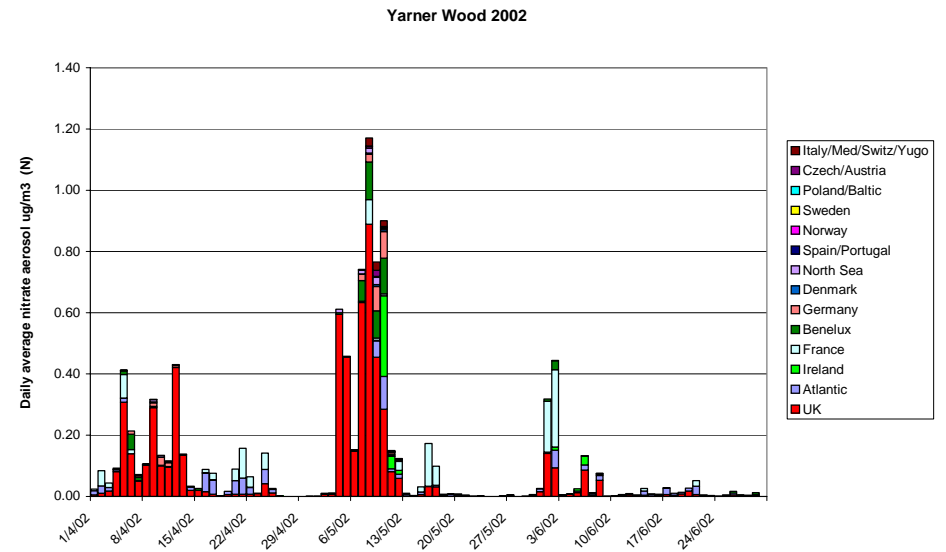
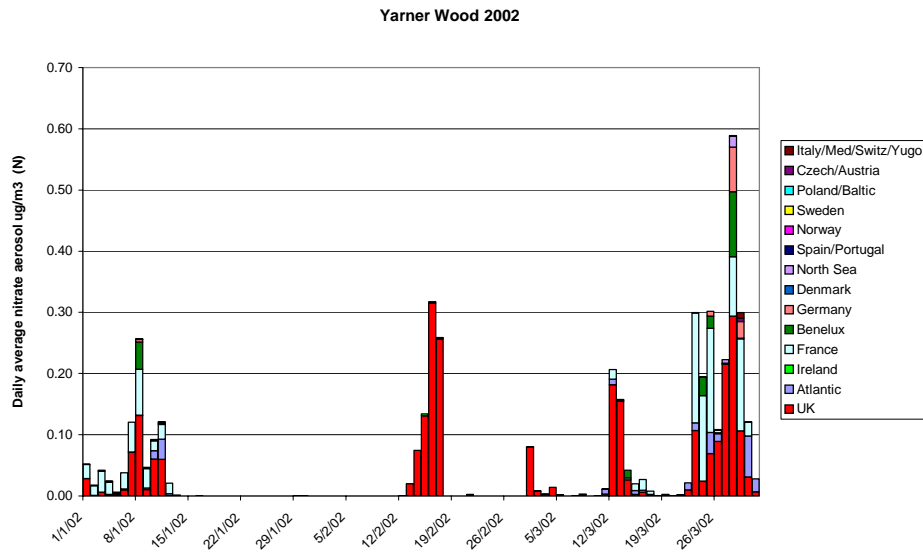


Figure V-16. Daily attribution of nitrate aerosol at Yarner Wood for 2002.

#### 4. Year to year variability of sulphate aerosol import

In this section, a subset of ten of the measurement sites has been selected for clarity. The sites chosen represent a good geographical spread and a mixture of urban and rural locations. Table V-6 and Table V-7 show percentages of sulphate aerosol at UK receptors split by country of origin for 2002 and 2003. (Data shown in Table V-6 are a subset of the data shown in Table V-3.)

The percentage contributions presented in Table V-7 show the same overall picture as was seen in 2002. However, it is interesting to note that there is a marked increase in the contributions from the Benelux countries and Germany in 2003, reflecting the different air mass pathways that dominated the synoptic flow during this year. In 2003, over 60% of the sulphate aerosol in London was from sources outside the UK. The three biggest contributors were: France (26.9%), Germany (10.1%) and Benelux (9.5%). These results highlight the effects of the year to year variability of the meteorology, and indicate that not only do the overall amounts imported each year differ, but the relative importance of source regions change, as does the effect on different parts of the UK, depending on the dominant air mass pathways. The contribution from shipping is very similar in both years, with the exception of Yarner Wood, which sees a substantial decrease from 18.4% to 10.6%. The contributions range from 4.7% to 18.4%, which is smaller to the range predicted by STOCHEM for the year 2000, 10% to 27% (see Chapter II, pages 42-43). Given the different resolutions, emissions and chemistry of the NAME and STOCHEM models, the agreement in these two estimates is reasonable.

**Table V-6.** Percentage contributions to sulphate aerosol in 2002.

Site	UK	Ireland	France	Benelux	Germany	Denmark	Shipping	Other Countries
Edinburgh	65.8	14.0	7.3	2.5	3.7	1.2	4.7	0.8
Eskdalemuir	60.0	18.1	7.7	2.6	4.3	1.2	5.2	0.9
Lough_Navar	24.1	51.3	7.4	2.7	4.7	0.8	8.0	0.8
High_Muffles	60.9	8.7	11.4	5.6	6.1	1.3	5.1	0.9
Mace_Head	23.4	43.9	10.1	3.8	6.4	1.0	10.2	1.1
Birmingham	60.3	6.8	15.3	4.7	4.2	0.9	6.9	0.8
Harwell	53.6	4.3	23.7	4.9	3.8	0.9	7.8	1.0
London	46.7	3.6	28.8	6.5	5.1	0.9	7.5	1.1
Barcombe_Mills	38.2	3.5	38.1	5.1	4.8	0.7	8.6	1.0
Yarner_Wood	36.0	12.4	23.3	4.2	4.3	0.5	18.4	0.9

**Table V-7.** Percentage contributions to sulphate aerosol in 2003.

Site	UK	Ireland	France	Benelux	Germany	Denmark	Shipping	Other Countries
Edinburgh	56.9	14.7	5.7	5.1	8.9	1.7	5.4	1.6
Eskdalemuir	51.7	17.8	7.9	4.6	8.8	1.1	6.6	1.4
Lough_Navar	23.8	48	8.9	3.9	6.4	0.9	7	1.1
High_Muffles	58	8.3	9.7	5.9	9.9	1.4	5.4	1.4
Mace_Head	18.9	45.1	14.2	3.4	5.4	0.9	10.9	1.1
Birmingham	58.6	5.6	12.5	6.5	8.9	0.8	5.9	1.1
Harwell	47.6	4.2	21.6	7.9	9	0.8	7.4	1.5
London	39.8	3.8	26.9	9.5	10.1	0.9	7.4	1.6
Barcombe_Mills	28.7	3.2	37.5	9.9	10	0.8	8.2	1.6
Yarner_Wood	36.8	6.4	26.6	7.8	9.5	0.9	10.6	1.3

### (c) Estimation of contribution of natural sources to fine and coarse particles

#### 1. Introduction

There is growing interest in suspended particulate matter because of its potential adverse impact on human health, visibility and climate. In order to address this issue the EU have put in place concentration limits for PM<sub>10</sub> (particles with a diameter less than 10 µm) under the new Air Quality Directive. Stage 1 limits, to be achieved by 2005, are an annual mean value of 40 µg PM<sub>10</sub> m<sup>-3</sup> with a 24 hour limit of 50 µg PM<sub>10</sub> m<sup>-3</sup> to be exceeded fewer than 35 days a year. While it is generally recognised that natural sources can contribute significantly to particulate matter, information quantifying the extent of these sources remains scarce. In order to determine the likelihood of meeting the EU targets it is necessary to identify the frequency and scale of PM<sub>10</sub> events due to natural sources. An emission parameterisation for a range of natural sources of primary PM<sub>10</sub> has been developed within the NAME model. The accuracy of the emission terms is then to be verified against observed data for specific episodes for which the natural component is thought to contribute significantly to levels of PM<sub>10</sub>. Once model validation has been completed satisfactorily, estimates may then be made regarding the contribution of natural sources to air quality in the UK

Particulate matter is modelled using a number of bin sizes to describe adequately the size distribution of particulates up to 10 µm in diameter. Data from the model will initially be split into two size categories, 10 µm and 2.5 µm, to facilitate comparison with field measurements. This distinction between PM<sub>10</sub> and PM<sub>2.5</sub> will be applied to all modelled

components of particulate matter: anthropogenic, natural and secondary components (generated by atmospheric chemistry within NAME). The use of these two sizes will allow receptor modelling to analyse the dominant sources that contribute towards PM<sub>10</sub> and PM<sub>2.5</sub>.

To achieve these goals a comprehensive literature review was undertaken which has identified the main sources of natural particulate matter in the atmosphere. These sources include contributions from the re-suspension of road dust, the uplift of dust, soil and sea salt, as well as those sources of a biological nature such as pollen, fungal spores and bacteria. Work has initially focused on the contribution from sea salt for which a reasonable amount of information is available in the literature. Data regarding the emission of salt particles from the sea were gathered and incorporated into a parameterisation scheme within the NAME model. In this scheme both the emission rate and the particle size distribution are determined as a function of the surface wind speed. Thereafter the sedimentation of the particles is calculated explicitly as a function of the particle size. The sea salt scheme and its performance are discussed in section 2 below. The implementation of the dust emission and deposition scheme from the climate model into NAME, and some studies of episodes with high dust levels, is described in section 3.

## 2. Modelling the formation and transport of sea salt

A scheme which models the emission of sea salt particles using two bin sizes to represent particles between 0.1µm and 10 µm in diameter (Gong and Barrie, 1997) has been implemented into NAME. The most important mechanism for the generation of sea-salt aerosols is through the entrained air bubbles bursting during whitecap formation. Additional energy supplied by the wind to the sea surface causes direct production of sea-salt particles through the production of spumes. The parameterisation implemented into NAME includes both the generation of sea salt particles indirectly through production by bubbles and directly through production by spumes. Both the emission rate and the particle size distribution are determined as a function of the surface wind speed. As with the Saharan dust, other parameters such as dry deposition, gravitational settling and in-cloud and below-cloud scavenging were also investigated.

In order to validate the sea salt particle scheme the model was run for a three month spell over the autumn of 1998. This timeframe was chosen as there were a number of instances during

which it was thought that sea salt could have contributed significantly to the levels of PM<sub>10</sub> observed.

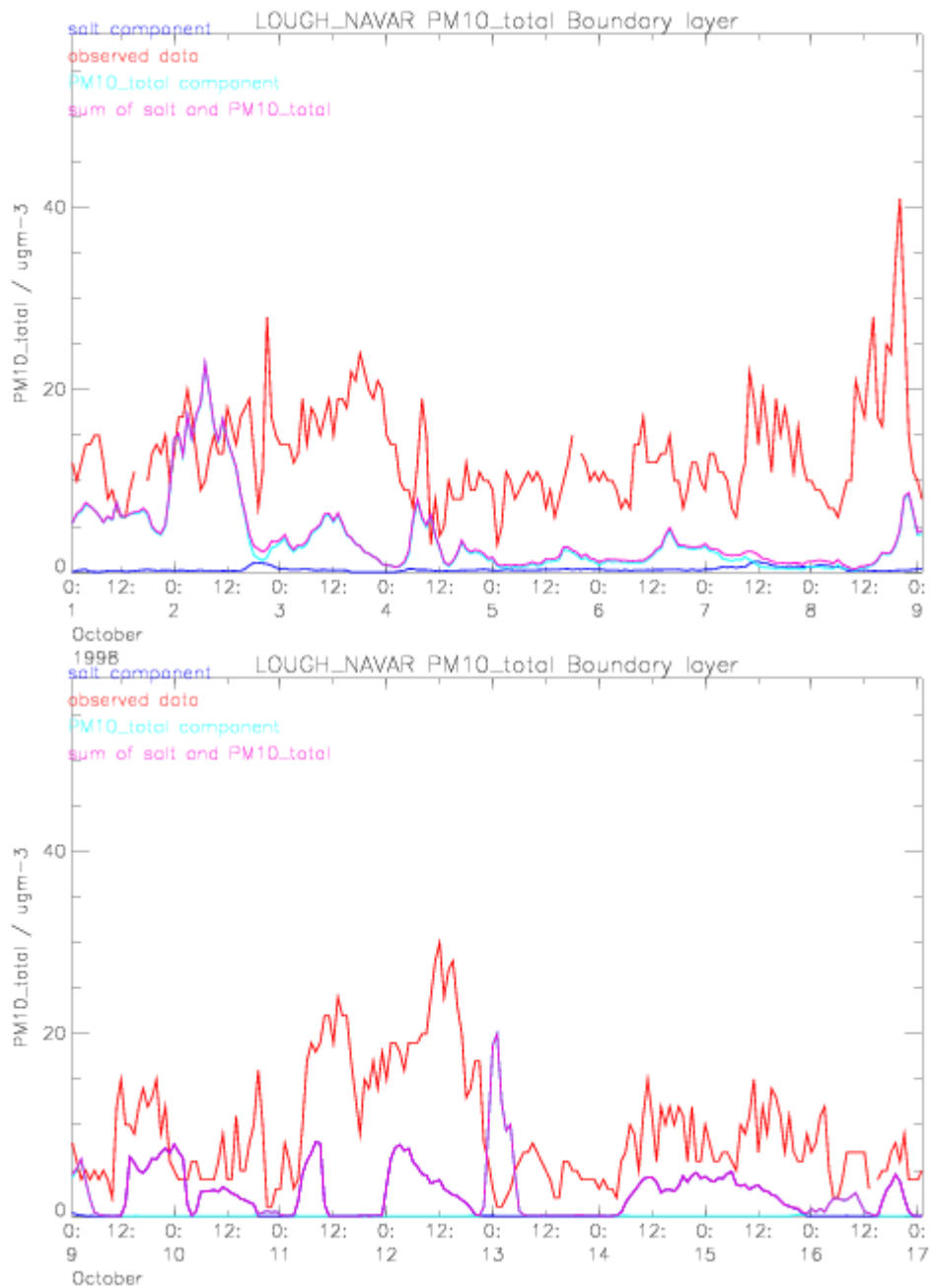


**Figure V-17.** Observed and modelled total PM<sub>10</sub> levels for 1<sup>st</sup> – 17<sup>th</sup> October 1998.

Figure V-17 shows model results for the first half of October 1998 for Lough Navar (a rural observation site in Northern Ireland). The sea salt component is labelled as “salt component”. A model run was also performed using NAME in conjunction with NAEI / EMEP emissions of primary pollutants together with the chemistry to generate secondary PM<sub>10</sub>. The output

from this model run was labelled as “PM10\_total component” with the sum of these labelled as “Sum of salt and PM10\_total”. These are both plotted against the observed PM10 data acquired from The UK National Air Quality Information Archive.<sup>4</sup>

The model predicts that, apart from the 2<sup>nd</sup> October, sea salt does not contribute significantly to the levels of PM10 observed during the first eight days of the simulation. However, during the second half of the timeframe shown here there are a number of instances where sea salt is predicted to be the major component of the observed PM10 at this remote site. As expected, model predictions at inland and urban environments show sea salt to be a much smaller component of observed PM10 than at coastal sites. As such the model may be used at present to identify potential sea salt episodes, but in order to assess the accuracy of the concentrations the model generates, comparisons against speciated PM10 data are required. Such data were not available during this contract.

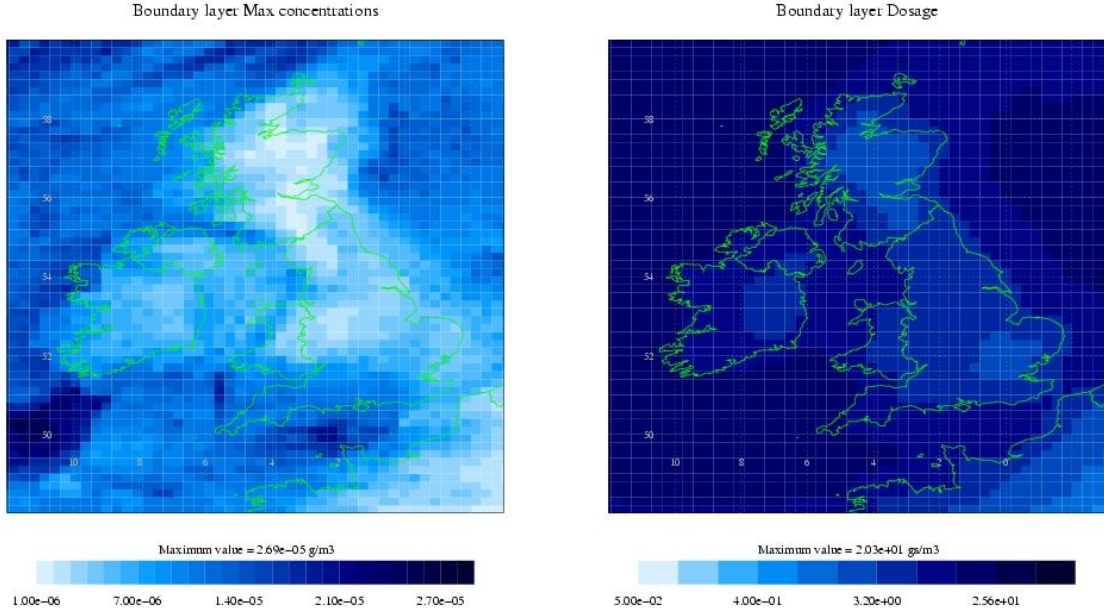


**Figure V-18.** Model output highlighting the maximum concentration and the cumulative concentrations of sea salt over the period 1.10.98 – 31.12.98.

Model results showing the maximum sea salt concentrations and cumulative totals over a three month period from 1<sup>st</sup> October to 31<sup>st</sup> December 1998 are shown in Figure V-18. This study indicates that sea salt alone is unlikely to produce an exceedence of the air quality objectives, as the maximum air concentration (daily averaged) over land is around 10 µg m<sup>-3</sup>.

<sup>4</sup>(<http://www.airquality.co.uk/archive/index.php>).

These results also suggests that while inland areas generally experience lower amounts of sea salt than coastal regions, sea salt is still a significant component of inland PM<sub>10</sub> levels. Further model runs were performed over the same three month period for the year 2003 and also for August 1999 to May 2000. These results were broadly similar to those shown in Figure V-18, indicating a relatively steady contribution from sea salt to PM<sub>10</sub> levels each year.

### 3. Modelling the transport of Saharan dust

#### (i) Validation of the dust scheme

A dust scheme based on that used in the Hadley Centre's climate model (Woodward, 2001) has been implemented within NAME to simulate the emission and transport of Saharan sand using six bin sizes from 0.06 µm to 60 µm in diameter. This dust emission scheme has been used within the climate model to investigate the radiative impact of mineral dust. In this scheme both the emission rate and the particle size distribution are determined as a function of the surface wind speed. Other than the emission scheme, additional factors that were investigated include the sedimentation mechanism and both the dry and wet deposition of sand particles. These quantities are now calculated explicitly as a function of the particle size. The performance of the dust scheme was assessed using three case studies of dust events.

#### *Case Study (1)*

First, the accuracy of the dust emission terms and loadings predicted by NAME were assessed. A dust event on the 19<sup>th</sup> to 21<sup>st</sup> July 2004 was identified and some Meteosat-8 images were acquired in order to validate the extent of the dust plume predicted by NAME (Figure V-19). Results from the Naval Research Laboratory model NAAPS are also shown for comparison.

One factor that should be borne in mind is that accurate soil moisture information required by the emission scheme was not currently available. Therefore, soil moisture values used were monthly mean values obtained by averaging 30 years of modelled values from a climate model simulation. Despite this simplification, the model represents satisfactorily the evolution of the dust over this three day period. Figure V-19 shows the satellite imagery together with results from NAME and also from the NAAPS model (developed by NRL) for the 19<sup>th</sup> July 2004 at 1200 UTC. These results demonstrate that NAME has picked out the main features of the dust event and compares favourably with other model predictions.

However, the dust loadings predicted by NAME are considerably larger than those from the NAAPS model

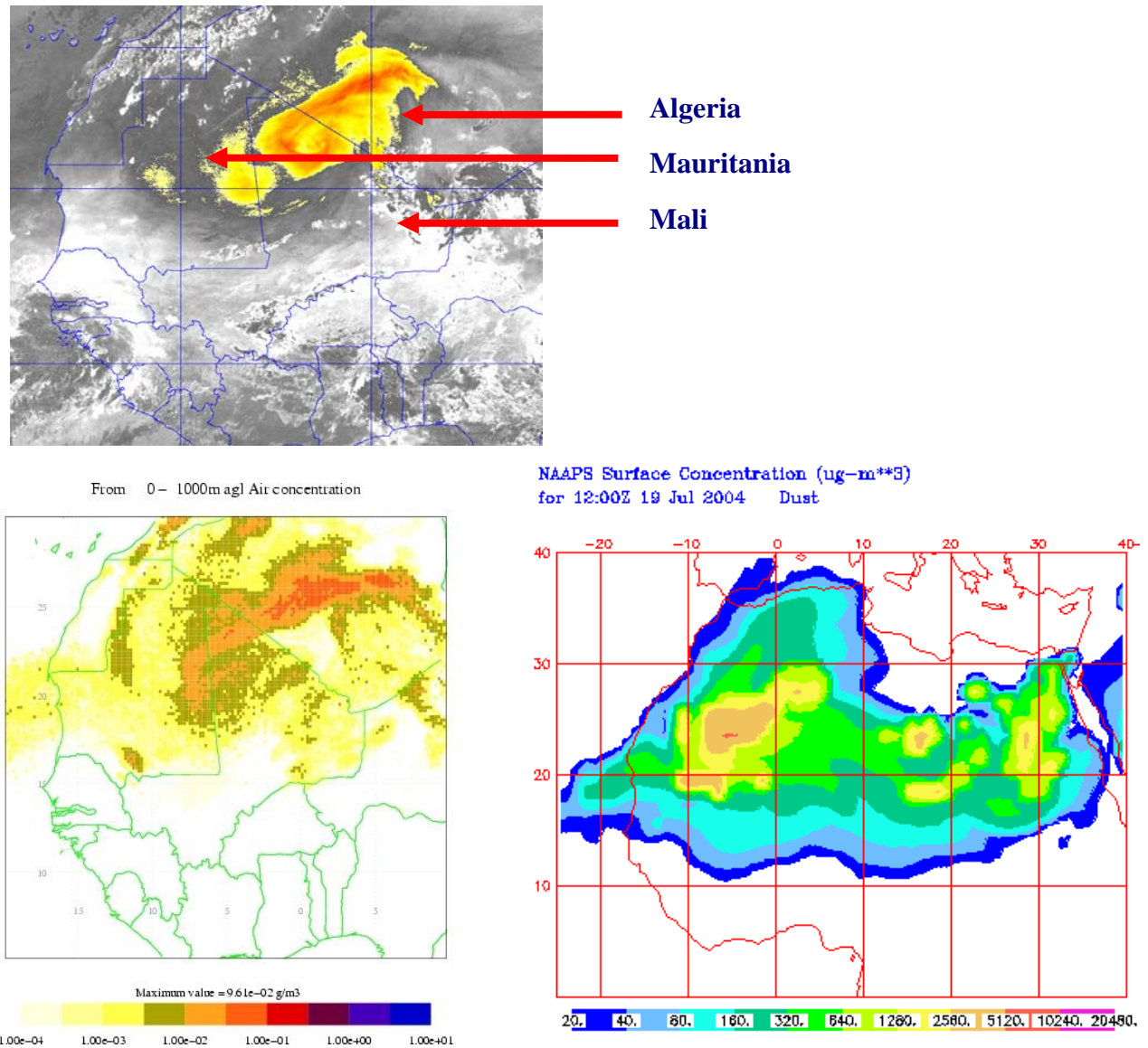


**Figure V-19.** Satellite imagery (top left panel) and modelled dust loadings from NAME (bottom left panel) for 19<sup>th</sup> July 2004 at 1200 UTC. Results from the Naval Research Laboratory NAAPS model are also shown (bottom right panel).

### Case Study (2)

Further validation of the dust scheme within NAME was carried out by simulating the dust event reported by Rodriguez et al. (2002), because PM<sub>10</sub> and TSP (total suspended particles) measurements are available at two sites (Morella and Monagrega) in north east Spain. As demonstrated by the three day back trajectories shown in the lower 3 panels of Figure V-20,

between 24<sup>th</sup> and 27<sup>th</sup> Aug 2000, particulates measured at Morella and Monagrega could well have originated from Africa.

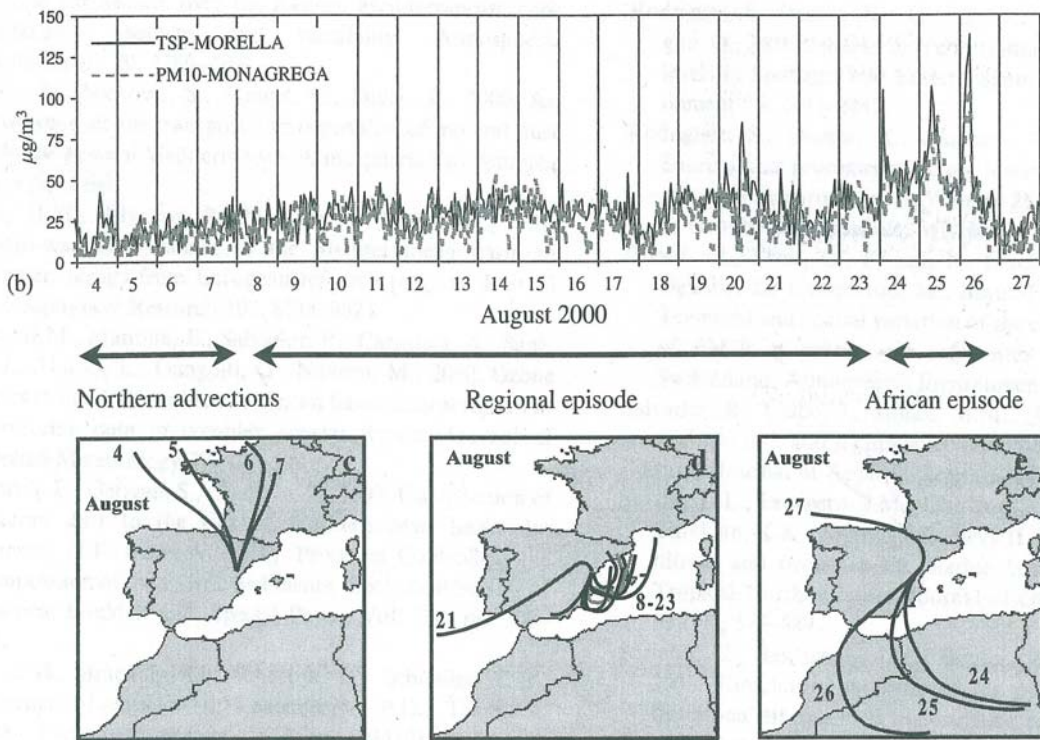


**Figure V-20.** Observed mass of particulates and trajectories (Rodriguez et al., 2002).

While the timing and the profile of the modelled peaks at Morella and Monagrega (Figure V-21) compare reasonably well the measurements (top panel of Figure V-20), the concentrations generated by NAME are again much greater than those measured at the observation sites (upper panel of Figure V-20).

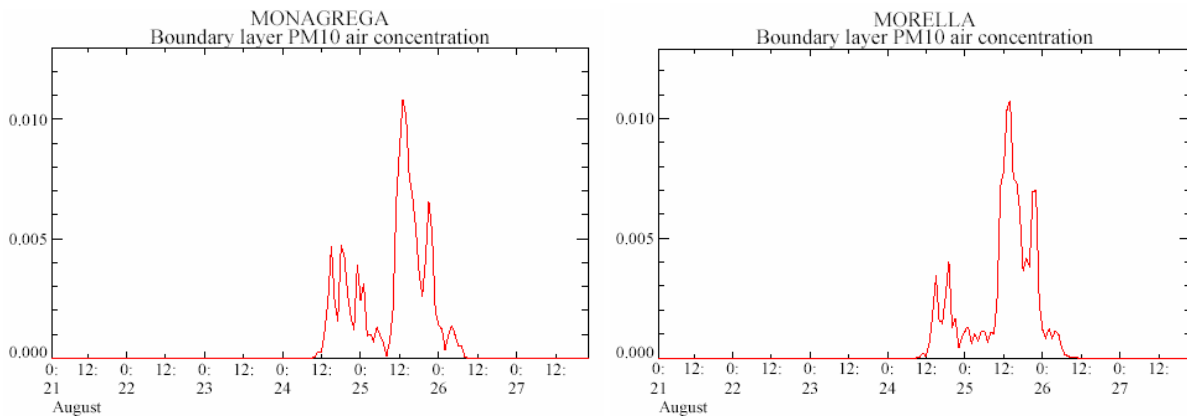


**Figure V-21.** Modelled Saharan dust contribution to PM<sub>10</sub> (g m<sup>-3</sup>) over the period 21<sup>st</sup> – 28<sup>th</sup> August 2000 at Monagrega and Morella.

As well as the lack of accurate soil moisture information, the resolution of NAME (and hence the driving data, such as soil types and fractions, as well as the meteorology) will also impact on the results. The first comparison of the modelled results with satellite observations and the simulation by the NAAPS model (see Figure V-19) focused on a small area over the Sahara, and used a resolution of  $0.18^\circ \times 0.18^\circ$ . However, in order to run the model over a larger area to simulate transport of dust to Spain, it was necessary to run NAME at a lower resolution ( $0.83^\circ \times 0.55^\circ$ ). NAME was run at these two resolutions over the same time period for the Western Sahara. The higher resolution simulation (Figure V-22, left panel) picks up the dust event highlighted in section 2(i) whereas the model run at lower resolution does not represent the event nearly as well (Figure V-22, right panel). This result is clearer if each of the panels in Figure V-22 are compared Figure V-19. In the latter case, the dust concentrations are much smaller.

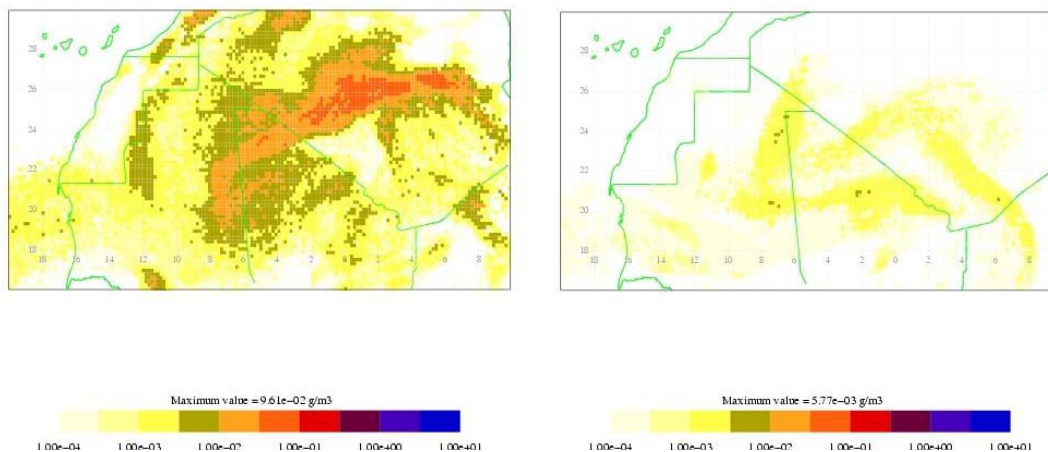


**Figure V-22.** Modelled TSP masses for the 19<sup>th</sup> July 2004 at 1200 UTC, at  $0.18^\circ \times 0.18^\circ$  resolution (left panel) and  $0.83^\circ \times 0.55^\circ$  resolution (right panel).

### *Case Study (3)*

There was an episode in March 2000 when significant amounts of dust from the Sahara were transported to the UK during which time loadings as high as  $292 \mu\text{g m}^{-3}$  were recorded in Plymouth. The modelled dust loadings at selected days between the 25th February and 5th March 2000 are shown in Figure V-23. The transport of dust from the Sahara to the UK is clearly shown. While the timing of the arrival of the dust proves to be accurate, work is presently ongoing to quantify the amounts arriving at the UK. As with the Spanish episode described in case study (2), NAME is over predicting the amounts transported to the UK.

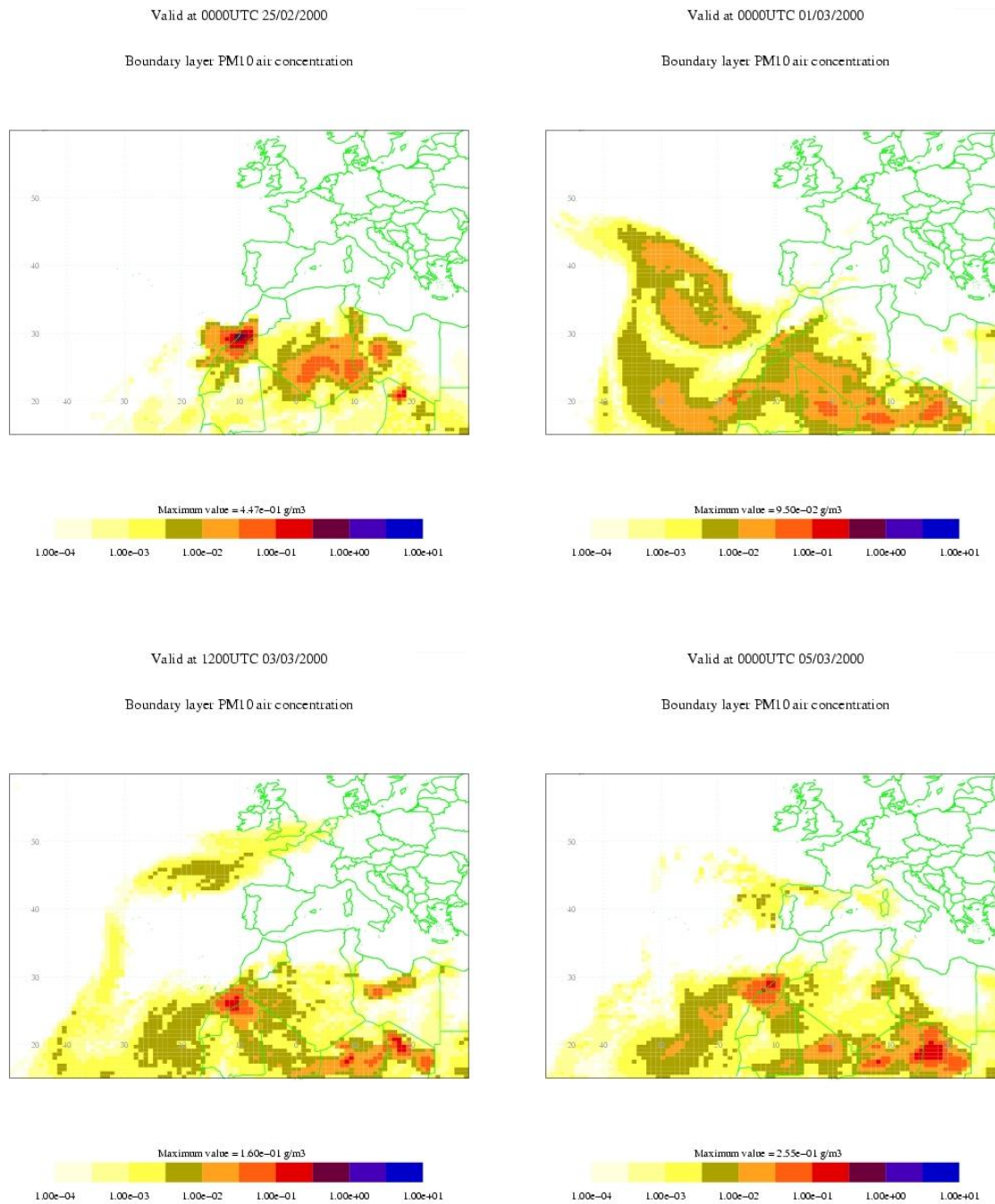


**Figure V-23.** Model output highlighting the dust generation and transportation. Plots are for 0000 UTC 25/2/2000, 0000 UTC 1/3/2000, 1200 UTC 03/3/2000 and 0000 UTC 5/3/2000.

Further work on the dust scheme in NAME has focused on the validity over a 1 – 14 day time period. Other than the emission scheme, additional factors that were investigated include the sedimentation scheme and both the dry and wet deposition of sand particles. These deposition rates are now calculated explicitly as a function of the particle size. Modelled dust is generated at three size categories, 1  $\mu\text{m}$ , 2.5  $\mu\text{m}$  and 10  $\mu\text{m}$  to facilitate comparison with field measurements acquired at these size ranges ( $\text{PM}_1$ ,  $\text{PM}_{2.5}$ , and  $\text{PM}_{10}$ ).

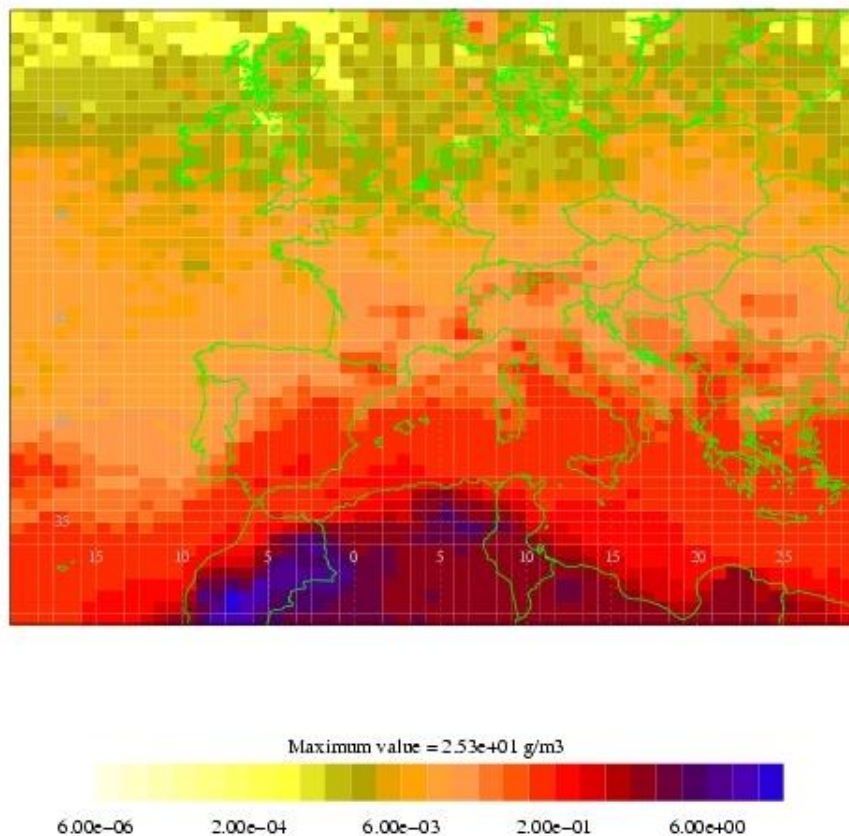


**Figure V-24.** Cumulative concentrations of dust over Europe for the year 2000 from NAME.

While the NAME model has the ability to identify the main plume of dust (Figure V-19), satellite imagery is not able to quantify the amounts of dust present in each layer of the atmosphere. In addition to the resolution issues highlighted earlier, there are a number of uncertainties with respect to the input parameters used in the emission scheme. These include the clay fraction, the soil moisture content, the surface wind speed and the vegetation fraction. Therefore, studies were undertaken examining the affect of these parameters on the resulting maximum concentration of dust observed at Plymouth during this episode. The model results were found to be very sensitive to the changes in these input parameters. This also helps explain the sensitivity of the model to the resolution at which it is run. Clearly if the model is run at higher resolution the input parameters used by the dust scheme will be more representative of the area that they are representing.

In addition to using the model to examine specific instances in which dust is thought to contribute significantly to levels of particulate matter, it is also possible to run the model over

a longer period of time to assess the impact of dust across Europe. Figure V-24 show the cumulative concentration of dust as predicted by NAME for the year 2000. Despite the uncertainties regarding the amounts of dust being emitted by the scheme, using the model in this fashion allows assessments to be made regarding the geographical impact of Saharan dust across Europe. For example it can be seen from Figure V-24 that areas of north East Spain could well be more affected by dust from the Sahara than Portugal for example. While charts such as Figure V-24 can provide useful information, further work is required to improve the accuracy of the emission scheme in order to achieve more realistic results. For example characterising the soil moisture on the basis of climatologically data is a simplification which clearly needs to be addressed.

#### (ii) Contributions to the DABEX and DODO flight campaigns

The atmospheric dispersion group provided support to the flight campaigns “Dust and Biomass Experiment” (DABEX) and “Dust Outflow and Deposition to the Ocean” (DODO) (see <http://www.metresearch.com/dabex/>). These campaigns were based in Niamey and Dakar during the month of January 2006 and will provide useful data with which to validate the dust modelling that the group performs. In addition these campaigns were also useful in allowing the dispersion group to demonstrate our operational capabilities. Forecasts were produced twice daily over the whole of the Sahara and were critical in planning the flight routes. As well as supplying the dust forecast a biomass burning forecast was also provided initiated manually using satellite imagery to identify sources of biomass burning. Initial feedback was very positive regarding the biomass forecasts. Although the dust forecast generally worked well, on a number of occasions dust was observed that the model had not predicted. In order to address this problem, “ad hoc” runs were performed in which the dust was initiated manually and tracked within the model.

#### **(d) Photochemical oxidant modelling within NAME**

##### 1. Ozone

Considerable progress has been made with modelling ozone in NAME. Ozone modelling in the Lagrangian framework has proved a difficult problem. Whilst a Lagrangian model is suited to following the dispersion of air parcels simulating the release of pollutants from anthropogenic sources (i.e. traffic or industrial sources) it is less well suited to modelling a chemical species that is being generated throughout the atmosphere, and is present as a

background species. The previous version of the model treated species that were globally present but not directly released into the atmosphere as static fields, held on the 3-dimensional grid on which the chemistry was calculated.

The released species and their chemical products are transported in the model atmosphere as masses held on air parcels. In order to calculate loss terms for primary species and production terms for secondary species due to the chemical reactions occurring, it is necessary to calculate species concentrations from the masses carried by the air parcels. This is done by effectively constructing a three-dimensional grid over the model domain, and adding up the contributions to the mass of each species from the air parcels within that grid box, from which a concentration can then be calculated. Concentrations of background species, i.e. those species not directly released into the atmosphere, but that are globally present, are also held on this three-dimensional grid, and all the species concentrations are then passed to the chemistry module. After the chemical reactions have taken place, the new concentrations of the species carried on the air parcels must be converted back to masses and re-assigned back to the air parcels. By using the information about the plume of air parcels before the chemistry occurred, it is possible to allocate production and loss terms in proportion with the original amount of primary species carried in the parcel. This method reduces the artificial diffusion of a species within the chemistry grid box.

The new concentrations of the background species, including ozone, were then stored on the three-dimensional grid for use in the next time step, so although the precursors for ozone formation were being advected in the model the actual ozone was not. The most obvious way to tackle the advection of ozone would be to simply initially release ozone air parcels throughout the model domain with a mass sufficient to represent background ozone, and then subsequently feed in parcels carrying background ozone from the model domain boundaries. The parcels could then be advected and interact with anthropogenic emissions and the chemistry scheme could then calculate the production and loss as before. Unfortunately, this approach is prohibitively expensive in terms of memory and model run time as many millions of air parcels would be required to properly represent the ozone field. Instead, an approach has been developed which uses a combination of the existing model air parcels that are released to represent the anthropogenic emissions and the static background field.

The NAME photo-oxidant scheme has been tested using the August 2003 ozone episode which was particularly notable for its long duration, high temperatures and the highest recorded ozone concentrations over London in the last ten years. The model was run at a horizontal resolution of 10 km over a domain 11.0° W to 12.4° E and 46.0° N to 61.7° N, with vertical layers of 200 m depth up to 2 km and a further 4 levels up to the top of the model domain at 20 km. The model was run from the 28<sup>th</sup> July to 16<sup>th</sup> August and hourly average modelled ozone concentrations have been compared with a number of rural and urban sites around the UK. Figure V-25 shows the model data plotted against the observations at London Bloomsbury and Narberth. The model is shown in red and the observed data in blue. Where there is missing data in the observations, the corresponding model data has not been plotted. Narberth is a rural site on the west coast of Wales, and London Bloomsbury is an urban centre.

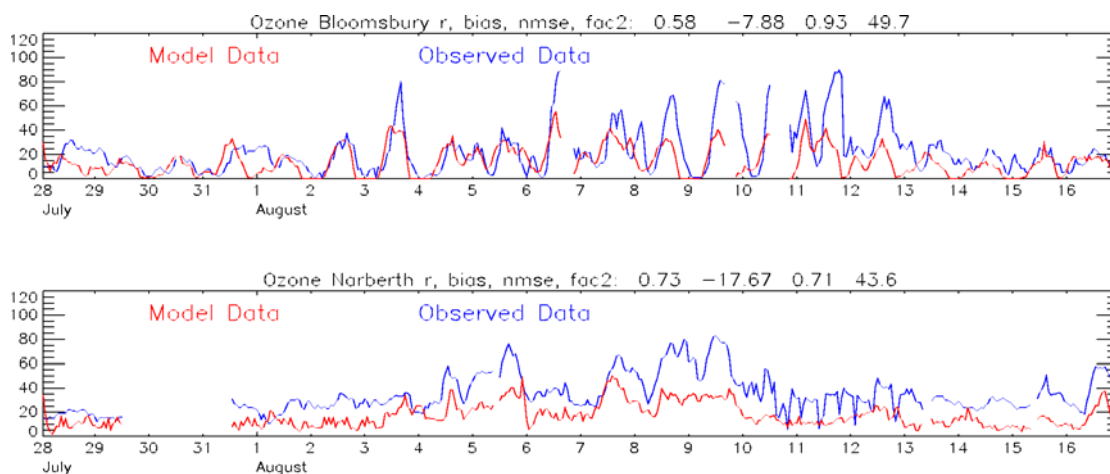


**Figure V-25.** Ozone levels predicted by the NAME model and observations at London Bloomsbury and Narberth.

At Bloomsbury the model is capturing the diurnal cycle observed reasonably well with a correlation of 0.58. The model is generally under-predicting the observed concentrations though most notably during the episode from the 8<sup>th</sup> - 13<sup>th</sup> August. At Narberth we see that there is a much less pronounced diurnal cycle than is evident at Bloomsbury. The model has represented the overall pattern of the observed ozone at Narberth very well, indicated by a correlation of 0.73. The model clearly captures the start of the elevated concentrations on 4<sup>th</sup> August, with a decrease on the 6<sup>th</sup>, before levels rise again on the 7<sup>th</sup>. The marked difference in the two sites on the 6<sup>th</sup> August is due the effects of different air masses. Narberth was receiving relatively clean air from the South West of France, where as London was receiving

highly polluted air from the industrial areas of Germany and France on that day. The model captures these differences, though in each case under-predicts the observed concentration. The overall bias at Narberth is larger than at London and we can see that the model is underestimating the observed concentration both prior to the episode and during it.

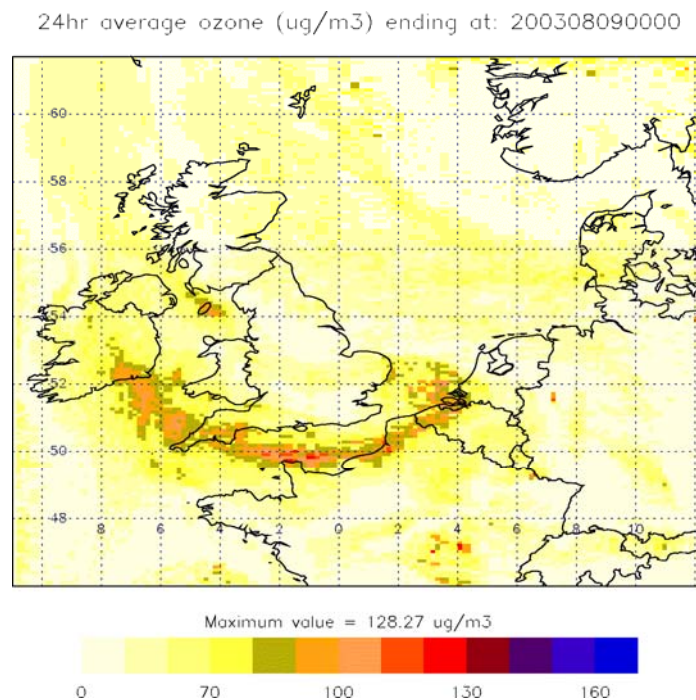


**Figure V-26.** A 24 hour average map of ozone concentration produced by the NAME model for 8<sup>th</sup> August 2003. The contours are: 0, 30, 50, 70, 80, 90, 100, 110, 120, 130, 140, 150, 160, 170  $\mu\text{g m}^{-3}$ ).

At Bloomsbury the model is capturing the diurnal cycle observed reasonably well with a correlation of 0.58. The model is generally under-predicting the observed concentrations, most notably during the episode from the 8<sup>th</sup> - 13<sup>th</sup> August. At Narberth we see that there is a much less pronounced diurnal cycle than is evident at Bloomsbury. The model has represented the overall pattern of the observed ozone at Narberth very well, indicated by a correlation of 0.73. The model clearly captures the start of the elevated concentrations on 4<sup>th</sup> August, with a decrease on the 6<sup>th</sup>, before levels rise again on the 7<sup>th</sup>. The marked difference in the two sites on the 6<sup>th</sup> August is due the effects of different air masses. Narberth was receiving relatively clean air from the South West of France, where as London was receiving very polluted air from the industrial areas of Germany and France on that day. The model captures these differences, though in each case under-predicts the observed concentration. The overall bias at Narberth is larger than at London and we can see that the model is underestimating the observed concentration both prior to the episode and during it.

As a further comparison, the 24 hour average ozone levels predicted by NAME and the PREV’AIR model for the 8<sup>th</sup> August are shown in Figure V-26 and Figure V-27 respectively. Focusing on the area represented by both models we can compare the predictions. The general pattern observed in and around the UK is similar between the two models, with low levels inland in the UK (dark blue in PREV’AIR, pale yellow in NAME) and much higher concentrations in the English Channel and the coast. However, the magnitudes from the PREV’AIR model are much greater than those seen in NAME, with the entire PREV’AIR map being above  $50 \mu\text{g m}^{-3}$  and most of the NAME map being below  $50 \mu\text{g m}^{-3}$ . The peak concentration seen in NAME in the English Channel is  $128 \mu\text{g m}^{-3}$ , and in PREV’AIR is between 160 and  $170 \mu\text{g m}^{-3}$ . Looking into Europe the spatial pattern in NAME is less evident, in particular NAME does not capture the very high levels ( $\sim 200 \mu\text{g m}^{-3}$ ) modelled by PREV’AIR over Germany.

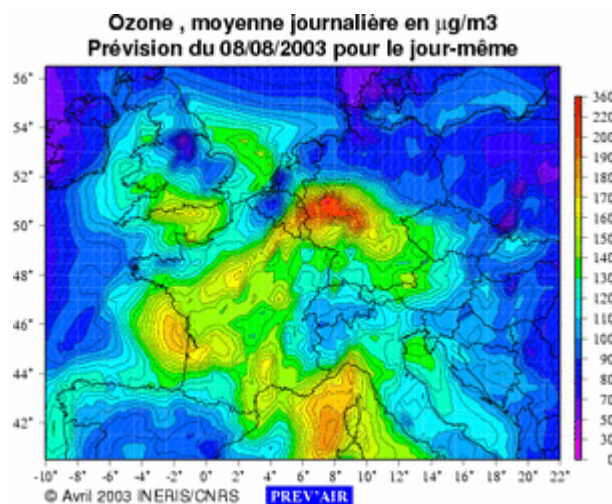


**Figure V-27.** A 24 hour average map of ozone concentration produced by the PREV’AIR model for 8<sup>th</sup> August 2003 in units of  $\mu\text{g m}^{-3}$ .

Figure V-28 shows a one hour average NAME map for the hour ending at 12:00 hours on 8<sup>th</sup> August. Whilst the ozone levels seen over much of the UK are still too low, the spatial pattern shows a much closer agreement with the PREV’AIR 24 hour average map shown in Figure V-27. In particular, NAME captures the elevated ozone levels over France and Germany very well. This close spatial agreement is very encouraging, showing that at least the daytime ozone production is working reasonably well in NAME, but perhaps too much ozone is lost in the night time.

1 hour average ozone (ug/m<sup>3</sup>) ending at: 200308081200

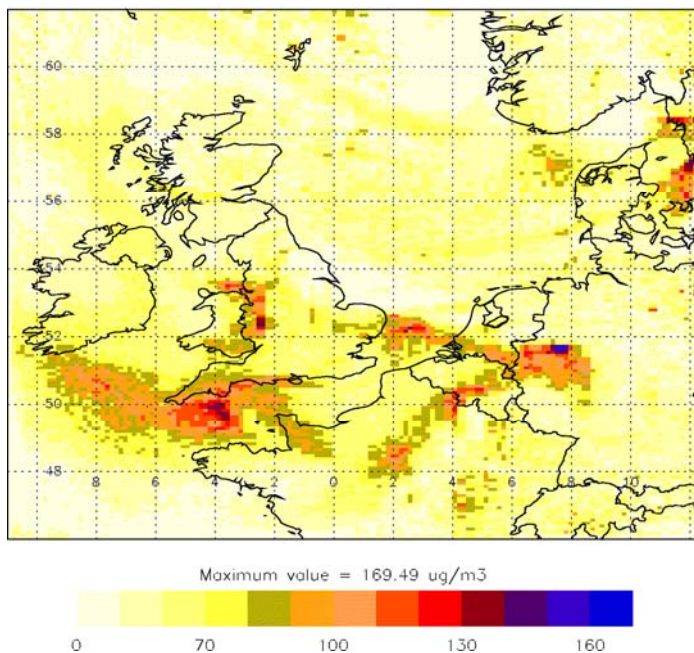


**Figure V-28.** A NAME model 1 hour average map of ozone concentration for 1200 hrs (hour ending) on 08 / 08 / 2003. (units  $\mu\text{g m}^{-3}$ )

In conclusion, the NAME model has been developed to a state in which it can make reasonable predictions of ozone at hourly timescales over a model domain including the UK and some of Europe. The model under-predicts both observations from the UK and the PREV' AIR model and this needs to be understood. One necessary improvement is the inclusion of biogenic emissions, most notably isoprene, which is known to have had a large effect on ozone levels over this particular episode (Lee et al., 2006), and to improving the representation of dry deposition of ozone within the model. The current deposition scheme for ozone is very simplistic allowing a dry deposition velocity over land of  $4 \text{ mm s}^{-1}$  and over sea of  $0.7 \text{ mm s}^{-1}$ . The model has been shown to be quite sensitive to the deposition velocity used, and a scheme which allowed differentiation between the deposition velocities used in urban and rural areas could prove very beneficial.

## 2. Nitrate aerosol

The NAME nitrate aerosol scheme previously reported (section (b)) has been replaced by a scheme described by Ackermann et al. (1995). Modelled nitrate aerosol levels using the old and new schemes are compared with observations at Harwell in Figures V-30 and V-31 respectively.

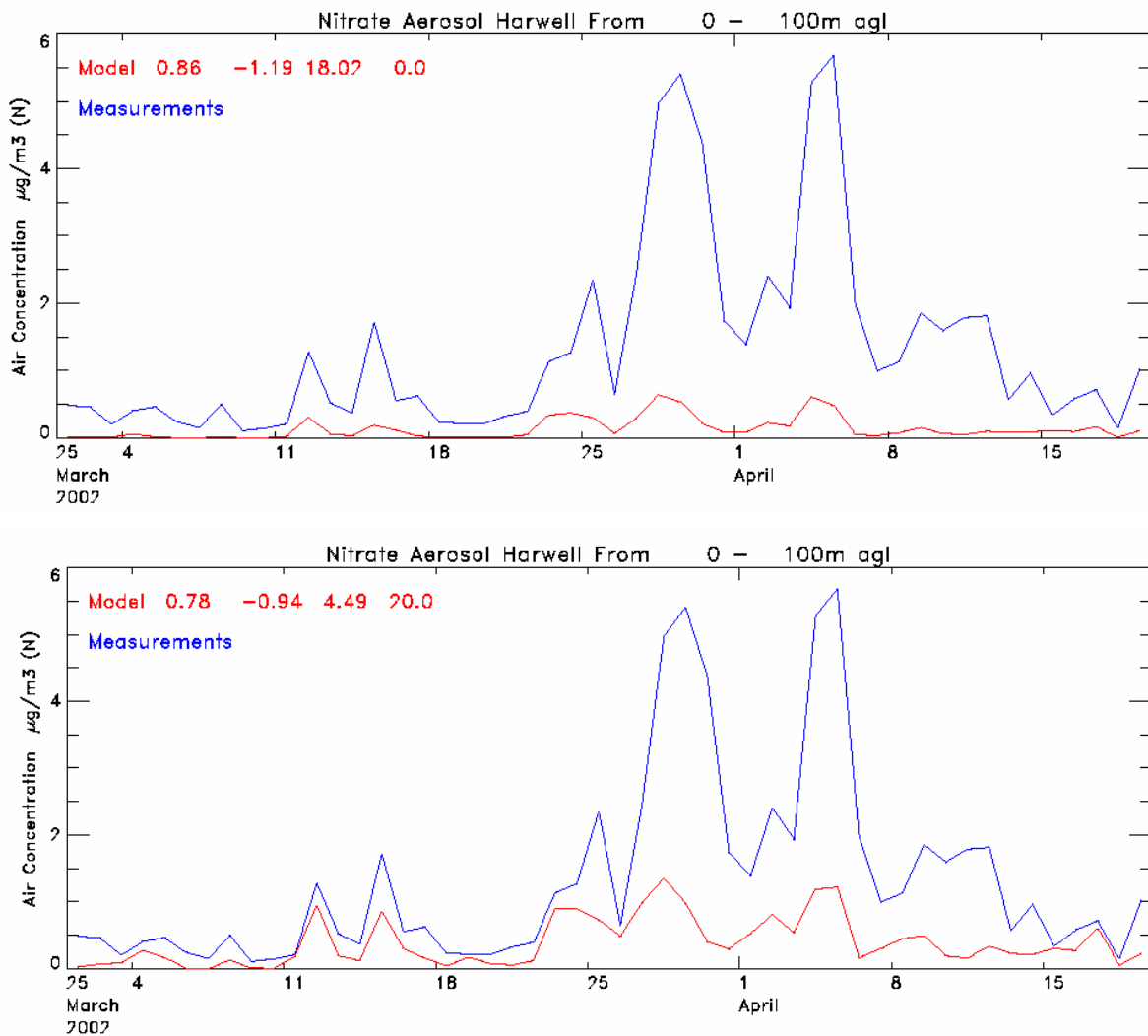


**Figure V-29.** Modelled nitrate aerosol concentrations for March and April 2002 at Harwell using the original scheme (top panel), and the improved scheme (lower panel).

These results indicate that the new scheme increases the amount of nitrate aerosol predicted by the model. During July, this has the effect of over predicting the amount of nitrate, whereas during March it generates results that more closely resemble the observed values.

The model was also run over the months of August and October to determine whether the new nitrate scheme consistently predicted more nitrate than the original scheme. This indeed was the case. Although the results using the new scheme are mixed, it has been implemented due to the fact that it is documented in the literature. Any future work would investigate the reason for the increased nitrate production by looking at the effect of the new nitrate parameterisation on the chemistry scheme as a whole.

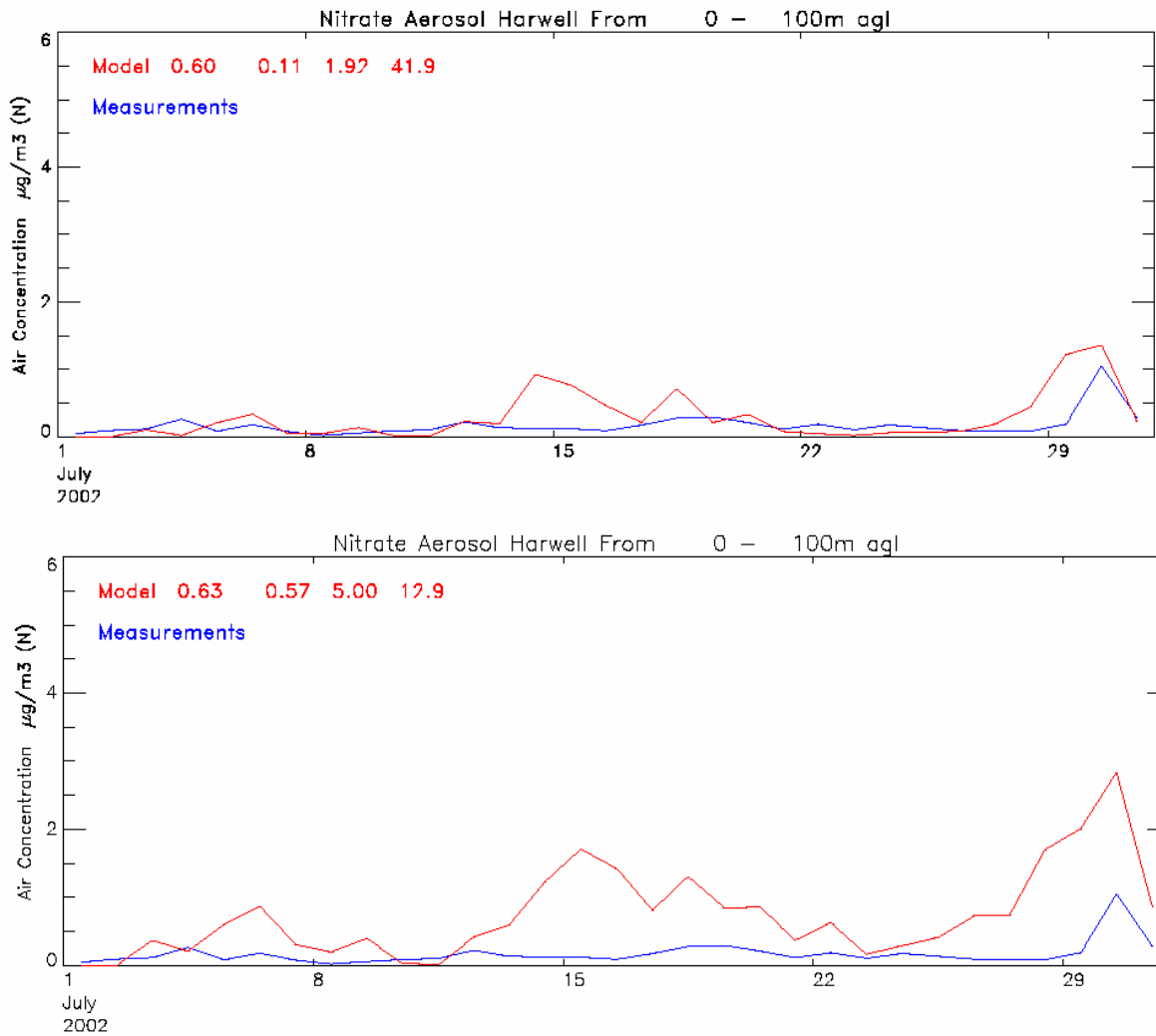


**Figure V-30.** Modelled nitrate aerosol concentrations for July 2002 at Harwell using the old scheme (upper panel) and the new scheme (lower panel).

### 3. Sulphate aerosols

A preliminary sensitivity study of the relationship between modelled sulphate aerosol production and liquid cloud water amount has been carried out. Although the modelled sulphate aerosol is generally quite reasonable, there are occasions when the model greatly over-predicts observed values, as can be seen in Figures V-33 and V-34. Sulphate aerosol production in the gas phase occurs at a steady but relatively slow rate. In the aqueous phase, however, large amounts of sulphate aerosol can be produced rapidly if the conditions are right. The aerosol is generated by reaction of dissolved  $\text{SO}_2$  with either hydrogen peroxide or ozone. The ozone pathway is limited by the cloud pH, and therefore can become self limited as sulphuric acid (dissolved sulphate aerosol) is produced. All available hydrogen peroxide is rapidly used up in aerosol production.

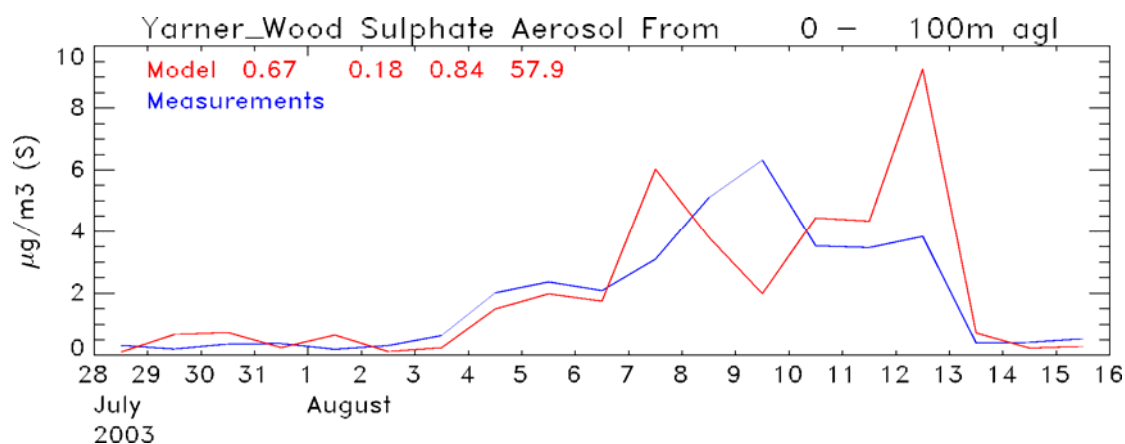


**Figure V-33.** Sulphate aerosol at Yarner Wood calculated using the current sulphate scheme which directly uses Unified Model cloud liquid water.

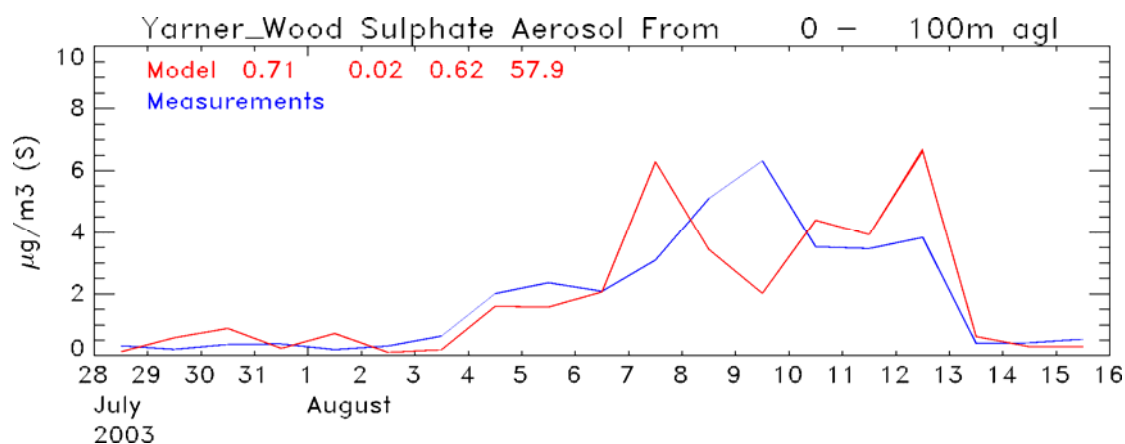


**Figure V-34** Sulphate aerosol at Yarner Wood calculated using the current sulphate scheme but with the Unified Model cloud liquid water value divided by two.

Looking at Figures V-33 and V-34 it can be seen that the large model peak on the 12<sup>th</sup> August has been considerably reduced by the halving of the cloud liquid water amount from the Unified model. The NAME sulphate scheme is clearly very sensitive to this parameter and further investigation is required. Confidence in the cloud liquid water value from the Unified model is not that high as it is a difficult quantity to verify. It would be useful to study the differences in aerosol production when using meteorological data at mesoscale resolutions (e.g. 4 – 50 km) and to assess the impact of reducing the cloud liquid water available to the chemistry over a wide range of locations and meteorological conditions.

## **(e) Conclusions**

The NAME model has been used successfully to respond to ad-hoc enquiries from Defra, most notably regarding the spread of the plume resulting from the fire at the Buncefield oil depot. The spread of the plume was accurately predicted (by comparing the modelled plume with satellite pictures), despite the uncertainties in the temperature of the fire and the amount of fuel burned. Continuous updates on the predicted spread of the plume were provided to the relevant authorities during the incident.

Unusually high levels of PM<sub>10</sub> were observed over parts of Scotland and northern England between the 8th and 10th of May 2006. Forward and backward trajectories were used with NAME to identify the source of the PM<sub>10</sub>, which was traced to forest fires in Russia. The path of the air during this period, and the low levels of pollutants in the air mass, ruled out pollution from continental Europe as a source.

The contribution of nitrate and sulphate aerosols to total aerosol levels over the UK was investigated. The NAME predictions were validated by comparison with observed levels of sulphate and nitrate aerosols at several locations in the UK. Given the relatively coarse resolution of NAME, the agreement between modelled and measured sulphate aerosol levels is satisfactory. NAME does not capture most of the peaks in the nitrate aerosol measurements, so the results should be treated with caution. Since this work was done, some improvement in the simulation of nitrate aerosol has been made, but NAME still tends to underpredict observed levels.

The simulation of dust emissions and transport to the UK by NAME has been improved. Comparisons with measurements made over Spain showed that NAME predicted the timing and shape of the dust transport well, but overpredicted the actual mass of dust. The dust emission was shown to be very sensitive to the soil moisture and resolution. In the latter case, a comparison of two simulations at low and high resolution showed that very little dust was produced by the low resolution run, whereas much more was emitted and transported by the high resolution run, which simulated the dust event more accurately. NAME was then successfully used to forecast dust events for two measurement campaigns in Africa. A dust storm over Athens was also investigated using NAME, and in this latter case the modelled and measured PM<sub>10</sub> levels agreed very well.

The contribution of emissions from different countries within Europe to observed levels of sulphate and nitrate aerosols over the UK was investigated. Of the total observed sulphate aerosol, the majority has been imported from nearby continental Europe, whereas for sulphur dioxide, UK emissions make up the largest proportion. The simulated sulphate aerosol levels were shown to be sensitive to the cloud liquid water content. Nitrate aerosol levels are less influenced by European emissions than sulphate aerosol levels; however, this result is highly uncertain, as NAME does not reproduce observed nitrate levels very well.

Progress in the simulation of ozone with NAME has been made. Comparisons with measurements and results from other models for the August 2003 summer, when very high ozone levels were measured over parts of Europe, showed that NAME captured the temporal variation and spatial patterns of the ozone levels, but tended to underpredict the absolute ozone levels. This underprediction is likely to be due to excessive deposition of ozone during the night-time, and the absence of natural hydrocarbons (i.e. isoprene) in the chemistry scheme; the very high emissions of the latter have been shown to be partly responsible for the very high ozone levels observed during parts of August 2003.

## Chapter VI. Summary and Conclusions

The change in surface ozone levels over Europe between 2000 and 2030 under three different emissions scenarios has been investigated. The scenarios were IIASA CLE (“likely”), IIASA MFR (“optimistic”) and SRES A2 (“pessimistic”). Under the CLE scenario, ozone levels were projected to be the same or slightly smaller in 2030 than 2000 over most of Europe, whereas when the MFR scenario was used ozone levels were significantly smaller over most of Europe. In both scenarios, ozone levels over the southern half of the UK and Benelux countries were projected to increase by about 5 ppb. When the A2 scenario was used, ozone levels over most of Europe were projected to be 6 – 10 ppb larger, but over the southern part of the UK and Benelux countries, ozone levels only rose by less than 3 ppb. Further investigation showed that  $\text{NO}_x$  emissions were the dominant controlling factor of the modelled ozone levels. These results suggest that current legislation regarding emissions of pollutants such as the National Emissions Control Directive will control surface ozone levels over Europe up to 2030, but that further significant reductions in ozone levels could be achieved with tighter restrictions on emissions. The impact of climate change on the modelled results is non-negligible in 2030, and acts to reduce modelled ozone values, but adds more uncertainty to the projections.

In the CLE and MFR scenarios, ozone levels over the southern half of the UK and the Benelux countries were projected to increase, despite the reductions in emissions. The production rate of ozone varies non-linearly with  $\text{NO}_x$  emissions and concentrations. When  $\text{NO}_x$  levels are very large, different chemical reactions which act to reduce the oxidation rate of VOCs (and hence ozone production) become important. When the  $\text{NO}_x$  emissions are decreased, these reactions become less important and so ozone production can increase. These results demonstrate that reducing emissions of pollutants does not always result in lower ozone levels. Reducing  $\text{NO}_x$  emissions generally will reduce ozone levels over Europe, but a reduction of 50% or more may be needed to control ozone levels over the Benelux countries and the southern part of the UK.

Additional model experiments were performed to look at the effect on modelled surface ozone levels if only Europe or the rest of the world (RoW) implemented emissions reductions. Using the CLE scenario, ozone levels over Europe are projected to fall between 2000 and

2030 if the RoW or just Europe follows this scenario, but rise if Europe does not. Under the MFR scenario, ozone levels decrease over Europe in all cases, even when it is assumed that Europe does nothing but the RoW follows this scenario. The ozone levels are the smallest if emissions from the entire world follow the MFR scenario. These results project that Europe receives high benefits from imposing strict controls on European emissions, but transport of pollutants from other regions can offset these benefits.

Further work on the effect of NO<sub>x</sub> emission changes concentrated on production by lightning. Vegetation distribution changes had a significant impact on the distribution and magnitude of the NO<sub>x</sub> production. In the future (2090s), the total amount of NO<sub>x</sub> was projected to remain the same, but the distribution was very different. More NO<sub>x</sub> was produced at mid-latitudes, and less in the tropics, owing to the dieback of the Amazon forest predicted by the Hadley Centre's model. However, projections of summer surface ozone levels over Europe were only slightly smaller (by 1-2 ppb) in the 2090s if NO<sub>x</sub> production by lightning was neglected.

The effect of emissions of pollutants from Asia on radiative forcing, and ozone levels over Europe, was assessed using emission pulses of NO<sub>x</sub>. These pulses caused changes in ozone and methane levels, from which the change in radiative forcing was calculated. The NO<sub>x</sub> pulse initially increased ozone levels (for 1 – 3 months) and in turn OH levels. The extra OH produced resulted in reduced methane levels, and also reduced ozone levels. Both the methane and ozone decreases decayed with a time constant between 10 and 15 years, because ozone levels are closely controlled by methane levels. The negative forcing (cooling) from the reduction in methane levels dominated the positive forcing (warming) from increased ozone levels. Initial experiments showed that the overall radiative forcing of the pulse decreased with increasing latitude.

Further experiments using pulses of NO<sub>x</sub> from different regions of Asia concentrated on the changes in ozone levels at Mace Head. Generally, pulses released from or very near the equator produced a net response of zero, i.e. the initial increase in ozone from the NO<sub>x</sub> pulse was equalled by the decrease caused by reduced methane levels. The ozone response at Mace Head became larger and more positive as the location of the pulse was moved further north.

In a similar set of experiments, the effects of pulses of NO<sub>x</sub> from various regions of North America were assessed. The initial ozone increase at Mace Head was larger, despite the fact

that the pulses were half the size of the Asian ones. A similar trend in the ozone response with the latitude of the pulse to that found with the Asian emissions was observed. Pulses emitted from southern regions produced a net ozone response at Mace Head of zero or a slightly negative value, whereas pulses emitted from more northerly regions gave a net positive ozone change. Changes in ozone levels over Europe in response to a given pulse from North America showed that the impact decreased both northwards and eastwards.

Exhaust gases from international shipping are currently unregulated. As land based emissions of NO<sub>x</sub> and SO<sub>2</sub> fall, the contributions from shipping will increase proportionately. For the year 2000, there is a significant contribution from shipping to sulphur deposited over Europe, as the fuel used in most ships has a very high sulphur content. Ozone levels are also enhanced by shipping emissions, contributing between 6 and 15% of modelled summer values over Europe. Legislation to reduce emissions from shipping will become more important as land-based emissions fall. The merchant fleet has increased by 35% over the last 50 years, and is projected to continue to increase, so such legislation will be even more important in the future.

The eutrophication and acidification of ecosystems from deposition of nitrogen and sulphur compounds was investigated. The NEC Directive sets targets on emissions, with the aim of reducing excess nitrogen deposition over Europe by 30%, compared with the situation in 1990. Using projections of emissions for the year 2030 as a proxy for 2010, significant reductions in nitrogen deposition, and hence land areas where a given critical load is exceeded, were modelled. Despite the differences between the model simulations and the exact specification of the NEC Directive, and uncertainties in the critical loads, the results suggest that the 30% reduction in areas having excess nitrogen deposition is achievable.

Projections of acid deposition further into the future indicate that acidification of soils may become a significant problem in south-east Asia and the eastern half of the USA during the 2090s. Climate change was found to make the problem worse, as more ammonia is oxidised in the aqueous phase, resulting in greater production of ammonium sulphate, one of the species responsible for acidification. The uncertainty in the critical loads for acidification means that the exact areas affected are difficult to identify. Further simulations, using different projections of future climate and emissions, would also be required to identify areas most at risk.

The effect of climate change on ozone levels over Europe in 2030 and 2100 were projected using the STOCHEM model. Even in 2030, climate change was found to have a significant influence on the predicted ozone levels, and more so in 2100. Stratosphere-troposphere exchange is projected to increase in the 2090s, and more ozone at the surface will have a stratospheric origin. However, overall ozone levels are smaller, owing to the increased destruction rate via the water vapour feedback. By 2100, changes in emissions and climate relative to the present day have the greatest impact on modelled future ozone levels. The stratospheric ozone impact is smaller, but is still significant.

The effect of changes in the distribution of vegetation on future ozone levels was investigated, including changes in emissions of isoprene. The biggest impact on simulated future surface ozone levels came from increased isoprene emissions due to the warmer climate. Dry deposition of ozone to vegetation is one of the key removal processes for ozone; however, the impact of vegetation distribution changes on the dry deposition of ozone was small. Isoprene emissions have been shown to have enhanced surface ozone levels over south-eastern parts of the UK during the summer 2003 heat wave, and as the climate warms, such episodes of very high ozone values may become more common.

Increased levels of CO<sub>2</sub> have an indirect effect on modelled future ozone levels. Plants absorb CO<sub>2</sub> via stomata, which are small pores on the surface of leaves. Larger CO<sub>2</sub> levels mean that the stomata do not need to open as widely to allow sufficient CO<sub>2</sub> for photosynthesis to enter the plant. Many trace gases, including ozone, are deposited to the inner surface of the leaves via the stomata. Hence, if the stomata do not open as widely, less ozone is deposited. Surface ozone levels were found to rise by 3 – 4 ppb over most of Europe if CO<sub>2</sub> levels were doubled, although the pattern of changes was very different in each season.

Reduced stomatal conductance also had a significant impact on modelled meteorology. When this impact was included, the modelled ozone changes were both positive and negative. The largest increases in ozone were 16 ppb over central Europe during the summer. However, this result is highly uncertain. A study of the exact long-term effect of stomatal conductance changes on meteorology and surface trace gas concentrations would require very long model simulations in order to identify robust changes and obtain meaningful statistics; such simulations were beyond the scope of the present contract.

Many results were contributed to the ACCENT Photocomp multi-model projections of future ozone levels, radiative forcing, and deposition fluxes. Six peer-reviewed publications have been published, and several of these have been referenced in Chapter 7 of the IPCC Fourth Assessment Report.

The NAME model has been used to respond to ad-hoc enquiries by DEFRA over the contract period. First, an explosion occurred at the Buncefield oil depot in Hemel Hempstead, Hertfordshire, at approximately 06:00 GMT on Sunday 11<sup>th</sup> December 2005. The explosion was heard over a wide area and is thought to have been caused by a leak from a petrol storage tank. The blaze is the largest industrial fire to date and at the height of the blaze, 20 tanks, each reported to hold up to three million gallons of refined fuel, were on fire. The NAME model was used to model the size, extent and movement of the resulting plume. Despite the uncertainties in the source release, comparison with satellite imagery showed good agreement between the geographical spread of the plume as predicted by NAME and satellite observations.

Secondly, unusually high PM<sub>10</sub> levels were measured over the UK by the air quality measurement network between 8th and 10th May 2006. Different sources of the PM<sub>10</sub> were investigated, including smoke from forest fires in Russia, pollen from Northern Europe, and European pollution. NAME was run in reverse, so that the origin of the air arriving at sites in the UK could be found. The resulting source maps indicated that these high levels of PM<sub>10</sub> were caused by smoke from Russian forest fires.

The NAME model has been used to study the origin of secondary inorganic aerosols in the UK. The study covered 2002 and 2003 and found significant variation in the amount of imported aerosol from Europe with location in the UK. For example in 2003 at Barcombe Mills (SE England), 28.7% of the sulphate aerosol was of UK origin with the largest European contribution coming from France (37.5%). In contrast in Edinburgh 56.9% of the sulphate aerosol was of UK origin with the next largest contribution coming from Ireland (14.7%). Significant differences were found between the results from the two years. These results reflect the importance of fully representing the transport of secondary aerosols over the European domain, and highlight the differences that can occur year to year through meteorology alone. This work contributed to the Air Quality Expert Group Report on Particulate Matter in the United Kingdom. It should be noted that aerosol formation and deposition will be affected by changes in temperature, cloud cover and rainfall.

The contribution of natural sources of aerosol to observed levels of PM<sub>10</sub> over the U.K. was investigated. Sea salt was found to make an important contribution to modelled levels, but would not cause an exceedence of air quality standards alone. The emissions and transport of Saharan dust to the UK and other countries was also investigated. Validation of NAME using case studies showed that the extent of the dust plumes, and their arrival at given locations was simulated well, but the model over-predicts the mass of dust (and hence PM<sub>10</sub> levels). Further tests showed that the model results were sensitive to the map of the different surface types, the soil moisture content, and the resolution of the model.

NAME has also been used to model the high ozone levels observed during the August 2003 heat wave. The model tended to underestimate observed levels of ozone, which is likely to be due to high deposition during the night-time, and the absence of natural hydrocarbons in the chemical scheme. Other work has shown that isoprene emissions were particularly high during the heat wave, and were a significant factor in the production of the very high ozone levels measured over south-east England.

## **Chapter VII. Suggestions for Future Work.**

In recent years, the importance of long-range transport of pollutants from different continents on local air quality has been recognised. Some work on this subject has been presented in this report, and the final report for contract EPG 1/3/164. Local emission reduction legislation has resulted in improved air quality over Europe. However, these local reductions are becoming increasingly offset by the transport of pollutants from other regions. Emission datasets used in this contract do not match exactly the limits proposed under legislation such as the NEC Directive. These datasets could be modified to match the emission limits of legislation, and so provide a more accurate assessment of their impact on eutrophication and air quality.

Within the framework of the Convention on Long-Range Transboundary Air Pollution (CLRTAP), the Task Force on Hemispheric Transport of Air Pollution (TF HTAP) has been set up to develop an understanding of the intercontinental transport of air pollutants in the Northern Hemisphere, and to produce estimates of the intercontinental flows of air pollutants for consideration in the review of protocols under the Convention. A set of multi-model experiments has been designed to investigate the long-range transport of air pollutants, and the effects of changes in emissions and background methane levels. STOCHEM would be used to perform these experiments, and the results presented at future meetings. Active participation in the analysis and writing of papers for peer-reviewed publication is also anticipated. The competing effects of increasing global background ozone levels and policies to reduce ozone levels under the NEC Directive would be investigated. Exposure of humans and crops and natural vegetation to ozone and PM could also be investigated. The health impacts of ozone would be quantified as far as possible using accepted methodologies. This work would involve interaction with London School of Hygiene and Tropical Medicine.

During the present contract, the technique of emission pulses has been used to quantify the radiative forcing consequences of tropospheric ozone precursor emissions, and more recently to begin the process of identifying intercontinental source-receptor relationships for ozone. Our initial work has used NO<sub>x</sub> emission pulses in North America and Asia to quantify ozone impacts across Europe. We propose to complete these initial studies and go on to look at the source-receptor relationships for other tropospheric ozone precursor gases of policy concern including methane, CO and VOCs.

The influence of aerosol loading on radiative forcing, the changing abundance of hydroxyl radicals and the resulting effects on the build up of greenhouse gases could be investigated. Damage to vegetation by ozone, and the resulting impact on climate and air quality is an important interaction that has only received a small amount of attention. We propose to investigate the damage to vegetation by ozone using an interactive vegetation model, in conjunction with CEH Wallingford.

The role of emissions from international shipping, and possibly aircraft, on air quality, acidification and eutrophication will be investigated. Currently, there are no restrictions on the emissions from ships or aircraft, and their numbers (and hence emissions) are expected to increase in the future. Presently, emissions from shipping are responsible for between 5 and 13% of observed ozone levels over Europe. Deposition of sulphur and nitrogen compounds from shipping is also increasing in importance as land-based sources decrease. We would use STOCHEM to investigate the contribution of shipping emissions to ozone levels and deposition of nitrogen and sulphur compounds over Europe under a range of future scenarios. The results will illustrate the uncertainty in the projections due to the emissions changes and future climate change.

STOCHEM would be further developed to simulate the production and transport of certain particles, such as ammonium nitrate and organic aerosols produced from the oxidation of naturally emitted hydrocarbons. Ammonium nitrate is only important in regions with high ammonia emissions, which in turn are produced from agricultural activities. Emissions of sulphur dioxide are declining as a result of legislation (such as CLRTAP and the NEC Directive), and so the formation of ammonium sulphate aerosols will also decline. Consequently, more ammonia is available for formation of ammonium nitrate. This latter species is not as thermally stable as ammonium sulphate, but still has the potential to be transported significant distances from its source regions and deposited to the surface. There may be significant impacts on ecosystems, via eutrophication. Interaction with CEH (Edinburgh) will occur on this subject.

In the process of analysing data obtained at Mace Head (under a contract with GA Division of DEFRA), a global biomass burning contribution to the observations of tropospheric background ozone at Mace Head has been identified for the 1998-1999 period. The mechanism underpinning these observations has not yet been characterised and two possible

explanations can be envisaged. The first involves the production of a reservoir of elevated ozone in the upper troposphere and the second the production of elevated levels of PAN by direct emission in the biomass burning fires. We propose to study the 1998 global biomass burning events using STOCHEM to elucidate the mechanism by which elevated ozone levels were observed across the EMEP network (Mace Head included) during the winter of 1998-1999.

A full life cycle for mercury has been added to STOCHEM and is fully operational on a global scale. The calculated elemental mercury concentrations at Mace Head agree with the available observations. In addition the model gives a complete continental attribution to the origins of the model mercury concentrations. We propose to study the continental attribution of mercury deposition across Europe and to provide input into the Review of the UN ECE Heavy Metals protocol and the EU Mercury Strategy.

The simulation of nitrate and sulphate aerosols by the NAME model has been improved, and the contribution of sea salt to total PM<sub>10</sub> levels has been assessed. However, there are a lack of measurements regarding the composition of aerosols, and meteorology of sufficient resolution. Such data have only been available within the last year. The aerosol simulation by NAME, in terms of mass and composition, could be improved by validation with these data.

## Glossary

AOT <sub>40</sub>	A metric used to assess possible damage to vegetation by ozone.
AQEG	Air Quality Expert Group.
CAFE	Clean Air for Europe.
CLRTAP	Commission on the Long Range Transport of Air Pollution.
Critical Load	Maximum deposition flux of a species or class of species that an ecosystem may withstand; above the critical load, damage to the ecosystem is likely to occur.
CUO	Cumulative (stomatal) Uptake of Ozone.
EC15	Those countries that have agreed to reduce their emissions of eutrophying compounds to given levels by 2010. They are Austria, Belgium, Denmark, Finland, France, Germany, Greece, Ireland, Italy, Luxembourg, The Netherlands, Portugal, Spain, Sweden, and the UK.
ECMWF	European Centre for Medium-Range Weather Forecasts.
EMEP	European Monitoring and Evaluation Programme.
GMD	Global Monitoring Division, part of NOAA.
GWP	Global Warming Potential.
HMs	Heavy Metals.
IIASA	International Institute for Applied Systems Analysis.
IPCC	Intergovernmental Panel on Climate Change.
MODIS	Moderate Resolution Imaging Spectroradiometer. A type of instrument aboard two satellites.
MOSES-II	Met Office Surface Exchange Scheme. The second version has an improved treatment of surface types and coastal regions.
NAME	The Met Office's Lagrangian dispersion model.
NAEI	National Atmospheric Emissions Inventory.
NECD	National Emissions Ceiling Directive.
NMSE	Normalised Mean Square Error.
NMVOC	Non-methane volatile organic compound.

NOAA	National Oceanic and Atmospheric Administration.
NO <sub>x</sub>	Nitrogen oxides; the sum of the concentrations of NO and NO <sub>2</sub> .
NPP	Net Primary Productivity.
NWP	Numerical Weather Prediction.
OX	Total oxidant, defined as the sum of the concentrations of ozone and nitrogen dioxide.
PM <sub>x</sub>	Sum of the mass of all particles with a diameter less than <i>x</i> . <i>x</i> usually has values of 10, 2.5 or 1.
POPs	Persistent Organic Pollutants.
RF	Radiative Forcing.
SRES	Special Report on Emission Scenarios, published by the IPCC.
SST(s)	Sea Surface Temperature(s).
STOCHEM	The Met Office's 3D Lagrangian chemistry-transport model.
VOC	Volatile Organic Compound, referring to most compounds containing carbon, hydrogen and oxygen emitted at the surface.

## References

- Ackermann I.J., Hass H., Memmesheimer M., Ziegenbein C., and Ebel A. (1995). The parametrization of the sulfate-nitrate-ammonia aerosol system in the long-range transport model EURAD. *Meteorology and Atmospheric Physics*, **57**, 101-114.
- Adams P.J., Seinfeld J.H., and Koch D.M. (1999). Global concentrations of tropospheric sulfate, nitrate, and ammonium aerosol simulated in a general circulation model, *Journal of Geophysical Research*, **104**, 13791-13823.
- Aselmann I. and Crutzen P.J. (1989). Global distribution of natural freshwater wetlands and rice paddies, their net primary productivity, seasonality and possible methane emissions. *Journal of Atmospheric Chemistry*, **8**, 307-358.
- Ashmore M., Emberson L., Karlsson P.E., and Pleijel H. (2004). New Directions: A new generation of ozone critical levels for the protection of vegetation in Europe. *Atmospheric Environment*, **38**, 2213-2214.
- Berntsen T., Fuglestad J., Myhre G., Stordal F., and Berglen T.F. (2005). Abatement of greenhouse gases. Does location matter? Paper presented to the 4th 'Non-CO2 greenhouse gases' Conference, Utrecht, Netherlands.
- Bobbink R. and Roelofs, G.-J. M. (1995). Nitrogen critical loads for natural and semi-natural ecosystems: the empirical approach. *Water Air and Soil Pollution*, **85**, 2413-2418.
- Butchart N., and Scaife A. A. (2001). Removal of chlorofluorocarbons by increased mass exchange between the stratosphere and troposphere in a changing climate, *Nature*, **410**, 799-802.
- Christensen T.R. and Cox P. (1995). Response of methane emissions from Arctic tundra to climatic change: Results from a model simulation. *Tellus*, **47B**, 301-309.
- Clapp L.J. and Jenkin M.E. (2001). Analysis of the relationship between ambient levels of O<sub>3</sub>, NO<sub>2</sub> and NO as a function of NO<sub>x</sub> in the UK. *Atmospheric Environment*, **35**, 6391-6405.
- Collins W.J., Stevenson D.S., Johnson C.E. and Derwent R.G. (1997). Tropospheric ozone in a global scale three dimensional Lagrangian Model and its response to NO<sub>x</sub> emission controls, *Journal of Atmospheric Chemistry*, **26**, 223-274.
- Collins W.J., Derwent R.G., Johnson C.E., and Stevenson D.S. (2002). The oxidation of organic compounds and their global warming potentials. *Climatic Change*, **52**, 453-479.
- Collins W.J., Derwent R.G., Garnier B.G., Johnson C.E., Sanderson M.G., and Stevenson D.S. (2003). Effect of stratosphere-troposphere exchange on the future tropospheric ozone trend. *Journal of Geophysical Research*, **108**, doi:10.1029/2002JD002617.
- Cox, P.M. (2001). Description of the TRIFFID dynamic global vegetation model, Hadley Centre Technical Note No.24, Met Office, Exeter, U.K. <http://www.metoffice.gov.uk/research/hadleycentre/pubs/HCTN>.

Cox P.M., Betts R.A., Jones C.D., Spall S.A., and Totterdell I.J. (2000). Acceleration of global warming due to carbon-cycle feedbacks in a coupled model, *Nature*, **408**, 184-187.

Cullen M.J.P. (1993). The Unified Forecast/Climate Model, *Meteorological Magazine*, (U.K.), 1449, 81-94.

Dentener F.D. and Crutzen P.J. (1993). Reaction of N<sub>2</sub>O<sub>5</sub> on tropospheric aerosols: Impact on the global distributions of NO<sub>x</sub>, O<sub>3</sub> and OH. *Journal of Geophysical Research*, **98**, 7149-7163.

Derwent R.G. and Malcolm A.L. (2000). Photochemical generation of secondary particulates in the United Kingdom. *Philosophical Transactions of the Royal Society of London Part A*, **358**, 1-15.

Dentener F.D., Stevenson D.S., Cofala J., Mechler R., Amann M., Bergamaschi P., Raes F., and Derwent R.G. (2005). The impact of air pollutant and methane emissions controls on tropospheric ozone and radiative forcing: CTM calculations for the period 1990-2030, *Atmospheric Chemistry and Physics*, **5**, 1731-1755.

Dentener F., et al. (2006). Nitrogen and sulfur deposition on regional and global scales: A multi-model evaluation, *Global Biogeochemical Cycles*, 20, GB4003, doi:10.1029/2005GB002672.

Derwent R.G., Collins W.J., Johnson C.E., and Stevenson D.S. (2001). Transient behaviour of tropospheric ozone precursors in a global 3-D CTM and their indirect greenhouse effects. *Climatic Change*, **49**, 463-487.

Derwent R.G., Collins W.J., Jenkin M. E., Johnson C.E. and Stevenson D.S. (2003). The global distribution of secondary particulate matter in a 3-D Lagrangian chemistry-transport model. *Journal of Atmospheric Chemistry*, **44**, 57-95.

DETR (2000). The Air Quality Strategy for England, Wales, Scotland and Northern Ireland. Working Together for Clean Air. Document Cm4548, SE2000/3, NIA7, Chapter 4. available at <http://www.defra.gov.uk/environment/airquality/strategy/index.htm>.

Erismann J. W., van Pul A. and Wyers P. (1994). Parametrization of surface resistance for the quantification of atmospheric deposition of acidifying pollutants and ozone, *Atmospheric Environment*, **28**, 2595-2607.

EMEP (1998). Numerical Addendum. MSC-W Status Report 1998 Part 2, EMEP/MSC-W 1/98, Norwegian Meteorological Institute, Oslo, Norway.

Essery R., Best M., and Cox P. (2001). MOSES 2.2 Technical Documentation, Hadley Centre Technical Note No.30, Met Office, Exeter, U.K. <http://www.metoffice.gov.uk/research/hadleycentre/pubs/HCTN>

Felzer B.S., Reilly J.M., Meilillo J.M., Kicklighter D.W., Wang C., Prinn R.G., Sarofim M., and Zhang Q. (2003). Past and future effects of ozone on net primary production and carbon sequestration using a global biogeochemical model, MIT Joint Program on the science and policy of global change, Report 103.

- Felzer B., Kicklighter D., Meilillo J., Wang C., Zhuang Q., and Prinn R. (2004). Effects of ozone on net primary production and carbon sequestration in the conterminous United States using a biogeochemistry model. *Tellus*, **56B**, 230-248.
- Fuhrer, J., Skärby, L., and Ashmore, M.R. (1997). Critical Levels for Ozone Effects on Vegetation in Europe. *Environmental Pollution*, **97**, 91-106.
- Fung I., John J., Lenerer J., Matthews E., Prather M., Steele L.P., Fraser P.J. (1991). Three-dimensional model synthesis of the global methane cycle. *Journal of Geophysical Research*, **96**, 13033-13065.
- Gong S.L. and Barrie L.A. (1997). Modelling sea-salt aerosols in the atmosphere 1. Model development, *Journal of Geophysical Research*, **102**, 3805-3818
- Guenther A., Hewitt C.N., Erickson D., Fall R., Geron C., Graedel T., Harley P., Klinger L., Lerdau M., McKay W.A., Pierce T., Scholes B., Steinbrecher R., Tallamraju R., Taylor J., and Zimmerman P. (1995). A global model of natural volatile organic compound emissions. *Journal of Geophysical Research*, **100**, 8873-8892.
- Hanna S.R. and Chang J.C. (1995). Comparison of predictions of the hybrid plume dispersion model with observations at the Kincaid power plant, *International Journal of Environment and Pollution*, **5**, 323-330.
- Hansen J., Sato M., and Ruedy R. (1997). Radiative forcing and climate response. *Climate Dynamics*, **13**, 547-560.
- IPCC (1994). *Climate Change 1994 – Radiative Forcing of Climate Change and an evaluation of the IPCC IS92 scenarios*, Cambridge University Press, Cambridge, U.K.
- IPCC (2001). *Climate Change 2001: The Scientific Basis. Contribution of Working Group I to the Third Assessment Report of the Intergovernmental Panel on Climate Change*, Houghton J.T., Ding Y., Griggs D.J., Noguer M., van der Linden P.J., Dai X., Maskell K., and Johnson C.A. (eds), Cambridge University Press, Cambridge, U.K.
- Jacob D. (2000). Heterogeneous chemistry and tropospheric ozone, *Atmospheric Environment*, **34**, 2131-2159.
- Johns T.C. et al. (2004). HadGEM1 - Model description and analysis of preliminary experiments for the IPCC Fourth Assessment Report, Hadley Centre Technical Note No.55, Met Office, Exeter, U.K. <http://www.met-office.gov.uk/research/hadleycentre/pubs/HCTN>.
- Johnson C.E., Stevenson D.E., Collins W.J., and Derwent R.G. (2001). Role of climate feedback on methane studied with a coupled ocean-atmosphere-chemistry model, *Geophysical Research Letters*, **28**, 1723-1726.
- Joshi M.M., Shine K.P., Ponater M., Stuber M., Sausen R., and Li L. (2003). A comparison of climate response to different radiative forcings in three general circulation models: Towards an improved estimate of climate change. *Climate Dynamics*, **20**, 843-854.

Kuylenstierna J.C.I., Cambridge H., Cinderby S., and Chadwick M.J. (1995). Terrestrial ecosystem sensitivity to acid deposition in developing countries, *Water Air and Soil Pollution*, **85**, 2319-2324.

Kuylenstierna J.C.I., Rodhe H., Cinderby S., and Hicks K. (2001). Acidification in developing countries: Ecosystem sensitivity and the critical load approach on a global scale, *Ambio*, **30**, 20-28.

Lee J.D., Lewis A.C., Monks P.S., Jacob M., Hamilton J.F., Hopkins J.R., Watson N.M., Saxton J.E., Ennis C., Carpenter L.J., Carslaw N., Fleming Z., Bandy B.J., Oram D.E., Penkett S.A., Slemr J., Norton E., Rickard A.R., Whalley L.K., Heard D.E., Bloss W.J., Gravestock T., Smith S.C., Stanton J., Pilling M.J., and Jenkin M.E. (2006). Ozone photochemistry and elevated isoprene during the UK heatwave of August 2003, *Atmospheric Environment*, **40**, 7598-7613.

Liao H. and Seinfeld J.H. (2005). Global impacts of gas-phase chemistry-aerosol interactions on direct radiative forcing by anthropogenic aerosols and ozone. *Journal of Geophysical Research*, **110**, doi:10.1029/2005JD005907.

Malcolm A. L., Derwent R.G. and Maryon R.H. (2000). Modelling the long range transport of secondary PM<sub>10</sub> to the UK, *Atmospheric Environment*, **34**, 881-894.

Matson P.A., McDowell W.H., Townsend A.R., and Vitousek P.M. (1999). The globalization of N deposition: ecosystem consequences in tropical environments, *Biogeochemistry*, **46**, 67-83.

Matyssek R., Wieser G., Nunn A. J., Kozovits A. R., Reiter I. M., Heerd C., Winkler J. B., Baumgarten M., Håberle K.-H., Grams T. E. E., Werner H., Fabian P., and Havranek W.M. (2004). Comparison between AOT40 and ozone uptake in forest trees of different species, age and site conditions, *Atmospheric Environment*, **38**, 2271-2281.

Mazzeo N.A., Venegas L.E., and Choren H. (2005). Analysis of NO, NO<sub>2</sub>, O<sub>3</sub> and NO<sub>x</sub> concentrations measured at a green area of Buenos Aires City during wintertime. *Atmospheric Environment*, **39**, 3055-3068.

Nickling W.G. and Gillies J.A. (1993). Dust emission and transport in Mali, West Africa, *Sedimentology*, **40**, 859-868

Meng Z. and Seinfeld J.H. (1996). Time scales to achieve atmospheric gas-aerosol equilibrium for volatile species. *Atmospheric Environment*, **30**, 2889-2900.

Pham M., Boucher O., and Hauglustaine D. (2005). Changes in atmospheric sulfur burdens and concentrations and resulting radiative forcings under IPCC SRES emission scenarios for 1990 – 2100, *Journal of Geophysical Research*, **110**, doi:10.1029/2004JD005125.

Physick W.L. and Maryon R.H. (1995). Near-source turbulence parametrization in the NAME model. UK Met Office Turbulence and Diffusion Note 218, Exeter, UK.

Pleijel H., Danielsson H., Ojanperä K., De Temmerman L., Högy P., Badiani M. and Karlsson P.E. (2004). Relationships between ozone exposure and yield loss in European wheat and

potato - a comparison of concentration- and flux-based exposure indices. *Atmospheric Environment*, **38**, 2259-2269.

Price C. and Rind D. (1992) A simple lightning parametrization for calculation global lightning distributions. *Journal of Geophysical Research*, **97**, 5929-5941.

Redington A.L., Derwent R.G., Ryall D.B., Matthew S., and Manning A.J. (2001). Pollution of the Urban Midlands Atmosphere: Development of an 'urban airshed' model for the West Midlands. Hadley Centre Technical Note 31, Met Office, Exeter.  
<http://www.metoffice.gov.uk/research/hadleycentre/pubs/HCTN/index.html>

Redington A.L. and Derwent R.G. (2002). Calculation of sulphate and nitrate aerosol concentrations over Europe using a Lagrangian dispersion model, *Atmospheric Environment*, **36**, 4425-4439.

Rodriguez S., Querol X., Alastuey A. and Mantilla E. (2002). Origin of high summer PM10 and TSP concentrations at rural sites in Eastern Spain, *Atmospheric Environment*, **36**, 3101-3112.

Ryall D.B. and Maryon R.H. (1998). Validation of the UK Met. Office's NAME model against the ETEX dataset, *Atmospheric Environment*, **32**, 4265-4276.

Sanderson M.G., Jones C.D., Collins W.J., Johnson C.E. and Derwent R.G. (2003). Effect of climate change on isoprene emissions and surface ozone levels, *Geophysical Research Letters*, **30**, 1936, doi:10.1029/GL017642.

Seinfeld J.H. and Pandis S.N. (1998). *Atmospheric Chemistry and Physics: From air pollution to climate change*, John Wiley & Sons, Inc., New York.

Shallcross, D.E. and Monks, P.S. (2000). New Directions: A role for isoprene in biosphere-climate-chemistry feedbacks. *Atmospheric Environment*, **34**, 1659-1660.

Shine K. P., Cook J., Highwood E.J., and Joshi M.M. (2003). An alternative to radiative forcing for estimating the relative importance of climate change mechanisms. *Geophysical Research Letters*, **30**, 2047, doi:10.1029/2003GL018141.

Simpson D., Ashmore M., Emberson L., Tuovinen J.-P., MacDougall M. and Smith R. I. (2003). Stomatal ozone uptake over Europe: Some preliminary results, in *Establishing ozone critical levels II*, Karlsson P.E., Selldén G., Pleijel H., Eds, UNECE Workshop Report IVL report 1523 B, IVL Swedish Environmental Research Institute, Gothenburg, Sweden.

Smith R.I., Fowler D., Sutton M.A., Flechard C., and Coyle M. (2000). Regional estimation of pollutant gas dry deposition in the U.K.: model description, sensitivity analyses and outputs, *Atmospheric Environment*, **34**, 3757-3777.

Stelson A.W. and Seinfeld J.H. (1982) Relative humidity and temperature dependence of the ammonium nitrate dissociation constant, *Atmospheric Environment*, **16**, 983-993.

Stevenson D.S., Doherty R.M., Sanderson M.G., Collins W.J., Johnson C.E. and Derwent R.G. (2004). Radiative forcing from aircraft NO<sub>x</sub> emissions: mechanisms and seasonal dependence. *Journal of Geophysical Research*, **109**, D17307, doi:10.1029/2004JD004759.

Stevenson, D. S., Doherty R.M., Sanderson M.G., Johnson C.E., Collins W.J., and Derwent R.G. (2005). Impacts of climate change and variability on tropospheric ozone and its precursors, *Faraday Discussions*, **130**, doi:10.1039/b417412g.

Stevenson D.S., et al. (2006). Multi-model ensemble simulations of present day and near future tropospheric ozone, *Journal of Geophysical Research*, **111**, doi:10.1029/2005JD00638.

Stillwell-Soller L.M., Klinger L.F., Pollard D., and Thompson S.L. (1995). The global distribution of freshwater wetlands. NCAR Technical Note NCAR/TN-416+STR, National Center for Atmospheric Research, Climate and Global Dynamics Division, Boulder, Colorado.

Sudo K., Takahashi M., and Akimoto H. (2003). Future changes in stratosphere-troposphere exchange and their impacts on future tropospheric ozone simulations, *Geophysical Research Letters*, **30**, 2256, doi:10.1029/2003GL018526.

Taiz, L. and Zeiger E. (1991). *Plant Physiology*, Benjamin/Cummings Publishing, Redwood City, California.

Targa J., Kent A., Stewart R., Coleman P., Bower J., Webster H., Taylor J., Murray V., Mohan R. and Aus C. (2006). Initial review of air quality aspects of the Buncefield Oil Depot explosion, Report no. AEAT/ENV/R/1784 Issue 1, AEA Technology Environment, Harwell, UK.

Wang X. and Mauzerall D.L. (2004). Characterizing distributions of surface ozone and its impact on grain production in China, Japan and South Korea: 1990 and 2020. *Atmospheric Environment*, **38**, 4383-4402.

Wild O. and Akimoto H. (2001). Intercontinental transport of ozone and its precursors in a three-dimensional global CTM, *Journal of Geophysical Research*, **106**, 27729-27744, 10.1029/2000JD000123.

Woodward S. (2001) Modelling the atmospheric life cycle and radiative impact of mineral dust in the Hadley Centre climate model, *Journal of Geophysical Research* **106**, 18155-18166.

Woodward S., Roberts D.L., and Betts R.A. (2005). A simulation of the effect of climate change-induced desertification on mineral dust aerosol, *Geophysical Research Letters*, **32**, doi:10.1029/2005GL023482.

Zeng G. and Pyle J. (2003). Changes in tropospheric ozone between 2000 and 2100 modeled in a chemistry-climate model, *Geophysical Research Letters*, **30**, doi:10.1029/2002GL016708.

## Annex A. Published Papers and Reports from this Project

W.J. Collins, R. G. Derwent, B. G. Garnier, C. E. Johnson, M. G. Sanderson, and D. S. Stevenson (2003). Effect of stratosphere-troposphere exchange on the future tropospheric ozone trend. *J. Geophys. Res.*, **108**, doi:10.1029/2002JD002617.

P. Cristofanelli, P. Bonasoni, W. Collins, J. Feichter, C. Forster, P. James, P. Kentarchos, W. Kubik, C. Land, J. Meloen, G.-J. Roelofs, P. Sigmund, M. Sprenger, C. Schnabel, A. Stohl, L. Tobler, L. Tositti, T. Tricj, and P. Zanis (2003). Stratosphere-to-troposphere transport: A model and method evaluations. *Journal of Geophysical Research*, **108**, doi:10.1029/2002JD002600.

R. G. Derwent, W. J. Collins, M. E. Jenkin, C. E. Johnson and D. S. Stevenson (2003). The global distribution of secondary particulate matter in a 3-D Lagrangian chemistry-transport model. *Journal of Atmospheric Chemistry* **44**, 57-95.

C. Granier, Y. Balkanski, S. Bekki, I. Bey, W. Collins, F. Dentener, L. Ganzefeld, S. Houweling, J.-F. Muller, J. Olivier, R. Sander, M. Sanderson, M. Schultz, J. Sciare, D. Stevenson, W. Sturges, and C. Zerefos (2003). Impact of climate change on tropospheric ozone. *Ozone-Climate Interactions*, edited by I. S. A. Isaksen, European Commission, number 81 (EUR20623), chapter 5, 97-114.

J. P. Meloen, P. Siegmund, P. van Velthoven, H. Kelder, M. Sprenger, H. Wernli, A. Kentarchos, G.-J. Roelofs, J. Feichter, C. Land, C. Forster, P. James, A. Stohl, W. Collins, and P. Cristofanelli (2003). Stratosphere-troposphere exchange: A model and method intercomparison, *J. Geophys. Res.*, **108**, doi:10.1029/2002JD002274.

G.-J. Roelofs, A. S. Kentarchos, T. Trickl, A. Stohl, W. J. Collins, R. A. Crowther, D. Hauglustaine, A. Klonecki, K. S. Law, M. G. Lawrence, R. von Kuhlmann, and M. van Weele (2003). Intercomparison of tropospheric ozone models: Ozone transport in a complex tropopause folding event, *J. Geophys. Res.*, **108**, 8529, doi:10.1029/2003JD003462

M. G. Sanderson, C. D. Jones, W. J. Collins, C. E. Johnson, and R. G. Derwent, (2003). Effect of climate change on isoprene emissions and surface ozone levels. *Geophysical Research Letters*, **30**, doi 10.1029/2003GL017642.

A. Stohl, P. Bonasoni, P. Cristofanelli, W. Collins, J. Feichter, A. Frank, E. Farster, H. Gerasopoulos, H. Gaggeler, P. James, T. Kentarchos, H. Kromp-Kolb, B. Kruger, C. Land, J. Meloen, A. Papayannis, A. Priller, P. Seibert, M. Sprenger, G.-J. Roelofs, H. E. Scheel, C. Schnabel, P. Siegmund, L. Tobler, T. Trickl, H. Wernli, V. Wirth, P. Zanis, and C. Zerefos (2003). Stratosphere-to-troposphere exchange: A review, and what we have learned from STACCATO. *J. Geophys. Res.*, **108**, doi:10.1029/2002JD002490.

R. G. Derwent, D. S. Stevenson, W. J. Collins, and C. E. Johnson (2004). Intercontinental transport of the ozone observed at surface sites in Europe. *Atmospheric Environment* **38**, 1891 – 1901.

R. G. Derwent. Global warming consequences of a future hydrogen economy. *Issues in Environmental Science and Technology* **20**, 25 – 33, (2004).

S. Solberg, D. Simpson, J. E. Jonson, A. G. Hjellbrekke, and R. Derwent. (2004). Chapter 6. Ozone. EMEP Assessment Report. Part I. Norwegian Meteorological Institute, Oslo, Norway.

D. S. Stevenson, R. M. Doherty, M. G. Sanderson, W. J. Collins, C. E. Johnson, and R. G. Derwent (2004). Radiative forcing from aircraft NO<sub>x</sub> emissions: mechanisms and seasonal dependence. *Journal of Geophysical Research* **109**, D17307, doi:10.1029/2004JD004759.

S. Solberg, D. Simpson, J. E. Jonson, A. G. Hjellbrekke and R. G. Derwent. Ozone. Part 1. EMEP Assessment Report.

F. Dentener, D. Stevenson, J. Cofala, R. Mechler, M. Amann, P. Bergamaschi, F. Raes and R. Derwent (2005). The impact of air pollutant and methane emission controls on tropospheric ozone and radiative forcing: CTM calculations for the period 1990-2030. *Atmospheric Chemistry and Physics* **5**, 1731-1755.

R. G. Derwent, D. S. Stevenson, R. M. Doherty, M. G. Sanderson, C. E. Johnson, J. Cofala, R. Mechler, M. Amann, and F. J. Dentener (2005). The contribution from ship emissions to air quality and acid deposition in Europe. *Ambio* **34**, 34-59.

R. G. Derwent, P. Grennfelt, O. Hov, J. Langner, A. Lindskog, and S. Solberg (2005). The development of European surface ozone. Implications for a revised abatement policy. EMEP-CCC Report 1/2005, Kjeller, Norway.

R. G. Derwent. (2005). Chapters 7 and 10. Particulate matter in the United Kingdom. Second report of the AQEG. DEFRA, London.

D. Ryall and A. Redington (2005). Contributions to chapters 6 and 8 of Particulate matter in the United Kingdom. Second report of the AQEG. DEFRA, London.

S. Solberg, R. G. Derwent, O. Hov, J. Langner, and A. Lindskog (2005). European abatement of surface ozone in a global perspective. *Ambio* **34**, 47-53.

D. Stevenson, R. Doherty, M. Sanderson, C. Johnson, W. Collins, and D. Derwent. (2005). Impacts of climate change and variability on tropospheric ozone and its precursors. *Faraday Discussions of the Royal Society of Chemistry* **130**, 41-57.

M. Athanassiadou, H. Flocas, M. A. J. Harrison, M. C. Hort, C. S. Witham, and S. Millington (2006). The dust event of 17 April 2005 over Athens, Greece. *Weather*, **61**, No. 5, 125-131.

F. Dentener, D. Stevenson, K. Ellingsen, T. van Noije, M. Schultz, M. Amann, C. Atherton, N. Bell, D. Bergmann, I. Bey, L. Bouwman, T. Butler, J. Cofala, B. Collins, J. Drevet, R. Doherty, B. Eickhout, H. Eskes, A. Fiore, M. Gauss, D. Hauglustaine, L. Horowitz, I. Isaksen, B. Josse, M. Lawrence, M. Krol, J.-F. Lamarque, V. Montanaro, J.-F. Muller, V. H. Peuch, G. Pitari, J. Pyle, S. Rast, J. Rodriguez, M. Sanderson, N. H. Savage, D. Shindell, S. Strahan, S. Szopa, K. Sudo, R. Van Dingenen, O. Wild, and G. Zeng (2006a). The global atmospheric environment for the next generation, *Environmental Science and Technology*, **40**, 3586-3594.

F. Dentener, J. Drevet, D. Stevenson, K. Ellingsen, T. Van Noije, M. Schultz, C. Atherton, N. Bell, I. Bey, T. Butler, B. Eickhout, A. Fiore, J. Galloway, C. Galy-Lacaux, U.C. Kulshrestha,

J.F. Lamarque, V. Montanaro, J.-F. Muller, J. Rodriguez, M. Sanderson, N. Savage, S. Szopa, K. Sudo, O. Wild, and G. Zeng (2006b). Nitrogen and Sulphur Deposition on regional and global scales: a multi-model evaluation, *Global Biogeochemical Cycles*, 20, GB4003, doi:10.1029/2005GB002672.

R. G. Derwent, P. G. Simmonds, S. O'Doherty, D. S. Stevenson, W. J. Collins, M. G. Sanderson, C. E. Johnson, F. Dentener, J. Cofala, R. Mechler, and M. Amann (2006). External influences on Europe's air quality: Baseline methane, carbon monoxide and ozone from 1990 to 2030 at Mace Head. *Atmospheric Environment*, **40**, 844-855.

M. Gauss, G. Myhre, I. S. A. Isaksen, V. Grewe, G. Pitari, O. Wild, W. J. Collins, F. J. Dentener, K. Ellingsen, L. K. Gohar, D. A. Hauglustaine, D. Iachetti, J.-F. Lamarque, E. Mancini, L. J. Mickley, M. J. Prather, J. A. Pyle, M. G. Sanderson, K. P. Shine, D. S. Stevenson, K. Sudo, S. Szopa, and G. Zeng (2006). Radiative forcing since preindustrial times due to ozone change in the troposphere and the lower stratosphere, *Atmospheric Chemistry and Physics*, **6**, 575-599.

M. G. Sanderson, W. J. Collins, C. E. Johnson and R. G. Derwent (2006). Present and future acid deposition to ecosystems: The effect of climate change. *Atmospheric Environment*, **40**, 1275-1283.

D. T. Shindell, G. Faluvegi, D. S. Stevenson, L. K. Emmons, J.-F. Lamarque, G. Petron, F.J. Dentener, K. Ellingsen, M. Amann, C.S. Atherton, N. Bell, D. J. Bergmann, I. Bey, T. Butler, J. Cofala, W. J. Collins, R. G. Derwent, R.M. Doherty, J. Drevet, H. J. Eskes, A. M. Fiore, M. Gauss, D. A. Hauglustaine, L. W. Horowitz, I. S. A. Isaksen, M. C. Krol, M. G. Lawrence, V. Montanaro, J.-F. Muller, G. Pitari, M. J. Prather, J. A. Pyle, S. Rast, J. M. Rodriguez, M. G. Sanderson, N. H. Savage, M. G. Schultz, S. E. Strahan, K. Sudo, S. Szopa, T. P. C. van Noije, O. Wild, and G. Zeng (2006). Multi-model simulations of carbon monoxide: Comparison with observations and projected near-future changes. *Journal of Geophysical Research*, 111, D19306, doi 10.1029/2006JD007100.

D. S. Stevenson, F. J. Dentener, M. G. Schultz, K. Ellingsen, T. P. C. van Noije, O. Wild, G. Zeng, M. Amann, C. S. Atherton, N. Bell, D. J. Bergmann, I. Bey, T. Butler, J. Cofala, W. J. Collins, R. G. Derwent, R. M. Doherty, J. Drevet, H. J. Eskes, A. Fiore, M. A. Gauss, D. A. Hauglustaine, L. W. Horowitz, I. S. A. Isaksen, M. C. Krol, J.-F. Lamarque, M. G. Lawrence, V. Montanero, J.-F. Müller, G. Pitari, M. J. Prather, J. A. Pyle, S. Rast, J. M. Rodriguez, M. G. Sanderson, N. H. Savage, D. T. Shindell, S. E. Strahan, K. Sudo, and S. Szopa (2006). Multi-model ensemble simulations of present-day and near-future tropospheric ozone. *Journal of Geophysical Research*, **111**, D08301, doi:10.1029/2005JD006338.

A. L. Redington and R. G. Derwent (2006). Import of inorganic aerosol to the UK: How significant is it? *Atmospheric Environment*, in press.

R. G. Derwent, D. S. Stevenson, R. M. Doherty, W. J. Collins, M. G. Sanderson, and C. E. Johnson (2007). Radiative forcing from surface NO<sub>x</sub> emissions: Spatial and seasonal variation. *Climatic Change*, (under review).

V. Eyring, D.S. Stevenson, A. Lauer, F.J. Dentener, T. Butler, W.J. Collins, K. Ellingsen, M. Gauss, D. A. Hauglustaine, I. S. A. Isaksen, M. G. Lawrence, A. Richter, J. M. Rodriguez, M. Sanderson, S. E. Strahan, K. Sudo, S. Szopa, T. P. C. van Noije, and O. Wild (2007). Multi-

model simulations of the impact of international shipping on atmospheric chemistry and climate in 2000 and 2030, *Atmospheric Chemistry and Physics*, **7**, 757-780.

M. G. Sanderson, W. J. Collins, D. L. Hemming, and R. A. Betts (2007). Stomatal conductance changes due to increasing carbon dioxide levels: Projected impact on surface ozone levels, *Tellus B*, in press.

## **Annex B. Meetings Attended.**

Results from this project were presented at the following meetings:

1. Beijing, 2005.
2. Seminar, Imperial College London, 3rd March 2004.
3. EMEP Task Force on Measurement and Modelling, Prague, 31st March - 2nd April 2004.
4. EMEP Workshop on Particulate Matter, New Orleans, USA, 20th - 22nd April 2004.
5. Colloquium, Hadley Centre, Met Office, Exeter, 27th April 2004.
6. EMEP Task Force on Health, Bonn, Germany, 5th - 7th May 2004.
7. Seminar, EU Café Secretariat, EU Brussels, 23rd - 24th June 2004.
8. Key-note Lecture, H2NET, Rutherford-Appleton Laboratory, Harwell, 14th July 2004.
9. 13th World Clean Air Congress, 23rd - 27th August, London, 2004.
10. 3rd IGAC conference, 5th - 10th September, New Zealand, 2004.
11. EMEP Steering Body, Geneva, 6th - 8th September 2004.
12. DEFRA Monitoring Strategy meeting, CEH, Edinburgh, 20th September 2004.
13. Intercontinental Transport of Air Pollution Workshop, North Carolina, USA, 21st - 22nd October 2004.
14. EMEP Task Force on Measurement and Modelling Workshop, Oslo, 22nd - 24th November 2004.
15. ACCENT workshop on Photocopy experiment (for IPCC AR4), 17th - 18th January, Oslo, 2005.
16. Lecture, Royal Meteorological Society, Atmospheric Chemistry Interest Group, University of Leicester, 17th March 2005.
17. EMEP Task Force on Measurement and Modelling, Zagreb, Croatia, 6th - 8th April 2005.
18. EMEP Task Force on Health, Bonn, Germany, 12 - 13th April 2005.
19. EMEP Task Force on Integrated Assessment Modelling, Berlin, 25th - 27th May 2005.
20. EMEP Task Force on Hemispheric Transport of Air Pollution, Brussels, 1st - 3rd June 2005.
21. EMEP Steering Body, Geneva, 5th - 7th September 2005.
22. ACCENT Symposium, 11th - 16th September, Urbino, Italy, 2005.
23. Royal Meteorological Society Annual Conference, 11th - 16th September, Exeter, 2005.
24. EMEP Task Force on Measurement and Modelling Workshop, Moscow, 13th - 14th October 2005.
25. EMEP Expert Group on PM, London, 8th November 2005.
26. EMEP Bureau, London, 8th - 9th November 2005.
27. UJCC Earth System Modelling workshop, Japan, 2005.
28. First iLEAPS conference, 21st - 26th January, Boulder, Colorado, 2006.
29. EMEP Task Force on Hemispheric Transport of Air Pollution, Washington DC, USA, 30th - 31st January 2006.
30. DEFRA modelling meeting, London, 27th February 2006.
31. EMEP Bureau, Geneva, 1st - 3rd March 2006.
32. EMEP Task Force on Measurement and Modelling, Helsinki, Finland, 10th - 12th May 2006.
33. NERC/DIAC meeting, Cambridge, 14th June 2006.
34. Transport, Atmosphere and Climate meeting, 26th - 29th June, Oxford, 2006.
35. Joint IGAC / CACGP / WMO Symposium, 18th - 22nd September, Cape Town, South Africa